

Ph.D 13172

- i -

MODELLING SEA ICE FLOE FIELDS

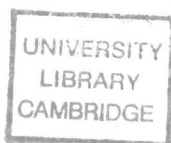
by

Iain Linklater Bratchie

A dissertation submitted for the degree of

Doctor of Philosophy

in the University of Cambridge



Churchill College,

Cambridge.

January 1984

## PREFACE

This dissertation is an account of my work carried out while a research student at the Scott Polar Research Institute and at the Meteorological Office during the period October 1980 to January 1984. During this time my supervisor at the Meteorological Office was Dr Howard Cattle. At the Scott Polar Research Institute during the period October 1980 to October 1981 my supervisor was Dr Vernon Squire, and from October 1981 to January 1984 my supervisor was Dr Peter Wadhams.

The dissertation does not exceed the regulations in length, and has not been submitted for a degree at any other university. It is the result of my own work and includes nothing which is the outcome of work done in collaboration.

Iain Linklater Bratchie

*Iain Bratchie*

January 1984

## ABSTRACT

This thesis is concerned with the modelling of sea ice, particularly in regions where it is composed of individual floes interacting through collisions. This has been done by modifying and extending existing models that have demonstrated their ability to simulate sea ice in various Arctic and Antarctic regions. The purpose of this study is the introduction of the representation of floes, in terms of their size and number, into a sea ice model, thus adding a feedback mechanism and a further output to the output fields normally produced by sea ice models, the ice velocity and the ice thickness distribution and the ice concentration.

Many of the physical processes concerning floes that are relevant to a sea ice model have not yet been investigated quantitatively. These aspects of floe behaviour used as model input are calculated from idealized mechanical models of a floe field. These include determinations of floe collision rates, side melting of floes and the cracking of floes in high winds. The strength of the pack ice is investigated, and in particular the effect of open water on the strength is considered. The shape of a plastic yield curve used in the model to determine the ice interaction forces is derived theoretically. The model used includes both thermodynamics and dynamics. The ice thickness characteristics and floe sizes change due to growing and melting, advection, floe cracking, floe collisions, and redistribution processes such as ridging and rafting. Daily wind and temperature data together with long term ocean currents are used as input to drive the model.

The results of a six month simulation of the sea ice development in the (East) Greenland region are presented and discussed together with a comparison with the observations.

#### ACKNOWLEDGEMENTS

I would like to thank Dr Peter Wadhams for all his advice, encouragement and interest throughout my stay at the Scott Polar. Thanks also to Dr Vernon Squire who started me on the road to sea ice modelling.

I am grateful to Dr Howard Cattle of the Meteorological Office for useful discussions and for his co-operation in all aspects of my work. I would like also to mention Dr Margaret Bottomley who tracked down some material, and who provided me with a place to live while in Bracknell. Pat Roberts deserves special mention for the hours of work she put into preparing the magnetic tapes containing the data.

The photographic work was done by Rob Massom of the Scott Polar.

I received grants from the Natural Environment Research Council and the Meteorological Office in Bracknell as part of a CASE (Co-operative Awards in Sciences of the Environment) award, and since October 1983 from the Arctic section of the Office of Naval Research, Washington. I am grateful for all their support.

## CONTENTS

PREFACE	ii
ABSTRACT	iii
ACKNOWLEDGEMENTS	iv
1. INTRODUCTION TO SEA ICE AND ITS MODELLING	
1.1 Introduction	1
1.2 History of sea ice modelling	4
1.3 Sea ice description	9
1.4 Marginal ice zones	10
1.5 Some general considerations regarding modelling	11
2. THE BASICS OF SEA ICE MODELLING	
2.1 Introduction	13
2.2 An ice model description	13
2.2.1 Basic equations	13
2.2.2 Internal ice stress	15
2.2.3 Ice distribution	17
2.3 The heat budget	19
2.3.1 Introduction	19
2.3.2 Determining growth rates in general	20
2.3.3 Short-wave radiation	21
2.3.4 Long-wave radiation	23
2.3.5 Bulk latent and sensible heat	24
2.3.6 Conductive flux	26
2.3.7 Testing the heat budget	26
2.4 Ice thickness distribution theory	29
3. ICE FLOES	
3.1 Spatial distribution of floes	38
3.2 Floe collisions	43
3.3 Floe size change	49
3.3.1 Introduction	49
3.3.2 Floe break up	50
3.3.3 Thermodynamic change in floe number density	65
3.3.4 Lateral melting	66
4. PACK ICE DYNAMICS	
4.1 Introduction	74
4.2 Ridging and rafting	74
4.2.1 A simple ridge building model	74
4.2.2 Rafting	88
4.3 Ice strength	89
4.3.1 Evaluating ice strength	89
4.3.2 Effect of open water on ice strength	100
4.4 Ice interaction	106
4.4.1 Introduction	106

4.4.2 A yield curve	108
5. INCORPORATING THEORY INTO THE NUMERICAL CODE	
5.1 Introduction	116
5.2 Ice thickness distribution	116
5.2.1 Representation of the ice thickness distribution	117
5.2.2 Ice redistribution	121
5.2.3 Analytic form of redistribution matrix	124
5.2.4 Numerical evaluation of the redistribution coefficients	126
5.2.5 A finer grid	126
5.3 Strength in the code	127
5.4 Floe number densities in the code	130
5.4.1 Floe size distribution	130
5.4.2 Floe size change	131
5.4.3 Continuous ice in a floe model	133
5.5 Thermodynamics in the code	134
5.5.1 Vertical changes	134
5.5.2 Lateral melting	137
6. THE MODEL SIMULATIONS	
6.1 Model inputs	142
6.1.1 The model grid	142
6.1.2 Initial thickness distribution	144
6.1.3 Oceanic heat flux and initial mixed layer temperature	146
6.1.4 Input winds and temperatures	149
6.1.5 Other thermodynamic inputs	149
6.1.6 Ocean currents	150
6.2 Application of the model to a standard simulation	152
6.2.1 Introduction	152
6.2.2 Variability of the model results	152
6.2.3 General features of the output fields	154
6.2.4 Distributions within single grid squares	173
6.2.5 Transects	181
6.3 Variations to the model	185
6.3.1 Introduction	185
6.3.2 Drift trajectories	190
6.3.3 Wind-induced currents	192
7. CONCLUSIONS AND FURTHER WORK	
7.1 Summary of the new features in this model	195
7.2 Future development of sea ice modelling	197
APPENDIX	199
BIBLIOGRAPHY	227
PLATES	236

## 1. INTRODUCTION TO SEA ICE AND ITS MODELLING

### 1.1 Introduction

The problem of concern in this thesis is the modelling of sea ice, particularly in regions where it is composed of individual floes interacting through collisions. This has been done by modifying and extending existing models that have demonstrated their ability to simulate sea ice in various Arctic and Antarctic regions. The purpose of this study is the introduction of the representation of floes, in terms of their size and number, into a sea ice model, thus adding a feedback mechanism and a further output to the output fields normally produced by sea ice models, the ice velocity, the ice thickness distribution and the ice concentration.

Many of the physical processes concerning floes that are relevant to a sea ice model have not yet been investigated quantitatively. These aspects of floe behaviour used as model input have been calculated from idealized mechanical models of a floe field.

Both thermodynamic and dynamic processes are important in sea ice variability. The model used for the present study was based upon a dynamic thermodynamic sea ice model that included a two-layer ice thickness parameterization (Hibler 1979). The computer code for this model has been published (Hibler 1980b) and was adapted to produce a 6-layer model, in which the ice is specified by a probability density function for the ice thickness. The floe number density was included as an additional parameter. The ice thickness categories evolve in time due to growth and melt, through horizontal advection to and from neighbouring grid squares, and by redistribution of ice during ridging and rafting. The floe sizes are parameterized by specifying the average radius of the floes within each thickness category. The floe size and the floe number density are related to the thickness distribution by assuming that the floes are circular. In a similar way to the ice thickness distribution, the floe

number density distribution evolves because of melting and growing of the ice. If floes grow in thickness, the floe number density in a thick ice category increases at the expense of the floe number density in a thinner category. In addition, lateral melting (included in the model) allows floes to decrease in radius while their number density remains unchanged. The floe number densities also change due to advection, from collisions, and from the cracking of floes due to the action of high winds.

The model has been applied to the (East) Greenland Sea where many ice types exist, from strong thick ice near the coast to thin ice near the ice edge which is observed to consist of floes of various sizes.

Chapter 1 includes an outline of the historical development of ice models as various levels of complexity were introduced to explain the observed ice drift patterns in the Arctic. In chapter 2, Hibler's (1979) sea ice model is described. This model, although considerably modified for this study, includes many of the aspects now regarded as necessary for inclusion in any reasonable sea ice model. Because of the large spatial variation in the thermodynamic parameters off East Greenland, the ice growth rates are calculated at each grid point. Chapter 2 includes also a description of the various thermodynamic factors and the calculation of ice growth rates. The method described utilizes formulae obtained from various thermodynamic models.

In chapter 3, the idea of a floe number density distribution is introduced and a number of analytic results obtained concerning floe fields. By considering the motion of a set of randomly scattered discs within a two-dimensional velocity field, an expression is obtained for the number of floe collisions occurring where there is an arbitrary strain rate expressed in terms of a shear and divergence.

Using the theory of flexible beams on elastic foundations, together with data available regarding floe tilting in wind, the cracking length of floes is calculated as a function of the applied wind speed and the floe thickness. The results indicate that there is a strong dependence of the cracking length upon the floe thickness, necessitating the introduction of a distribution of floe sizes in the model parameterization, rather than

using a single representative value.

Lateral melting of floes in summer is an important form of ice area loss. The relationship between the vertical and the lateral melt rate for floes is not known, so a simple theoretical treatment of floe melting was constructed to investigate the best suitable lateral melt rate for a model in which the floes are assumed to remain cylindrical.

In chapter 4 we consider the dynamics of pack ice deformation. In particular, a force model of the ice ridging process is presented that is simple enough to give an analytic expression for the ridge height in terms of the ice sheet thickness from which it was formed, and yet gives good quantitative and qualitative agreement with observed ridge heights. The ridging process is important in determining the ice strength needed in the momentum equation that gives the ice velocity. The determination of the ice strength in the context of ice thickness distribution theory is described and an analytic expression for the strength of an ice sheet of a single thickness is obtained that uses the ridge height formula calculated previously. The strength of a single ice thickness together with a fraction of open water is also obtained. By calculating the strength in this case by a method that takes into account the floe sizes present, a partial solution to one of the main problems of ice thickness distribution theory is obtained, that of the determination of the distribution of the ice involved in ridging as a function of the original ice thickness distribution.

The form of the collision rate obtained in chapter 3 is used to derive the shape of a yield curve which determines the relative amounts of internal shear and compressive stress that occur when the ice velocity field has non-zero shear or diverging strain rates. The choice of yield curve for sea ice models has in the past been a matter of intuition and this represents the first attempt to derive a yield curve shape from a physical model.

In chapter 5, the ways in which ideas and results derived in previous chapters may be included in practice into a numerical model are discussed.

Chapter 6 contains the details of the inputs to the model runs for the (East) Greenland Sea area and the setting up of the initial conditions. Results are presented and compared with the observed data. The conclusions are outlined in chapter 7.

The appendix contains the complete listing of the code as used for a typical run together with the output.

## 1.2 History of sea ice modelling

The early phase of sea ice modelling was characterized by initial observations leading to the formulation of theories to explain them. A classic example of this is the observation of Nansen that free ice did not drift in the direction of the wind, but consistently at an angle to the right of it. This led Ekman to formulate his boundary layer theories that explained the angular deviation of the ice drift as a consequence of the balance between the air and water stresses and the Coriolis force. The situation regarding the relationship between observations and theory has changed with experimental programmes designed to seek evidence to test already formulated theories. There are however many phenomena still without satisfactory physical explanations.

After Nansen's initial studies, further work on ice drift was carried out by Sverdrup (1928) who found evidence that ice-land and ice-ice interaction forces were causing significant departures from the Nansen theories of ice drift near the North Siberian coast. He assumed this resistance to be given by a coefficient of friction multiplied by the ice velocity. Using observed drift data from the Arctic, Zubov (1943) derived an empirical formula for ice drift which states that the ice moves in a direction parallel to the atmospheric isobars, and with a speed given by

$$V = 13000 \Delta p \quad (1)$$

where  $V$  is the drift speed in kilometres per month and  $\Delta p$  is the atmospheric pressure gradient in millibars per kilometre. Because of the fairly high degree of accuracy of this formula and its simplicity, it was

used for many years for long term Arctic drift trajectory calculations by Soviet researchers (Gordienko 1958). The formula does not work so well in regions where the ocean current is a dominant forcing. Reed and Campbell (1962) demonstrated from observations of the drift of ice station Alpha that internal ice resistance as well as the effect of gradient currents was important to the drift calculations. Campbell (1964) introduced terms for these two forces (the ice interaction term being more sophisticated than that assumed by Sverdrup) together with the three forces originally considered by Nansen, and obtained solutions to the resulting momentum equation. He also reviews the previous attempts to solve the momentum equation by leaving out various combinations of the forcing terms.

Sea ice models today generally include a solution to the ice momentum equation, at various positions on a two-dimensional grid, in an attempt to derive the ice velocity field over some geographic region. The development of models in this sense can be traced back to before computers became generally used. For example Zubov (1943) considers the deformation of a Lagrangian grid moving with ice that is deflected by the passage of a storm.

Another element of sea ice modelling that required consideration was the prediction of ice thicknesses or its distribution. Models that included these factors emerged in the 1950's. Some of these models are mentioned below. The ability to reproduce observed features of the ice circulation and distribution then became possible.

Drogaicev (1956) used a simple compactness ice model together with geostrophic wind fields and assuming ice drift  $10^\circ$  to the right of the isobars to give zones of convergence and divergence in the Arctic.

Campbell (1964), using an internal ice stress term of the form

$$K \nabla^2 u \quad u - \text{ice velocity} \quad (2)$$

simulated the anticyclonic gyre observed in the Beaufort Sea, although Felzenbaum (1958) had obtained this purely from long term wind input, the average pressure field having a high centred in the Beaufort. However, the

inclusion of the ice stress term resulted in a shift of the position of the gyre that more closely fitted the observations.

Models which include ice interaction terms proportional to  $\nabla^2 u$  aim to parameterize the effects of floe collisions by assuming that the associated energy losses give rise to viscous behaviour on the larger scale. This would give rise to a smoothing out of the resulting velocity field in that departures from locally averaged values would be resisted. This assumption may be valid for pack ice where there is a fair amount of open water but not for a compact ice cover.

Russian models with viscous terms include that of Ovsiyenko (1976) who investigated the wind drift of pack ice with a free boundary, using a constitutive law of the form

$$\sigma_{ij} = -(p + \mu \dot{\epsilon}_{kk}) \delta_{ij} + \mu \dot{\epsilon}_{ij} - \gamma \dot{\epsilon}_{ik} \dot{\epsilon}_{kj} \quad (3)^*$$

where the pressure term  $p$  is a function of the ice compactness evaluated from a simple random collision model of ice floes. Ovsiyenko concluded that the terms  $\mu$  and  $\gamma$  were negligible except for maximum compactness, thus leaving only a pressure term. Such an approach together with the more sophisticated collision calculations dealt with later in this study may prove to be a good approach to modelling ice very near the ice edge.

Models for forecasting need to be economical and simple to use so that care has to be taken with the choice of the physical parameters to include. Neralla and Liu (1979) have developed a sea ice model for use in predicting the ice compactness for short term local forecasting. They include the ice acceleration term, air and water stress, the Coriolis force and an internal ice resistance of the form  $\rho_i h \nabla \cdot (K \nabla u)$  where  $K$ , the horizontal kinematic eddy viscosity, has a linear dependence upon the ice concentration. The model can be run on a microcomputer producing reasonable results. Leppäranta (1981) describes a forecasting model for use in the Baltic Sea. The output gives ice type (level ice, ridged ice, open water) and is thus of direct use for shipping.

\*  $\sigma_{ij}$  and  $\dot{\epsilon}_{ij}$  are the stress and strain rate tensors and are dealt with in section 2.2.2.

inclusion of the ice stress term resulted in a shift of the position of the gyre that more closely fitted the observations.

Models which include ice interaction terms proportional to  $\nabla^2 u$  aim to parameterize the effects of floe collisions by assuming that the associated energy losses give rise to viscous behaviour on the larger scale. This would give rise to a smoothing out of the resulting velocity field in that departures from locally averaged values would be resisted. This assumption may be valid for pack ice where there is a fair amount of open water but not for a compact ice cover.

Russian models with viscous terms include that of Ovsiyenko (1976) who investigated the wind drift of pack ice with a free boundary, using a constitutive law of the form

$$\sigma_{ij} = -(p + \mu \dot{\epsilon}_{kk}) \delta_{ij} + \mu \dot{\epsilon}_{ij} - \gamma \dot{\epsilon}_{ik} \dot{\epsilon}_{kj} \quad (3)^*$$

where the pressure term  $p$  is a function of the ice compactness evaluated from a simple random collision model of ice floes. Ovsiyenko concluded that the terms  $\mu$  and  $\gamma$  were negligible except for maximum compactness, thus leaving only a pressure term. Such an approach together with the more sophisticated collision calculations dealt with later in this study may prove to be a good approach to modelling ice very near the ice edge.

Models for forecasting need to be economical and simple to use so that care has to be taken with the choice of the physical parameters to include. Neralla and Liu (1979) have developed a sea ice model for use in predicting the ice compactness for short term local forecasting. They include the ice acceleration term, air and water stress, the Coriolis force and an internal ice resistance of the form  $\rho_i h \nabla \cdot (K \nabla u)$  where  $K$ , the horizontal kinematic eddy viscosity, has a linear dependence upon the ice concentration. The model can be run on a microcomputer producing reasonable results. Leppäranta (1981) describes a forecasting model for use in the Baltic Sea. The output gives ice type (level ice, ridged ice, open water) and is thus of direct use for shipping.

\*  $\sigma_{ij}$  and  $\dot{\epsilon}_{ij}$  are the stress and strain rate tensors and are dealt with in section 2.2.2.

Another approach to sea ice modelling is the purely thermodynamic one in which the amount of ice in a region is determined by the amount of growing and melting which enable the ice to vary over a seasonal cycle. The most comprehensive study of this type was made by Maykut and Untersteiner (1971) in a one-dimensional simulation. Economical versions were produced by Semtner (1976). Such one-dimensional models have been made into three dimensional models (Washington et al 1976, Parkinson and Washington 1979, Parkinson and Herman 1980, Parkinson and Good 1982) to study the seasonal changes in the Arctic and Antarctic, but have limited ice dynamics. These sea ice models are useful in climate studies in that they may be easily incorporated into global circulation models. The effects on the ice sheets of changes in the atmospheric  $\text{CO}_2$  concentration may be investigated in this way (Manabe and Wetherald 1980). Predictions of ice edge positions where ice dynamics plays an important part are not valid though from such models. However, thermodynamic models have been combined with full dynamic sea ice models (Doronin 1970, Hibler 1980a). The ice model described in this study includes a heat budget calculation to determine time varying growth rates.

The sea ice model developed as part of the AIDJEX field programme (see for example Colony 1976, Pritchard 1977, Pritchard et al 1977) included a thickness distribution, and a momentum equation with the five forces already discussed, in which the internal ice stress is determined using an elastic plastic stress strain constitutive law. Hibler (1979, 1980a) developed the AIDJEX model further to produce a large scale dynamic thermodynamic sea ice model with non-linear advection terms that allows long term simulations. He used the model initially to simulate the seasonal cycle in the Arctic Basin although further studies have been carried out with the model on other geographical regions (Hibler and Ackley 1982). Hibler used a viscous plastic rheology for the ice interaction. Hibler's (1979) model is described in more detail later as it forms the basis of the dynamics used in the model developed here.

The more complicated plastic rheologies were introduced with the aim of being able to model the zones of intense shearing observed near coasts (Hibler et al 1974). For these plastic rheologies the ice yields only for ice of sufficient weakness (for a given forcing) and so should be able to

cope with areas of large shear, where viscous models would find difficulty.

The first application of a large scale numerical sea ice model to the East Greenland region was by Tucker (1982) using Hibler's two-layer model. He later repeated his study (Tucker 1983) using three different input datasets concluding that some available data fields contained incorrectly derived pressure fields which can substantially effect the resulting sea ice velocities.

Gaskill et al (1980) compared the free drift characteristics of a number of models. They concentrated on the wind and water stress formulations, concluding that those models incorporating stress terms proportional to the vertical air or water velocity gradients at the surface (Doronin (1970), Udin and Ullerstig (1976)) performed better than those employing stresses proportional to the square of relative air or water velocities. (Reed and Campbell 1962, Neralla et al 1980, Brown 1973, McPhee 1975, Hibler 1979). However, the former type requires more knowledge of the vertical structure of the surface boundary layers. The quadratic drag law formulations are simpler to apply.

The only models to take account of the finite size of floes, rather than simply using the ice area, are those of Timokhov (1967a, 1967b) and Solomon (1973). Timokhov derives equations based on the idea of collisions between floes caused by stochastic variations in their velocities. Solomon obtains ice interaction terms that depend on floe size, and concentration. However, both Timokhov and Solomon include only a one-dimensional treatment.

Recently model studies have attempted to simulate the processes occurring near the ice edge where there is much physical activity. These studies include that of Røed and O'Brien (1981, 1983) which predicts oceanic upwelling near an ice edge. This is a one dimensional model and has not yet been applied to a two-dimensional geographical region. Muench et al (1983) introduce a wave radiation term into the momentum balance to model the activity in the extreme ice edge zone.

As far as performance is concerned, the model best able to simulate observed ice edge position particularly in winter is the recently developed ice model of Hibler and Bryan (1983) that incorporates an

interacting ocean model to provide oceanic heat flux and time varying currents that are missing from previous models.

### 1.3 Sea ice description

The area of ice off East Greenland has been chosen for particular study in this thesis. This region is useful for testing a sea ice model because of the large variation in ice type present. Also a marginal ice zone and ice edge form part of the ice distribution there introducing an extra challenge to the ice modeller. Substantial areas of the ice consist of floes, a feature of the model developed here being the prediction of floe size distribution. We first describe the kinds of ice observed off East Greenland giving guidance to the kind of results that the model must be able to produce.

The East Greenland sea ice was described by Koch (1945), and a review including more recent observations was given by Wadhams (1981).

Apart from a very narrow area of ice frozen to the coast, which is called the ice foot, there are two main types of ice off East Greenland. They are 1) the fast ice, which is essentially fixed compared to 2) the pack ice, which comprises the majority of the ice area. Most of the fast ice is less than two metres in thickness although very thick (about 10m) ice can form after growing for many years in fjords and is known as sikussak (Walker and Wadhams 1979). In the Fram Strait region the average thickness of the drifting ice may reach 6m as indicated by submarine sonar data (Wadhams 1983b). Ice movement in the fast ice zone is prevented by grounded keels, giving rise to an apparent ice strength greater than that expected from ice thickness considerations alone.

The characteristic feature of the ice distribution and movement of ice in the Greenland Sea is a strong southward transport by the East Greenland Current that advects ice into regions where the thermodynamic conditions are such that ice would not grow there or survive unless it was continuously replaced. The pack ice can move with the currents and is susceptible to the effects of the winds. It consists of multiyear ice, generally about 3 years old, that originates in the Arctic and moves

across the pole in the Trans-Polar Drift Stream and passes together with slightly younger ice from north of Spitsbergen, through Fram Strait before moving south along the Greenland Current where the various ice types become mixed up. Ice divergence takes place in the vicinity of Fram Strait, where the East Greenland Current appears to accelerate. Here the opening of leads and polynyas allow new ice to grow, particularly in winter when the average air temperature can reach  $-28^{\circ}\text{C}$  (Crutcher and Merserve 1970). Some of the new ice occurs in the form of frazil ice because of the general level of turbulence. Thus new ice types will be expected within the areas of multiyear ice.

The physical properties of the ice in the Greenland Sea have only recently been studied (Overgaard et al 1983).

#### 1.4 Marginal ice zones

Man's interaction with the ice covered portions of the globe occur mostly near the ice edge, and in those regions which are ice-covered only for some part of the year. Such regions, known as seasonal sea ice zones, or marginal ice zones thus merit particular study. Knowledge of such regions is important for such activities as shipping and fishing as well as to the oil industry with its need to exploit all areas of the world. In Iceland for example the harbours become ice-bound in some winters but not others. The ability to forecast such situations then becomes of economic importance.

Marginal ice zones include the Greenland and Bering Seas, as well as parts of the Barents and the Labrador Seas. A large proportion of the area surrounding the Antarctic in winter is also a marginal ice zone.

Marginal ice zones may be characterized by their appearance. The ice in these regions is generally composed of floes of various shapes, sizes, and thicknesses. Using the Greenland Sea as an example, floes as large as 60 km in diameter have been observed in Fram Strait (Vinje 1977). Further south, the ice lies in a zone (in winter) parallel to the East Greenland coast. The area towards the edge is characterized by a gradual decrease in the

average floe size until, very near the ice edge, the action of ocean waves becomes significant giving rise to very small broken up floes. Floes larger than a few metres in diameter do not survive near the ice edge because of the level of activity there. This applies even to the thickest sea ice floes (Wadhams 1978).

This scheme is complicated by the motion of the floes whereby areas of small floes may be advected back away from the ice edge into the interior giving rise to large variations in floe size over comparatively short distances. Another complicating feature is that of bands of ice that break away from the ice edge. They remain relatively coherent as they drift away from the edge until they begin to melt in areas of warm water. Various mechanisms have been suggested for the formation and persistence of bands (Muench and Charnell (1977), McPhee (1982), Wadhams (1983a)). Along the ice edge, eddies have been observed, the effect of which is to disrupt any smoothness in the horizontal variation in ice properties, such as floe size (Wadhams et al 1979, Wadhams and Squire 1983).

The physics of marginal ice zones and ice edges include a number of additional complexities, concerned with the effects of the ice upon the factors that force it. In fact the ice-ocean-atmosphere system is totally interacting. Experimental programmes are now in progress (MIZEX-84) to study these interactions. To model all these interactions simultaneously would necessitate coupling ice, ocean and atmosphere models. The difficulties involved suggest that such a coupled model will not be achieved in the near future.

### 1.5 Some general considerations regarding modelling

With numerical models, it is possible to investigate the effects on sea ice of physical factors in a way not possible experimentally. This can be done by adjusting the physical parameters in the model and comparing the results with a standard set of results. There are, however, many factors preventing numerical sea ice models from ever truly representing reality. For example, stochastic variations in physical parameters such as the tensile strength of ice mean that their representation by single values

necessarily introduces errors. There are very few mechanical properties of sea ice for which there is little variation.

The degree of complexity of a model is another factor that should be considered. There is no point including highly sophisticated physics in a model if it has very little effect upon the results. Of course it may not be known to what extent some physical process is important, and here modelling can play a part.

Where a physical process is expected to be significant but its precise mathematical treatment is too difficult or beyond the scope of the model, it may be better to include some kind of approximate parameterization rather than nothing at all. Many of the early ice models included this sort of parameterization.

## 2. THE BASICS OF SEA ICE MODELLING

### 2.1 Introduction

In this chapter we introduce some of the details of fairly well established theory with regard to ice modelling. Firstly, we describe Hibler's (1979) two-layer model which serves as the basis of further development. A description of a simple heat budget calculation is given. Here there are a few minor modifications to existing models. Finally, an outline of ice thickness distribution theory of which extensive use is made later, is given.

### 2.2 An ice model description

#### **2.2.1 Basic equations**

In this section the major features of Hibler's sea ice model are outlined. Some of the components of the model have subsequently been altered to suit this particular study but the basic momentum equation and its method of numerical solution remain.

Sea ice is modelled as a two-dimensional continuum with spatially varying velocity  $\underline{u}(\underline{x})$ , and the ice thickness characteristics specified by two quantities  $h$ , the mean ice thickness over the grid square, and the compactness  $A$  which is the fraction of open water covered by ice. Thus, what is essentially a two-layer ice thickness distribution is set up, thin ice or open water and thicker ice.

The ice motion is determined from a momentum balance expressed by the following equation.

$$m \frac{Du}{Dt} = -mfk \wedge u + \tau_a + \tau_w - mg \nabla H + F \quad (1)$$

where

- $m$  - Ice mass per unit area
- $f$  - The Coriolis parameter
- $\underline{k}$  - Unit vector normal to the plane of the ice motion
- $\tau_a$  - Force on ice due to air stress
- $\tau_w$  - Force on ice due to water stress
- $\underline{g}$  - Acceleration of gravity
- $H$  - Sea surface dynamic height
- $\underline{F}$  - Force due to internal ice resistance

We consider the forcing terms on the right hand side of (1) in turn. The first term  $-mfk \wedge u$  is the Coriolis force and is a significant contribution to the momentum balance. The terms  $\tau_a$  and  $\tau_w$  are computed as follows

$$\tau_a = \rho_a C_a |\underline{U}_g| (\underline{U}_g \cos \phi + \underline{k} \wedge \underline{U}_g \sin \phi) \quad (2)$$

$$\tau_w = \rho_w C_w |\underline{U}_w - \underline{u}| [(\underline{U}_w - \underline{u}) \cos \theta + \underline{k} \wedge (\underline{U}_w - \underline{u}) \sin \theta] \quad (3)$$

where

- $\underline{U}_g$  - Geostrophic wind
- $\underline{U}_w$  - Geostrophic ocean currents
- $C_a$  - Air drag coefficient
- $C_w$  - Water drag coefficient
- $\rho_a$  - Air density
- $\rho_w$  - Sea water density
- $\phi$  - Air turning angle
- $\theta$  - Water turning angle

The geostrophic wind can be obtained from pressure data, and similarly, the geostrophic currents are obtained from maps of the sea surface dynamic height. Formulae (2) and (3) are thus quite convenient methods of estimating the water and wind stress for a long term climate model. The term  $-mg \nabla H$  represents the component of the gravitational force on the ice

in the direction parallel to the sea surface which is tilted in response to the ocean geostrophic currents. The sea surface dynamic height  $H$  is related to  $\underline{U}_w$  by the equation

$$\underline{U}_w = \hat{g} f^{-1} \underline{k} \wedge \nabla H \quad (4)$$

so that

$$-m \hat{g} \nabla H = m f \underline{k} \wedge \underline{U}_w \quad (5)$$

and the tilt effects can be combined with the Coriolis forces in the single term

$$m f \underline{k} \wedge (\underline{U}_w - \underline{u}) \quad (6)$$

The final term  $\underline{F}$ , the internal ice stress, depends on a number of other components of the model, specifically the rheology, the constitutive law and the ice strength. The evaluation of  $\underline{F}$  is now considered in more detail.

### 2.2.2 Internal ice stress

The choice of rheology determines how  $\underline{F}$ , the ice interaction term depends upon the motion of the ice. The frictional forces set up in the ice depend upon the relative velocities at various places, expressed in terms of a two-dimensional strain rate tensor  $\dot{\epsilon}_{ij}$ . Also the magnitude of the forces set up in the ice due to its motion will depend upon the strength of the ice, denoted  $p^*$ . For normal strain rates Hibler's model employs a viscous plastic rheology in which the internal ice stress  $\sigma$  has a value that lies on a particular curve (the yield curve) in a suitably defined coordinate system. The value of the stress is independent of the magnitude of the strain rate, and it is this property that characterizes plasticity. For very small strain rates, Hibler uses a linear viscous rheology so that the stress drops linearly to zero from its plastic value as the magnitude of the strain rate tends to zero. An elliptical yield curve is used (in the

$(\sigma_1, \sigma_{11})$  plane, where  $\sigma_1$  and  $\sigma_{11}$  are the principle components of stress). In a later chapter, the meaning of the shape of the yield curve is discussed.

Hibler expresses the stress tensor  $\sigma_{ij}$  in terms of the strain rate tensor  $\dot{\epsilon}_{ij}$  according to a non-linear constitutive law of the form

$$\sigma_{ij} = 2\eta\dot{\epsilon}_{ij} + \{\zeta - \eta\}\dot{\epsilon}_{kk}\delta_{ij} - \frac{1}{2}p^*\delta_{ij} \quad (7)$$

where  $\eta$  and  $\zeta$  are the shear and bulk viscosities respectively. These viscosities depend upon the strength as well as the strain rate. The forms that  $\eta$  and  $\zeta$  take as functions of  $\dot{\epsilon}_{ij}$  and  $p^*$  are determined by the choice of yield curve. For the elliptical yield curve with eccentricity  $e$ , as used by Hibler, the viscosities are

$$\zeta = \frac{p^*}{2\sqrt{\dot{\epsilon}_1^2 + e^{-2}\dot{\epsilon}_{11}^2}} \quad (8)$$

and

$$\eta = \zeta/e^2 \quad (9)$$

The terms  $\dot{\epsilon}_1$  and  $\dot{\epsilon}_{11}$  are functions of the components of the strain rate tensor and are defined by

$$\begin{aligned} \dot{\epsilon}_1 &= \dot{\epsilon}_{11} + \dot{\epsilon}_{22} \\ \dot{\epsilon}_{11} &= \sqrt{(\dot{\epsilon}_{22} - \dot{\epsilon}_{11})^2 + 4\dot{\epsilon}_{12}\dot{\epsilon}_{21}} \end{aligned} \quad (10)$$

Once the stress  $\sigma_{ij}$  has been obtained from the given strain rate and the ice strength, the components of the ice interaction term in the momentum equation (1) are given by

$$F_i = \frac{\partial \sigma_{ij}}{\partial x_j} \quad (11)$$

### 2.2.3 Ice distribution

The momentum equation when solved (numerically) gives the ice velocity field  $u(x)$ . Some of the terms in the equation, in particular the ice interaction term, depend upon the amount and thickness of the ice. These quantities evolve in time by advection which is determined by the velocity field. In addition, thermodynamic effects alter the ice thickness characteristics and so affect the ice strength. Thus the momentum equation giving  $u$  and depending upon  $p^*$ , and the advection and thermodynamic equations giving  $h$  and  $A$  and depending upon  $u$ , give a coupled system of equations. The evolution of  $h$  and  $A$  are given by (using a one-dimensional version of the equations for illustration)

$$\frac{\partial h}{\partial t} = -\frac{\partial (uh)}{\partial x} + S_h \quad (12)$$

and

$$\frac{\partial A}{\partial t} = -\frac{\partial (uA)}{\partial x} + S_A \quad (13)$$

where the thermodynamic terms are given by

$$S_h = f(h/A)A + (1-A)f(0) \quad (14)$$

and

$$S_A = \begin{cases} (f(0)/h_0)(1-A) & \text{if } f(0) > 0 \\ 0 & \text{if } f(0) < 0 \end{cases} + \begin{cases} 0 & \text{if } S_h > 0 \\ (A/2h)S_h & \text{if } S_h < 0 \end{cases} \quad (15)$$

Here,  $f(h)$  is the growth rate of ice of thickness  $h$ , and  $h_0$  is the demarkation thickness between thick and thin ice. Also, the compactness  $A$  is forced to remain less than or equal to one. Equations (12) to (15) represent a simple form of the ice thickness distribution equation which is examined in detail later so that here it suffices to mention that the equations are designed to include such concepts as the increase in thickness during ridging when the compactness becomes unity and the ice field converges. Also the term  $S_A$  allows rapid freezing of open water to occur by letting its fraction  $(1-A)$  decay exponentially, and, during melting conditions, the amount of thin ice resulting from the melting of the thick ice will occur relatively slowly.

The values for the growth rate function  $f(h)$  used in Hibler's (1979) Arctic study were those calculated by Thorndike et al (1975) using Maykut and Untersteiner's (1971) numerical thermodynamic model. The values however may also be obtained by performing a complete heat budget calculation at each time step. Semtner (1976) and Hibler (1980a) show how this may be done efficiently. A similar heat budget calculation is dealt with later for use in the model developed here and is described in more detail then.

Finally, the ice strength is determined by the formula

$$P^* = P \exp[-K(1-A)] \quad (16)$$

where  $P$  and  $K$  are fixed empirical constants. This equation was not derived from a study of the mechanics of deforming ice but rather, chosen just to give a sharp drop in strength as the amount of open water increases from zero, and also to incorporate an increase in strength as the ice thickness

increases. A more detailed treatment of the ice strength is given in section (4.3).

### 2.3 The heat budget

#### 2.3.1 Introduction

As we have seen, the thermodynamics, in Hibler's models and in the thickness distribution evolution equations, enter in the form of a growth rate function  $f(h,t)$ . This growth rate  $(dh/dt)$  is a function of the ice thickness  $h$ , but not the ice type. Different growth rates might be expected for new ice compared to multiyear ice due to their relative surface albedos. Such modifications will not be made in this treatment and average values of albedo and other thermodynamically important quantities will be used.

The general problem of determining the growth rates  $f(h)$  is <sup>that</sup> of solving the time dependent heat equation within the ice with appropriate boundary conditions at the top and bottom surfaces, as well as including heat source terms within the interior of the ice itself. A direct attack on the one-dimensional problem was attempted by Maykut and Untersteiner (1971). This model included the effects of a snow cover and salinity inputs. The surface boundary conditions were computed by means of evaluating the heat fluxes, which govern the growth rates. Semtner (1976) constructed versions of the Maykut and Untersteiner model which included just a few ice layers with linear temperature profiles. These yielded results reasonably close to those of Maykut and Untersteiner but considerably more economically, making it possible to evaluate the growth rates over a horizontal grid, as was done by Parkinson and Washington (1979). In their model, useful parameterizations of the long-wave and short-wave radiation terms as functions of obtainable climatic variables were given.

### 2.3.2 Determining growth rates in general

As part of a numerical climate model, growth rates are needed not only at every time step and at each grid point, but also for a variety of ice thicknesses. Thus, an efficient method is required to generate these quantities. Semtner (1976) considers a simple method of obtaining growth rates from a one layer (slab) model which assumes a temperature profile linear with depth. Hibler (1980a) also assumes a linear temperature profile with a surface heat budget calculation in order to calculate the ice growth rates. In this study, the heat budget is calculated in a way similar to that given by Hibler, except that the latent heat transfer is given in terms of the relative humidity, and an albedo dependence on ice thickness is also included. Also stability-dependent heat transfer coefficients will be used (including these can affect the ice edge position in large scale numerical models; personal communication, H. Cattle). The details of the heat budget calculations are now discussed.

Using the convention that fluxes towards the ice surface are taken positive, the surface heat balance equation may be written

$$(1-\alpha)F_s + F_L + F_{\text{sen}}^{(T_o)} + F_{\text{lat}}^{(T_o)} - F_L^{\uparrow(T_o)} + (K/h)(T_{\text{mix}} - T_o) = 0 \quad (17)$$

where  $\alpha$  is the ice surface albedo,  $F_s$  and  $F_L$  represent the incoming short-wave and long-wave radiation,  $F_{\text{sen}}^{(T_o)}$  and  $F_{\text{lat}}^{(T_o)}$  are the sensible and latent heat flux terms, and are functions of the ice surface temperature  $T_o$ . The final term included here is the heat conductivity to the surface through the ice from the bottom surface. After solving (17) numerically for  $T_o$ , the heat budget growth rate  $f_b(h)$  may be evaluated from

$$f_b(h) = -[(1-\alpha)F_s + F_L + F_{\text{sen}} + F_{\text{lat}} - F_L^{\uparrow} + F_o]/Q_I \quad (18)$$

where each of the terms within the bracket is a heat input or output to the ice slab as a whole.  $Q_I$  is the volumetric heat of fusion of ice ( $302 \text{ MJ m}^{-3}$ ). The additional term  $F_o$  represents the oceanic heat flux transmitted through the mixed layer to the ice and is included at this stage in Hibler's (1980a) thermodynamic model although in the model developed here, the term enters into the heat budget by raising the

temperature of an oceanic mixed layer which subsequently produces bottom and side melting of the floes.

The ideal situation as far as a numerical sea ice model incorporating thermodynamics is concerned, would be to have the growth rates themselves as observed input. Failing this, direct observational data for the terms in (17) and (18) would be useful. However, even this situation is somewhat unrealistic in terms of the amount and scale of the data needed to run a climate simulation. Fortunately, most of the quantities used in the thermodynamics are expressible using theoretical and empirical relationships in terms of more basic thermodynamic quantities that are available in the form of long term datasets for substantial geographic regions. These relationships we now outline.

### 2.3.3 Short-wave radiation

The short-wave radiation, denoted  $F_s$  in equation (18) originates from the sun, and is a major component of the heat balance. Although  $F_s$  is a measurable quantity, it is more convenient in a large scale numerical model to use the empirical formula of Zillman (1972),

$$Q_s = \frac{S_0 \cos^2 Z}{1.085 \cos Z + (2.7 + \cos Z)e_a 10^{-5} + 0.1} \quad (19)$$

where  $S_0$  is the solar constant taken to be  $1353 \text{ Wm}^{-2}$ .  $Z$  is the solar zenith angle and can be calculated as a function of the hour angle  $HA$ , the latitude  $\phi$  and the declination  $\delta$  by the formula

$$\cos Z = \sin \phi \sin \delta + \cos \phi \cos \delta \cos HA \quad (20)$$

$e_a$  is the atmospheric vapour pressure in Pascals.

The declination  $\delta$  can be calculated as a function of the time of year approximately as follows.

$$\delta = 23.44^\circ \cos[(172 - \text{DAY})\pi/180] \quad (21)$$

The hour angle HA can be determined by the formula

$$HA = (12 - \text{Solar time in hours})\pi/12 \quad (22)$$

It should be noted that (19) applies only if  $\cos Z \geq 0$ , for otherwise the sun is below the horizon and  $Q_s = 0$ .

In (19),  $Q_s$  is the incoming short-wave radiation for clear skies. For cloud covered skies characterized by the quantity C, the fraction of the celestial dome with cloud, the short-wave radiation  $Q_s$  is modified by multiplying by the factor  $1 - 0.6C^3$ , thus

$$F_s = (1 - 0.6C^3)Q_s \quad (23)$$

Various empirical formulae giving the change in short-wave radiation with cloudiness have been suggested (see Maykut 1983 for a review), the form used in equation (23) being due to Laevastu (1960). Monthly averaged and hourly data give different results when used to obtain cloudiness-radiation relationships. The reasons for this are not yet known. Monthly or seasonally averaged values are suitable for climate models. Factors such as increased cloudiness as is observed near an ice edge may have to be taken into account when modelling ice edge phenomena.

<sup>those</sup> For  $\Delta$  climate models, in which the equations are integrated using a time step of the order of a day, it is better to average  $F_s$  over a 24 hour period. In practice, since  $F_s$  is symmetric about solar noon, the average over a suitably chosen 12 hour period may be used.

The term  $F_s$  is multiplied by the factor  $1 - \alpha$  to account for the short-wave radiation reflected at the surface. For  $T_o < 273.16^\circ\text{K}$  an ice thickness dependent albedo is used of the form (Maykut 1983)

$$\alpha(h) = 0.44h^{0.28} + 0.08 \quad (24)$$

derived from the albedo measurements of refreezing ice in leads (Weller 1972). This formula indicates the rapid change of albedo as the ice thickness varies near zero. The albedo for the case when the surface temperature is  $273.16^{\circ}\text{K}$  (or above) is set slightly lower than given by (24). To reduce the albedo by the same proportion as does Hibler (1980a), we multiply the albedo from (24) by the factor 0.8213 when  $T_0 = 273.16^{\circ}\text{K}$ . The purpose of this is to reduce the albedo when, particularly in summer, melt pools appear on the ice surface.

### 2.3.4 Long-wave radiation

As with the case of short-wave radiation, empirical or theoretically derived formulae for long-wave radiation are most useful in determining the heat balance in a climate model.

The incoming long-wave energy at the ice surface, consisting of the black body radiation from the atmosphere, almost balances the upward radiation emitted by the ice itself. Usually there is a net loss of radiation at the ice surface. The long-wave radiation considered has wavelengths in the range  $5 - 50\mu\text{m}$  corresponding to the black body spectrum for a temperature of about  $250\text{K}$ , whereas the short-wave radiation considered in the previous section has wavelengths of the order  $0.1 - 3\mu\text{m}$  due to a black body temperature of that of the sun's surface of  $6000\text{K}$  (Fleagle and Businger 1963).

The downward long-wave radiation depends on the temperature and humidity profiles through the atmosphere, from which  $F_L$  may be calculated although in polar regions there is sparse data concerning the vertical structure of the atmosphere. A convenient derived formula for  $F_L$  was obtained by Idso and Jackson (1969) which depends on air temperature  $T_a$ , of the form

$$F_L = \sigma T_a^4 \{1 - 0.261 \exp[-7.77 \cdot 10^{-4} (T_a - 273)^2]\} \quad (25)$$

where  $\sigma$  is Stefan's constant. The term in the curly brackets is the emissivity  $\epsilon_0^*$  of the atmosphere for clear skies. For cloudy skies an effective emissivity  $\epsilon_0$  can be used where

$$\epsilon_O = \epsilon_O^* (1 + nC) \quad (26)$$

and so

$$F_L = \epsilon_O \sigma T_a^4 \quad (27)$$

C is the cloudiness, as before, and n is an empirical parameter that varies slightly depending upon the time of year.

The upward long-wave radiation  $F_L \uparrow$  depends upon the surface temperature according to

$$F_L \uparrow = \epsilon_S^* \sigma T_O^4 \quad (28)$$

where  $\epsilon_S^*$  is the surface emissivity.

### 2.3.5 Bulk latent and sensible heat

The sensible heat transfer  $F_{sen}$  occurs because of the temperature difference between the ice surface  $T_O$  and that of the atmosphere,  $T_a$ . It is parameterized by the relation,

$$F_{sen} = D_1 |U_g| (T_a - T_O) \quad (29)$$

where  $D_1$  is the bulk sensible heat transfer coefficient, and  $|U_g|$  is the geostrophic wind speed.

The coefficient  $D_1$  can be expressed in the form

$$D_1 = \rho_a c_p C_H \quad (30)$$

where  $\rho_a$  is the density of air,  $c_p$  is the specific heat of dry air, and  $C_H$  is the transfer coefficient of sensible heat, or the Stanton number. The values of  $c_p$  and  $C_H$  as used in the AIDJEX models, by Parkinson and Washington (1979), and Hibler (1980a) are

$$\begin{aligned} c_p &= 1004 \text{ J kg}^{-1} \text{ K}^{-1} \\ C_H &= 1.75 \cdot 10^{-3} \end{aligned} \quad (31)$$

From measurements by Joffre (1982), the Stanton number can vary depending on whether the surface boundary layer is stable ( $T_{\text{air}} > T_o$ ) or unstable ( $T_{\text{air}} < T_o$ ). The value given in (31) corresponds to unstable situations, whereas for stable conditions the Stanton number  $C_H$  is rather less, giving rise to less heat transfer. We thus drop  $C_H$  to  $10^{-3}$  if  $T_{\text{air}} > T_o$ , this value corresponding to the lower values of  $C_H$  as measured by Joffre in near neutral conditions.

The latent heat  $F_{\text{lat}}$  is associated with the heat released during phase changes, and has a bulk parameterization of the form (Andreas and Ackley 1982)

$$D_2 |U_g| [\bar{f} q_s(T_a) - q_s(T_o)] \quad (32)$$

where  $q_s(T)$  is the saturation specific humidity at temperature  $T$ , and  $\bar{f}$  is the relative humidity.

The terms  $q_s(T_a)$  and  $q_s(T_o)$  may be calculated using Murry's (1967) formula,

$$q_s(T_a) = \frac{\epsilon e_s}{p - (1 - \epsilon)e_s} \quad (33)$$

where  $\epsilon$  is the ratio of the molecular weight of water vapour to that of dry air, taken to be 0.622, and with  $e_s$  the saturation vapour pressure (Pascals), given by

$$e_s = 611 \times 10^a [(T - 273.16)/(T - b)] \quad (34)$$

where the empirical parameters  $a$  and  $b$  are given by  $(a, b) = (9.5, 7.66)$  when there is an ice cover and  $(a, b) = (7.3, 35.86)$  for open water. In equation (32) the bulk latent heat transfer coefficient  $D_2$  takes values

that depend on whether there is ice or not, and so whether sublimation or evaporation is taking place. Over water  $D_2 = 5.69 \times 10^3 \text{ Jm}^{-3}$  and over ice  $D_2 = 6.45 \times 10^3 \text{ Jm}^{-3}$  (Hibler 1980a).

### 2.3.6 Conductive flux

In the simple slab model considered here, a temperature profile, linear with depth is assumed, so that there is a constant conductive heat flux (upward) in the ice of magnitude

$$(K/h)(T_{\text{mix}} - T_o) \quad (35)$$

where  $K$  is the conductivity and,  $T_{\text{mix}}$  is the upper water temperature, or the temperature of the ice at its lower boundary.

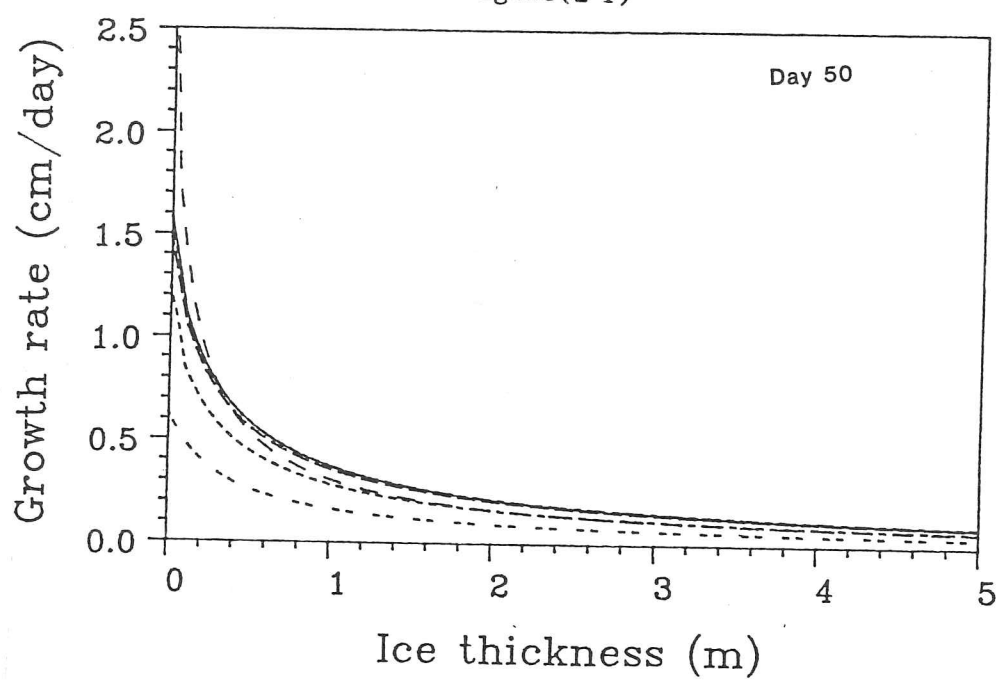
More sophisticated models include a number of points through the ice for which the temperature is solved, a linear temperature profile being assumed to exist between these points. Semtner (1976) compares the results obtained from the various models. The single slab models perform favourably compared to the sophisticated models, despite their simplicity.

### 2.3.7 Testing the heat budget

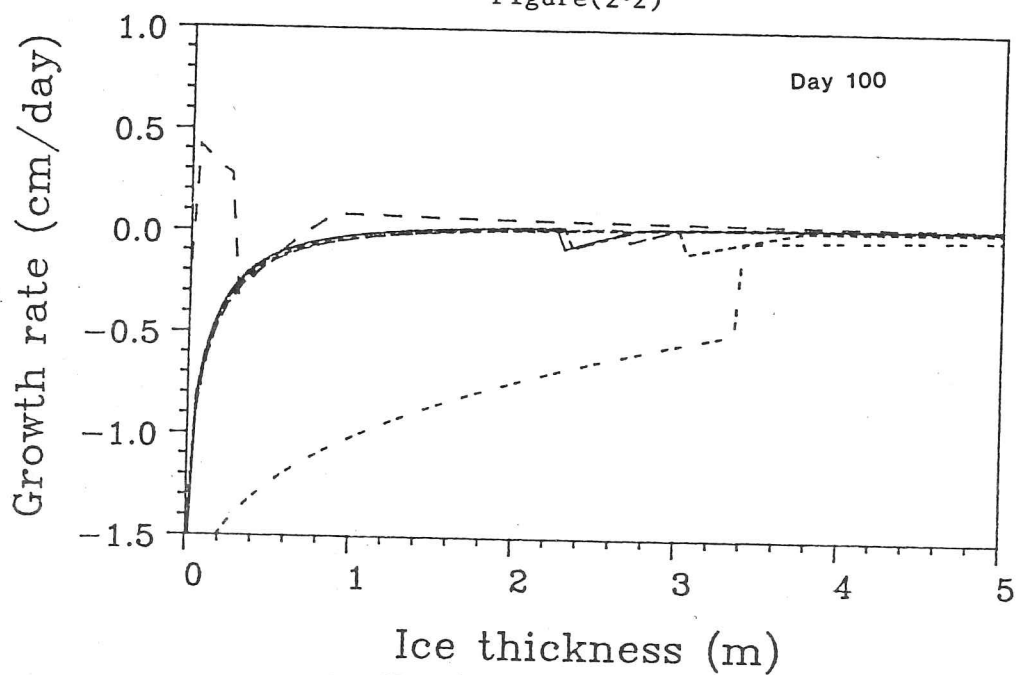
The heat budget calculation as described here was tested with various input parameters to determine their relative importance. The results are best described pictorially. The growth rates  $f_b(h)$  were obtained for values of ice thickness ranging from 0 to 5 m. The thermodynamic conditions were calculated with short-wave radiation corresponding to different times of the year (Julian days 50, 100 and 150), together with various humidities, cloudiness factors, and air temperatures.

Figures (2.1), (2.2) and (2.3) show the growth rates plotted against the ice thickness obtained by varying the values of each of the thermodynamic inputs in turn from a standard set. The growth rates for zero ice thickness (open water) in the diagrams correspond to water at freezing point. If the water temperature is above freezing the growth rate (heat absorption) would be different. The standard set plotted with a solid line were

Figure(2.1)



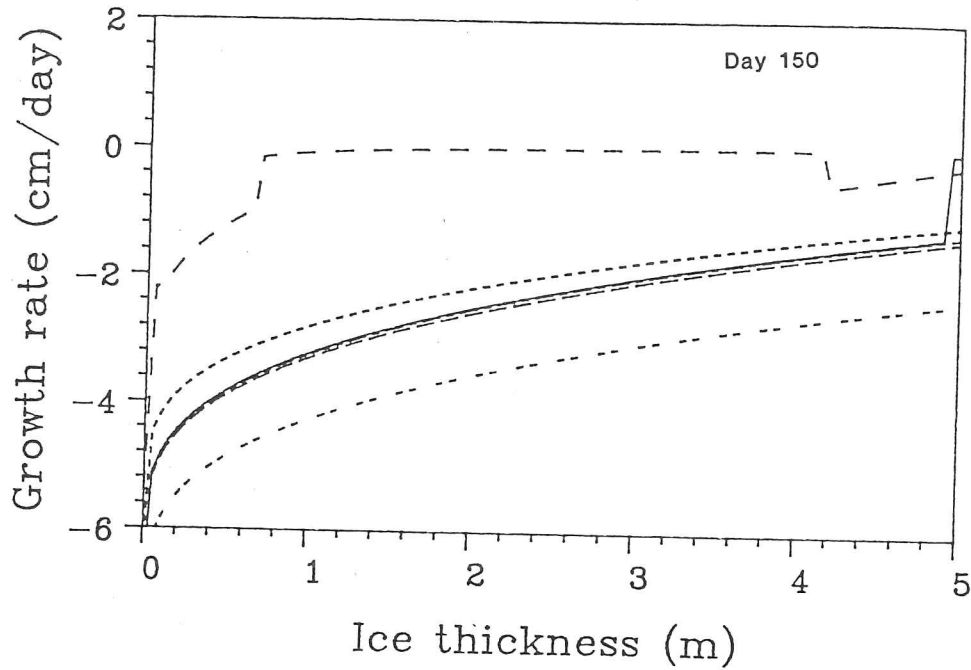
Figure(2.2)



Testing the sensitivity of the growth rate calculations to variations in the input parameters.







See the next page for the key to the diagrams.

Figure(2.3)



Testing the sensitivity of the growth rate calculations to variations in the input parameters.

The linestyles indicate the growth rates as calculated by changing each of the following input parameters.

	Standard
	Cloudiness
	Humidity
	Wind speed
	Temperature
	Pressure

calculated for an atmospheric pressure of 970mbar, an air temperature of  $270^{\circ}\text{K}$ , a wind speed of  $1\text{ms}^{-1}$ , a relative humidity of 50% and a cloudiness factor of 50%. Tests were done increasing the pressure to 1030mbar, increasing the air temperature to  $275^{\circ}\text{K}$ , increasing the wind speed to  $5\text{ms}^{-1}$  and changing the humidity and cloudiness to 70%.

The wind speed and temperature changes were found to have the greatest effect on the growth rates, especially for thin ice. The humidity and cloudiness changes which represent the range of observed monthly average values had only a small effect on the growth rates. The pressure change had almost no effect at all. Thus in calculating the thermodynamic heat budget for the growth rates, the wind speed and air temperatures should be specified at each grid point and time step, whereas for the cloudiness, humidities and pressures, single monthly average values would be sufficient.

#### 2.4 Ice thickness distribution theory

An area of sea ice has, in a local region, many thicknesses of ice as well as areas of open water. It would clearly be inadequate to model such an area by considering it to be composed of one thickness, say the mean thickness. For example, an area consisting of 50% open water and 50% 2m ice would not be able to resist deformation, whereas an area consisting of 100% 1m ice would be comparatively strong. The first remedy would be to parameterize the area by giving the fraction of open water together with the mean thickness of the ice present. Although a considerable improvement, there is still difficulty in choosing the appropriate thermodynamic growth rates for such a representation. In growing conditions, thin ice grows an order of magnitude faster than thick ice so that it is not possible to obtain the change to the mean thickness caused by such growth. Calculations by Thorndike *et al* (1975) using Maykut and Untersteiner's (1971) ice growth rate model gave a growth of 1.95 cm/day for 0.5m ice but for 3m ice this growth rate is down to 0.27cm/day (the conditions used in the calculation were for January 1 in the Central Arctic).

A description of sea ice in terms of the thickness distribution stems from observations that ice is not uniform and a desire to indicate the relative amounts of the various kinds of ice present in a region. Wittmann and Schule (1966) produced cumulative ice thickness diagrams for various regions in the Arctic. They concluded from the observations that between 13 and 18% of the ice area consisted of ridges of thickness considerably greater than the average ice thickness. Using submarine data Williams *et al* (1975) were able to estimate percentages of various categories of ice cover along transects in the Arctic. Submarine data has been obtained on subsequent cruises (Wadhams 1980a) to provide detailed thickness distribution graphs. These kinds of data prompted the development of a theory to explain the time evolution of the thickness categories due to thermodynamic and dynamic causes. Thorndike *et al* (1975) describe such a theory. Here we describe the development of the theory in a way that leads to its use in a numerical sea ice model.

The thickness distribution  $g(h)$  is defined such that the quantity

$$\int_{h_1}^{h_2} g(h) dh \quad (36)$$

is the fraction of the area of ice of thickness in the range  $(h_1, h_2)$ . From this definition  $g(h)$  acts as a probability density function for thickness. In particular integrating over the entire range of thicknesses gives a probability of one, thus

$$\int_0^{\infty} g(h) dh = 1 \quad (37)$$

The thickness distribution may vary from place to place and may evolve in time so that

$$g = g(h, x, t) \quad (38)$$

and is defined at a point  $\underline{x}$  by measuring  $g(h)$  within some region  $R$  that includes  $\underline{x}$  and taking the limit as  $R \rightarrow 0$ .

Thorndike et al (1975) derive the following equation to represent the evolution of  $g(h)$ .

$$\frac{\partial g}{\partial t} = -\nabla \cdot (\underline{u}g) - \frac{\partial (fg)}{\partial h} + \psi \quad (39)$$

The three terms on the right represent, respectively, the flux divergence of  $g$ , the changes in  $g$  due to thermodynamic processes and the changes in  $g$  due to mechanical redistribution. Hibler (1980a) introduced a fourth term on the right hand side of (39) to account for lateral melting of floes. This term  $\bar{F}_L$  is such that

$$\int_0^\infty \bar{F}_L dh = 0 \quad (40)$$

because lateral melting conserves area in that open water is created to compensate for the loss of ice. It is assumed that the amount of ice in all the thickness categories are reduced by the same percentage with the amount depending on the quantity of heat available. This assumes that the lateral melt rate is independent of ice thickness, so that the volume loss is linearly dependent on the ice thickness. This assumption is consistent with the lateral melting analysis outlined in the next chapter.

The quantity  $\underline{u}$  in the first term  $-\nabla \cdot (\underline{u}g)$  is the two-dimensional ice velocity so that

$$-\nabla \cdot (\underline{u}g) = -g\nabla \cdot \underline{u} - \underline{u} \cdot \nabla g \quad (41)$$

represents influx of ice due to convergence and changes due to advection.

The second term

$$-\frac{\partial (fg)}{\partial h} \quad (42)$$

includes  $f$  which is a function of  $h$  and is the ice growth rate  $dh/dt$ . This term is thus analogous to the flux divergence term with  $f$  corresponding to the velocity  $u$ , except that it represents the transfer of ice between vertical thickness levels rather than horizontal ones.

The final term  $\Psi$  accounts for the changes in  $g$  that do not change the \* ice volume within a region but merely alter the relative amounts in each category. Thus, this term parameterizes redistributive processes such as ridging and rafting.  $\Psi$  depends on  $g$  and  $u$  in a rather complicated way and so is discussed in more detail.  $\Psi$  is a function of  $h$  because it describes the change in  $g(h)$  for each thickness category  $(h, h+dh)$ .

We can write down two general properties of the redistribution function. Firstly, by integrating equation (39) and noting (37) we obtain

$$\int_0^{\infty} \Psi dh = \nabla \cdot u \quad (43)$$

The volume of ice is expressed as

$$\int_0^{\infty} h g(h) dh \quad (44)$$

so that to assume that no ice volume is created during ridging gives

$$\int_0^{\infty} h \Psi dh = 0 \quad (45)$$

\* Note that here the symbols  $\psi$  and  $\Psi$  are equivalent.

Now to derive a more explicit form for  $\Psi$  showing its dependence on the ice velocity we consider first the simplest cases of pure divergence and pure convergence.

Horizontal variations in  $u$  are expressed by the (symmetric) strain rate tensor

$$\dot{\epsilon}_{ij} = \frac{1}{2} \left( \frac{\partial u_i}{\partial x_j} + \frac{\partial u_j}{\partial x_i} \right) \quad (46)$$

It is often found more convenient to express the strain rate in terms of the sum and difference of the eigenvalues of  $\dot{\epsilon}_{ij}$ . Thus we define the two strain rate invariants  $\dot{\epsilon}_I$  and  $\dot{\epsilon}_{II}$  by

$$\begin{aligned} \dot{\epsilon}_I &= \dot{\epsilon}_{11} + \dot{\epsilon}_{22} \\ \dot{\epsilon}_{II} &= 2 \sqrt{-\det(\dot{\epsilon}_{ij} - \frac{1}{2} \dot{\epsilon}_{kk} \delta_{ij})} \\ &= \sqrt{(\dot{\epsilon}_{22} - \dot{\epsilon}_{11})^2 + 4\dot{\epsilon}_{12}\dot{\epsilon}_{21}} \end{aligned} \quad (47)$$

$\dot{\epsilon}_I$  is the divergence of the velocity field,  $\nabla \cdot u$ , and  $\dot{\epsilon}_{II}$  is a measure of the rate of shear of the field. Sometimes another set of strain rate invariants proves useful. These are denoted by  $|\dot{\epsilon}|$  and  $\theta$ .

$$|\dot{\epsilon}| = \sqrt{\dot{\epsilon}_I^2 + \dot{\epsilon}_{II}^2} \quad (48)$$

gives the amount of deformation and  $\theta = \tan^{-1}(\dot{\epsilon}_{II}/\dot{\epsilon}_I)$  depends on the relative amounts of shear and divergence. If the strain rate is specified as a point in the  $(\dot{\epsilon}_I, \dot{\epsilon}_{II})$  plane, then  $|\dot{\epsilon}|$  and  $\theta$  are its polar coordinates.

In terms of the velocity gradients,

$$\begin{aligned} \dot{\epsilon}_I &= \frac{\partial u}{\partial x} + \frac{\partial v}{\partial y} \\ \dot{\epsilon}_{II} &= \sqrt{\left( \frac{\partial u}{\partial x} - \frac{\partial v}{\partial y} \right)^2 + \left( \frac{\partial u}{\partial y} + \frac{\partial v}{\partial x} \right)^2} \end{aligned} \quad (49)$$

During pure divergence ( $|\dot{\epsilon}| = \nabla \cdot \mathbf{u}$ ), open water is created so that the thickness distribution changes by increasing the value of  $g(h)$  at  $h = 0$  only. This means that in these circumstances  $\Psi$  is proportional to a delta function  $\delta(h)$  and from (43) we see that

$$\Psi = \delta(h) |\dot{\epsilon}| \quad (50)$$

During pure convergence ( $|\dot{\epsilon}| = -\nabla \cdot \mathbf{u}$ ), ice redistribution will have to take place due to the flux of ice into the region considered. Then the redistribution function  $\Psi$  is written

$$\Psi = w_r(h, g) |\dot{\epsilon}| \quad (51)$$

where  $w_r(h, g)$ , called the ridging mode, describes the way each thickness level is changed during ice redistribution. For ice of a particular thickness, area will be lost as it ridges to thicker ice, but there will also be a gain in area due to the thinner ice ridging to that thickness. The function  $w_r(h, g)$  gives the net rate of change of area of thickness  $h$  per unit strain rate  $\nabla \cdot \mathbf{u}$ .

The way the thickness categories change described by  $w_r(h, g)$  depends on the thickness distribution present so that the redistribution function is a functional dependent on  $g(h)$ .

The dependence of  $w_r$  upon  $g(h)$  is still an open question but here we describe the form assumed by Thorndike et al (1975). Firstly, we note that with (51), conditions (43) and (45) become

$$\int_0^{\infty} w_r(h, g) dh = -1 \quad (52)$$

and

$$\int_0^{\infty} h w_r(h, g) dh = 0 \quad (53)$$

Then  $w_r(h, g)$  may be split into two components

$$w_r(h, g) = \frac{-a(h) + z(h)}{\int_0^{\infty} \{a(h) - z(h)\} dh} \quad (54)$$

where  $a(h)$  is the distribution of ice ridged, and  $z(h)$  is the distribution thus formed. The denominator in (54) ensures that  $w_r(h, g)$  is normalized to -1 as in (52).  $a(h)$  is a probability density function and so is normalized to 1, thus

$$\int_0^{\infty} a(h) dh = 1 \quad (55)$$

Thus it must be remembered that  $a(h)$  is normalized with respect only to the ice involved in ridging so that  $a(h)dh$  does not give the actual amount of area lost in ridging, that quantity being given by

$$\frac{a(h)}{\int_0^{\infty} \{a(h) - z(h)\} dh} \quad (56)$$

Thorndike et al (1975) hypothesized that  $a(h)$  could be related to  $g(h)$  by a relation of the form

$$a(h) = b(h)g(h) \quad (57)$$

where  $b(h)$  is some weighting factor. Noting that thin ice tends to deform more easily than thick ice, Thorndike et al (1975) chose

$$b(h) = \max\left\{0, \frac{2}{G^*} \left(1 - \frac{G(h)}{G^*}\right)\right\} \quad (58)$$

This assumes that only a fraction  $G^*$  of the thinnest ice is ridged with a bias toward the thinnest ice within that range. A reasonable choice for  $G^*$  is 0.15.  $G(h)$  is the cumulative thickness distribution so that

$$G(h) = \int_0^h g(h') dh' \quad (59)$$

The factor  $2/G^*$  in (58) means that

$$\int_0^\infty b(h)g(h) dh = 1 \quad (60)$$

as required by (55).

The function  $z(h)$  can be deduced from  $a(h)$  from the way ridges are assumed to be formed. If ridges are produced as described in section (4.2), then analytic expressions for  $z(h)$  can be obtained for some distributions  $a(h)$ . In section (4.3) regarding ice strength,  $z(h)$  is calculated when  $a(h)$  is a delta function.

Having established, with equations (50) and (51), the redistribution function for pure divergence and pure convergence, the next step is to postulate that for an arbitrary strain rate  $\dot{\epsilon}$ , which is composed of a divergence  $\dot{\epsilon}_d$ , and a shear  $\dot{\epsilon}_s$ , the redistribution function is a linear combination of the two forms. Thus

$$\psi = |\dot{\epsilon}| \{ \alpha_o(\theta) \delta(h) + \alpha_r(\theta) w_r \} \quad (61)$$

Thus the coefficients  $\alpha_o(\theta)$  and  $\alpha_r(\theta)$  of the ridging modes  $|\dot{\epsilon}|\delta(h)$  and  $|\dot{\epsilon}|w_r$ , depend only on  $\theta$ . Substituting (61) into (43) and noting (52) we obtain

$$\alpha_o(\theta) - \alpha_r(\theta) = \cos\theta \quad (62)$$

so that  $\psi$  is known to within one function.

For pure divergence  $\theta = 0$ , so from (61) we immediately see that

$$\alpha_o(0) = 1 \quad \alpha_r(0) = 0 \quad (63)$$

In the case of pure convergence,  $\theta = \pi$  so similarly,

$$\alpha_o(\pi) = 0 \quad \alpha_r(\pi) = 1 \quad (64)$$

Rothrock (1975) shows how a knowledge of the amount of ridging, specified by the coefficient  $\alpha_r(\theta)$ , in an arbitrary deformation can be related to the yield function and yield curve of plasticity theory. He equates the rate of working  $\sigma_{ij}\dot{\epsilon}_{ij}$  in deforming the material to rates of production of potential energy and the loss of energy in frictional processes. The energy equation he derives expressed in terms of the stress and strain rate invariants is

$$\sigma_1\dot{\epsilon}_1 + \sigma_{II}\dot{\epsilon}_{II} = |\dot{\epsilon}|\alpha_r(\theta)p^* \quad (65)$$

where  $p^*$  is the strength of the material in pure compression. In a later section an explicit expression for  $\alpha_r(\theta)$  is derived from physical arguments so that  $\psi$  may be determined completely.

In subsequent chapters the ideas introduced with thickness distribution theory are used to calculate  $p^*$  for an area of pack ice containing many different thicknesses of ice.

### 3. ICE FLOES

#### 3.1 Spatial distribution of floes

Some areas of sea ice, such as marginal ice zones, contain distributions of floes of various shapes and sizes. This situation is modelled here by considering an idealized floe field in which variations in floe shape are neglected - all the floes being considered circular.

A floe field, within a region  $R$ , is described by the quantities  $A$ ,  $n$  and  $r$ . The compactness,  $A$ , is the fraction of the sea surface covered by ice, and  $n$  is the number of floes per unit area. These may be related to a third quantity  $r$ , the average floe radius in  $R$ , according to

$$A = n\pi r^2 \quad (1)$$

Later we split  $n$  into a distribution  $n(h)$ , of floe number densities for each ice thickness category, but for the moment only the average floe number density need be considered. Within  $R$ , the discs or floes can be considered randomly distributed in the sense that there is no preferred position for any given floe, but with the constraint that no two floe centres can be closer than  $2r$  apart.

The information provided by a knowledge of the spatial distribution of a set of floes together with their velocities at some moment is sufficient to determine the instantaneous collision rate. In fact it is necessary only to consider the floes that at some time are just about to touch. We can regard the floe field as homogeneous so that we need consider only one typical floe which we subsequently refer to as the reference floe. We take the centre of the reference floe as the origin of the coordinate system. In particular, polar coordinates  $(\rho, \psi)$  may be used so that the reference floe edge satisfies  $\rho = r$ . Also, it is found convenient to express floe

velocities relative to this origin. The floe collision problem is thus reduced to determining the distribution of floes that at some moment are almost touching the reference floe. The concept of closeness of floes can be made more precise by defining a floe to be close to the reference floe if its centre lies at a distance in the range  $2r$  to  $2(r+\delta\rho)$  from the origin, where  $\delta\rho \ll r$ .

For a region sparsely populated with floes, the expected number of floe centres in the annulus  $\rho = [2r, 2(r+\delta\rho)]$  is the product of its area,  $\delta S$ , and the floe number density and is thus  $n\delta S = 8\pi nr\delta\rho$ . This value is accurate only in the limit  $A \rightarrow 0$  since we have not restricted the possibility of floes overlapping.

If non-overlapping discs are scattered randomly then each one has about 6 'neighbours', and of course, for close packing each disc has exactly 6 neighbours. From this we can find an expression for the expected number of floe centres in the annulus  $\delta S$  that is accurate not just for low floe densities.

The problem becomes tractable if one assumes that near the reference floe there are 6 floe centres uniformly distributed in the annulus defined by the range

$$\left[2r, \frac{2r}{\alpha\sqrt{A}}(1-\beta A^2)\right], \quad A = n\pi r^2 \quad (2)$$

$\alpha$  and  $\beta$  are as yet undetermined scaling constants. The constant  $\alpha$  scales the upper limit simply because as the floe number density decreases, the floes get further apart. The constant  $\beta$  accounts for the finite size of the floes further out restricting the distance that the neighbouring floe can drift.

The expected number of floes with centres in the annulus  $\rho = [2r, 2(r+\delta\rho)]$  is

$$\frac{6(8\pi r\delta\rho)}{\pi\left\{\frac{4r^2}{\alpha^2 A}(1-\beta A^2)^2 - 4r^2\right\}} \quad (3)$$

From the low density approximation, this expression must tend to  $8\pi nr\delta\rho$  as  $A \rightarrow 0$  which implies that  $\alpha^2 = 2/3$ . For close packing we let the upper limit in (2) tend to  $2r$  as  $A \rightarrow 1$  which gives  $\beta = 1-\alpha$ .

The expression (3) becomes

$$Ln\delta S \quad (4)$$

where

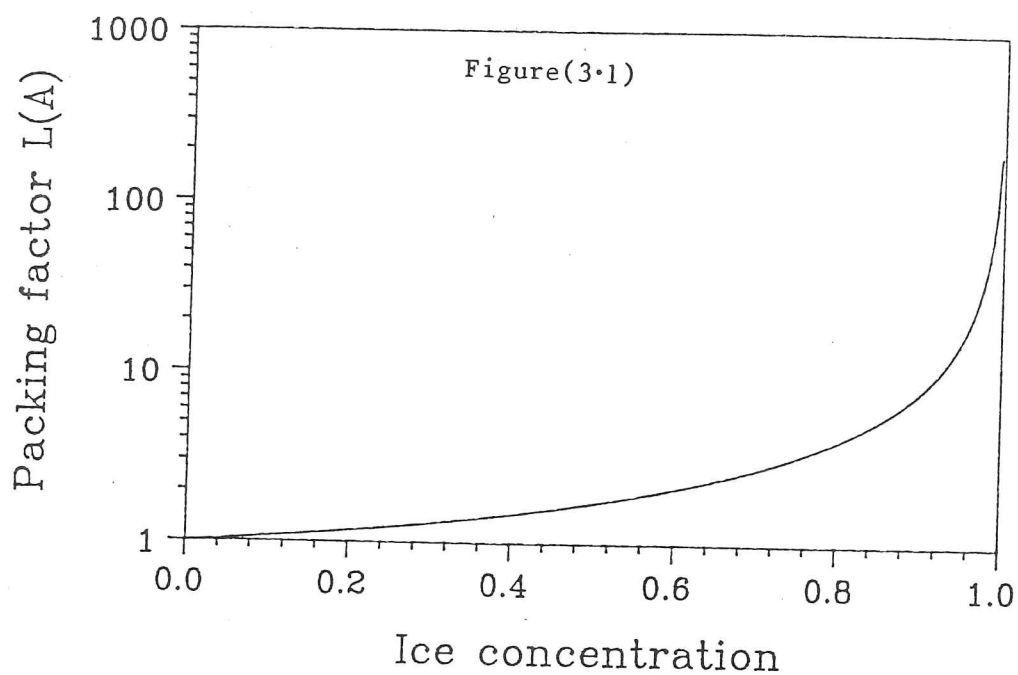
$$L(A) = \frac{1}{[1-(1-\alpha)A^2]^2 - \alpha^2 A} \quad (5)$$

and  $\delta S$  is the area of the annulus  $\rho = [2r, 2(r+\delta\rho)]$ .

This means that close to a given floe the local floe number density is  $L(A)$  times as great as the overall floe number density  $n$ . The function  $L(A)$  increases rapidly near  $A = 1$  as is indicated in figure (3.1).

The previous calculation for discs may be done analogously for line segments in one dimension. In the one-dimensional case however, the situation is sufficiently simple for an exact analytical solution for the expected number of 'close' floes to be obtained as a function of the compactness. It would be useful to compare the exact solution with that obtained by a method for one dimension that is analogous to the approximate method employed in the two-dimensional case.

Suppose that along an infinite line, there are distributed  $n$  line segments (floe) per unit length, and that each floe is of length  $2r$ . The compactness of the floes is then  $A = 2nr$  and the expected gap between the floes is



The rapid increase of  $L(A)$  as the compactness reaches unity indicates the increased number of collisions likely to occur between floes.

$$\frac{1}{n} - 2r = \frac{1-A}{n} \quad (6)$$

The probability density function  $p(x)$  for the width of the gap between floes is thus the Poisson distribution for points on a line with density  $n/(1-A)$  per unit length. Hence

$$p(x) = \frac{n}{1-A} \exp\left[\frac{-nx}{1-A}\right] \quad (7)$$

The probability that a gap is less than  $2\delta\rho$ , or that two floe centres are closer than  $2(r+\delta\rho)$  apart is

$$\int_0^{2\delta\rho} p(x) dx = \frac{2n\delta\rho}{1-A}, \quad \delta\rho \ll \frac{1-A}{2n} \quad (8)$$

Now to obtain the value of  $p(x)$  at  $x = 2r$  by the method employed for the case of discs, assume that  $p(x)$  for the centre of a floe neighbouring the reference floe is uniformly distributed in the range

$$[2r, \frac{\alpha r}{A}(1-\beta A)] \quad (9)$$

As before,  $\alpha$  and  $\beta$  are scaling constants to be determined by considering limiting compactnesses.

Thus given the range in which the nearest floe centre can lie, the expected number of floe centres in the range  $[2r, 2(r+\delta\rho)]$  is

$$\frac{4\delta\rho}{\frac{\alpha r}{A}(1-\beta A) - 2r} \quad (10)$$

$\alpha$  and  $\beta$  can then be determined by considering the limiting cases for which  $A \rightarrow 0$  and  $A \rightarrow 1$ . For  $A \rightarrow 0$  the expected number of floe centres within  $[2r, 2(r+\delta\rho)]$  is simply  $2n\delta\rho$ . For (10) to give this limit,  $\alpha = 4$ . In the case  $A \rightarrow 1$  the upper limit  $(\alpha r/A)(1-\beta A)$  should tend to  $2r$ , hence  $\beta = 1/2$ . Hence the expected number of floes within a distance  $2\delta\rho$  from the reference floe is  $2n\delta\rho/(1-A)$ .

We see that in one dimension, the exact and approximate solutions are in fact identical. This suggests that the approximate solution to the two-dimensional problem may be usable. The equality of the implied collision rates for the two methods is thus assured.

### 3.2 Floe collisions

We are not concerned here with the 'random' collisions caused by the small scale variation in the floe velocity field but rather the collisions due to the differential mean drift of neighbouring floes. The energy losses associated with 'random' bumping of floes may be calculated in a way similar to the analysis given below for the 'strain rate' collisions. This requires additional information regarding the magnitude of the random components of the floe velocity field.

The problem then is to determine for a floe in a velocity field with strain rate specified by  $\dot{\epsilon}$ , and  $\dot{\epsilon}_{\parallel}$ , the resulting rate at which collisions occur with other floes. We have to determine the area within which a floe centre has to be for it to be involved in a collision in some small time  $\delta t$ .

Suppose that a two-dimensional ice velocity field  $u(x)$  varies on a scale much larger than the floe radius  $r$ . If the reference floe with centre at  $x_0$  has velocity  $u(x_0)$  then the velocity field close by at  $x$  is

$$u(x) = u(x_0) + (x-x_0) \cdot \nabla u(x_0) \quad (11)$$

neglecting terms small compared to  $(x-x_0) \cdot \nabla u$ . With the centre of the reference floe as the origin,  $x_0 = 0$ , the relative velocity of a floe close to the origin is thus given by

$$u(x) = x \cdot \nabla u(0) \quad (12)$$

Thus, close to the reference floe we consider only linear variations in the velocity field. Expressing the relative velocity of a floe in polar coordinates  $(\rho, \psi)$ , and using equation (12), the radial velocity  $u_\rho$  is given by

$$\begin{aligned} u_\rho &= \frac{u \cdot x}{|x|} \\ &= \frac{1}{\rho} \left[ \left( \frac{\partial u}{\partial x} x + \frac{\partial u}{\partial y} y \right) x + \left( \frac{\partial v}{\partial x} x + \frac{\partial v}{\partial y} y \right) y \right] \quad * \\ &= \rho \left[ \frac{1}{2} \left\{ \frac{\partial u}{\partial x} + \frac{\partial v}{\partial y} \right\} + \frac{1}{2} \left\{ \frac{\partial u}{\partial x} - \frac{\partial v}{\partial y} \right\} \cos 2\psi + \frac{1}{2} \left\{ \frac{\partial u}{\partial y} + \frac{\partial v}{\partial x} \right\} \sin 2\psi \right] \quad (13) \end{aligned}$$

since  $x = \rho \cos \psi$  and  $y = \rho \sin \psi$ . Hence if we define

$$\dot{\epsilon}_{\parallel} \sin \phi = \frac{\partial u}{\partial x} - \frac{\partial v}{\partial y} \quad (14)$$

and

$$\dot{\epsilon}_{\parallel} \cos \phi = \frac{\partial u}{\partial y} + \frac{\partial v}{\partial x} \quad (15)$$

then we have

$$u_\rho = \frac{1}{2} \rho \{ \dot{\epsilon}_{\parallel} + \dot{\epsilon}_{\parallel} \sin(\phi + 2\psi) \} \quad (16)$$

The transverse velocity  $u_\psi$  can be similarly found to be

$$u_\psi = \frac{1}{2} \rho \{ \omega + \dot{\epsilon}_{\parallel} \cos(\phi + 2\psi) \} \quad (17)$$

where

\*

Note that here the symbols  $\psi$  and  $\Psi$  are equivalent.

$$\omega = \frac{\partial v}{\partial x} - \frac{\partial u}{\partial y} \quad (18)$$

is the magnitude of the vorticity of the floe velocity field. However only the radial velocity component is of interest for the purpose of calculating the floe collision rate. For another floe to collide with the reference floe at an angle in the range  $(\psi, \psi + \delta\psi)$ , the radial velocity  $u_\rho$  has to be negative for that value of  $\psi$ , and its centre has to be within the shaded parallelogram shown in figure (3.2).

The total area within which a floe centre has to be to collide in a time  $\delta t$  is

$$\delta A = - \int_0^{2\pi} \min\{0, u_\rho(\psi, \rho=2r)\} 2r \, d\psi \, \delta t \quad (19)$$

$$= -2r^2 |\dot{\epsilon}| \delta t \begin{cases} 0 & 0 < \theta < \frac{1}{4}\pi \\ 4 \int_{\psi_0}^{\frac{3}{4}\pi} (\cos\theta + \sin\theta \sin 2\psi') \, d\psi' & \frac{1}{4}\pi < \theta < \frac{3}{4}\pi \\ \int_0^{2\pi} (\cos\theta + \sin\theta \sin 2\psi') \, d\psi' & \frac{3}{4}\pi < \theta < \pi \end{cases} \quad (20)$$

where  $\psi$  has been replaced by  $\psi' = \psi + \phi/2$  and the angle  $\psi_0$  is such that

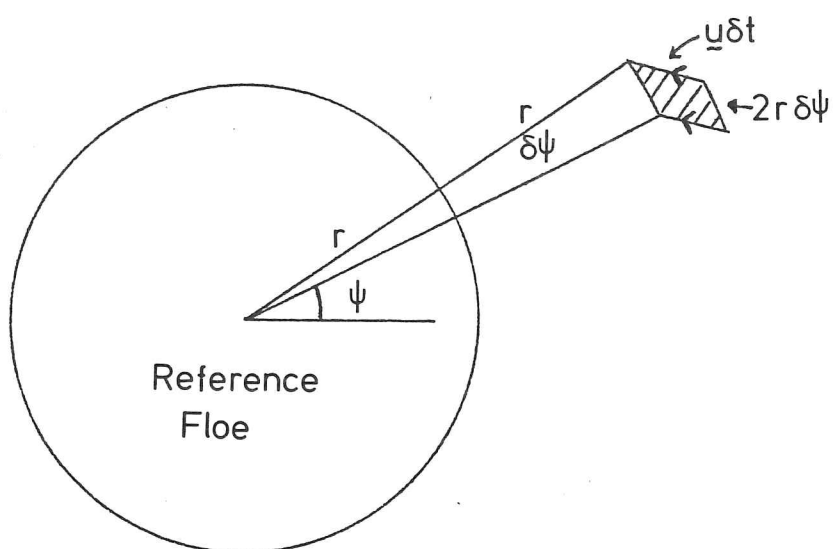
$$\sin 2\psi_0 = -\cot \theta \quad \frac{1}{4}\pi < \psi_0 < \frac{3}{4}\pi \quad (21)$$

Then we have

$$\delta A = 4\pi r^2 |\dot{\epsilon}| \alpha(\theta) \delta t \quad (22)$$

where  $\alpha(\theta) =$

Figure(3.2)



The shaded parallelogram contains the centres of floes about to collide with the reference floe in a time  $\delta t$ .

$$\left\{ \begin{array}{ll} 0 & 0 < \theta < \frac{1}{4}\pi \\ -\frac{1}{\pi} \cos^{-1}(\cot\theta) \cos\theta + \frac{1}{\pi} \sqrt{\sin^2\theta - \cos^2\theta} & \frac{1}{4}\pi < \theta < \frac{3}{4}\pi \\ -\cos\theta & \frac{3}{4}\pi < \theta < \pi \end{array} \right. \quad (23)$$

The inverse cosine function takes its principal value. The function  $\alpha(\theta)$  increases monotonically from 0 to 1 as  $\theta$  varies from 0 to  $\pi$  and is shown in figure (3.3).

The number of collisions in time  $\delta t$  is the product of  $\delta A = 4\pi r^2 |\dot{\epsilon}| \alpha(\theta) \delta t$  and the local floe number density,  $L(A)n$ , thus the collision rate is

$$4\pi r^2 n L |\dot{\epsilon}| \alpha(\theta) \quad (24)$$

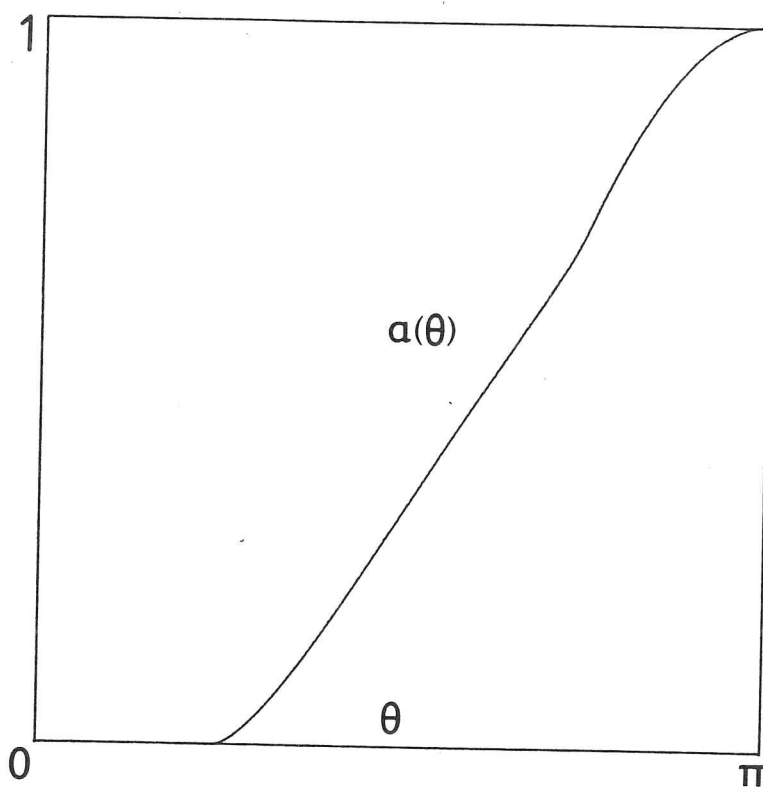
For a unit area containing  $n$  floes, the collision rate is thus

$$\begin{aligned} 2\pi r^2 n^2 L |\dot{\epsilon}| \alpha(\theta) &= \frac{2LA^2 |\dot{\epsilon}| \alpha(\theta)}{\pi r^2} \\ &= 2LA |\dot{\epsilon}| \alpha(\theta) n \end{aligned} \quad (25)$$

where a factor of 2 in (24) is lost because each collision involves two floes.

Results (24) and (25) are, in principle, experimentally verifiable. Also they are a convenient starting point for describing several aspects of floe behaviour, and will be used in this and the next chapter to derive further theoretical results. The MIZEX-84 experimental programme includes the deployment of 3-axis accelerometer arrays on floes to measure collisions. The results will be supplemented by other measurements such as the floe drift rate and floe size.

Figure(3.3)



The function  $\alpha(\theta)$  giving the floe collision rate for an arbitrary deformation type relative to that for pure convergence.

### 3.3 Floe size change

#### 3.3.1 Introduction

The average floe radius  $r$  may change thermodynamically or dynamically. The floe radius decreases during periods of lateral melting. Floes also change size due to collisions. A number of outcomes to collisions have been observed. The floes may bounce apart elastically, coalesce, or break up. However, when considering floe sizes in the context of a climate model, the collisions considered are those due to the differential mean drift of the floes. These collisions would be expected to give rise to the coalescing of floes with a ridge produced along the region of contact. Collisions are thus considered to increase the average floe size.

For thin floes such as found in the Bering Sea, floe collisions often result in rafting, the overriding of one floe by another. This has the effect of producing a single larger floe.

With these assumptions, the floe number density  $n$  would satisfy a two-dimensional continuity equation of the form

$$\frac{Dn}{Dt} + n\nabla \cdot \mathbf{u} = S_n \quad (26)$$

where  $S_n$  is a source term for floe number density, due to collisions. From the mean velocity field within which the floes move, the collision rate per unit area may be expressed, from the previous section as,

$$\frac{2LA^2|\dot{\epsilon}|\alpha(\theta)}{\pi r^2} = 2LAN|\dot{\epsilon}|\alpha(\theta) \quad (27)$$

The assumption that the floes stay together when they collide implies that  $n$ , the floe number density, decreases by 1 for each collision. Hence

$$S_n = -2LA|\dot{\epsilon}|\alpha(\theta)n \quad (28)$$

The sink term  $S_n$  giving the rate of decrease of floes is thus proportional to the number of floes. So, neglecting other methods of floe size change, an exponential decay in the number of floes is expected with the decay constant depending on the ice concentration and the strain rate of the velocity field. This is not strictly true because changes in compactness would be expected to accompany changes in floe number density. Equation (26) may then be written

$$\frac{\partial n}{\partial t} + \nabla \cdot (\underline{u}n) = -2LA|\dot{\epsilon}|\alpha(\theta)n \quad (29)$$

For a full sea ice model in which the compactness  $A$  undergoes time evolution, the average floe size may be calculated from  $A = \pi n r^2$  using the current value of  $A$ .

### 3.3.2 Floe break up

Often, in a particular region, there is a characteristic floe size, suggesting that there is some mechanism, determined by the local physical conditions, responsible for their formation. However, there is a very large range of observed floe sizes (from tens of kilometres down to just a few metres) so that it is unlikely that a single mechanism is at work. We must therefore look for several possible mechanisms that could cause a uniform and infinite ice sheet to crack into floes or indeed for a large floe to crack into smaller units. We must consider each mechanism in turn and determine the physical conditions required to cause floe cracking together with the size of the floe thus produced. The characteristic floe size will be the least value of the floe size predicted by the various mechanisms for which local physical conditions suggest floe cracking to occur.

For the very large floes observed, there is some doubt about whether they are actually a single entity. Observations by Ackley and Hibler (1974) taken from two surface stations on what appeared, from aerial photographs, to be continuous ice, experienced a relative drift.

There is some difficulty in explaining the size of the largest floes produced. It is possible that their scale is determined by variations in the forcing, of which a major component is the wind. The situation is complicated by the fact that no ice field exists that is formed of perfectly uniform ice of constant strength. Suppose some mechanism suggests the formation of a floe of the order of a hundred kilometres in diameter. Such a result must be treated with caution since over these distances the physical properties are likely to vary considerably. Consider the following simple example. A semi-infinite ice sheet of thickness  $h$  is subjected to an off-ice wind giving rise to a surface stress  $\tau$ . The internal stress at  $x = L$  would then be  $\tau L$ . Equating this with  $\sigma_{\max} h$  where  $\sigma_{\max}$  is the tensile strength of sea ice gives a breaking length of

$$L = \frac{\sigma_{\max} h}{\tau} \quad (30)$$

$\text{Nm}^{-2}$

For  $h = 1\text{m}$ ,  $\sigma_{\max} = 10^5$  and  $\tau = 0.5\text{Nm}^{-1}$ , this gives  $L = 200\text{Km}$ . If  $\sigma_{\max}$  and  $h$  were not constant along the floe then depending on the amount of variation, it is possible that the tension  $\tau x/h(x)$  exceeds  $\sigma_{\max}(x)$  for some  $x$  much less than  $L$  giving rise to floes of the order of a few kilometres.

Because of the large variation in the physical properties of ice over large distances it is not feasible to predict the sizes of extremely large ice features other than, as we have done here, to estimate the orders of magnitude involved. A more complete analysis would have to take into account the stochastic nature of the ice properties. This would require more comprehensive datasets than exist at present concerning the variation in sea ice properties.

Sodhi (1977) investigates the arched fracture lines that are visible from satellite imagery of the ice which is forced through the Bering Strait and in the Amundsen Gulf. He explains these using the theory of granular media forced through a narrowing passage. In this way large floes of the order of 20-60 km may be produced.

We now turn our attention to mechanical processes that would be expected to produce floes less than one kilometre in length. Evans and Untersteiner (1971) considered the formation of thermal cracks in an ice sheet due to a sufficiently large difference in air and water temperatures. For 3m ice, a temperature difference of  $20^{\circ}\text{K}$  was able to give rise to cracks 200m apart. The analysis was performed using the coefficient of thermal expansion for brine-free ice. Evans (1971) extended the theory to include a salinity dependent coefficient of thermal expansion. The results were similar to the brine free case suggesting that this mechanism could explain cracking in sea ice.

Schwaegler (1974) suggests that cracking due to isostatic imbalances caused by the variation in ice sheet thickness is possible. However, results presented by Ackley et al (1976) using observed ice profiles show that the internal ice stresses would not be enough to cause fracture. They also point out that stresses caused by isostatic imbalances would have sufficient time to subside due to plastic creep.

We next consider the wind-induced flexure of ice sheets. This flexure may be directly caused by the wind or indirectly in that the wind-induced motion of the floe causes interaction with the ocean in such a way as to produce vertical forces. Also, winds increase the sea surface roughness and swell which may similarly cause flexure and break up of floes.

There are little data and no satisfactory theories to explain wind-induced flexure and fracturing of ice floes. Browne and Crary (1958) observed the tilting of Fletcher's ice island, T-3, and found a correlation between the time series for this tilt and the atmospheric pressure. Weber and Erdelyi (1976), as part of the AIDJEX pilot study, placed tilt measuring devices on an ice floe and found a good correlation between the tilt and the wind speed. They put forward the suggestion that the floe tilt was caused by the couple exerted by the wind on the top surface and the water traction on the floe bottom. This, however, predicted tilts far smaller than those actually observed. In fact, subsequently it became known (personal communication from Weber to Wadhams) that the sense of the tilt was opposite to that predicted by their calculations and that the floe was behaving as a planing dinghy in that the down-wind end of the

floe tilted up.

Coon and Evans (1977) criticised the assumption made by Weber and Erdelyi that the floe behaved rigidly. They suggested that consideration should be made of the elastic character of ice floes. They thus utilized the theory of non-rigid beams on elastic foundations to represent a floating ice floe. They concluded that for normal winds the bending stresses were insufficient to cause cracking but that the angle of deflection of the end of the floe was of the order of magnitude of the Weber and Erdelyi observations, and hence that wind-induced tilting of floes could not cause cracking. The slope at the end of the floe is largest and the magnitude quickly decays away from the edge. For a wind stress of  $0.5 \text{ Nm}^{-2}$  and for 3m ice they calculated a tilt at the end of the floe of  $3.16 \cdot 10^{-6}$  radians. This should according to their equation (13) be  $0.316 \cdot 10^{-6}$  radians. Thus they cannot satisfactorily explain the tilts of  $30 \cdot 10^{-6}$  radians actually observed by Weber and Erdelyi (1976), who presumably did not place their tilt measuring device at the edge of the floe. One can conclude from their analysis, however, that the wind and water surface tractions alone are not sufficient to explain the observed tilts even when consideration is taken of the flexure of ice floes.

This means that one must accept that floes do tilt in a way that is closely dependent on the wind speed but that the tilt is caused indirectly by the wind. It is possible that features on the underside of the floe cause deflection of water as the floe moves giving rise to vertical forces on the floe.

In this section, we attempt to use the observations of Weber and Erdelyi (1976), bearing in mind that the floe might have been flexing, to find a maximum floe size that can exist for a given wind field.

Beams on elastic foundations behave rigidly or flexibly depending on their length. A length scale  $\lambda^{-1}$ , called the characteristic plate length, occurs in beam theory and only those beams whose length is greater than about  $\lambda^{-1}$  behave flexibly.  $\lambda$  is defined by

$$\lambda^4 = \frac{k}{4D} \quad (31)$$

where  $k$  is the foundation modulus, which is the upthrust per unit length of the beam required to cause a unit vertical deflection. In the case of a body floating in water,  $k$  is  $\rho_w \hat{g}$ .  $\hat{g}$  is the acceleration of gravity.  $D$  is the flexural rigidity, which for a plate is

$$D = \frac{Eh^3}{12(1-\nu^2)} \quad (32)$$

Here,  $E$  is Young's modulus and  $\nu$  is Poisson's ratio for sea ice. If we take  $E/(1-\nu^2) = 10^{10} \text{ Nm}^{-2}$ , then for 3m ice, the characteristic plate length  $\lambda^{-1}$  is about 55m.

Weber and Erdelyi (1976) found the tilt of a floe by measuring the variations in the levels of two points on the floe at a distance 120m apart. Thus we see that the flexure of the floe must be taken into account when interpreting their data.

Suppose a semi-infinite beam has an applied load  $P$  at  $x = 0$ . The angle of deflection of the beam and the bending moment, for  $x > 0$ , are given by Hetenyi (1946), with a sign change because we consider an upthrust, as

$$\begin{aligned} \theta(x) &= \frac{2P\lambda^2}{k} \exp(-\lambda x) [\cos \lambda x + \sin \lambda x] \\ M(x) &= \frac{P}{\lambda} \exp(-\lambda x) \sin \lambda x \end{aligned} \quad (33)$$

The maximum bending moment occurs at  $x = (\pi/4)\lambda^{-1}$  and has the value  $(P/\lambda\sqrt{2})\exp[-\pi/4]$ . In terms of the deflection at  $x = 0$ ,  $\theta_0$ ,

$$M_{\max} = \frac{k\theta_0}{2\sqrt{2}\exp[\pi/4]\lambda^3} \quad (34)$$

Now the bending stress  $\sigma$  is related to the bending moment by

$$\sigma = \frac{6M}{h^2} \quad (35)$$

so that from (34) we obtain

$$\sigma = \frac{3\rho_w g (\lambda^{-1})^3}{\sqrt{2} \exp[\pi/4] h^2} \theta_0 \quad (36)$$

Thus, for an observed tilt  $\theta_0$ , we expect a maximum bending stress given by (36). A floe tilting sufficiently to give a bending stress exceeding  $\sigma_{\max}$ , the tensile strength of sea ice, will break.

If we substitute  $\lambda^{-1} = 55\text{m}$  and  $\theta_0 = 30 \cdot 10^{-6}$  radians, which is the extreme range of tilt measured by Weber and Erdelyi (1976), equation (36) gives  $\sigma \approx 5 \cdot 10^3 \text{Nm}^{-2}$  which is about 20 times smaller than the breaking stress. Thus the floe was in no danger of breaking up due to wind tilting. Now to proceed with the analysis, an estimate of the relation between the tilt,  $\delta$ , measured by Weber and Erdelyi's device and the tilt at the floe end,  $\theta_0$ , must be made. For the moment we assume they are equal ( $\delta = \theta_0$ ) and if necessary make adjustments once the results have been obtained. Equation (36) should thus be replaced with the following expression for the maximum bending moment in the floe,

$$\sigma = \frac{3\rho_w g (\lambda^{-1})^3}{\sqrt{2} \exp[\pi/4] h^2} \delta \quad (37)$$

where  $\delta$  is the deflection measured in Weber and Erdelyi's (1976) data.

Clearly, the floe for which Weber and Erdelyi (1976) made observations was long with regard to its rigidity in that its length exceeded the characteristic plate length,  $\lambda^{-1}$ , for sea ice of its thickness. Thus the analysis for a semi-infinite beam as has been carried out so far is applicable.

To deal with the situation for a short floe, a different theory is needed. The presence of the second free end to the floe has, as we shall see below, a substantial effect on the relation between the applied force  $P$  and the angle of tilt.

The analysis proceeds as for the case of the semi-infinite beam except that it has a free end at  $x = L$ . From Hetenyi (1946), the tilt  $\theta(x)$  and bending moment  $M(x)$  are

$$\begin{aligned}\theta(x) &= \frac{2P\lambda^2}{k} \frac{1}{\sinh^2 \lambda L - \sin^2 \lambda L} [\sinh \lambda L (\sin \lambda x \cosh \lambda x' \\ &\quad + \cos \lambda x \sinh \lambda x') + \sin \lambda L (\sinh \lambda x \cos \lambda x' + \cosh \lambda x \sin \lambda x')] \\ M(x) &= \frac{P}{\lambda} \frac{\sinh \lambda L \sin \lambda x \sinh \lambda x' - \sin \lambda L \sinh \lambda x \sin \lambda x'}{\sinh^2 \lambda L - \sin^2 \lambda L}\end{aligned}\quad (38)$$

where  $x' = L - x$ . Now if we assume that the beam is short in that  $\lambda L \ll 1$ , then the trigonometric and hyperbolic trigonometric terms may be replaced by the first two terms of their series expansions. Keeping only the highest order terms, this yields the following expressions for the tilt and bending moment for the beam.

$$\begin{aligned}\theta(x) &= \frac{6P}{kL^2} \\ M(x) &= PLX(1-X)^2\end{aligned}\quad (39)$$

where  $X = x/L$ . The bending moment has a maximum at  $X = \frac{1}{3}$  with a value

$$M_{\max} = \frac{4}{27} PL \quad (40)$$

Hence, noting (35), the maximum bending stress is given in terms of the angle of tilt by

$$\sigma = \frac{4\rho_w g L^3}{27h^2} \theta \quad (41)$$

It is worth noting at this point that Weber and Erdelyi (1976) gave a similar formula for the maximum bending moment in a tilting 'rigid' beam. However, they obtained

$$\sigma = \frac{\rho_i g L^3}{6\sqrt{3}h^2} \theta \quad (42)$$

Coon and Evans (1977) gave a maximum bending stress which is half that of Weber and Erdelyi (1976). In fact there is no unique formula for the maximum bending moment as a function only of the tilt; it depends on the method by which the beam is tilted. For example, in the case of a beam tilted by applying a moment about its centre, the relationship between  $\sigma$  and  $\theta$  is

$$\sigma = \frac{\rho_w g L^3}{12\sqrt{3}h^2} \theta \quad (43)$$

which is similar to the Coon and Evans (1977) value except that they have the factor  $\rho_i$  instead of  $\rho_w$ . Since floe tilting seems more likely to be caused by an upthrust at the leading end of the floe rather than an applied couple (either by way of a concentrated couple or from an upthrust in combination with a downthrust at another part of the floe), formula (41) would seem more applicable.

The only tilt measurements that are related to the wind speed are those of Weber and Erdelyi (1976) so we again have to use these with the floe bending models to predict the tilt of a small floe.

Weber and Erdelyi (1976) made observations on only one floe. To obtain an empirical law for the tilt of a floe of arbitrary length and thickness, based on these observations, it is necessary to assume a mechanism to explain the tilt and then determine theoretically the dependence on factors such as the floe thickness  $h$  and the wind speed  $U_{10}$ .

The procedure is to use (33) to determine the upthrust  $P$  needed to give rise to a tilt at the floe end of  $\theta_0 = \delta$ , where  $\delta$  is the tilt measured on

Weber and Erdelyi's (1976) floe for a given wind condition. We obtain,

$$P = \frac{1}{2} \rho_w g (\lambda^{-1})^2 \delta \quad (44)$$

We now assume that a short floe of length  $L$  is subjected to the same loading  $P$  at one end. Equation (39) then gives the tilt of this short floe as

$$\theta = \frac{3(\lambda^{-1})^2 \delta}{L^2} \quad (45)$$

from which the maximum bending stress may be found from (41) to be

$$\sigma = \frac{4 \rho_w g L (\lambda^{-1})^2 \delta}{9 h^2} \quad (46)$$

Summarizing, given a floe in a wind field, we first determine the tilt expected from the Weber and Erdelyi (1976) floe if it had the same thickness as the given floe. This tilt is denoted  $\delta$ . We next calculate  $\lambda^{-1}$  for the floe and so determine if it is to be classified as a 'long' or 'short' floe. If the floe is long then  $\sigma$  in equation (37) is calculated and if it is greater than  $\sigma_{\max}$  the floe will crack producing floes of length  $(\pi/4)\lambda^{-1}$ . The short floe theory with  $L = (\pi/4)\lambda^{-1}$  is then used to determine if subsequent cracking of the pieces occurs. If the given floe is already short then formula (46) is used immediately without first using the semi-infinite beam theory. The method is to solve (46) for  $L$  with  $\sigma = \sigma_{\max}$  to determine the largest floe that can exist in the wind field without cracking.

There is still one implicit assumption here that needs to be checked. That is, that a floe of length  $(\pi/4)\lambda^{-1}$  produced according to the semi-infinite floe theory will not, if subjected to the same forcing that produced it, continue to break according to the short floe theory. This is checked as follows. Suppose a semi-infinite beam cracks due to a load  $P$  at

its end. From (33), the maximum bending moment in a long floe  $M_{\max}^{\infty}$  is given by

$$M_{\max}^{\infty} = \frac{1}{2} P \lambda^{-1} \exp[-\pi/4] \sqrt{2} \quad (47)$$

A short beam of length  $L = (\pi/4) \lambda^{-1}$  will from (40) have a maximum bending moment of

$$M_{\max}^L = \frac{4}{27} P (\pi/4) \lambda^{-1} \quad (48)$$

so that since  $M_{\max}^L / M_{\max}^{\infty}$  is

$$\frac{\pi \sqrt{2} \exp[\pi/4]}{27} \approx 0.361 \quad (49)$$

which is less than unity, the bending moment in the fragments of the large floe does not exceed the maximum bending moment.

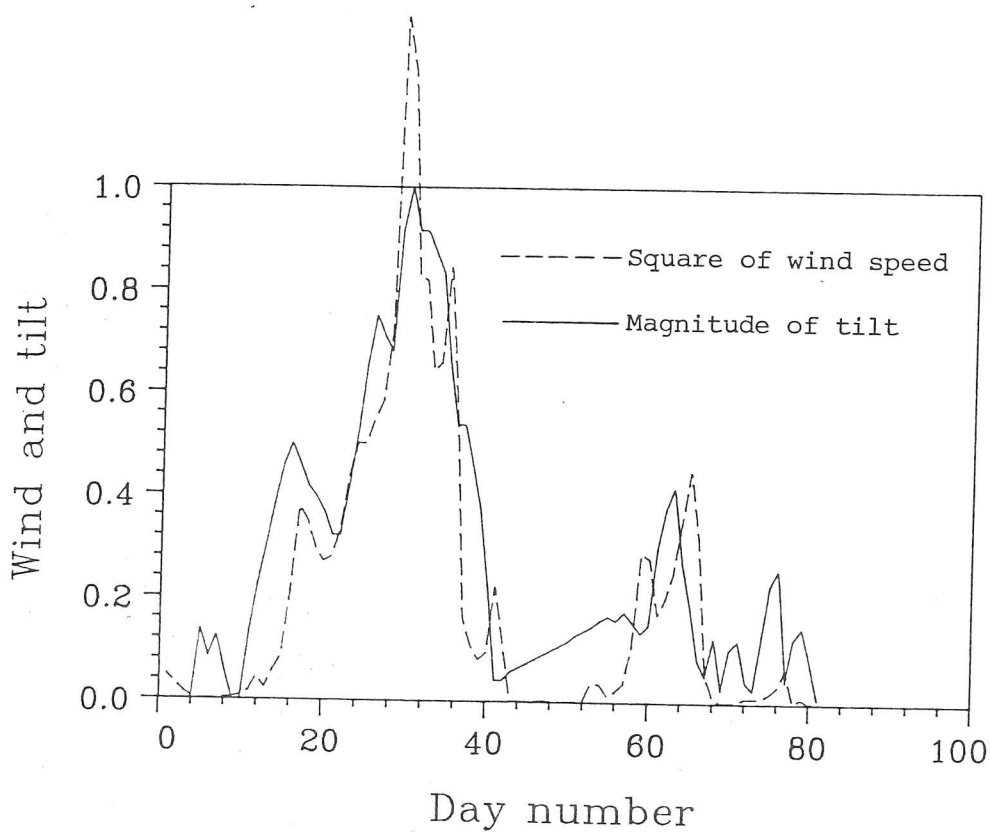
We now turn our attention to the mechanisms that might cause floe bending. We have assumed that an upthrust is produced at the leading edge of the floe. The tilt produced will again depend on whether we have a long or short floe. Considering first the long floe, the tilts will depend on the thickness  $h$  and the wind speed  $U_{10}$ . Suppose the upthrust at the end of the floe is caused by the downward deflection of water by a number of keels at the down-wind end of the floe. In this case the upthrust would be expected to be proportional to the square of the wind speed. As far as the thickness is concerned, we see from (31), (32) and (33) that the tilt is proportional to  $h^{-3/2}$ . Thus an empirical law relating the wind speed with the tilt should be of the form,

$$\delta = C h^{-3/2} U_{10}^2 \quad (50)$$

Weber and Erdelyi (1976) suggest that the tilt angle  $\delta$  is linearly related to  $U_{10}$ . The corresponding data curves agree quite well. However, by

Figure(3.4)

The square of the wind velocity plotted against the magnitude of the tilt, the scaling having been adjusted to give the best eye fit between the two curves. (After Weber and Erdelyi 1976)



rescaling the graphs a good fit between the curves for tilt and  $U_{10}^2$  can be obtained (see figure (3.4)). From the data, it is possible to derive the approximate law

$$\delta = 0.66 \cdot 10^{-6} U_{10}^2 \quad (51)$$

where  $\delta$  is measured in radians.

So, taking the thickness of the Weber and Erdelyi (1976) floe to be 3m, the expression for tilt, (50), becomes

$$\delta = 3.43 \cdot 10^{-6} h^{-3/2} U_{10}^2 \quad (52)$$

This may be substituted into (37) and (46) to give the maximum bending stresses for long and short floes as

$$\sigma = \frac{3\rho_w g (\lambda^{-1})^3 C U_{10}^2}{\sqrt{2} \exp[\pi/4] h^{7/2}} \quad (53)$$

and

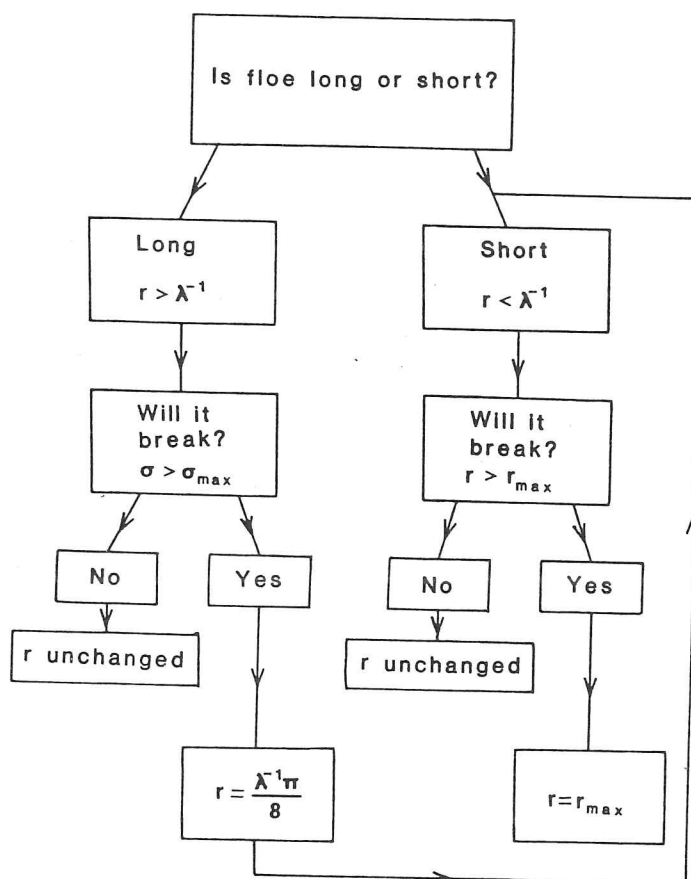
$$\sigma = \frac{4\rho_w g L (\lambda^{-1})^2 C U_{10}^2}{9 h^{7/2}} \quad (54)$$

where  $C = 3.43 \cdot 10^{-6}$ . Thus a long floe will break into floes of length  $(\pi/4)\lambda^{-1}$  if  $\sigma$  in (53) exceeds  $\sigma_{\max}$ . Solving (54) for  $L$  with  $\sigma = \sigma_{\max}$  will give the maximum size that the floes can be in the wind field  $U_{10}$ . If  $L/2$  is taken to be the radius of the floe, then (54) may be rearranged to give the maximum size of short floes in a wind  $U_{10}$  as

$$r_{\max} = \frac{9 h^{7/2} \sigma_{\max}}{2 \rho_w g (\lambda^{-1})^2 C U_{10}^2} \quad (55)$$

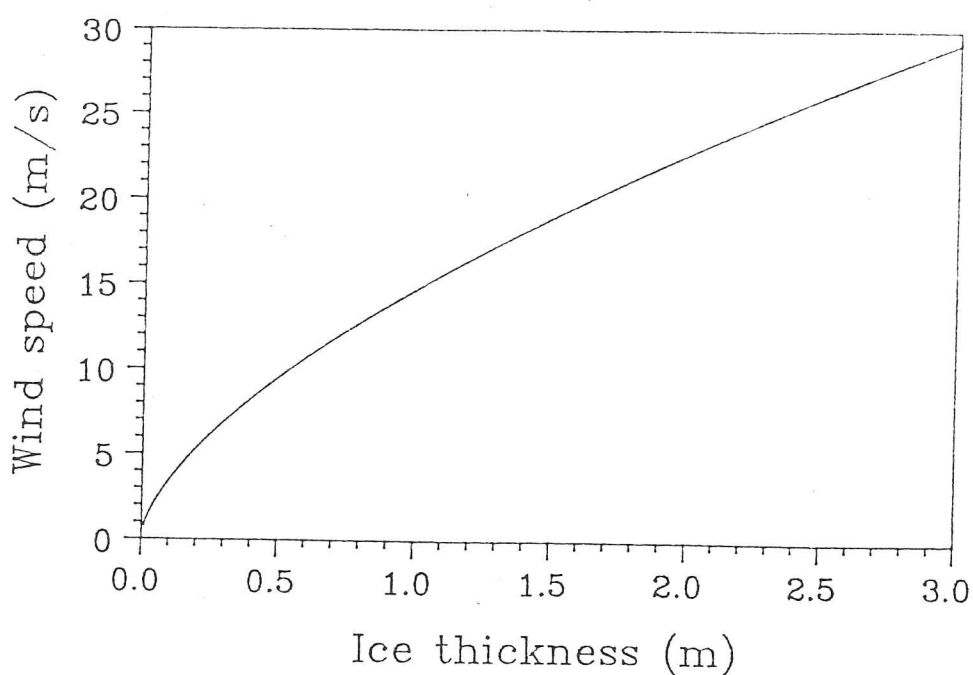
The line of reasoning regarding the breaking of long and short floes is

Figure(3.5)



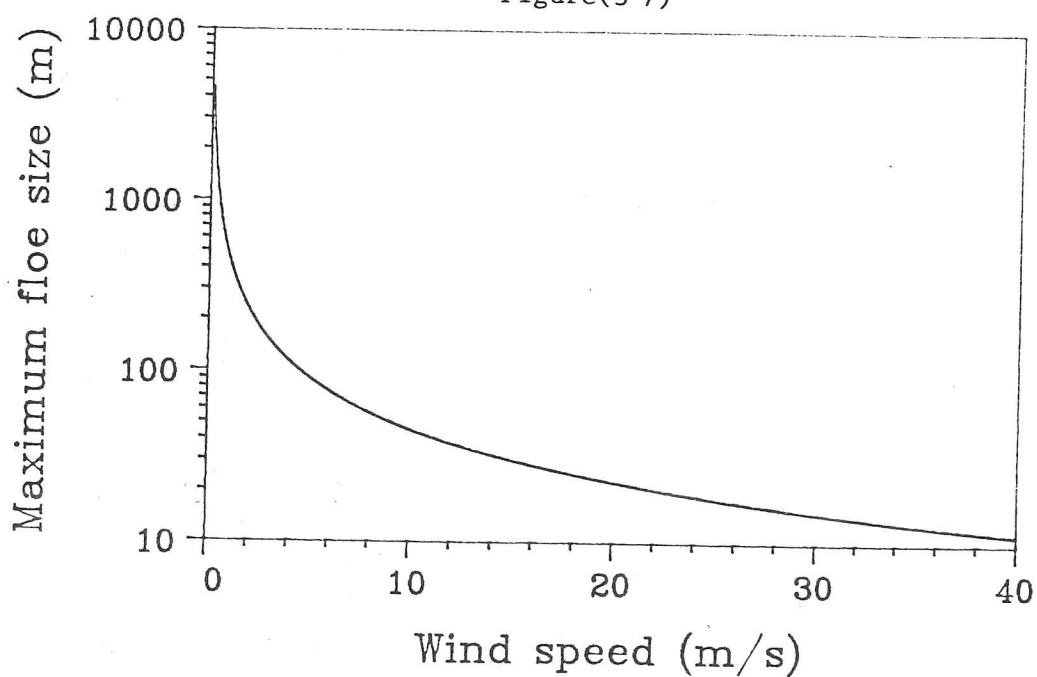
The line of reasoning involved in determining whether a floe will break up or not.

Figure(3.6)



The wind speed needed to break a floe according to the long floe equations.

Figure(3.7)



The radius of a floe three metres thick able to survive a given wind according to short floe theory.

traced in figure (3.5)

Figures (3.6) and (3.7) show the relationship between wind speed and the cracking of floes. Figure (3.6) shows the wind speed needed to crack a long floe. From this we see that only rarely will floes of more than 1m in thickness crack when in the interior of the pack. A wind speed of about  $16\text{ms}^{-1}$  is needed for this. As is mentioned below, wave action will be responsible for breaking the thicker floes. Another complicating factor is the variation of the tensile strength of ice  $\sigma_{\text{max}}$  which may be important during summer when melting may cause weakness of the ice structure.

In figure (3.7) we see the maximum size  $r_{\text{max}}$  that floes can be in a given wind field, according to the short floe formulae. The plotted curve is applicable to a floe of thickness 3m. The part of the curve for which large values of  $r_{\text{max}}$  are given is not relevant since only short floes will be tested for breaking using the formula. The comments regarding the variation in ice tensile strength apply to short floe breaking as well as to long floe breaking. The values that these curves indicate for breaking of floes seem reasonable, so without further evidence, we can take our assumption leading to equation (37), that the tilt as measured by Weber and Erdelyi is equal to the tilt at the floe end.

When considering a floe field consisting of many thickness categories, the dependence of  $r_{\text{max}}$  upon  $h$  in (55) means that the floe radius  $r$  averaged over a region depends on the ice thickness distribution  $g(h)$ . Suppose an area of pack ice initially consisting of short floes with a distribution  $g(h)$  is subjected to a wind of speed  $U_{10}$ . Any floes with radius larger than  $r_{\text{max}}$  given by equation (55) would then crack. The fraction of floes with thickness in the range  $(h, h+dh)$  is  $g(h)dh$ , and if initially the floes have radius  $r$ , then subsequently they will have radius  $\min\{r, r_{\text{max}}(h)\}$ . The average floe size resulting from the action of the wind is thus

$$\bar{r} = \int_0^{\infty} \min\{r, r_{\text{max}}(h)\} g(h) dh \quad (56)$$

Note that if  $\min\{r, r_{\text{max}}(h)\} = r$  for all  $g(h) \neq 0$ , then  $\bar{r} = r$ .

The preceding analysis, which stems from a single set of observations relating wind speed and floe tilt, concludes that if a thick floe tilts with the wind, then a sufficiently thin floe would break in the same wind. However, no mechanism has been suggested which fully explains the tilting. One mechanism which involves flexure and floe tilting (see page 52), but which can explain the break-up of floes is that due to the transfer to and subsequent propagation of ocean waves in the pack ice (Robin 1963). Measurements in the Fram Strait region (Wadhams 1978) suggest that the wave energy decays exponentially with distance into the pack, the waves of shorter wavelength decaying most rapidly. Wadhams found the decay rate such as to imply floe breaking to a distance of a few tens of kilometers into the pack. Kozo and Tucker (1974) found that further south in Denmark Strait, it was necessary to travel 165 km into the pack before its character was similar to that of the Central Arctic.

We should perhaps note that the resulting sizes of floes produced according to wave-breaking theory are similar to that given in this section since both rely on the elastic property of ice floes which depend upon the characteristic plate length  $\lambda^{-1}$ . The full theory of wave-induced break-up could be incorporated into a sea ice model by applying observed ocean wave amplitude fields which decay within the pack. In the model developed for this study, no explicit consideration of wave-induced break-up is included. However, to simulate the extreme break-up of floes observed near the ice edge, an ad hoc method is used in which the equations derived here for floe break-up are used with the ice tensile strength reduced in proportion to the ice concentration. Although this method of parameterizing wave-induced break-up has the advantage of being simple and requires knowledge only of the local wind speeds, it is not based upon any direct physical arguments. Because of this, we must regard the equations for floe break-up only as empirically derived, to be modified as and when observations of floe break-up in connection with wind speed become available. Such observations should note the break-up of any thin ice present in a region, even if it contributes only a small fraction of the total area. As part of an empirical approach we may regard the wind speed as a measure of the level of physical activity, the wind acting indirectly to cause floe break-up. For example, wind causes local ocean surface waves which, as we have mentioned, can cause floe break-up.

Alternatively, the wind can produce waves in the ice directly (Hunkins 1962). Also, general turbulence can cause random floe collisions resulting in impulsive forces on floes. There are more complicated mechanisms involving a combination of some of the mechanisms already mentioned, such as the variation in wave group velocity associated with changes in the horizontal compressive stress within floes (Mollo-Christensen 1983). These can lead to enhanced wave amplitudes in regions where the group velocity is zero with possible fracturing of the floe. Before we can determine quantitatively the relationship between floe tilt and wind speed, we cannot do better than to use empirical relationships and will continue to use the floe breaking formulae derived here, but bearing in mind the limitations involved.

### 3.3.3 Thermodynamic changes in floe number density

When dealing with collisions, only the average floe number density,  $n$ , has been considered. However, in order to more fully model the spatial distribution and changes in floe size it is necessary to consider a distribution of floe sizes at each point. This is motivated from observations of floe fields which show large variations in the floe sizes present at any location. The analysis of the previous section suggests that floe break up and the subsequent size of the residual pieces depend strongly upon the thickness of the floe involved. Thus a suitable way of considering a floe distribution is to consider the floe number density for each thickness category  $(h, h+dh)$ . Thus we obtain a floe number density distribution  $n(h)$  such that

$$\int_0^{\infty} n(h) dh = n \quad (57)$$

It is possible for the floe size distribution to change without altering the total number of floes. Such redistributions occur, for instance, during vertical melting and growing in exactly the same way as when the relative areas of each thickness level change during thermodynamic redistribution.

Thus during growing, the numbers of floes in the thicker ice categories increase at the expense of a thinner category. There are some differences in behaviour between the thickness distribution  $g(h)$  and the floe number density distribution  $n(h)$ . The distribution  $n(h)$  is not normalized as is  $g(h)$ : there is no limit to the number of pieces a floe may break up into. When the thinnest floes melt, open water is created which changes  $g(h)$ , but for  $n(h)$ , the floes simply disappear.

By adding a thermodynamic term to the floe number density equation (29) we obtain an equation for the evolution of  $n(h)$  that is analogous to the ice thickness distribution equation (2.39), thus

$$\frac{\partial n}{\partial t} + \nabla \cdot (\underline{u}n) + \frac{\partial (fn)}{\partial h} = \psi_n + F_n \quad (58)$$

where the third term on the left indicates the thermodynamic changes to  $n$ . The term  $\psi_n$  represents the changes to  $n$  occurring during collisions and fracture. The final term only loosely similar to the lateral melting term  $\bar{F}_L$  represents the changes to  $n$  occurring when new ice forms from open water or melts completely. The functional form of  $\psi_n$  is complicated and totally different from that of  $\psi_n$ , <sup>the redistribution function of equation (2.39)</sup> Handling  $\psi_n$  in a model is best done by converting the floe number densities into the equivalent floe sizes for each thickness category and make the necessary changes to the floe radius as outlined in this chapter before converting back to floe number densities.

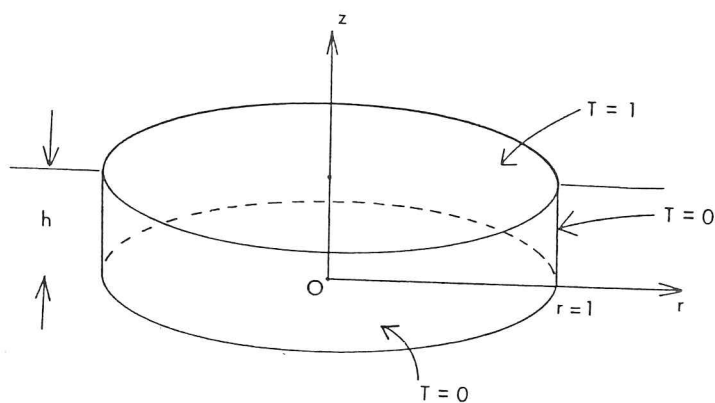
### 3.3.4 Lateral melting

Consider the situation in which heat is absorbed into the ocean mixed layer, through leads. The heat is assumed to mix underneath the ice floes and melt them from below as well as from the sides. This melting from the sides, known as lateral melting, is an important component of the change in ice geometry through thermodynamic effects, especially when there is a high floe number density and there exists a large length of floe edge per unit area. A specific problem associated with lateral melting is to determine the rate at which melting occurs laterally compared to that at

which it occurs vertically.

The more general problem is to determine how and at what rate an arbitrarily shaped ice floe will melt when immersed or floating in water which is at a temperature above freezing, such that melting will occur. This problem cannot be solved analytically even in simple cases because of the difficulties introduced by the boundary condition, namely the shape of the boundary of the ice, being one of the unknowns. However, we make some assumptions here which simplify the problem and enable some kind of a solution to be obtained for the case of a disc or a large floe with thickness small compared to its horizontal extent. The method consists of assuming that the upper surface of the ice floe is maintained at a constant low temperature and the surfaces below the water line are at a temperature slightly higher than that necessary to initiate melting. Laplace's equation  $\nabla^2 T = 0$ , is solved for the body with these Dirichlet boundary conditions. The next step is to look at the isotherm for which melting will occur.

The temperature of the water surrounding the ice is assumed to be just enough to make the surface layer melt, so that the melting-isotherm will be very close to the original surface. We can assume that the body will melt in a short time so that the new surface coincides with this isotherm. The solution to Laplace's equation for the original body may be modified to give the solution of the newly melted body by specifying the temperature on the old melting-isotherm as zero. The new isotherms will have the same shape as before but with slightly different values of  $T$ . We thus reach the conclusion that a body will melt in such a way as to assume the shape of its isotherms in the solution to Laplace's equation. We assume also that the body melts slowly compared to the time required for the ice to reach thermal equilibrium internally, so that a quasi-static situation is obtained and the heat equation may be solved for the body without including the time dependent term. We can obtain the solution to Laplace's equation for a disc with boundary conditions as shown in figure (3.8). To simplify matters we take the temperature at the top surface to be 1 and at the bottom and curved surfaces to be zero. The height of the disc is  $h$  and its radius is  $l$ . The solution may be obtained by separation of variables and is expressed as a series of Bessel functions thus



Figure(3.8)

The boundary conditions used to determine the temperature distribution within a disc.

$$\sum_{p=1}^{\infty} \frac{2 J_0(\lambda_p r) \sinh \lambda_p z}{\lambda_p J_1(\lambda_p) \sinh \lambda_p} \quad (59)$$

However this solution for a given isotherm,  $T = \text{constant}$ , does not give a very useful indication of the relation between the variables  $r$  and  $z$ .

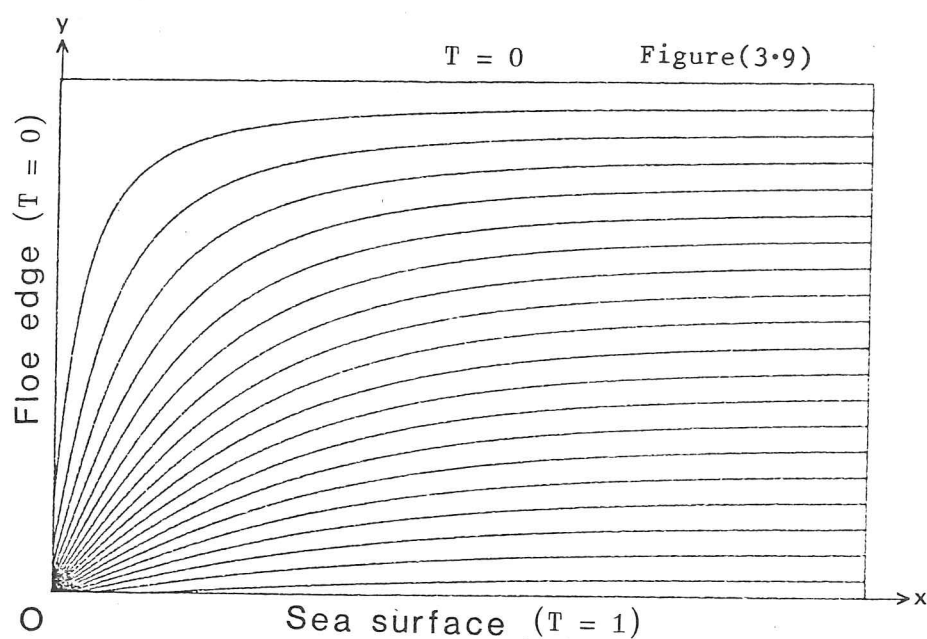
We thus solve the problem in a rectangular region shown in figure (3.9). For simplicity we take the height as  $\pi$  with boundary conditions  $T = 0$  for  $x = 0$  and  $y = \pi$  and  $T = 1$  for  $y = 0$  in the region  $x > 0$ . The solution of Laplace's equation in this region may be solved by summing two known solutions. Firstly, the solution in which the two longer sides have zero temperature and the side  $x = 0$  has a Dirichlet boundary condition  $T(0, y) = (y/\pi) - 1$ . The second solution is simply  $T(x, y) = 1 - (y/\pi)$ . The first solution can be obtained by Fourier superposition which together with the second solution gives

$$T(x, y) = 1 - \frac{y}{\pi} - \frac{2}{\pi} \tan^{-1} \left[ \frac{e^{-x} \sin y}{1 - e^{-x} \cos y} \right] \quad (60)$$

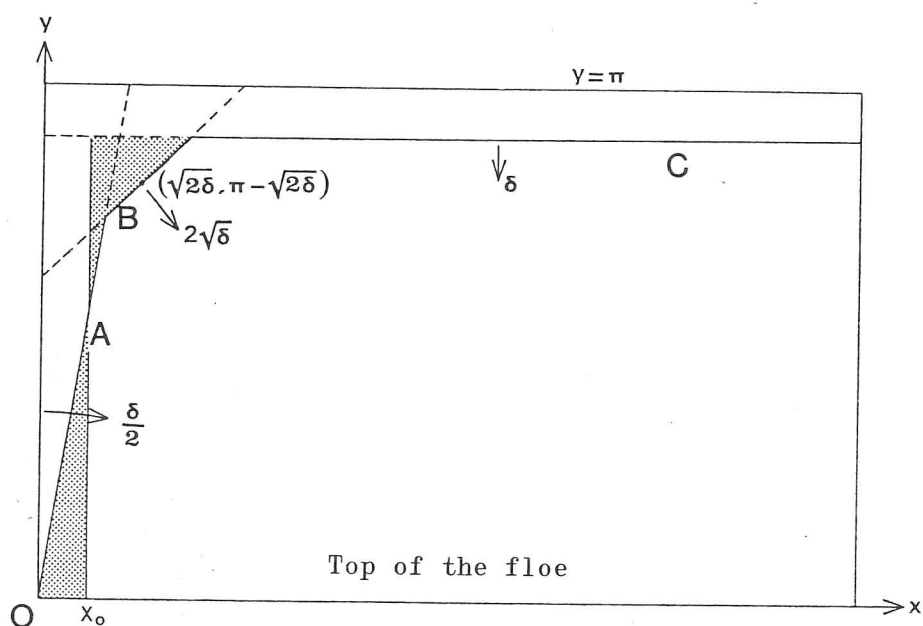
The isotherms for this solution are shown in figure (3.9). Thus we assume that for a rectangular floe left undisturbed within well mixed water of a temperature sufficient to melt the ice, the floe will melt so that its profile at subsequent times follows the isotherms as they appear in figure (3.9). The figure shows the 'bathtub' shape that is observed in laboratory experiments with melting ice blocks (Russell-Head 1980, Gebhart et al 1983) It is convenient in the following analysis to re-express (60) in the form

$$T(x, y) = \frac{1}{\pi} \tan^{-1} \left[ \frac{\sin y \sinh x}{1 - \cos y \cosh x} \right] \quad (61)$$

where  $(-\pi/2) < \tan^{-1} < \pi/2$  in (60) and  $0 < \tan^{-1} < \pi$  in (61). Thus the  $\tan^{-1}$  function in (60) is the principle value of the function, whereas the  $\tan^{-1}$  function in (61) is a modified  $\tan^{-1}$  function. A typical isotherm



The isotherms or the lines of melting at the edge of an infinite rectangular floe when the temperature distribution is assumed to obey Laplace's equation in two dimensions.



Figure(3.10) An approximation to the mode by which floes melt laterally. The arrows give the relative speeds with which various parts of the floe melt.

$T = \text{constant}$  starts at the origin at an angle  $T\pi/2$ . It then meets the asymptote  $y=\pi T$  at  $x = \infty$ .

In a simple model in which vertical melting of floes as well as lateral melting (but retaining vertical edges) is allowed, the problem is to determine the relation between the vertical and lateral melt rate that best describes the melting patterns shown in figure (3.9).

One way to approach this problem is to assume that the floe melts very slightly so that it decreases in thickness by  $\delta \ll 1$ . If we further assume that the floe remains rectangular, then in principle a calculable amount of lateral melt is needed to give the correct total volume melted.

We consider the isotherm  $T = \delta/\pi$  and expressing (61) in the form  $y = f(x)$  we need to find  $x_0$  such that

$$\int_0^{x_0} f(x) dx = \int_{x_0}^{\infty} [\pi - \delta - f(x)] dx \quad (62)$$

$x_0(\delta)$  would then give, as a function of the vertical melt  $\delta$ , the amount of lateral melt needed to retain a rectangular cross section and give correct total volume melt.

Solving (62) in practice is difficult because there is no simple way to re-express (61) in the form  $y = f(x)$ . However, since  $\delta \ll 1$  we may assume  $\tan \delta \approx \delta$  and write (61) in the form

$$\delta(1 - \cos y \cosh x) = \sin y \sinh x \quad (63)$$

Equation (63) may be used to give the  $\delta/\pi$  isotherm for the following cases.

- 1)  $x$  small (The edge of the floe)  
 $y = 2 \tan^{-1}(x/\delta)$
- 2)  $x$  small and  $y \approx \pi$  (The corner of the floe)  
 $y = \pi - (2\delta/x)$

3)  $x$  not small and  $y \approx \pi$  (The bottom of the floe)

$$y = \pi - \delta \coth(x/2)$$

By examining these three cases, we see that it is possible to enclose the slightly melted floe by a polygonal region as shown in figure (3.10). Case (1) gives a tilting of the floe edge away from the vertical. This is shown by line A in figure (3.10) which has a gradient  $2/\delta$ . From case (2) which is the equation of a rectangular hyperbola, we obtain line B of slope 1, touching the curve at  $(x,y) = (\sqrt{2\delta}, \pi - \sqrt{2\delta})$ . Case (3) tells us that line C,  $y = \pi - \delta$ , encloses the curve,  $\pi - \delta$  being the value that the isotherm asymptotes to as  $x \rightarrow \infty$ .

As the floe melts, line A tilts, its angle changing at a rate with order of magnitude  $\delta$ . Similarly line C drops at a rate proportional to  $\delta$ . However line B proceeds away from the corner  $(0, \pi)$  at a significantly faster rate (proportional to  $\sqrt{\delta}$ ). Thus we would expect to see any corners of the floes melt most rapidly.

Now we redistribute the ice of the floe so that it is again vertical (along the line  $x = x_0$ ), and determine  $x_0$  such that the two shaded regions in figure (3.10) are equal.  $x_0$  can be determined from simple geometry to be

$$x_0 = \left[ \frac{\pi}{4} + \frac{4}{\pi} \right] \delta + (\text{Higher order terms in } \delta) \quad (64)$$

The higher order terms in  $\delta$  in (64) may be neglected if we consider the limit as  $\delta \rightarrow 0$ . We then obtain the relation  $(x_0/\delta) = (\pi/4) + (4/\pi) \approx 2.05$  which gives us the rate at which lateral melting occurs compared to vertical melting. Thus in a model of floes consisting of squat cylinders with vertical sides, including a lateral melt rate equal to 2.05 times the vertical melt rate will give the best approximation to the melting suggested in figure (3.9).

It should be mentioned that the factors that we have ignored here if included would tend to increase the lateral melt rate compared to the vertical melt. For instance, if the heat was not effectively transported beneath the ice in the mixed layer, then more melting would be expected near the leads. Another factor would be the breaking off of small pieces of

the floe at the edge which would melt more quickly in the water. Also a significant amount of melting occurs due to wave action (Wadhams et al 1979). This acts at the water line producing a 'wave-cut' which destroys the profile suggested by the calculations here. The result of the long term wave action and melting is to produce an underwater sill with a flat top (Alekseev and Buzuev 1973). Again an additional contribution to the loss of ice from the side of the floe would result from including wave-induced melting in the calculations. Such melting could occur even when there is net heat loss from the leads. Thus if we decide to use the factor  $(\pi/4) + (4/\pi)$  to give the lateral melt rate, it should be borne in mind that it is really a lower limit.

## 4. PACK ICE DYNAMICS

### 4.1 Introduction

A full understanding of the large scale deformation of pack ice, which is important in climate studies, can be achieved only when a study has been made of the small scale processes that accompany such deformation. These include ridging and rafting.

The average thickness of the pack ice in a region where there is convergence, will tend to increase (by ice conservation). In general an area of pack ice will consist of a variety of thicknesses, and it is the thinnest ice that will be crushed in a converging flow field. Determining which thicknesses are crushed and by how much was discussed in section (2.3) concerning redistribution theory.

The size and shape of ridges produced during pack ice deformation determines the strength of the ice, an important factor in determining the magnitude of the internal ice resistance, or ice interaction term. In this chapter we aim to derive the ice interaction terms using, where possible, mechanistic models of the underlying physical processes.

### 4.2 Ridging and rafting

#### **4.2.1 A simple ridge building model**

Although relatively thick ice is able to ridge, it will do so substantially only after any nearby thin ice has ridged. The thin ice, often newly grown ice in leads, breaks up into rubble and piles into a ridge-like structure. The thin ice continues to break up and feed rubble into the ridge until some limiting ridge height is reached, a height that

depends on the strength of the original ice sheet.

In this section the thickness of the original, or parent, ice sheet is  $h_1$  and the ridge height which is the distance from the tip of the sail to the bottom of the keel, is  $h_2$ . For the situation in which thin ice in a lead is ridging,  $h_1$  will be the thickness of the ice in the lead. The frequent occurrence of ridges in pack ice suggests that ridging is an important method of ice redistribution.

Tucker and Govoni (1981) conclude from observations of 30 ridges in 5 locations off Prudhoe Bay, Alaska, that there is a dependence of the ridge heights on the maximum block thickness from which the ridge is composed. In other words, that the ridge height is a function of the parent ice thickness.

In early studies of ice redistribution theory (Thorndike et al, 1975; Rothrock, 1975), a linear ridging law was used, so that  $h_2$  the ridge height is related to the parent ice thickness  $h_1$  by

$$h_2 = kh_1 \quad (1)$$

where  $k$  is a constant. This rule was chosen not as an accurate formula for ridge heights but to simplify the interpretation of the results obtained using redistribution theory. The Tucker and Govoni (1981) observations suggest that (1) is far from adequate and that a square root dependence such as

$$h_2 = \sqrt{Hh_1} \quad (2)$$

used in Hibler's (1980a) variable ice thickness model, is a better formula for an appropriate constant  $H$ , than is equation (1). Equation (2) has the additional advantage that it can be derived (Hibler 1980a) from a geometrical argument by assuming that ridges have triangular cross section and are formed from leads of constant width.

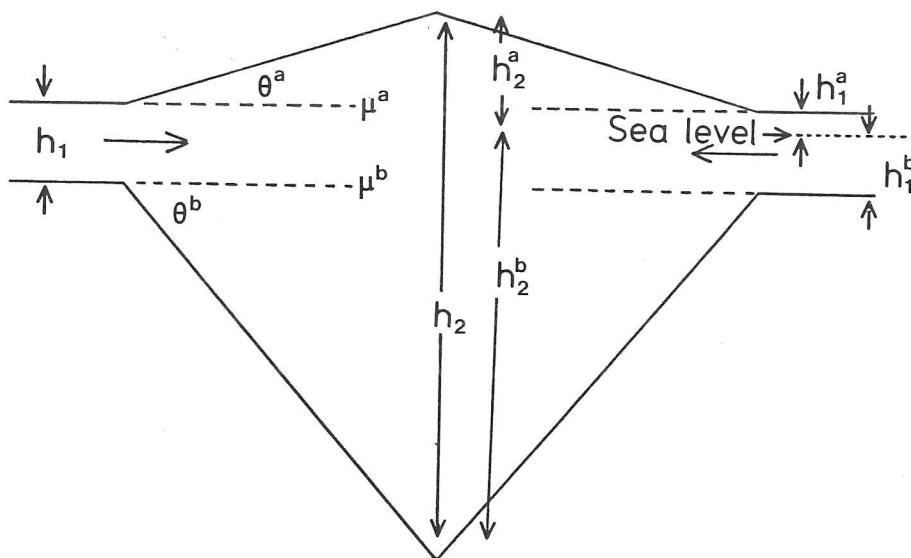
Results from a numerical model of the ridge building process (Parmerter and Coon, 1972) tend to confirm that  $k$  in equation (1), rather than being constant, should decrease with increasing  $h_1$ .

Rothrock (1975) calculates the potential energy and frictional losses occurring when an ice sheet of thickness  $h$  slides into a rubble field of thickness  $kh$ . In this way he derived an estimate of the ice strength. Here mechanical arguments are used similar to those of Rothrock (1975) but for a different purpose. Firstly some idealized shape is chosen to represent the cross-section of a typical ridge. An ice strength dependent on its thickness is assumed, and the size of the resulting ridge calculated. A ridge shape is chosen that is conveniently handled mathematically and is also reasonably in accord with observations. Figure (4.2) shows a possible idealization of a 'typical' ridge cross section. A ridge of this shape is however not in isostatic equilibrium and, if the ice were to deform, an adjustment due to the buoyancy of the keel would take place resulting in a shape something like that shown in figure (4.3). An altogether more convenient shape to deal with mathematically is shown in figure (4.1). The ridge is assumed to be in isostatic equilibrium at each point. This model represents the keel well, but not the small steep-sided sail shown in figure (4.2). This is perhaps not such a serious deficiency because the keel contains a far greater proportion of ice than the sail. Also since the shapes in figures (4.3) and (4.1) are in isostatic equilibrium, the volumes of ice in the keels and sails are correctly represented. It is important in a redistribution model to ensure that the correct volume of thin ice is used up in forming a ridge. Figure (4.1) is thus chosen to represent a 'typical' ridge, and the theoretical results obtained should be compared with keel data rather than sail data. The angle of inclination of the keel  $\theta^b$  is fixed, and is chosen to agree with observed values. Other dimensions are calculated by assuming that throughout the ridging process, the ice remains in isostatic balance. By definition

$$h_j^a + h_j^b = h_j \quad j = 1, 2 \quad (3)$$

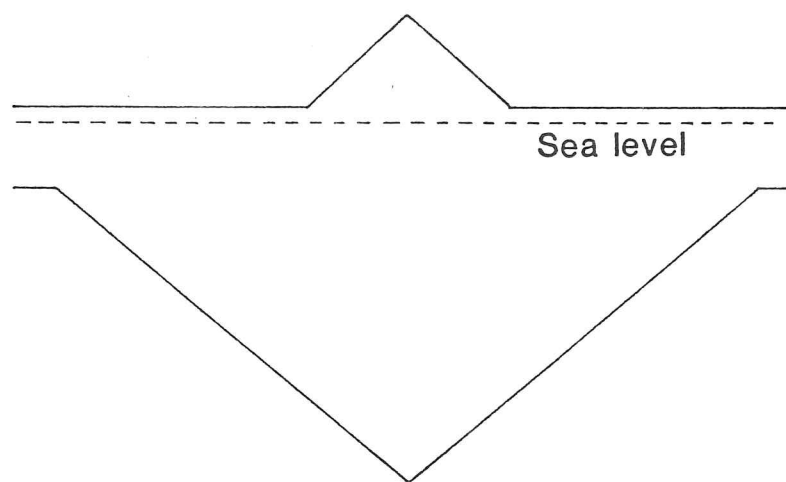
The superscripts  $a$  and  $b$  refer to quantities above and below sea-level respectively.

Figure (4.1)



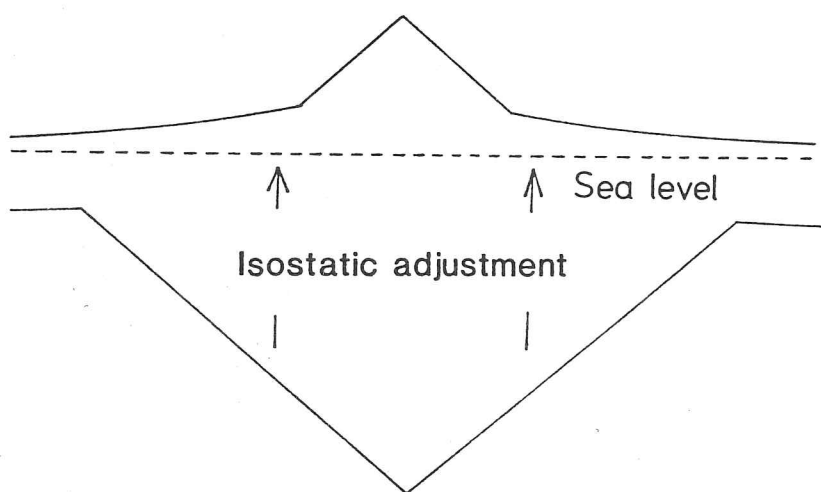
The assumed cross section of a ridge used in calculating the height of ridges produced  $h_2$  as a function of the original ice thickness  $h_1$ .

Figure (4.2)



Idealization of a ridge cross section

Figure (4.3)



The cross section of a ridge after undergoing isostatic adjustment.

During ridging, the ice will not have a continuous structure, but will contain many air gaps between the blocks. Below the sea surface, the gaps will contain water. The fractional volume of the ridge structure consisting of the air and water gaps is defined as the porosity  $n_0$ . The simplifying assumption is made that the porosity is constant throughout the ridge and in particular above and below the water line. In fact the porosity varies considerably within the pack ice, but here a single 'average' value is chosen. With this assumption isostasy implies,

$$\rho_i h_j^a = (\rho_w - \rho_i) h_j^b \quad j = 1, 2 \quad (4)$$

Combining (3) and (4) gives,

$$h_j^a = \frac{(\rho_w - \rho_i)}{\rho_w} h_j \quad j = 1, 2 \quad (5)$$

$$h_j^b = \frac{\rho_i}{\rho_w} h_j \quad j = 1, 2 \quad (6)$$

From the geometry of the ridge and from (5) and (6),

$$(h_2^a - h_1^a) \cot \theta^a = (h_2^b - h_1^b) \cot \theta^b \quad (7)$$

Here  $\rho_i$  and  $\rho_w$  are the densities of ice and sea water respectively.

The ridging strength is regarded as the horizontal stress that an ice sheet can exert before it yields. Intuitively it is expected that this strength should increase with increasing ice thickness. The ideas behind ice strength are dealt with in more detail in the next section. The force required to increase the gravitational potential energy of the ridge  $F_{\text{pot}}$  together with the frictional forces  $F_{\text{fric}}$  involved in the ridge building are calculated. It is assumed that when

$$P(h_1) = F_{\text{pot}} + F_{\text{fric}} \quad (8)$$

the ridge has reached its maximum height  $h_2$ . Consider the left half of the ridge. The gravitational potential energy of the sail is

$$\begin{aligned}
 & (1-n_o)\rho_i \hat{g} \cot \theta^a \int_{h_1^a}^{h_2^a} y(h_2^a - y) dy \\
 &= \frac{1}{6} (1-n_o)\rho_i \hat{g} \cot \theta^a (h_2^a + 2h_1^a)(h_2^a - h_1^a)^2 \\
 &= \frac{1}{6} (1-n_o)\rho_i \hat{g} \cot \theta^a \left[ \frac{\rho_w - \rho_i}{\rho_w} \right]^3 (h_2 + 2h_1)(h_2 - h_1)^2
 \end{aligned} \tag{9}$$

where  $\hat{g}$  is the acceleration of gravity.

The potential energy of the keel can be similarly calculated, to give

$$\begin{aligned}
 & -\frac{1}{6} (1-n_o)\rho_i \hat{g} \cot \theta^b (h_2^b + 2h_1^b)(h_2^b - h_1^b)^2 \\
 &= -\frac{1}{6} (1-n_o)\rho_i \left( \frac{\rho_i}{\rho_w} \right)^3 \hat{g} \cot \theta^b (h_2 + 2h_1)(h_2 - h_1)^2
 \end{aligned} \tag{10}$$

The potential energy of the keel due to buoyancy is similarly found to be

$$\frac{1}{6} (1-n_o)\rho_w \left( \frac{\rho_i}{\rho_w} \right)^3 \hat{g} \cot \theta^b (h_2 + 2h_1)(h_2 - h_1)^2 \tag{11}$$

Adding (9), (10) and (11) and using (7) to eliminate  $\theta^a$  in favour of  $\theta^b$  gives the total isostatic potential energy as

$$\frac{1}{6} (1-n_o)(\rho_w - \rho_i) \frac{\rho_i^2}{\rho_w^2} \hat{g} \cot \theta^b (h_2 + 2h_1)(h_2 - h_1)^2 \tag{12}$$

It is not necessary to consider the potential energy of the ice of thickness  $h_1$  since only changes in potential energy are of concern.

Since

$$\text{P.E.} = \int F_{\text{pot}} dl \tag{13}$$

where  $l$  is the length of pack ice fed into the ridge, it is necessary to relate  $l$  to changes in  $h_2$ . From

$$lh_1 = \left[ \frac{1}{2}(h_2^a - h_1^a)^2 \cot \theta^a + \frac{1}{2}(h_2^b - h_1^b)^2 \cot \theta^b \right] (1 - n_o) \quad (14)$$

which represents volume conservation during ridging, one gets using (5), (6) and (7)

$$lh_1 = \frac{\rho_i}{2\rho_w} \cot \theta^b (h_2 - h_1)^2 (1 - n_o) \quad (15)$$

From which

$$h_1 \frac{dl}{dh_2} = \frac{\rho_i}{\rho_w} (1 - n_o) \cot \theta^b (h_2 - h_1) \quad (16)$$

So

$$\begin{aligned} F_{\text{pot}} &= \frac{d(\text{P.E.})}{dl} = \frac{d(\text{P.E.})/dh_2}{dl/dh_2} \\ &= \frac{1}{2} \frac{\rho_i}{\rho_w} (\rho_w - \rho_i) g h_1 (h_2 + h_1) \end{aligned} \quad (17)$$

The frictional forces are calculated by assuming that the incoming ice (generally ice in leads) slides along in contact with the forming ridge (shown in figure 4.1) as it breaks up and that the coefficient of friction at the surface above sea-level is  $\mu^a$  and that below is  $\mu^b$ . Cohesion between the surfaces is not assumed.

The friction on the upper surface is

$$\begin{aligned}
& \mu^a \int_0^{(h_2^a - h_1^a) \cot \theta^a} (1 - n_o) \rho_i g x \tan \theta^b dx \\
& = \frac{1}{2} (1 - n_o) \mu^a g \frac{\rho_i^2}{\rho_w^2} (\rho_w - \rho_i) \cot \theta^b (h_2 - h_1)^2
\end{aligned} \tag{18}$$

and on the lower surface is

$$\frac{1}{2} \mu^b (1 - n_o) g (\rho_w - \rho_i) \frac{\rho_i^2}{\rho_w^2} \cot \theta^b (h_2 - h_1)^2 \tag{19}$$

The total friction is thus,

$$\frac{1}{2} (\mu^a + \mu^b) (1 - n_o) g (\rho_w - \rho_i) \frac{\rho_i^2}{\rho_w^2} \cot \theta^b (h_2 - h_1)^2 \tag{20}$$

Substituting (17) and (20) into (8) gives

$$C_b h_1 (h_2 + h_1) + C_f (h_2 - h_1)^2 = P(h_1) \tag{21}$$

where,

$$C_f = \frac{1}{2} (\mu^a + \mu^b) (1 - n_o) g (\rho_w - \rho_i) \frac{\rho_i^2}{\rho_w^2} \cot \theta^b \tag{22}$$

and

$$C_b = \frac{1}{2} \frac{\rho_i}{\rho_w} (\rho_w - \rho_i) g \tag{23}$$

Equation (21) is a simple quadratic equation in  $k = h_2/h_1$ , the physically realistic solution of which is

$$k = 1 - \frac{C_b}{2C_f} + \left[ \frac{C_b^2}{4C_f^2} - \frac{2C_b}{C_f} + \frac{P(h_1)}{C_f h_1^2} \right]^{\frac{1}{2}} \quad (24)$$

for

$$h_1 < \left( \frac{P(h_1)}{2C_b} \right)^{\frac{1}{2}} \quad (25)$$

Thus, starting from an expression  $P(h_1)$  for the ridging strength of ice of thickness  $h_1$ , it is possible to derive an expression for the height  $h_2 = kh_1$  of ridges formed.

If  $P(h_1)$  is taken to have a quadratic dependence on  $h_1$ , then equation (21) implies that  $k$  is a constant and thus gives the linear ridging law, as in equation (4). Ice of thickness  $h_1$  has a buckling strength proportional to  $h_1^{3/2}$ . Parmerter (1974) gives the buckling strength as

$$\sqrt{\frac{E\rho_w \hat{g}}{12(1-\nu^2)}} h^{3/2} \quad (26)$$

It may be inappropriate to use this to estimate the ridging strength of an ice sheet that is initially fractured or broken up. Here, the strength,  $P(h_1)$ , of a single thickness ice sheet is taken to depend linearly upon  $h_1$ , thus

$$P(h_1) = P^* h_1 \quad \text{Nm}^{-1} \quad (27)$$

The linear dependence of the ridging strength in equation (27) is consistent with the ice strength term used in Hibler's (1979) two-layer model.

In this ridging model, the frictional terms are calculated assuming a uniform ice sheet sliding between piles of rubble blocks. The choice of values of the coefficients  $\mu^a$  and  $\mu^b$  is questionable because no account is taken of the sharp corners of the blocks digging into each other

preventing slipping. Values of  $\mu^a$  and  $\mu^b$  are thus chosen at the upper limit of observed values for ice-ice or for ice-steel contact (Zubov 1943). The keel angle  $\theta^b$  may be related to  $\mu^b$  from a simple model of a block resting in equilibrium due to friction on a slope. This gives

$$\mu^b = \tan \theta^b \quad (28)$$

which may be used to estimate  $\mu^b$ .

The density of sea water at temperatures and salinities found in sea ice regions is about  $1025 \text{ kgm}^{-3}$ . The choice of a single value of density of sea ice is not easily justified. Actual sea ice densities depend on the amount of salt and air trapped internally (Cox and Weeks 1982). As ice ages and brine drainage occurs, the density of the ice decreases. The best that can be done for this problem is to consider that since ridging frequently involves thin ice which is new, then  $\rho_i$  should be chosen to be that of ice with a high salt content. Kovacs (1972) notes that undeformed sea ice has a density in the range  $870$  to  $930 \text{ kgm}^{-3}$ . Cox and Weeks give formulae for ice density in terms of the salt and air content as well as the temperature. For ice with high salinity a high density is expected.

For the ridging strength given in the form of equation (27), the constant  $P^*$  is considered as a free parameter to be found by comparing the values given by equation (27) with those available from observations.

In order to compare the data of Tucker and Govoni (1981) with the predicted values of  $h_2$ , we take their data for the observed ridge heights  $h$ , as plotted against the maximum block thickness  $t$ , and adjust the values of  $h$  to account for settling since the time of formation of the ridge. We estimate that the height of the ridge when formed,  $h_2$ , is given in terms of  $h$  and  $t$  by

$$h_2 = (h-t) \frac{1-n''_0}{1-n'_0} + t \quad (29)$$

This assumes that the ridge formed with a porosity  $n'_0$  and that it subsequently settled to  $n''_0$ , but that the part of the ridge composed of the original ice sheet of thickness  $t$  remained with zero porosity throughout the ridging process. Attempts to fit the function  $h_2(h_1)$  as given by (24) to the Tucker and Govoni (1981) observations suggest that the best fit is obtained in the range 0-2m if  $P^*$  is chosen such that the product of  $P^*$  and  $(\mu^a + \mu^b)$  is about  $9000 \text{ Nm}^{-2}$ .

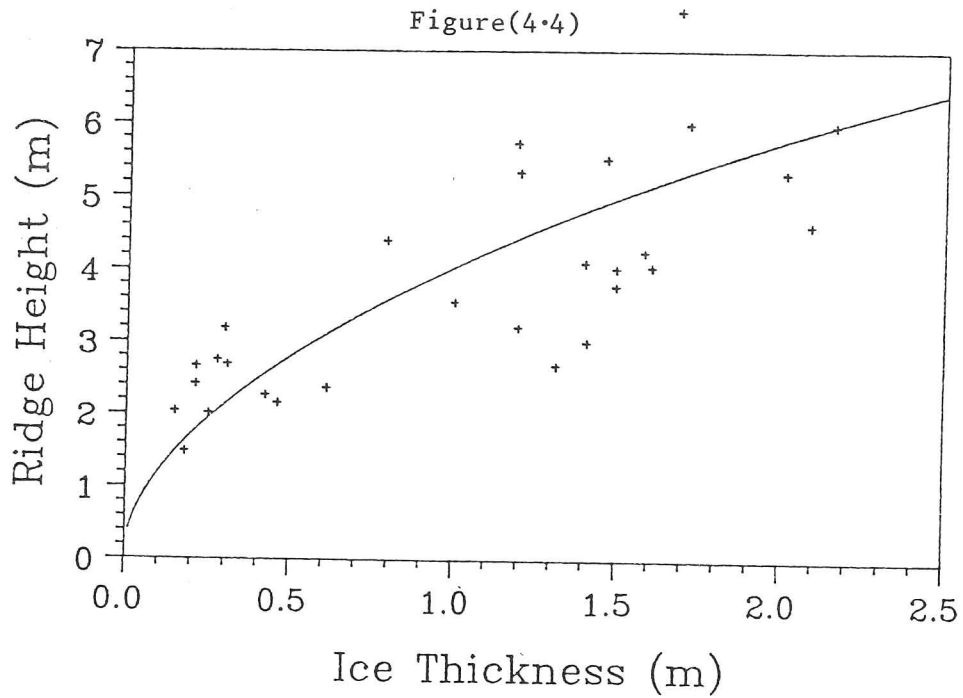
For  $h_1 > P^*/2C_b$ , (24) predicts either  $h_2 < h_1$  or that  $h_2$  is complex, both of which are not physically meaningful, and indicates that no ridging can take place. Indeed if such a ridge were artificially constructed from rubble blocks, it would immediately collapse if unsupported. Hence

$$h_2 = h_1 \quad \text{if} \quad h_2 > \frac{P^*}{2C_b} \quad (30)$$

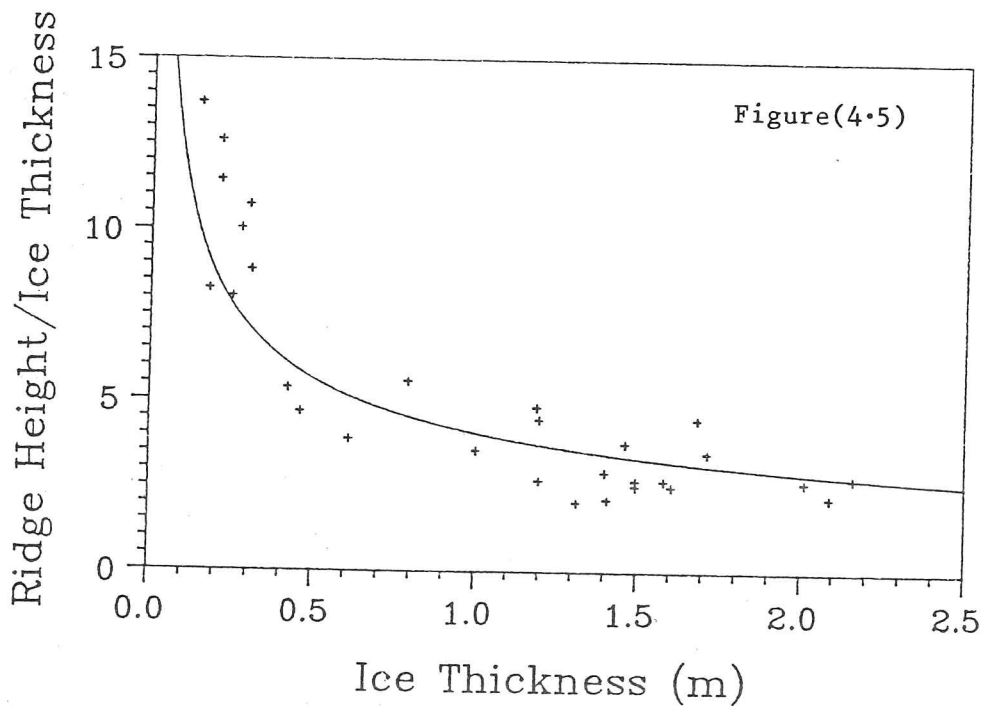
Figure (4.4) shows  $h_2$  plotted against  $h_1$  for the following values of the physical constants.

$$\begin{aligned} \mu^a &= \mu^b = 0.5 \\ \theta^b &= 26^\circ \\ \rho_i &= 922 \text{ kg m}^{-3} \\ \rho_w &= 1025 \text{ kg m}^{-3} \\ n_0 &= 0.3 \\ \bar{g} &= 9.82 \text{ m}^{-2} \\ P^* &= 9000 \text{ Nm}^{-2} \end{aligned}$$

The + signs in figure (4.4) represent the adjusted observations of Tucker and Govoni (1981). Figure (4.5) shows the ratio  $k = h_2/h_1$  plotted against  $h_1$  and indicates the drop in  $k$  as  $h_1$  increases. If  $h_2$  is plotted for values of  $h_1$  outside the range of the Tucker and Govoni (1981) observations (figure 4.6) then a maximum ridge height of about 9m is predicted. This is not consistent with observations that have been made of much larger ridges of about 20m to 30m. The largest observed ridge to date <sup>had a keel draft</sup>  $\Delta$  of 50m (W.K.Lyon, personal communication, 1983). If  $(\mu^a + \mu^b)$  is reduced and  $P^*$  increased, then (24) could account for these large ridges as well as the Tucker and Govoni (1981) observations. However, it is undesirable to reduce  $(\mu^a + \mu^b)$  so that it is no longer within physically realistic limits.

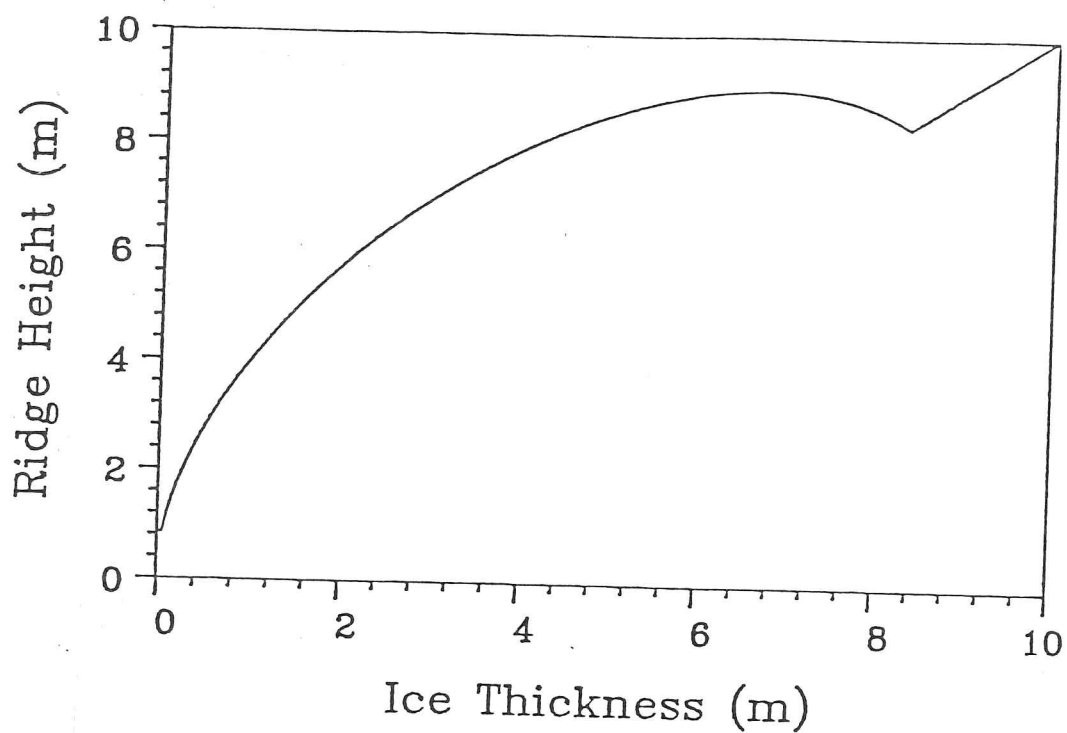


A comparison of the derived ridge height formula  $h_2(h_1)$  with the observations of Tucker and Govoni (1981).



The ratio of ridge height to parent ice thickness - a comparison with the Tucker and Govoni observations showing the observed decrease of this quantity with increasing parent ice thickness.

Figure(4.6)



The height of ridges produced from parent ice of a single thickness according to a simple force model that assumes triangular ridges produced.

It is more likely that the large ridges may be accounted for by the regional variability of  $P^*$  or that they are formed by mechanisms different from those assumed in this section.

#### 4.2.2 Rafting

Rafting occurs when two ice sheets collide in such a way that one of the sheets overrides the other. If both sheets are equally thick, this effectively doubles the ice sheet thickness in a region. Parmerter (1974) calculates that rafting will occur if the ice sheets are thin enough. If they are not then one of them will fracture to form blocks from which a conventional ridge can be built. Parmerter calculates the crossover thickness between ridging and rafting for young ice as 0.17m. This is a value that is consistent with that reported by Kovacs (1972), but still must be taken only as a representative value because of the variability of the physical properties of ice used in its calculation. Kovacs (1972) also reports that ice of 1m has been observed to raft. Rafting is often observed with 40-60 cm thick ice in the Bering Sea due to wave activity.

Since thin ice tends to raft and thick ice to ridge, it may be necessary to modify equation (24) with the condition  $h_1 > 0.17\text{m}$ . Parameterization of rafting may be incorporated into a sea ice model that includes ice thickness redistribution by considering a redistribution of the form

$$h_2 = 2h_1 \quad \text{for } h_1 < 0.17\text{m} \quad (31)$$

Note that the redistribution suggested by (31) does not describe the production of triangular ridges and so must be treated in a different way to equation (24) when considering the ice thickness distribution changes during deformation.

### 4.3 Ice strength

#### 4.3.1 Evaluating ice strength

It is vital to incorporate the idea of ice strength into any dynamic sea ice model. Expressed simply, thin ice is weak and thick is strong. The strength of ice in a model is a measure of its resistance to deformation. The dependence of the resistance on the type of deformation is dealt with in the next section. In this section, we are concerned with the magnitude of, say, the compressive resistance of ice and its dependence on the ice thickness. In fact we consider the ice strength in terms of the more general idea of an ice thickness distribution.

Qualitatively, for a region where the greatest percentage of the area consists of thin ice categories and open water, the ice strength would be small, and ice would thus deform easily. Strong ice would include that near coastal regions which is thick and relatively difficult to deform. The variation in ice strength from strong to weak as one moves seaward, accounts for the shear zone observed in such regions.

Hibler's (1979) two layer sea ice model represents the ice in a region by two quantities; the average ice thickness  $h$ , and the compactness  $A$ . As mentioned before, strength is included by the term

$$P^* = Ph \exp\{-K(1-A)\} \quad (32)$$

The quantity  $(1-A)$  is the amount of open water and  $P$  is an empirically determined constant. The constant  $K$  is taken to be 20. This equation, which has been adopted by subsequent ice modellers (Røed and O'Brien, 1983) expresses, in mathematical terms, the idea that the strength decreases rapidly when even a small amount of open water appears. The notion that the strength increases for thicker ice is included in equation (32) by a linear dependence of the ice strength on the thickness  $h$ . We shall investigate the dependence of the ice strength upon the amount of open water in more detail later. In a general area of pack ice, many different

thicknesses of ice are present, so that during a process of deformation, different thickness categories of ice will be involved. A full description of the ice strength should thus be dependent on the ice thickness distribution  $g(h)$ .

The gravitational potential energy of an area of sea ice containing many thicknesses is

$$PE[g(h)] = C_b \int_0^{\infty} h^2 g(h) dh \quad (33)$$

Following Rothrock (1975) we evaluate the rate of production of potential energy by distribution by differentiating (33) with respect to time and eliminating the time rate of change of  $g(h)$  by using the ice thickness distribution equation (2.39). This gives,

$$C_b \int_0^{\infty} h^2 \dot{\psi} dh \quad (34)$$

The redistribution function  $\dot{\psi}$  can be expressed as

$$\dot{\psi} = |\dot{\epsilon}| \{ \alpha_o(\theta) \delta(h) + \alpha_r(\theta) w_r(h, g) \} \quad (35)$$

where the terms are defined in chapter 2. By substituting (35) into (34) one obtains

$$C_b \int_0^{\infty} h^2 \dot{\psi} dh = |\dot{\epsilon}| \alpha_r(\theta) p_p^* \quad (36)$$

where  $p_p^*$  is defined as

$$p_p^* = c_b \int_0^{\infty} h^2 w_r(h) dh \quad (37)$$

This quantity  $p_p^*$  is the strength of the ice with respect to potential energy considerations. Rothrock (1975) thus regards the strength as the potential energy produced per unit area per unit strain in pure convergence.

By expressing the rate of loss of energy by frictional work, during ice redistribution, in the form

$$R_{\text{fric}} = |\dot{\epsilon}| \alpha_r(\theta) p_f^* \quad (38)$$

Rothrock (1975) obtains an expression for  $p_f^*$ , the strength due to frictional considerations. Firstly, he expresses  $R_{\text{fric}}$  in the form

$$\int_0^{\infty} E_{\text{fric}} R_{\text{area}} dh \quad (39)$$

where  $E_{\text{fric}}$  is the frictional energy loss in ridging per unit area of pack ice fed into the ridge, and  $R_{\text{area}}$  is the rate of loss of this area per unit area per unit width of the ridge. Rothrock (1975) calculates  $E_{\text{fric}}$  by considering a model of ridging, similar to that used in section (4.2), but in which he assumes that ice of thickness  $h$  breaks up during deformation, producing a rubble field of thickness  $kh$ , where  $k$  is taken as a constant. The corresponding strength derived from frictional energy loss considerations, Rothrock (1975) derived as

$$p_f^* = c_f \int_0^{\infty} \frac{h^2 a(h)}{1-(1/k)} dh \quad (40)$$

where

$$c_f = \frac{(\rho_w - \rho_i) \mu^b g}{2 \tan \theta^b} \left( \frac{\rho_i (k-1)}{\rho_w} \right)^2 \quad (41)$$

The total ice strength is given by  $p_p^* + p_f^*$ .

Later we derive expressions for  $p_p^*$  and  $p_f^*$  as in (37) and (40) but based upon the ridge model described previously.

In his multi-layer model Hibler (1980a) calculated the strength numerically, but essentially used the formula given by equation (37). His method consists of artificially increasing the thickness distribution term  $g(h)$  to  $g'(h)$  so that the distribution is no longer normalized to unity, thus

$$\int_0^{\infty} g'(h) dh > 1 \quad (42)$$

If  $g'(h) = (1+\phi)g(h)$ , then by redistributing the thin ice categories of  $g'(h)$ , as described in the section on redistribution theory, so that a new normalized distribution  $g''(h)$  is obtained, the strength may be obtained from the expression

$$p_p^* = (C_b/\phi) \int_0^{\infty} \{g''(h) - g'(h)\} h^2 dh \quad (43)$$

From the definition of the redistributor  $w_r(h)$  of redistribution theory, it may be seen that in this case it is given by

$$w_r(h) = (1/\phi) \{g''(h) - g'(h)\} \quad (44)$$

so that (43) is simply an application of equation (33) for this particular redistributor. Equation (43) may also be seen as the difference in potential energies given by (33) of the distributions  $g''(h)$  and  $g'(h)$ , divided by the increment factor  $\phi$ .

Our aim now is to calculate the strength of a single thickness of ice with the method used by Rothrock (1975), but assuming that ice deforms to produce ridges as described in the previous section. In the process of this we derive expressions for determining the strength  $p^*$  of more general distributions. Equation (37) may be used directly to give the strength  $p_p^*$  once  $w_r(h)$  has been calculated. However, equation (40) must be modified since its form depends on the particular method of ridge production assumed by Rothrock.

Instead of assuming that ice of thickness  $h_1$  ridges to a single valued thickness  $h_2$ , we assume that the ice involved in the ridging process is uniformly distributed between the values  $h_1$  and  $h_2(h_1)$ . If  $h_2$  is the ridge height function introduced previously, (equation 24) then our redistribution assumption is consistent with that of having triangular ridges. An area of ice of one thickness  $h_1$ , has a thickness distribution given by

$$g(h) = \delta(h-h_1) \quad (45)$$

Consider a unit area of ice of thickness  $h_1$  totally converted into ridges. If the resulting distribution is

$$g(h) = \begin{cases} 0 & 0 < h_1 \\ c & h_1 < h < h_2 \\ 0 & h > h_2 \end{cases} \quad (46)$$

then from volume conservation,

$$\int_0^{\infty} h \delta(h-h_1) dh = \int_{h_1}^{h_2} c h \, dh \quad (47)$$

We thus obtain

$$c = \frac{2h_1}{h_2^2 - h_1^2} \quad (48)$$

By conserving volume in this way, and noting that the redistributor  $w_r(h)$  is normalized to -1 in that

$$\int_0^{\infty} w_r(h) dh = -1 \quad (49)$$

it is possible to obtain the redistributor for the distribution given by (45) as

$$\begin{aligned} w_r(h) = & -\frac{h_2 + h_1}{h_2 - h_1} \delta(h - h_1) \\ & + \frac{h_1}{(h_2 - h_1)^2} [H(h - h_1) + H(h_2 - h)] \end{aligned} \quad (50)$$

$H$  is the Heaviside step function defined by

$$H(h) = \begin{cases} 1 & h > 0 \\ 0 & h < 0 \end{cases} \quad (51)$$

We recapitulate here on the meaning of the redistributor  $w_r(h)$ . For any ice distribution  $g(h)$ , the redistributor  $w_r[g(h);h]$  tells us the relative changes that the various categories of ice that make up  $g(h)$  undergo when the ice deforms in pure compression. By specifying the type of ridges to be formed in deforming an initially uniform ice sheet, we essentially specify the redistributor for the distribution (45). Equation (50) can be compared with the general expression for the mechanical redistributor  $w_r(h)$  given by

$$w_r(h) = \frac{-a(h) + z(h)}{-\int_0^{\infty} \{-a(h) + z(h)\} dh} \quad (52)$$

so that

$$a(h) = \delta(h-h_1) \quad (53)$$

is the distribution of ice that is ridged, and

$$z(h) = \frac{h_1}{h_2^2 - h_1^2} [H(h-h_1) + H(h_2-h)] \quad (54)$$

is the distribution of ice formed when  $a(h)$  is redistributed. Since  $w_r(h)$  is normalized, the first and second terms in equation (50) give the actual areas of ice involved in ridging to form the distribution (46). We can immediately obtain the strength  $p_p^*$  by substituting (50) in (37) to obtain

$$p_p^* = \frac{1}{3} C_b h_1 (2h_2 + h_1) \quad (55)$$

This gives the strength  $p_p^*$  of the  $\delta$ -function thickness distribution. For a general distribution  $g(h)$ , and an assumed distribution of the ice involved in ridging, it is possible to calculate the new ice distribution  $z(h)$  and proceed as before to obtain  $p_p^*$  from equation (37). However, a more direct method is to note from equations (45) to (48) that a unit area of ice of thickness  $h_1$  which ridges, undergoes a potential energy change given by

$$C_b \int_{h_1}^{h_2} h^2 \frac{2h_1}{h_2^2 - h_1^2} dh - C_b \int_0^{\infty} h^2 \delta(h-h_1) dh \quad (56)$$

where the potential energies for the distributions before and after ridging are given by equation (33). The expression (56) simplifies to

$$\frac{1}{3} C_b h_1 \frac{h_2 - h_1}{h_2 + h_1} (2h_2 + h_1) \quad (57)$$

Redistribution of ice occurs when  $g(h)$  becomes non-normalized by the introduction of areas of various thickness categories by advection. The function  $a(h)$  enables us to deduce from  $g(h)$  the distribution of ice thicknesses that are lost when ridging occurs. The actual areas of ice involved in the redistribution process depend upon the amount by which  $g(h)$  becomes non-normalized. The function  $a(h)$  gives us only the relative area losses from each of the thickness levels.

Suppose that it is known by how much each thickness category is reduced through redistribution and that these areas are described by the distribution  $a'(h)$ . Thus the area of ice lost from the  $(h, h+dh)$  thickness level is given by  $a'(h)dh$ . Since not all the ice in a distribution would be expected to ridge, the distribution  $a'(h)$  is not normalized to 1, and in fact

$$\int_0^{\infty} a'(h) dh < 1 \quad (58)$$

If  $a'(h)$  is taken to be the areal distribution that is lost when the distribution  $(1+\phi)g(h)$  is renormalized, then by using Hibler's method for determining ice strength from equation (43) we have

$$p_p^* = \frac{1}{3} \frac{C_b}{\phi} \int_0^{\infty} h_1 \frac{h_2 - h_1}{h_2 + h_1} (2h_2 + h_1) a'(h_1) dh_1 \quad (59)$$

To determine the frictional strength,  $p_f^*$  of a general distribution  $g(h)$  in terms of  $a'(h)$ , we first note, as does Rothrock (1975), that the frictional energy loss per unit area loss,  $E_{fric}$ , is given by the frictional force per unit ridge width. Hence, from equation (20)

$$E_{\text{fric}} = C_f(h_2 - h_1)^2 \quad (60)$$

Now, we note that during deformation described by  $|\dot{\epsilon}|$  and  $\theta$ , the rate of area loss of ice of thickness  $(h_1, h_1 + dh_1)$  is

$$R_{\text{area}} = |\dot{\epsilon}| \alpha_r(\theta) a'(h_1) dh_1 \quad (61)$$

so that  $R_{\text{fric}}$  becomes, from equation (39), (60), (61) and (38),

$$\frac{|\dot{\epsilon}| \alpha_r(\theta)}{\phi} \int_0^\infty C_f(h_2 - h_1)^2 a'(h_1) dh_1 = |\dot{\epsilon}| \alpha_r(\theta) p_{\text{f}}^* \quad (62)$$

which immediately gives  $p_{\text{f}}^*$ . For the  $\delta$ -function thickness distribution,  $a'(h)$  is, from the first term in equation (50), given by

$$a'(h_1) = \frac{h_2 + h_1}{\phi(h_2 - h_1)} \delta(h - h_1) \quad (63)$$

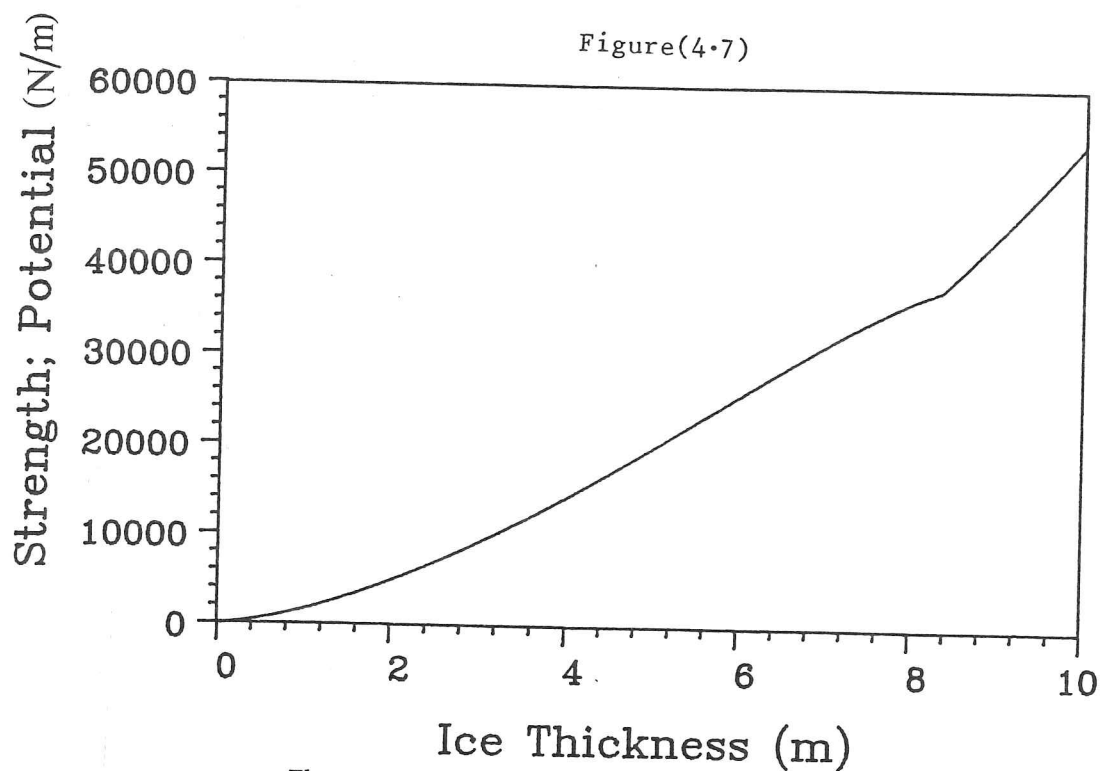
By substituting (63) into (62) and comparing the result with equation (38), the frictional strength is found to be

$$p_{\text{f}}^* = C_f(h_2^2 - h_1^2) \quad (64)$$

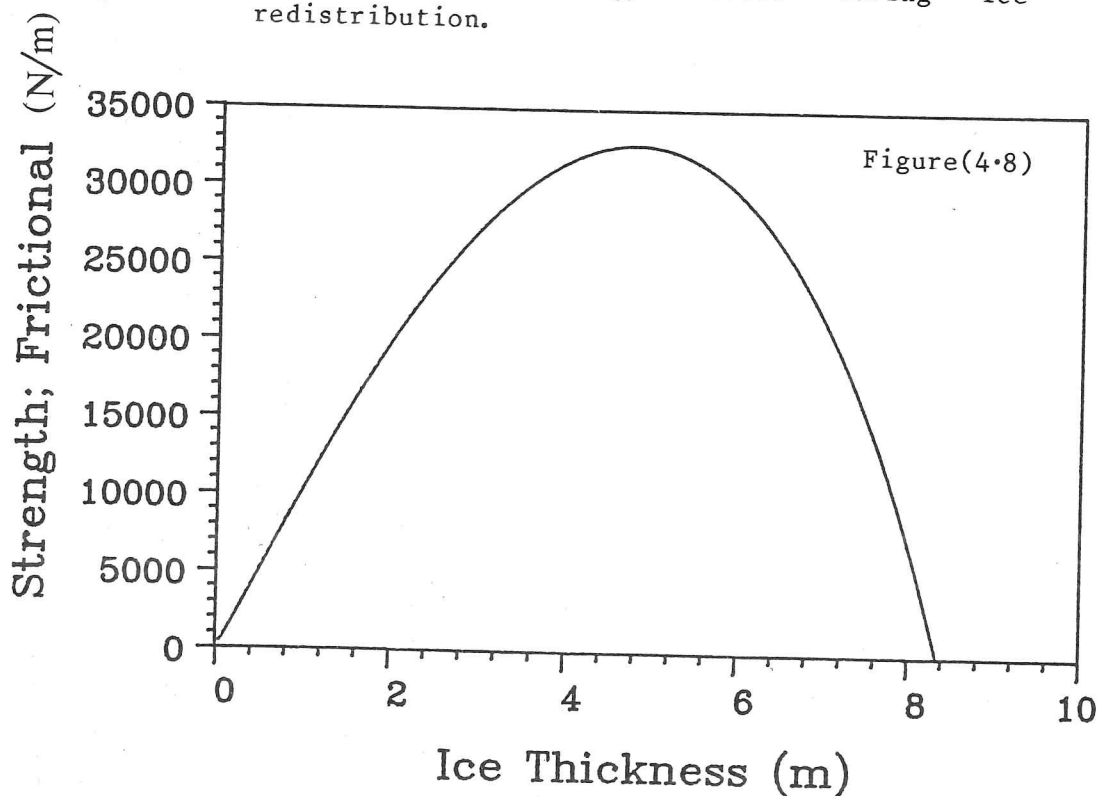
The total strength of an area of pack of a single thickness  $h_1$  is simply

$$\begin{aligned} p^* &= p_{\text{p}}^* + p_{\text{f}}^* \\ &= \frac{1}{3} C_b h_1 (2h_2 + h_1) + C_f(h_2^2 - h_1^2) \end{aligned} \quad (65)$$

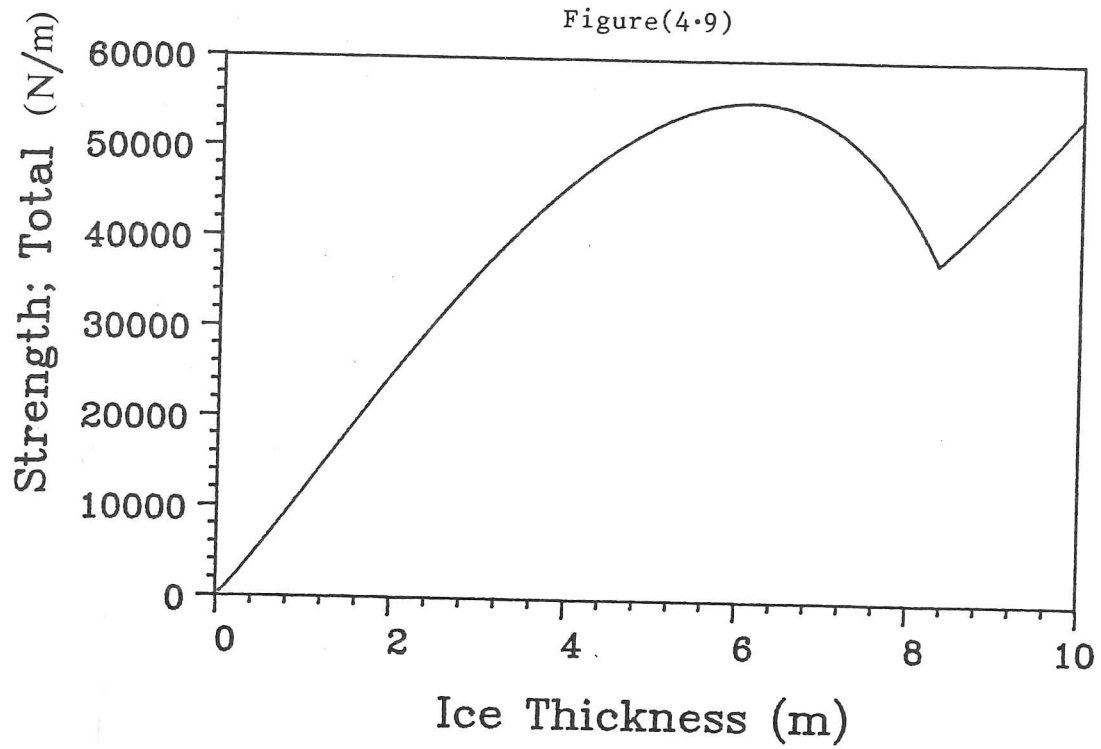
Figures (4.7) and (4.8) show the two components of the predicted ice strength for ice of uniform thickness. Figure (4.9) shows the total strength.



The component of the strength of a single thickness of ice obtained from a consideration of the potential energy losses during ice redistribution.



As above but only the part of the strength obtained by considering the frictional energy losses during redistribution.



The strength of a single thickness of ice according to ice redistribution theory when assuming ridges produced by deformation are of a height predicted by force model.

### 4.3.2 The effect of open water on ice strength

We have employed Rothrock's (1975) method to obtain the strength of ice of a single thickness. If a certain amount of open water is present, then a considerably lower strength would be expected.

Take as the initial distribution

$$g(h) = \alpha \delta(h) + (1-\alpha) \delta(h-h_1) \quad (66)$$

This distribution represents a fraction  $\alpha$  of the area as open water, and the rest, ice of thickness  $h_1$ . If the distribution is subjected to pure compression then some open water will be lost and some of the ice will ridge. There is a choice in determining the relative amounts of open water loss and ice ridging. This choice can be expressed by a free parameter  $\beta$  in the annihilator  $a(h)$  of the distribution (66). Thus  $a(h)$  is expressed

$$a(h) = \beta \delta(h) + (1-\beta) \delta(h-h_1) \quad (67)$$

We consider two methods of evaluating  $\beta$  later. Proceeding as before and noting that if the distribution (67) were to ridge totally, a distribution

$$z(h) = \begin{cases} 0 & h < h_1 \\ \frac{2(1-\beta)h_1}{h_2^2 - h_1^2} & h_1 < h < h_2 \\ 0 & h > h_2 \end{cases} \quad (68)$$

would be produced. Since

$$-\int_0^\infty \{-a(h)+z(h)\} dh = \frac{h_2+(2\beta-1)h_1}{h_2+h_1}, \quad (69)$$

we can write the redistributor as

$$\begin{aligned}
w_r(h) = & \frac{h_2+h_1}{h_2+h_1(2\beta-1)} [-\beta\delta(h)-(1-\beta)\delta(h-h_1)] \\
& + \frac{(1-\beta)h_1}{h_2^2-h_1^2} \{H(h-h_1)+H(h_2-h)\}
\end{aligned} \quad (70)$$

Equation (37) then gives the potential energy derived strength as

$$p_p^* = \frac{\frac{1}{3} C_b(1-\beta)(2h_2+h_1)(h_2-h_1)h_1}{h_2-h_1+2\beta h_1} \quad (71)$$

The frictional strength  $p_f^*$  is found from the redistributor to be (using analysis similar to that used in deriving (64))

$$p_f^* = \frac{C_f(h_2-h_1)^2 h_1(h_2+h_1)(1-\beta)}{h_2+h_1(2\beta-1)} \quad (72)$$

Writing the total strength of the distribution containing a fraction  $\alpha$  of open water as  $p^*(\alpha)$ , we see from (65), (71) and (72) that

$$p^*(\alpha) = \frac{(1-\beta)(h_2-h_1)}{h_2-h_1+2\beta h_1} p^*[\delta(h-h_1)] \quad (73)$$

When  $\beta$  is known as a function of  $\alpha$ , (73) demonstrates the effect on the ice strength of the presence of open water.

Thorndike et al (1975) suggest that the distribution of ice that becomes ridged may be obtained by weighting the original distribution with the factor

$$\frac{2}{G^*} \max \left\{ 1 - \frac{G(h)}{G^*}, 0 \right\} \quad (74)$$

where  $G(h)$  is the cumulative thickness distribution defined by

$$G(h) = \int_0^h g(h') dh' \quad (75)$$

and  $G^*$  is a constant usually taken to be 0.15. This means that 15% of the ice undergoes ridging, with the thinner ice ridging in preference to the thicker. For the initial distribution (66), the distribution ridged is thus

$$a(h) = \frac{\alpha}{G^*} \left( 2 - \frac{\alpha}{G^*} \right) \delta(h) + \left( 1 - \frac{\alpha}{G^*} \right)^2 \delta(h - h_1) \quad (\alpha < G^*) \quad (76)$$

so that comparing with (67),

$$\beta = \frac{\alpha}{G^*} \left( 2 - \frac{\alpha}{G^*} \right) \quad (\alpha < G^*) \quad (77)$$

If  $\alpha > G^*$ , then only open water is removed and no ice is ridged, so that

$$a(h) = \delta(h) \quad (78)$$

implying that

$$\beta = 1 \quad (\alpha > G^*) \quad (79)$$

With  $\beta$  given by (77) and (79), the strength  $p^*(\alpha)$  given by (73) becomes

$$p^*(\alpha) = \frac{(G^* - \alpha)^2}{G^{*2} + \frac{2\alpha(2G^* - \alpha)}{k - 1}} p^* [\delta(h - h_1)] \quad (\alpha < G^*) \quad (80)$$

and

$$p^*(\alpha) = 0 \quad (\alpha > G^*) \quad (81)$$

where  $k = h_2(h_1)/h_1$ . Thus with the Thorndike *et al* (1975) assumptions, the strength drops from the value  $p^*[\delta(h-h_1)]$  as the amount of open water increases until it reaches zero when  $\alpha = 1-A = G^*$ . Figure (4.10) shows this drop in strength for three different ice thicknesses, with  $G^*$  taken to be 15%.

The picture of a floe field introduced in section (3.1) may be used to give a method of calculating  $\beta$  to give another estimate of the ice strength when open water is present. The factor  $\beta$  depends on how much ice area is lost during each floe collision. Thus we must extend our ideas of collisions in terms of the circular floe model, in which a collision between two floes is assumed to produce one floe consisting of two touching discs with any ice area lost accounted for independently in the ice redistribution equation. We must modify this assumption in order to calculate  $\beta$ .

Suppose that two floes of radius  $r$  and thickness  $h_1$  collide and that a triangular ridge of length  $l(r)$  and height  $h_2(h_1)$  is produced. For our original picture of a floe collision  $l(r)$  would be zero no matter how large the floes. It is more reasonable to suppose that  $l(r)$  depends on the floe size. A linear dependence would be expected on the basis that fields of floes of differing radii appear similar. We thus obtain

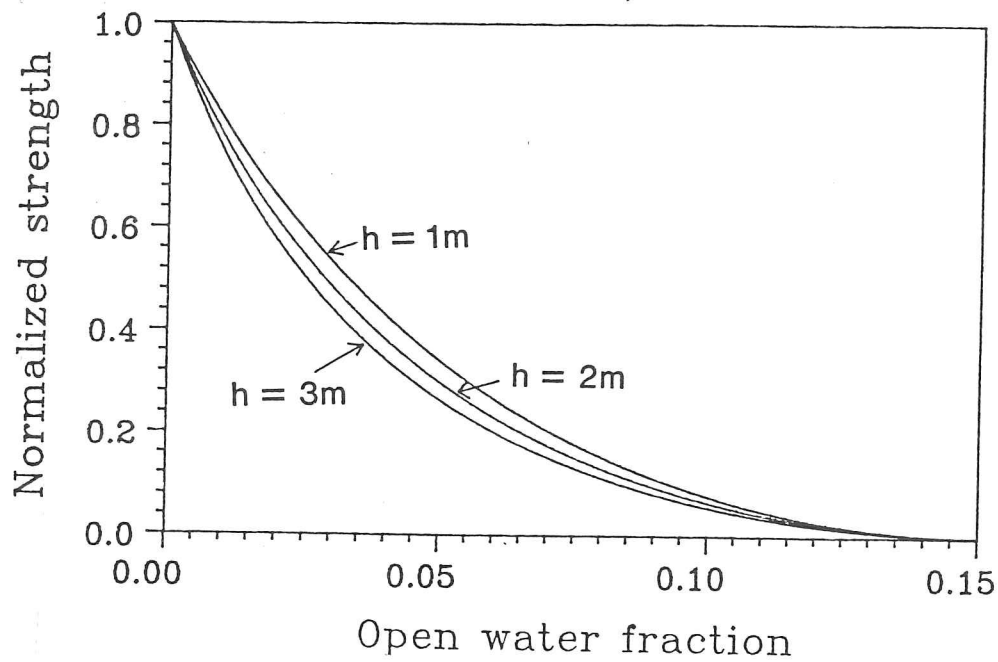
$$l = cr \quad (82)$$

where  $c$  is a constant. For floes touching at a single point  $c = 0$ . Only for elongated floes colliding side-on could a ridge larger than  $2r$  be produced so that in normal conditions

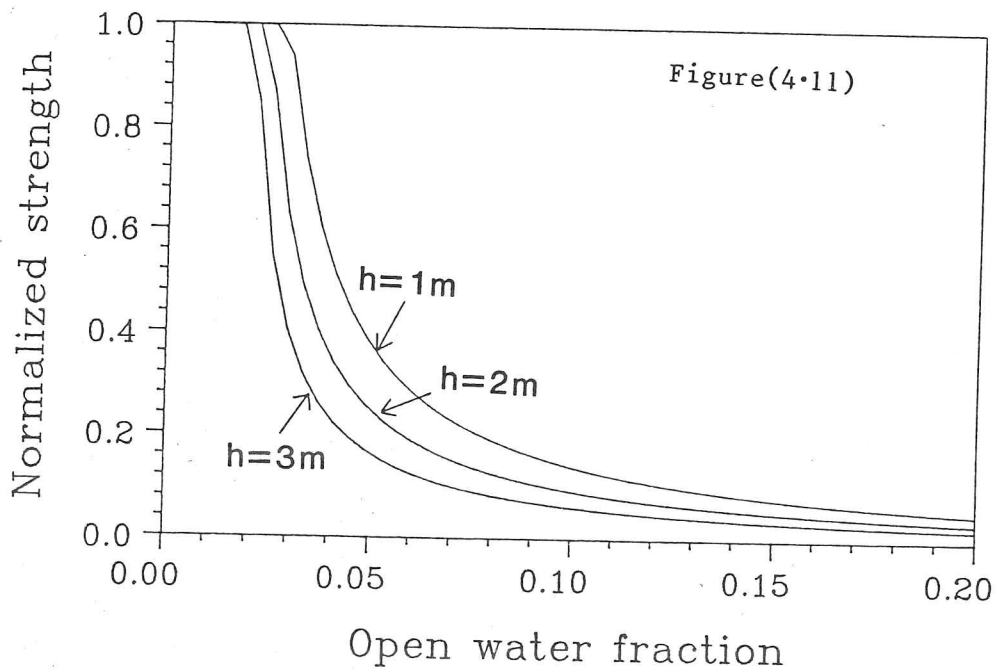
$$0 < c < 2 \quad (83)$$

Until measurements are made relating floe size to ridge length, the value  $c$  must be guessed.  $c = 1$  or perhaps a little less would seem reasonable.

Figure(4.10)



The drop in strength with increased open water amount according to the Thorndike et al (1975) ice distribution theory.



The drop in strength as the amount of open water is increased when floe size is taken into account.

The volume of ice in a length  $l$  of ridge of the type described in section (4.2) would be

$$\frac{\rho_i}{\rho_w} (h_2 - h_1)^2 \cot \theta^b l(r) \quad (84)$$

If the area lost is  $A_r$ , then by equating volumes

$$A_r h_1 = \frac{\rho_i}{\rho_w} (h_2 - h_1)^2 \cot \theta^b l(r) \quad (85)$$

Now the rate of collisions per unit area found in section (3.3) is

$$\frac{2LA^2 |\dot{\epsilon}| \alpha(\theta)}{\pi r^2} \quad (86)$$

So that the rate of loss of area per unit area is

$$\frac{2LA^2}{\pi r^2} |\dot{\epsilon}| \alpha(\theta) \frac{\rho_i}{\rho_w} \frac{(h_2 - h_1)^2}{h_1} \cot \theta^b l(r) \quad (87)$$

which can be equated with (see equation (67))

$$(1 - \beta) |\dot{\epsilon}| \alpha_r(\theta) \quad (88)$$

to give

$$\beta(\alpha) = 1 - \frac{2L(1-\alpha)^2 \rho_i (h_2 - h_1)^2 \alpha(\theta)}{\pi r \rho_w h_1 \alpha_r(\theta)} \cot \theta^b c \quad (89)$$

The strength of the ice predicted by this method is thus obtained by substituting this expression for  $\beta(\alpha)$  into equation (73). Figure (4.11)

shows the resulting strengths for floes of radius 300m and for three thicknesses of ice, in which also,  $\alpha(\theta) = \alpha_r(\theta)$  is assumed. This assumption is discussed in the next section. Comparing figure (4.10) with figure (4.11), we see a rather sharper drop in ice strength as the open water amount increases, although the strength never drops to zero due to collisions occurring, albeit infrequently, even in low concentrations. A maximum strength is predicted until open water exceeds about 3% in this case because the number of collisions predicted for the high ice concentrations, becomes too large for a full sized ridge to form for each collision.

#### 4.4 Ice interaction

##### 4.4.1 Introduction

In this section, we are concerned with the determination of the ice interaction term,  $E$ , in the momentum equation. This term depends on the velocity gradients that occur during ice deformation. Energy losses accompany such deformation so that the ice behaves as if it has a viscosity. No energy losses of this kind occur during pure translation, only when there is shear or divergence.

Stresses in a material can be calculated by considering the energy losses associated with the physical processes that accompany deformation. If the energy loss during some process depends on the amount of deformation but not on the rate at which the deformation occurs, then the resulting stresses are independent of the magnitude of the strain rate. A material with this property is described as plastic.

Ice ridging is a small scale physical process that occurs during large scale deformation of pack ice. Assume, such as in Parmerter and Coon's (1972) ridge building model that the energy required to form a ridge depends on its potential energy and the work done against frictional forces during its production. The amount of energy thus needed is independent of the rate at which the ridge is built, supporting the plastic hypothesis for pack ice.

In a two-dimensional ice field, the stress state can be represented by the stress tensor with components  $\sigma_{ij}$  which have dimensions of force per unit length. Stress invariants  $\sigma_I$  and  $\sigma_{II}$  can be defined in a way similar to the strain rate invariants  $\dot{\epsilon}_I$  and  $\dot{\epsilon}_{II}$ . Thus

$$\sigma_I = \frac{1}{2}(\sigma_{11} + \sigma_{22}) \quad (90)$$

$$\sigma_{II} = \frac{1}{2}\sqrt{(\sigma_{22} - \sigma_{11})^2 + 4\sigma_{12}\sigma_{21}} \quad (91)$$

where  $-\sigma_I$  is the pressure component of the ice stress and  $\sigma_{II}$  is a measure of the shear stress.

The stress  $\sigma_{ij}$  can be related to the strain rate  $\dot{\epsilon}_{ij}$  by a constitutive equation of the form

$$\sigma_{ij} = 2\eta\dot{\epsilon}_{ij} + \{\zeta - \eta\}\dot{\epsilon}_{kk}\delta_{ij} - \frac{1}{2}p^*\delta_{ij} \quad (92)$$

where  $\eta$  and  $\zeta$  are the shear and bulk viscosities and  $p^*$  is a pressure or ice strength term. The stress  $\sigma_{ij}$  gives  $F$  according to the rule

$$F_i = \frac{\partial \sigma_{ij}}{\partial x_j} \quad (93)$$

The stress depends on the strain rate in a more complicated way than at first equation (92) suggests. This is because the viscosity terms  $\eta$  and  $\zeta$  themselves are functions of  $\dot{\epsilon}_{ij}$ . The way  $\eta$  and  $\zeta$  depend on  $\dot{\epsilon}_{ij}$  is determined by the yield function chosen to describe the way the ice behaves plastically.

For a two-dimensional plastic medium, a yield function  $F(\sigma_I, \sigma_{II})$  can be defined such that no strain occurs for values of  $\sigma$  with  $F < 0$  and that the medium yields when  $F = 0$ . The curve in the  $(\sigma_I, \sigma_{II})$  plane defined by  $F(\sigma) = 0$  is known as a yield curve. It is plotted in the  $(\sigma_I, \sigma_{II})$  plane which covers all possible stress states in two dimensions. The curve defines all the possible stress states that can exist in the medium when it is deforming. The normal flow rule states that the stress at a point on

the yield curve occurs when the material is deforming with a strain rate which has a direction normal to the yield curve at that point. The normal flow rule can be deduced from the assumption that non-negative work is done on the material when the point representing its stress state passes along a closed curve (Drucker 1950). Another general property of yield curves implied by this is that they are convex. This assumption implies a further property that the directions of the  $(\dot{\epsilon}_I, \dot{\epsilon}_{II})$  axes and the  $(\sigma_I, \sigma_{II})$  axes coincide. Because the sign of the shear rate is arbitrary, so the yield curve would be expected to be symmetric about the  $\sigma_I$  axis.

Having mentioned some of the general properties of yield curves, we go on to determine a particular example from physical considerations, in particular the idea that the ice is composed of finite sized floes that interact by colliding. The viscosities that this yield curve implies are then calculated so that they may be used in equation (92) to give  $\sigma_{ij}$  from which  $F$  may be found from (93).

#### 4.4.2 A yield curve

In this section we aim to derive the viscosities that could be used in a viscous plastic sea ice model, based on the notion that the ice field is composed of finite floes.

The collision rate given by (86) is a product of kinematic variables  $|\dot{\epsilon}|$  and  $\alpha(\theta)$  and variables associated with the physical structure of the floe field,  $A$ ,  $n$  and  $r$ . We assume that ice ridges are produced as a result of collisions and that the rate of production of ridges, and hence the rate of loss of energy, is proportional to  $|\dot{\epsilon}|\alpha(\theta)$ , the kinematic term in (86). Thus

$$\sigma_I \dot{\epsilon}_I + \sigma_{II} \dot{\epsilon}_{II} \propto |\dot{\epsilon}| \alpha(\theta) \quad (94)$$

The ridging coefficient  $\alpha_r(\theta)$  used by Rothrock (1975) in (2.65) is normalized so that  $\alpha_r(\pi) = 1$ . The quantity  $\alpha(\theta)$  is likewise normalized so by comparing (94) with (2.65), we can write

$$\sigma_1 \dot{\epsilon}_1 + \sigma_n \dot{\epsilon}_n = |\dot{\epsilon}| \alpha(\theta) p^* \quad (95)$$

Equating  $\alpha(\theta)$  and  $\alpha_r(\theta)$  is the simplest possible assumption we can make about these functions. There are many points that should be included when making a fuller study of ice interaction. Firstly, the model used in this calculation does not incorporate an ice thickness distribution except that the amount of open water is specified. Thus we cannot properly include ridging. The occurrence of collisions gives information regarding the initiation of a ridge but not its subsequent development. In particular, in this model, less ridging occurs as a result of glancing collisions because of the smaller area in which a floe has to be for it to collide, but no account is taken of smaller ridges being produced as a result, requiring less energy. The derivation of  $\alpha(\theta)$  is based on a model of the pack that is most applicable in the case where there is enough open water present to significantly reduce the ice strength, i.e., its resistance to pure compression. Thus in fact we are dealing with the case in which there is very little ice ridge formation. The importance of  $\alpha(\theta)$  is that it gives a indication of relative amounts of ridging for the various types of flow, even though the amount of ridging is small. It is  $\alpha(\theta)$  that will be used to give the shape of a plastic yield curve whereas its size, which depends on the ice strength, is not determined by this model. The function  $\alpha_r(\theta)$  in the case where there is no open water and the ice strength is high, cannot be deduced from a collision model.

Despite all these difficulties, further examination of the derivation of  $\alpha(\theta)$  in section (3.2) reveals an unexpected bonus. Suppose that a continuous ice cover is deforming with uniform spatial gradients. Suppose also that the ice cannot support tension so that open water is produced by divergence with no loss of energy. Then the loss of area of ice due to ridging from a circular region  $2r$  in diameter is given by (3.22). Thus the rate of loss of area due to ridging per unit area (which defines  $|\dot{\epsilon}| \alpha_r(\theta)$ ) is  $|\dot{\epsilon}| \alpha(\theta)$ . Hence  $\alpha_r(\theta) = \alpha(\theta)$ . Thus we see that although  $\alpha(\theta)$  refers to the ridging amount for weak ice in which there is a significant amount of open water, it may also refer to that for a continuous ice cover. The intermediate cases, such as when the ice cover consists of highly compacted floes, require further study.

An attempt to find a function  $\alpha_r(\theta)$  from satellite observations has been made (Pritchard and Coon 1981) and the following function has been suggested as a fairly good representation of the situation.

$$\alpha_r(\theta) = \begin{cases} 0 & 0 \leq \theta \leq \pi/3 \\ 1 - 3\theta/2\pi - \cos\theta & \pi/3 < \theta \leq 2\pi/3 \\ -\cos\theta & 2\pi/3 < \theta \leq \pi \end{cases} \quad (96)$$

The comparison between  $\alpha_r(\theta)$  given by (96) and  $\alpha(\theta)$  as evaluated in (3.23) is shown in figure (4.12). The functions differ slightly and in particular, equation (96) predicts no ice interaction for strain rates with  $\theta$  in the range  $(\pi/4) < \theta < (\pi/3)$  whereas the derived function  $\alpha(\theta)$  does indicate some interaction in this range.

By considering general properties of plastic materials, Drucker (1950) derived the normal flow rule, which specifies that for a stress on the yield curve,  $\theta$  is equal to the angle between the normal to the yield curve at that point and the  $\sigma_1$  axis, and can be written in the form

$$\dot{\epsilon}_1 = \lambda \left. \frac{\partial F}{\partial \sigma_1} \right|_{F=0}, \quad \dot{\epsilon}_{11} = \lambda \left. \frac{\partial F}{\partial \sigma_{11}} \right|_{F=0} \quad (97)$$

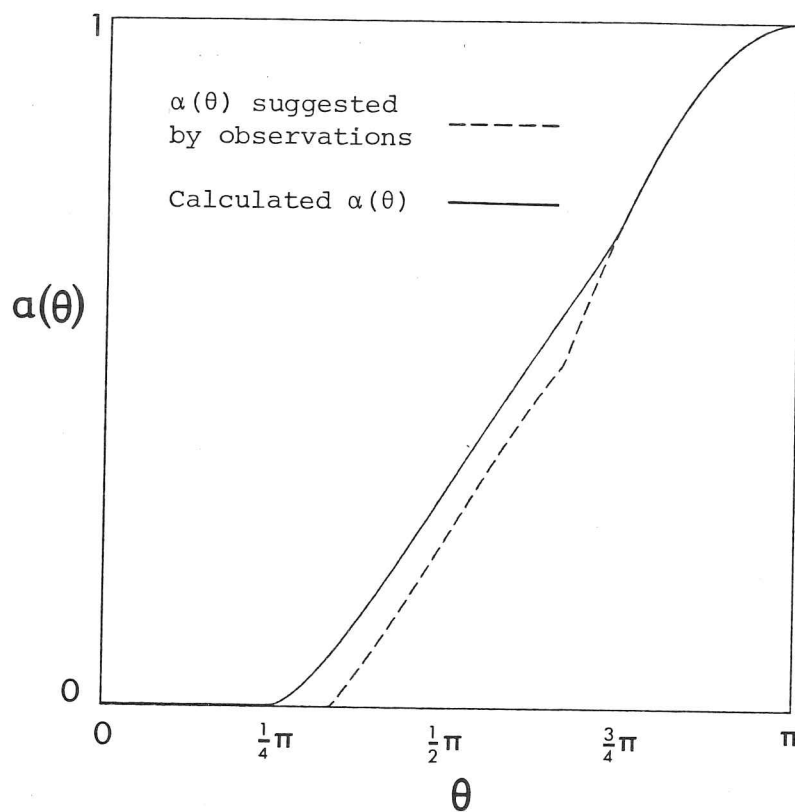
The normal flow rule states nothing about the magnitude of  $\dot{\epsilon}_1$ , only its direction with respect to the  $\dot{\epsilon}_1$  and  $\dot{\epsilon}_{11}$  axes. Hence  $\lambda$  is just a constant that remains undetermined.

The energy equation (95) can be written (Rothrock 1975)

$$\sigma_{11} = -\cot\theta \sigma_1 + \frac{p^* \alpha(\theta)}{\sin\theta} \quad (98)$$

where  $\alpha(\theta)$  is given by (3.23) and the normal flow rule is expressed in the form

Figure(4.12)



The function  $\alpha(\theta)$  giving the relative amounts of area loss through ridging as a function of the deformation type.

$$\frac{d\sigma_{II}}{d\sigma_I} = -\cot \theta \quad (99)$$

where  $\sigma_{II}$  has been regarded as a function of  $\sigma_I$ .

Equation (98) defines a family of straight lines in the  $(\sigma_I, \sigma_{II})$  plane with the parameter  $\theta$ . The envelope of this family of lines satisfies (99) and is thus the yield curve. For  $0 < \theta < \frac{1}{4}\pi$  the lines all pass through the origin and for  $\frac{3}{4}\pi < \theta < \pi$  they all pass through the point  $(-p^*, 0)$ . For  $\frac{1}{4}\pi < \theta < \frac{3}{4}\pi$ ,  $\theta$  can be eliminated from (99) and (98) to give

$$\sigma_{II} = \left\{ \frac{d\sigma_{II}}{d\sigma_I} \sigma_I - \frac{p^*}{\pi} \right\} \cos^{-1} \left( -\frac{d\sigma_{II}}{d\sigma_I} \right) \frac{d\sigma_{II}}{d\sigma_I} + \sqrt{1 - \left( \frac{d\sigma_{II}}{d\sigma_I} \right)^2} \quad (100)$$

Since the yield curve is the envelope of the straight line solutions of (98) we require the singular solution of the differential equation (100) which is

$$\sigma_{II} = -\frac{p^*}{\pi} \sin \left[ \frac{\pi}{p^*} \sigma_I \right] \quad (101)$$

The full yield curve is symmetric about the  $\sigma_I$  axis and is thus as shown in figure (4.13).

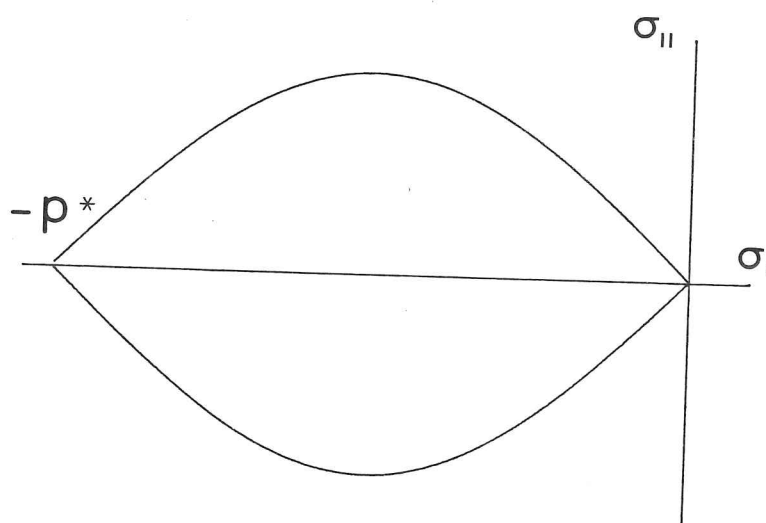
The pointed ends of the yield curve indicate that a range of values of  $\theta$  rather than a single value give rise to a particular stress.

To calculate the bulk and shear viscosities that this yield curve implies we first note that the expression for the stress tensor in equation (92) gives

$$\sigma_I = \zeta \dot{\epsilon}_I - \frac{1}{2} p^* \quad (102)$$

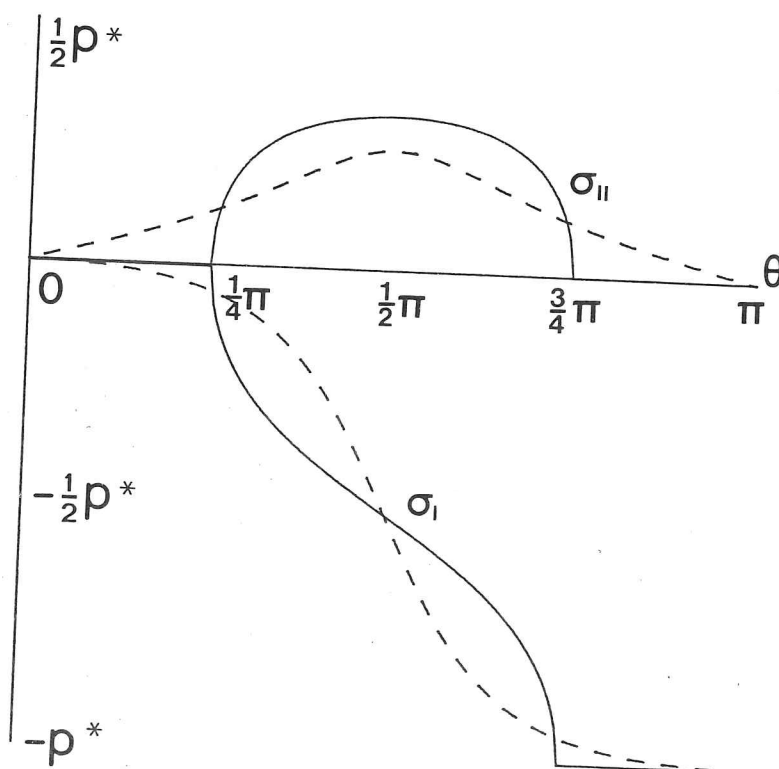
and

Figure(4.13)



The derived sine wave lens yield curve.

Figure(4.14)



The shear stress and negative pressure as a function of the type of deformation as implied by the sine wave lens yield curve. The dashed line shows the same for an elliptical yield curve of eccentricity 2.

$$\sigma_{\parallel} = \eta \dot{\epsilon}_{\parallel} \quad (103)$$

For  $\frac{1}{4}\pi < \theta < \frac{3}{4}\pi$ , we use the flow rule in the form of equation (97) to obtain

$$\dot{\epsilon}_1 = \lambda \pi \cos\left(\frac{\pi}{p^*}\right) \quad (104)$$

and

$$\dot{\epsilon}_{\parallel} = \lambda \pi \quad (105)$$

Thus

$$\sigma_1 = -\left(\frac{p^*}{\pi}\right) \cos^{-1}\left(\frac{\dot{\epsilon}_1}{\dot{\epsilon}_{\parallel}}\right) \quad (106)$$

The minus sign occurs so that the inverse cosine function can take its principal value. From (101) and (106) we obtain

$$\sigma_{\parallel} = \frac{p^*}{\pi} \frac{\sqrt{\dot{\epsilon}_{\parallel}^2 - \dot{\epsilon}_1^2}}{\dot{\epsilon}_{\parallel}} \quad (\dot{\epsilon}_{\parallel} > 0) \quad (107)$$

Comparing (106) and (107) with (102) and (103) we obtain the required viscosities,

$$\eta = \frac{p^*}{\pi} \frac{\sqrt{\dot{\epsilon}_{\parallel}^2 - \dot{\epsilon}_1^2}}{\dot{\epsilon}_{\parallel}^2} \quad (108)$$

$$\zeta = \frac{p^*}{2\dot{\epsilon}_1} - \frac{p^*}{\pi\dot{\epsilon}_1} \cos^{-1}\left(\frac{\dot{\epsilon}_1}{\dot{\epsilon}_{\parallel}}\right) \quad (109)$$

valid for  $\dot{\epsilon}_{\parallel} > 0$  and  $\frac{1}{4}\pi < \theta < \frac{3}{4}\pi$ . For  $\theta < \frac{1}{4}\pi$  the viscosities are  $\eta = 0$  and  $\zeta = p^*/2\dot{\epsilon}_1$ , and for  $\frac{3}{4}\pi < \theta < \pi$  we have  $\eta = 0$  and  $\zeta = -p^*/2\dot{\epsilon}_1$ , which are the viscosities at the end points of the yield curve.

Figure (4.14) shows the stresses  $\sigma_1$  and  $\sigma_{11}$  as functions of  $\theta$ . The dashed curves are the results obtained from Hibler's (1979) elliptical yield curve with  $e = 2$ .

The similarities in the stress curves between those derived from the sine wave yield curve and Hibler's elliptical yield curve, reflect the similarities in the shapes of the yield curves themselves. Both satisfy the deductions from Drucker's (1950) hypothesis regarding plastic materials, in that they are closed convex curves. In addition, they both pass through the origin and the point  $(-p^*, 0)$ .

For the sine wave yield curve zero stress occurs for  $\theta < \frac{1}{4}\pi$  for which  $\dot{\epsilon}_1 > \dot{\epsilon}_{11}$ . In this state no collisions occur and leads of all orientations within the pack ice open up.

One conclusion that can be drawn from the shape of the sine wave lens yield curve is that as long as the convergence is larger than the shear, then the actual value of the shear has no effect on the ice rheology, and similarly, if the divergence is larger than the shear, then the pack ice is essentially drifting freely and the ice interaction term is zero.

If we assume that energy is lost through ridging in proportion to the area loss in the regions where neighbouring points approach, and that where neighbouring points move apart, there is no energy loss, then a sine wave lens yield curve is implied. Thus, compared to other yield curves, the sine wave lens yield curve makes the least number of assumptions about the nature of the physical processes involved in ice deformation, so that it is a canonical yield curve. If, for instance, account is taken of the differing types of ridges produced in pure compression and in shear, then a modified yield curve would be expected.

## 5. INCORPORATING THEORY INTO NUMERICAL CODE

### 5.1 Introduction

The theory that has been developed in the previous chapters must be modified before it can be included into a numerical model. There are a number of reasons for this, of which perhaps the most important is the necessity to construct discrete versions of continuous functions, such as the ice thickness distribution. Integrals become finite sums, necessarily incurring certain amounts of inaccuracies. During the development of the code, techniques can be utilized that minimize such errors.

In this chapter we also mention some of the factors that have to be included in the code that are not connected with any real physics but are necessary only to avoid non-physical results.

During a redistribution of ice thicknesses various amounts of ice are lost from each category. The amounts lost determine the amounts of ice added to higher categories as well as the potential energy changes and frictional energy losses. Thus by obtaining coefficients giving the amounts of ice and energy produced by destroying unit areas of each category, the necessary changes to each of these quantities may be evaluated for arbitrary deformations. The first part of this chapter deals with the evaluation of these coefficients.

### 5.2 Ice thickness distribution

### 5.2.1 Representation of the ice thickness distribution

Solving the thickness distribution equation analytically is not possible because of its highly complex nature. A numerical solution within the context of a climate model demands the construction of a finite set of thickness levels. Hibler (1980a) uses 10 thickness levels for his variable thickness Arctic ice model in which the category widths are small for thin ice and increase for the thicker ice levels. This is because the growth rate function

$$f(h) = \frac{dh}{dt} \quad (1)$$

varies mostly for small values of  $h$ . Rothrock (1983) points out some other difficulties associated with the numerical integration of the thickness distribution equation (2.39). In particular, the formation of thin ice from the freezing of open water must be handled carefully. Some of these problems may be overcome by constructing more thickness levels so that the vertical grid is finer. In some cases however, this tends to smear out some of the structure of the distribution as the integration proceeds. Also, in climate models where the sea ice is specified on a two-dimensional grid, the addition of a large number of levels in the third dimension increases considerably the computational burden, particularly with respect to the amount of store needed. Better results can be obtained by letting the thickness levels float so that they follow the characteristics of equation (1). This allows the correct thermodynamic changes to be made to the thickness levels. However, in this case, grid squares in the horizontal direction will in general have thickness distribution levels that do not mesh together so that difficulties are introduced in modelling horizontal redistribution processes such as advection. With all these shortcomings we have to compromise with the choice of the form of the vertical grid used.

The model used here is general with respect to the number of levels, as long as there are three or more. There is no limit to the maximum number of levels except for the constraints introduced by storage requirements. It is possible to have useful results with as few as four levels.

For a grid consisting of four levels, the thickness distribution is expressed by the four quantities

$$G_1, G_2, G_3, G_4 \quad (2)$$

The first of these,  $G_1$ , is taken to be the fraction of open water present. The quantities  $G_2$ ,  $G_3$ , and  $G_4$  are the fractional areas of ice within thickness categories defined below, whereas  $G_1$  is the area of a single thickness. For this reason  $G_1$  is by nature different from  $G_2$ ,  $G_3$ , and  $G_4$  and so is treated differently.

We consider the thickness levels to be specified by their limits, so that there are four thickness values

$$H_1, H_2, H_3, H_4 \quad (3)$$

and that  $H_i - H_{i-1}$  is the width of the  $i$ 'th thickness level. Since the lowest level represents open water,  $H_1 = 0$ . The values in (3) are considered fixed except for the top level  $H_4$ , which is allowed to vary.  $H_4$  is thus taken to be the value of the maximum thickness of ice present in the region that  $g(h)$  describes. The variable top level is useful in that a knowledge of  $G_4$  and  $H_4$  together, gives an indication of the character and amount of ridges present in the distribution  $g(h)$ .

A disadvantage of a totally fixed grid is that any ice thicker than the maximum thickness level will have to be redistributed within the lower thickness levels. To reduce the amount of error introduced in this way, the top level will have to be made large compared with the maximum ice thickness expected. In that case, unless a large number of thickness levels are added to represent the thicker ice, there will be little information given regarding  $g(h)$  for large  $h$ . By choosing appropriate values for  $H_i$ , the thickness levels can be chosen to represent physically different categories of ice. For example, if the following values are chosen

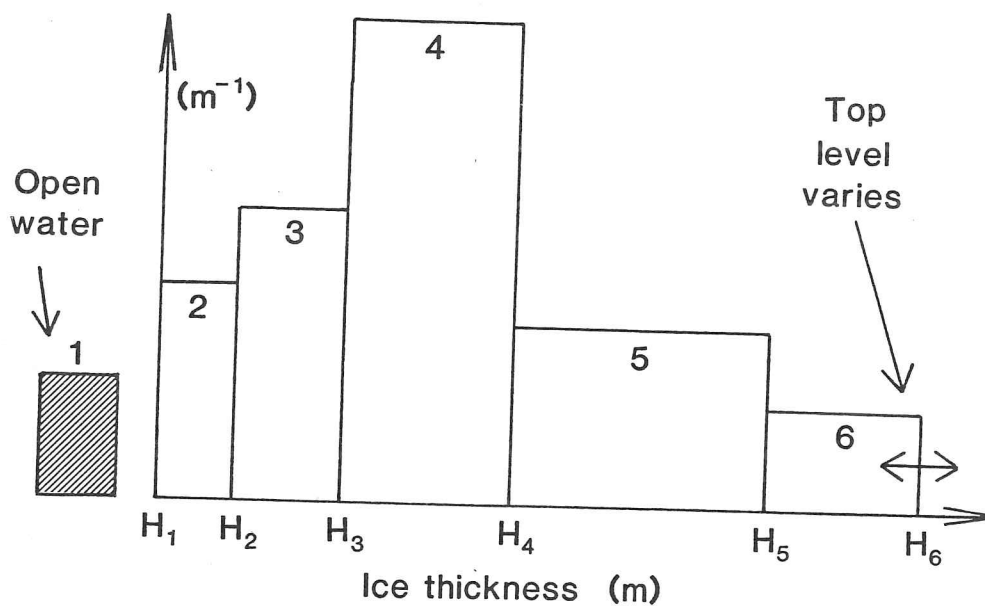
$$\begin{aligned}
 H_1 &= 0 \\
 H_2 &= 0.5\text{m} \\
 H_3 &= 2.0\text{m} \\
 H_4 &= > 2.0\text{m}
 \end{aligned}
 \tag{4}$$

then  $G_1$  would represent the fraction of open water as always,  $G_2$  would represent young ice,  $G_3$  would be the fraction of older first-year ice and finally,  $G_4$  would give the fraction of multiyear or ridged ice. Of course these can only be approximate categorizations but they should be enough to give a reasonably full description of the ice field.

A problem remaining is to adequately represent the formation of thin ice,  $G_2$ , by the quick freezing of open water  $G_1$ . Suppose that during one time step, which can be as little as a few hours, all the open water freezes over producing a layer of ice a few centimetres thick. This means that  $G_1$  becomes reduced to zero, and that the area of thin ice increases by  $G_1$ . However, from (4), the thin ice has thickness 0.5m, so that regardless of how thin the newly formed ice really is, the model takes it to be on average 0.25m thick. In other words, too much ice volume would be created. This can be partially overcome if some modification is made to our physical picture of the freezing process. We suppose that newly formed thin ice, rather than remaining as a coherent sheet of nilas, is blown by the wind and buffeted by the waves until it piles up against other more substantial pieces of ice. We thus postulate a minimum thickness that ice in the form of a solid structure can be. A fifth thickness level can then be introduced at this value. Then when new ice forms at a certain rate, we calculate the increase to the lowest ice level by forcing volume conservation and replacing the requisite amount of open water. This concept is consistent with the formation of 'grease' ice which does not have a solid consistency until a reasonable thickness is built up, often as a result of piling up against solid floes (Bauer and Martin 1983).

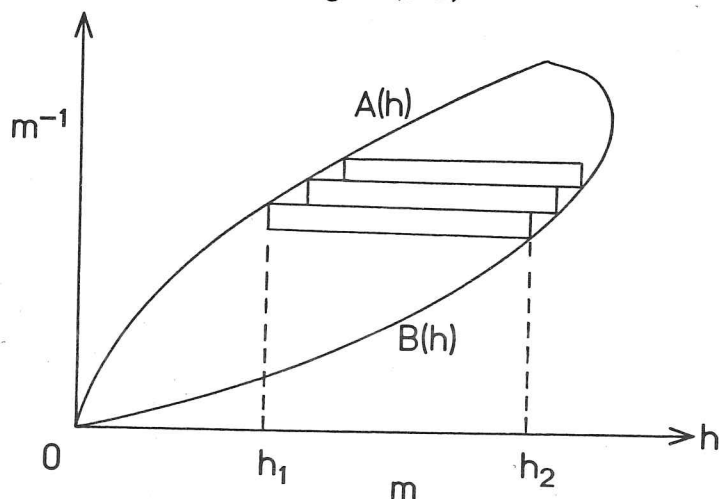
If there are five or more vertical thickness levels, then included in the code is a routine that calculates the values  $H_1, H_2, \dots, H_n$  in such a way that the level widths increase smoothly as  $h$  increases. Hibler (1980a) used such a grid in which the level widths  $H_i - H_{i-1}$  increases according to a Gaussian formula. If there are only four thickness levels, then choosing

Figure(5.1)



Schematic representation of the vertical thickness distribution grid used in the code.

Figure(5.2)



The construction of a distribution of ridged ice from an arbitrary initial distribution by summing the resulting distribution from elemental strips each consisting of the ice distribution within a set of triangular ridges.

a value for the thinnest ice level and the highest fixed ice level, completely determines the vertical grid. Figure (5.1) shows the spacings for a 6 level grid.

### 5.2.2 Ice redistribution

At each grid point, the information about the ice distribution is given in the form of four or five numbers representing the thickness distribution, and similarly for the floe number density. At each time step during the model run it is necessary to update each of these quantities.

We concentrate now on the thickness distribution. Although representing a continuous distribution with just a few values is a fairly crude approximation, we would like to retain as much accuracy as possible when calculating the various redistributions at each time step. The method employed is to consider the actual continuous thickness distribution to be constructed by assuming that the ice is uniformly distributed within the thickness levels. This means that the distribution would resemble a histogram. It is then possible, analytically or numerically, to any desired accuracy to determine the resulting continuous thickness distribution. In order to proceed with the next time step, the new thickness distribution is interpolated back to the finite grid for subsequent use by the model.

In order to keep to a minimum the calculations performed at each time step, as much as possible concerning the redistribution is calculated at the start of the model run. We describe here the way the mechanical redistribution is performed for a finite grid and is essentially the same as that used by Hibler's (1980a) multi-layer model. For an N-layer model, the areas of ice in each category are denoted by

$$G_1, G_2, \dots, G_N \quad (5)$$

where  $G_1$  is the area of open water. Suppose that during the course of the time step, areas have been added and subtracted until the distribution is no longer normalized to 1, so that

a value for the thinnest ice level and the highest fixed ice level, completely determines the vertical grid. Figure (5.1) shows the spacings for a 6 level grid.

### 5.2.2 Ice redistribution

At each grid point, the information about the ice distribution is given in the form of four or five numbers representing the thickness distribution, and similarly for the floe number density. At each time step during the model run it is necessary to update each of these quantities.

We concentrate now on the thickness distribution. Although representing a continuous distribution with just a few values is a fairly crude approximation, we would like to retain as much accuracy as possible when calculating the various redistributions at each time step. The method employed is to consider the actual continuous thickness distribution to be constructed by assuming that the ice is uniformly distributed within the thickness levels. This means that the distribution would resemble a histogram. It is then possible, analytically or numerically, to any desired accuracy to determine the resulting continuous thickness distribution. In order to proceed with the next time step, the new thickness distribution is interpolated back to the finite grid for subsequent use by the model.

In order to keep to a minimum the calculations performed at each time step, as much as possible concerning the redistribution is calculated at the start of the model run. We describe here the way the mechanical redistribution is performed for a finite grid and is essentially the same as that used by Hibler's (1980a) multi-layer model. For an N-layer model, the areas of ice in each category are denoted by

$$G_1, G_2, \dots, G_N \quad (5)$$

where  $G_1$  is the area of open water. Suppose that during the course of the time step, areas have been added and subtracted until the distribution is no longer normalized to 1, so that

$$\sum G_i^! \neq 1 \quad (6)$$

If

$$\sum G_i^! < 1 \quad (7)$$

then the area of open water is increased until the distribution is normalized. Thus

$$\begin{aligned} G_1'' &= G_1^! + (1 - \sum G_i^!) \\ &= 1 - \sum_{i=2}^n G_i^! \end{aligned} \quad (8)$$

and the other areas remain unaltered thus

$$G_i'' = G_i^! \quad i = 2, \dots, N \quad (9)$$

If however

$$\sum G_i^! > 1 \quad (10)$$

then mechanical redistribution takes place. An  $N \times N$  matrix  $\gamma$  is constructed such that  $\gamma_{ij}$  is the increase in area in level  $j$  caused by the loss through redistribution of a unit area from level  $i$ . A set of category reductions  $G_i^*$  are calculated from the values  $G_i^!$  by applying the annihilator function  $a(h)$  of redistribution theory. These category reductions  $G_i^*$  give only the relative losses from each level,  $i$ , so to determine the actual reductions, they are multiplied by a constant such that the resulting distribution is normalized.

Writing the relative loss from level  $i$  as  $\lambda_i$  for which the net gain to level  $j$  is  $\gamma_{ij}\lambda_i$ , we write the net loss to level  $j$  as

$$G_j^* = \lambda_j - \sum_i \gamma_{ij}\lambda_i \quad (11)$$

Thus  $G_j''$  is given by

$$G_j'' = G_j' - \frac{G_j^*}{\sum G_i^*} (\sum G_i' - 1) \quad (12)$$

because then the resulting distribution  $G_j''$  is normalized to 1,

$$\sum G_j'' = 1 \quad (13)$$

It is quick computationally to calculate  $G_j''$  at each time step from (12) once the values  $\gamma_{ij}$  are known. These values can be calculated at the start of the run and remain constant. We now describe how the values of  $\gamma$  may be calculated analytically.

From the definition of  $\gamma$ , the coefficients  $\gamma_{ij}$  may be obtained by considering a unit area of ice uniformly distributed in the range  $(H_{i-1}, H_i)$ , and allowing all the ice to become ridged. Although, from a real distribution, only a fraction of the ice will ridge, we consider a hypothetical situation in which all the ice ridges. This is because the coefficients  $\gamma_{ij}$  refer to areas of ice formed per unit area ice annihilated.

The distribution of the ice annihilated is

$$a'(h) = \begin{cases} \frac{1}{H_i - H_{i-1}} & H_{i-1} < h < H_i \\ 0 & \text{otherwise} \end{cases} \quad (14)$$

The ice described by  $a'(h)$  is ridged to produce a new distribution  $n'(h)$ . The coefficients of  $\gamma$  are then given by

$$\gamma_{ij} = \int_{H_{j-1}}^{H_j} n'(h) dh \quad (15)$$

### 5.2.3 Analytic form of redistribution matrix.

We firstly describe a method of obtaining an analytic expression for  $n'(h)$  in terms of a general distribution  $a'(h)$  assuming that ice of thickness  $h_1$  forms triangular ridges of height  $h_2(h_1)$ . Although this is interesting in its own right, even for a simple distribution  $a'(h)$  as in (14), the function  $n'(h)$  obtained is too complicated for the integral in (15) to be evaluated to give  $\gamma_{ij}$ .

Thus, we also describe a numerical method of calculating  $\gamma_{ij}$  that is completely general with respect to the manner in which ice redistribution is assumed to take place.

The concept of considering an entire area of ice of thickness  $h_1$  forming ridges as described in section (4.2) was introduced in section (4.3) to derive the strength of a general thickness distribution. This was done by straightforwardly integrating the potential energy changes that occurred during the loss of ice from each thickness element  $(h, h+dh)$ . This idea can be extended to calculate the actual distribution  $a'(h)$  of ridges.

The difficulty here arises because the ice from the element  $(h_1, h_1+dh_1)$  redistributes through a range of thicknesses  $(h_1, h_2)$ . The new distribution can be obtained by summing up the elemental strips produced by the redistribution from each thickness element  $(h, h+dh)$ . This is shown in figure (5.2). From the element  $(h_1, h_1+dh_1)$  an area  $a'(h_1)dh_1$  is redistributed uniformly between  $h_1$  and  $h_2$ . Volume conservation gives the value of the new distribution between  $h_1$  and  $h_2$  as

$$a'(h) = \frac{2h_1}{h_2 - h_1} dh_1 \quad (16)$$

We imagine that the elemental strips are stacked on top of one another starting with the strips near  $h = 0$ . The left and right hand ends of the stacked strips trace out two curves (in the limit as the elements  $dh_1 \rightarrow 0$ )  $A(h)$  and  $B(h)$ . Constructed in this way curve  $A(h)$  would be given by

$$A(h) = \int_0^h a'(h_1) \frac{2h_1}{h_2^2 - h_1^2} dh_1 \quad (17)$$

since the height of the stack at  $h$  is just the sum of the heights of each of the elements whose left hand end starts before  $h$ . The curve  $B(h)$  would then be given by

$$B(h) = A\{h_2^{-1}(h)\} \quad (18)$$

where  $h_2^{-1}(h)$  is the function inverse to  $h_2$  in that if  $h_2 = h_2(h_1)$  then  $h_1 = h_2^{-1}(h_2)$ . The resulting distribution would then be given by

$$n'(h) = \max\{A(h), B(h)\} - \min\{A(h), B(h)\} \quad (19)$$

Taking  $a'(h)$  to be the distribution in (14),  $A(h)$  may be evaluated analytically for certain simple functions  $h_2(h_1)$ .

By substituting the ridge height formula (4.24) into (16), with  $a'(h)$  given by (14) the function  $A(h)$  can be evaluated. The result

$$\int \frac{dx}{\sqrt{x}\sqrt{b-x}+ax} = \frac{2}{1+a^2} \left[ a \ln(\sqrt{b-x} + a\sqrt{x}) + \sin^{-1}\left(\sqrt{\frac{x}{b}}\right) \right] \quad (20)$$

is needed for this, where  $a$  and  $b$  are constants.  $B(h)$  is then calculated from (18) using the inverse function  $h_1 = h_2^{-1}(h)$  given by

$$h_1 = \frac{P^* + (2C_f - C_b)h \pm \sqrt{[P^{*2} + 2h(2C_f - C_b)P^* - h^2(8C_f - C_b)]}}{2(C_f + C_b)} \quad (21)$$

The resulting expression is too cumbersome to deal with further so that it is at this point that the limit of the analytic approach is reached. Since the evaluation of the integral obtained by substituting (21) into the

expression obtained for  $A(h)$  is not possible, we can only evaluate (15) numerically. If however a numerical method is needed a more direct method applicable to arbitrary functions  $h_2(h_1)$  may be used and is described below.

#### 5.2.4 Numerical evaluation of redistribution coefficients

The coefficients  $\gamma_{ij}$  are evaluated numerically by dividing  $(H_{i-1}, H_i)$  into a large number of elements. The ice originally contained within the element  $(h, h+dh)$  is uniformly redistributed in the range  $h+\frac{1}{2}\delta h$  to  $h_2(h+\frac{1}{2}\delta h)$ .

The area of ice then created within the range  $(H_{j-1}, H_j)$  is noted, and such areas summed for each thickness element in the range  $(H_{i-1}, H_i)$ . The total area obtained is then  $\gamma_{ij}$ .

This method gives the coefficients  $\gamma_{ij}$  for any function  $h_2(h)$ . Also, the method may easily be extended to include modes of redistribution other than by the formation of triangular ridges.

#### 5.2.5 A finer grid

A particular kind of error is likely to occur when evaluating the changes to the thickness distribution through ridging, especially when there are few thickness levels. This occurs when  $H_L - H_{L-1}$  is large enough for there to be a significant difference between  $h_2(H_{L-1})$  and  $h_2(H_L)$ . Suppose that during an ice redistribution process, that ice up to a maximum  $h^*$  is involved in ridging. If  $H_{L-1} < h^* < H_L$  then only the ice in the region  $H_{L-1}$  to  $h^*$  should ridge. However, because the thickness levels are ridged as a whole, so the whole of the level  $(H_{L-1}, H_L)$  will in this case be ridged. Thus, although the correct loss of ice from the  $L$ 'th level is evaluated, incorrect information regarding the increase in ice to the upper levels is calculated.

For this reason, before ridging takes place, the thickness grid is interpolated to a fine thickness grid in which each of the coarse grid thickness levels is uniformly divided into a number of finer levels. The changes to the fine grid thickness levels are calculated due to ridging

and the new thickness distribution interpolated back to the coarse grid again. The number of fine thickness levels within each coarse thickness level is a matter of choice. The larger the number chosen, the greater is the amount of computer time required. Later in this chapter, we show results of some experiments in which the number of thickness levels within the coarse and the fine grids are changed, giving an indication of how few levels may be included without incurring significant errors.

### 5.3 Strength in the code

In section (4.3) the theory concerning the determination of the strength of the ice,  $p^*$  as a functional of the ice thickness distribution  $g(h)$  was dealt with. We saw that for an arbitrary distribution  $g(h)$  the strength may be found by renormalizing, by ridging, the distribution  $(1+\phi)g(h)$  where  $\phi$  is small. If  $a'(h)$  represents the ice destroyed through ridging then formulae (4.59) and (4.62) may be used to determine  $p^*$  by

$$p^* = p_p^* + p_f^* \quad (22)$$

This procedure may be adapted to the determination of the strength of an ice thickness distribution described as in the code by the areal fractions  $G_1, G_2, \dots, G_N$ . The method is to increase each of the  $G_L$  by the increment  $\phi G_L$  as for the continuous case and allow the distribution to ridge. If the actual fractional areas of ice from each thickness category are recorded during the ridging process, and if they are denoted  $A_L$ , then the strength may be determined from

$$p^* = (1/\phi) \sum_L \Gamma_L A_L \quad (23)$$

where  $\Gamma_L$  are constant strength coefficients that are calculated at the start of the run. They are given by

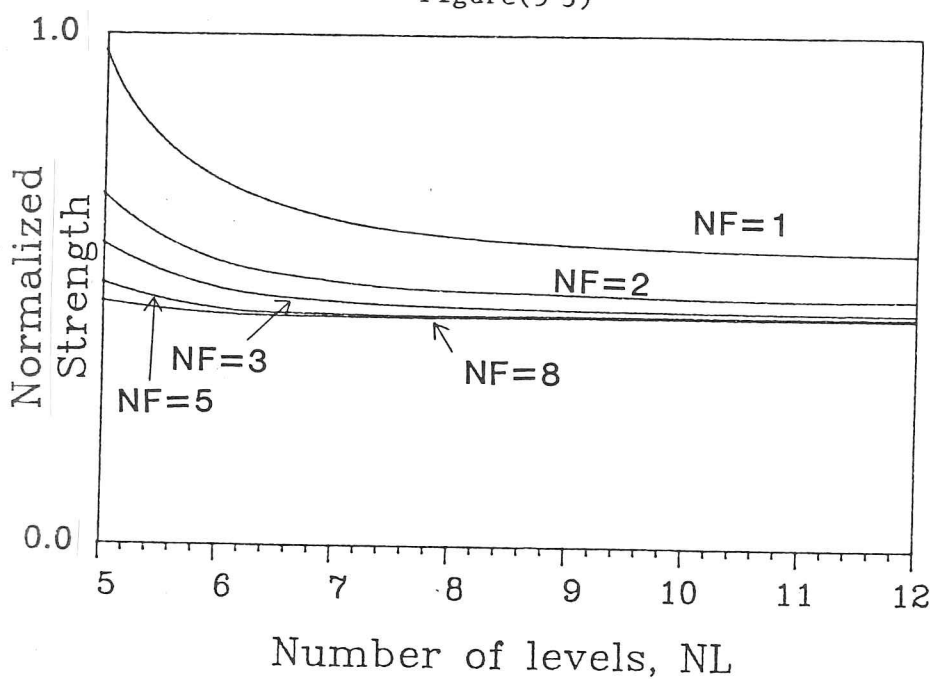
$$\Gamma_L = \int_{H_L-1}^{H_L} \left[ C_f (h_2(h) - h)^2 + \frac{1}{3} C_b \frac{(2h_2(h) + h)(h_2(h) - h)h}{h_2(h) + h} \right] dh \quad (24)$$

and are evaluated numerically. The coefficient  $\Gamma_N$  does have to be calculated at each evaluation of the strength because of the variable value of  $H_N$ . Equation (24) still applies though once  $H_N$  is known.

Because the strength determination relies on ridging being carried out, which as we have seen may be inaccurate when there are only a few thickness levels, the coefficients  $\Gamma_L$  are calculated for the fine grid used when evaluating the changes to the thickness distribution from ridging.

To investigate the kind of errors introduced by taking few thickness levels, a number of runs of the model were performed on a small (3x3 velocity field) test grid in which the number of refinements to each layer for the ridging procedure, NFINE were varied. The strength of the ice in one of the grid cells after 40 half-day time steps was evaluated in each run. All the grid cells initially contained a 100% cover within the thinnest ice level ( $G_2 = 1$ ). This is so that the same initial conditions could be applied for each of the runs, the thinnest ice level always having the same width, in this case 0.25m. Ice growth conditions were applied. The October growth rates for the Arctic as calculated by Thorndike et al (1975) were used. This test would thus pick up errors introduced during the ridging process, the thermodynamic growing of the ice, and the strength evaluation, by changing the number of thickness levels used. Figure (5.3) shows the variation of the model results for NL from 5 to 12, and for NFINE = 1, 2, 3, 5 and 8. The curves show that when there are more than 6 levels reasonable accuracy is achieved when NFINE is greater than one. For 5 or 6 levels accurate results may be obtained by taking NFINE to be 3 or more. For the standard simulations described in the next chapter, 6 levels were used (NL = 6) with NFINE, the number of refinements to each level during ridging, equal to four. In this case, we are essentially using an 18 level model to evaluate ice strength and to perform ridging.

Figure(5.3)



The value of the strength as measured in one grid cell after 40 time steps of growth. Values have been plotted for a range of thickness levels NL and for various numbers of refinements to the vertical grid used when evaluating strength or performing ridging.

## 5.4 Floe number densities in the code

### 5.4.1 Floe size distribution

The average floe number density in a region, or a grid square, is denoted  $n$ . A real floe field consists of many different floe sizes, usually from the very small up to some maximum cut-off size. (Goodman et al 1980). Thus, there may be some difficulties introduced by trying to model the floe field by considering only the average floe number density,  $n$ . In section (3.3) we saw that many of the factors that determined the size of newly formed floes, depended upon the ice thickness  $h$ . Wind-induced fracture of floes would give small floes for thinner ice and conversely, large floes for thicker ice (if the thick ice can be made to break at all). Having divided up the thickness into a number of levels, or thickness categories, in order to increase the amount of information provided by the representation of the ice thickness, it would seem that an analogous procedure could be carried out for floe sizes. One method would be to give the fractional area covered by each floe size category. Another would be to give the number of floes per unit area of each floe size. There would be a difficulty involved here in delimiting the range of floe sizes to be used for each size range. In addition there would be a loss of information involved in taking a finite number of possible floe sizes, particularly because of the large number of possible floe sizes that exist and would have to be coped with in a model. Instead of choosing to represent the range of floe sizes present at a single place by one of the two methods mentioned so far, we take advantage of the fact, already pointed out, that the floe sizes depend very much upon the ice thicknesses involved and consider floes of various thicknesses rather than of various lateral extents. Thus we specify the average floe number density  $n_L$  for each thickness category. This preserves more information regarding the actual floe sizes making up the pack ice. The disadvantage of this method is that it implies that each floe is of more or less uniform thickness, and that the thicker ice, which generally consists of ridged ice in contact with thinner ice, is considered as separate thick floes. It would not be easy to overcome this difficulty because, given a thickness distribution  $g(h)$  we

cannot a priori decide whether or not the upper levels (h large) consist of ridged ice or genuinely thick floes of uniform ice thickness.

Formally, we consider floe number densities  $n_2, n_3, \dots, n_N$  such that  $n_L$  is the number of floes per unit area with thickness lying in the range  $(H_{L-1}, H_L)$ . Clearly

$$\sum_2^N n_L = n \quad (25)$$

An average floe size  $r_L$  for each thickness level may be defined by the relation

$$G_L = \pi n_L r_L^2 \quad (26)$$

for which  $r_L$  would be the floe radius for circular floes. Note that  $n_1$  is not defined. In the code only the values of  $n_L$  and  $G_L$  are held in store and a conversion to  $r_L$  is made when it is more convenient to deal with floe sizes (such as for floe breaking) and then convert back to  $n_L$ . Processes such as advection are best handled by varying  $n_L$  directly.

#### 5.4.2 Floe size change

Equation (3.58) is split into two stages in the code. Firstly, the advection is performed according to the equation

$$\frac{\partial n_L}{\partial t} + \nabla \cdot (\underline{u} n_L) = 0 \quad (27)$$

for each of the thickness levels  $L = 2, \dots, N$ . This is done in the same way as the advection of the thickness level areas  $g(h)$ .

The change in floe number density due to the coalescing of floes within a large scale straining velocity field was obtained in chapter 3 and is given by

$$\frac{dn}{dt} = -2LA|\dot{\epsilon}|\alpha(\theta)n \quad (28)$$

This equation may be solved simply to give

$$n(t) = n(0)\exp\{-2LA|\dot{\epsilon}|\alpha(\theta)t\} \quad (29)$$

where  $n(0)$  is the floe number density at time  $t = 0$ , and it has been implicitly assumed that

$$2LA|\dot{\epsilon}|\alpha(\theta) \quad (30)$$

is constant in time. This is clearly not true for long periods of time where any of the factors  $L$ ,  $A$ ,  $|\dot{\epsilon}|$  or  $\alpha(\theta)$  in (30) may vary. However, in practice (29) is used to determine  $n(t+\Delta t)$  in terms of  $n(t)$ , where  $\Delta t$  is the length of the time step, and because of the nature of the staggered time marching used in this model, the values of  $L$ ,  $A$ ,  $|\dot{\epsilon}|$  and  $\alpha(\theta)$  are those evaluated at time  $t+\frac{1}{2}\Delta t$ , giving second order accuracy in time. Thus, when the floes are not being broken up by the action of the wind or the waves, we assume an exponential decay in their number within each time step. Whether or not the number of floes in a region is able to decrease, with a corresponding increase in floe size, according to this mechanism, depends upon whether the wind is strong enough to break the floes up again. For this reason we allow the floe number to decrease according to (29) before subjecting the floes to the effects of the wind and waves. When  $A = 1 - G_1$  is close to unity, the function  $L(A)$  may become very large, thus giving rise to a very sudden drop in  $n$ . This represents the situation that occurs when the pack ice stops behaving as floes and becomes continuous. Thus, in a floe model we must include the possibility of a continuous pack being formed. The transfer from a floe model to a continuous model occurs when equation (29) predicts a sudden drop in  $n$ . This idea is discussed in more detail below.

### 5.4.3 Continuous ice in a floe model

Consider a floe field described by an array of grid squares, within each of which is specified the relative areas of open water and the various ice thicknesses together with the average floe sizes for each thickness category. There needs to be special care taken if the implied floe sizes become of the same order of magnitude or larger than the grid size. For, in this case we are dealing with a continuous ice cover, not a floe field. If the predicted floe size, obtained from the relation  $G_L = \pi n_L r_L^2$ , is larger than some specified value, related to the grid size, then the code abandons the floe modelling for that particular grid square and thickness level  $L$  and sets

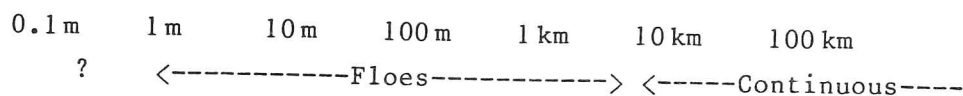
$$n_L = \frac{G_L}{\pi(\Delta x)^2} \quad (31)$$

where  $\Delta x$  is the grid length. Thus where we do not expect to find floes the model does not try to predict sizes. Instead of using the grid length  $\Delta x$  here, any large value may be chosen. The value only serves to indicate the floe size beyond which they are no longer considered as floes.

A newly formed ice cover is considered to be continuous in that its initial value for the floe number density is given by (31). Conversely, if all the floes of some thickness range melt then the floe number density,  $n_L$ , is set to zero.

We have considered one circumstance in which a floe field would have to be thought of as continuous. That is when the predicted floe size becomes large. A floe field would also have to be thought of as continuous if its compactness became unity. In this model, this would occur in a region experiencing a converging ice velocity field. If the fraction of open water drops below  $10^{-12}$  then the ice cover is taken to be continuous and the floe number density dropped so that the floe radius is equal to the grid length. The value  $10^{-12}$  is arbitrary - any low value will do. Even a value of  $10^{-9}$  would represent only 10 square metres of open water in a 100 km grid square.

The following figure shows schematically the range of floe sizes best dealt with in a model with grid size of the order 10 km to 100 km.



Although the floe model is able to produce floes of less than about 1m, such values should be regarded as meaning only that the ice consists of very broken up fragments.

## 5.5 Thermodynamics in the code

### 5.5.1 Vertical changes

We now consider the numerical treatment of the thermodynamic term in the thickness distribution equation. The thermodynamic part of the thickness distribution equation may be written

$$\frac{\partial g}{\partial t} + \frac{\partial (fg)}{\partial h} = 0 \quad (32)$$

where  $f(h)$  is the growth rate  $(dh/dt)$  of ice of thickness  $h$ . The second term in (32) behaves as an advection term for  $g$  with  $f$  analogous to velocity and  $h$  representing distance. Thus we expect many of the problems associated with the numerical representation of advection or conservation laws in general.

We will discuss the way in which growth and melt are handled with respect to the variable thickness grid described above, and in particular, mention ways in which some of the inherent problems associated with numerical representation of (32) are dealt with to suit the particular problems we are concerned with.

If we consider a typical thickness level, number  $L$ , then growth and melt may be achieved very simply. If the growth rate  $f(h)$  for that level is

positive, so that we have growth, then the area of ice in that level  $G_L$  will decrease and be added to that of the  $L+1$ 'th level. Similarly, if melting occurs then  $f(h) < 0$  and a decrease in  $G_L$  is accompanied by an increase in the  $L-1$ 'th level. The special cases where the  $L$ 'th level is the top or bottom level are treated separately.

So far, we have talked about the growth or melt of level  $L$  without reference to which value of  $h$  we are considering when calculating  $f(h)$ . For level  $L$  which extends from  $H_{L-1}$  to  $H_L$ , there may be a range of values of  $f(h)$ , especially if the thickness level is large. In particular,  $f(h)$  may even change sign within the range  $(H_{L-1}, H_L)$ . So, do we take  $f(H_{L-1})$ ,  $f(H_L)$  or perhaps  $f\{\frac{1}{2}(H_{L-1} + H_L)\}$  as the representative growth rate of level  $L$ ? Hibler (1980a) chose  $f\{\frac{1}{2}(H_{L-1} + H_L)\}$  as the representative value. This would be reasonable when a large number of thickness levels are used (in this context, about 10 levels, as used by Hibler, would be enough). If fewer levels are desired, then problems will arise, problems best illustrated by an example. Suppose we have four levels in all, the first representing open water. Suppose further that ice in level 2 is growing ( $f > 0$ ) and that ice in level 3 is melting. Clearly we would expect an equilibrium thickness lying somewhere within levels 2 or 3. If the equilibrium thickness lay in level 2 then it would be reasonable that during a time integration of the thermodynamic equation (32), all the ice from level 3 would be transferred to level 2. However, this would not occur within the regime so far mentioned. Instead, a balance between the rate at which the ice was being transferred from level 2 to level 3 and that in the opposite direction would be set up. It wastes levels to represent a particular thickness of ice by their relative values, especially when two levels may span the entire thickness range from zero to the maximum fixed value.

This situation is overcome by concentrating not on the growth or melt of particular levels but rather, on the growth or melt at the thickness values between the levels, i.e. at the values  $H_L$ . Thus the value of  $f$  is evaluated at  $H_L$  and the growth performed by reducing the area of ice in level  $L$  by the appropriate amount and increasing that of level  $L+1$  by the same. Melt would occur with a reduction from level  $L+1$  and an increase to level  $L$ .

As an example, suppose we have growth at  $H_L$ . So  $f(H_L) > 0$ , then in time  $\Delta t$ , the value of  $G_L$  would drop by the amount

$$\frac{G_L f(H_L) \Delta t}{H_L - H_{L-1}} \quad (33)$$

and the value  $G_{L+1}$  would increase by the same amount.

If  $f(H_L) < 0$ , then  $G_L$  would increase by

$$\frac{-G_{L+1} f(H_L) \Delta t}{h_{L+1} - h_L} \quad (34)$$

and  $G_{L+1}$  would decrease by this amount. The cases of the thermodynamic changes occurring to the upper and lower levels need now to be considered. Melting of the thinnest ice layer is straightforward except that open water is formed rather than a thinner layer of ice. The increase in open water would be given by (34) with  $L = 1$ . In addition to melting of the thinnest ice, the value  $f(H_1) = f(0)$  determines the amount of heat absorbed by open water used to melt the ice from below and laterally. This is described in more detail in the section on lateral melting.

The situation in which new ice is formed from open water has been discussed previously in connection with the choice of the type of thickness grid to be used. The increase in the ice of level 2 due to freezing of open water in time  $\Delta t$  is given by

$$\frac{G_1 f(0) \Delta t}{H_2 - H_1} \quad (35)$$

The situation that occurs for the top two thickness levels is complicated by the fact that the top thickness level is variable and so must vary in response to growth and melt. If there are  $N$  thickness levels, then  $H_{N-1}$  is the value of the maximum fixed thickness level, and  $H_N$  will vary. If  $f(H_{N-1}) > 0$  then  $G_{N-1}$  will decrease and  $G_N$  will increase. Also,  $f_N$

may need to be increased if  $f(H_{N-1})$  is sufficiently large. This is the one case in which  $f(h)\Delta t$  may exceed the level width. This is because we allow the possibility of the top level reducing in width to zero if no ice exists there. If  $G_{N-1} > 0$ , then  $H_N$  is readjusted to the value

$$\max\{H_N, H_{N-1} + f(H_{N-1})\Delta t\} \quad (36)$$

If  $f(H_N) > 0$ , then no change occurs to  $G_N$  but providing  $G_N > 0$ , then  $h_N$  is increased by  $f(H_N)\Delta t$ .

In the case of melting of the top levels ( $f(H_{N-1}) < 0$ ,  $f(H_N) < 0$ ), we must allow for the possibility of the entire top level melting and the top level  $H_N$  dropping down to the value  $H_{N-1}$ .

Thus we have considered all the possibilities of growth and melt of all the layers, including the possible total melt of the top variable layer or its increase from the growth of the  $N-1$ 'th layer.

### 5.5.2 Lateral melting

The growth rate as calculated by the heat budget is given by the function  $f_b(h)$ . The growth rate for ice of zero thickness is thus  $f_b(0)$ . If  $f_b(0) > 0$  then ice is grown at that rate. If however,  $f_b(0) < 0$  then no ice can be melted. Instead, it is assumed that heat is absorbed through the leads (areas of open water) into the upper mixed layer of the ocean. This heat is then able to melt ice from the bottom of the floes as well as from their vertical sides. If all the ice melts or there is none to begin with, then the heat absorbed but not used to melt ice is recorded as a mixed layer temperature increase.

In the case where ice is melted, the volume lost from the floe edges depends upon the perimeter of the floes per unit area, which depends on the floe sizes and number densities.

The total floe perimeter per unit area may be written

$$s = \sum_L 2\pi r_L h_L n_L \quad (37)$$

where  $h_L$  is the average thickness of the  $L$ 'th ice thickness category. Now suppose the rate of bottom melting of the floes is  $f^b$ . The sides of the floes will then melt at a rate  $[(\pi/4) + (4/\pi)]f^b$  so that the total rate of loss of volume through ice melting can be expressed

$$\left\{ \frac{\rho_i}{\rho_w} \left[ \frac{\pi}{4} + \frac{4}{\pi} \right] s + (1 - G_1) \right\} f^b \quad (38)$$

This may be equated with the rate of loss of ice volume as calculated from the heat absorbed through leads

$$-\min\{0, f_b(0)\} G_1 \quad (39)$$

By equating the two volume melt rates (38) and (39), the vertical bottom melt rate  $f^b$  may be evaluated.

The code is written so that if any artificial adjustment of the thickness distribution occurs, then an adjustment is made to the thermodynamic budget so that total energy is conserved. The type of thickness distribution changes envisaged here are those concerned with the adjustments necessary to correct the effects of numerical errors, such as the production of areas containing small negative values of the thickness distribution (for example, as produced by the second order accurate advection routines). In this case the thickness distribution value would be set to zero and the extra ice needed to be melted to conserve energy would be added to the term in equation (39). If an extra volume rate of melt of  $\dot{v}$  were needed to balance the energy budget, then from (38) and (39) the final value for  $f^b$  would be given by

$$\frac{\dot{v} - \min\{0, f_b(0)\} G_1}{\frac{\rho_i}{\rho_w} \left[ \frac{\pi}{4} + \frac{4}{\pi} \right] s + (1 - G_1)} \quad (40)$$

The oceanic heat flux  $F_o$  which is assumed to enter the mixed layer at a depth of 30m, gives another source of both lateral and bottom melting. Numerically this term can be handled by including it with the  $\dot{v}$  term.

Having now established the rate  $f^b$  at which the bottom of the floe will melt, the lateral melt is handled indirectly. During the model run,  $f^b$  gives the melting rate at the start of a time step. As the floe melts,  $f^b$  would in fact change as the floe became thinner. This is the error caused when modelling a continuously changing process with forward time steps at discrete intervals. Thus instead of calculating the increase in open water according to the lateral melt at the start of the time step which can be deduced from  $f^b$ , rather we use an indirect approach taken whereby the difference between the volume melted due to bottom melting  $f^b$  and the volume that should be melted according to the heat budget, is calculated. The difference between the two volumes is converted into a mixed layer temperature rise. Ice is removed from each thickness category equally and at the same time the amount of open water is increased to compensate, until either the temperature has reduced to freezing or all the ice has melted, in which case the water temperature remains above freezing. Using the lateral melting term  $F_L$  introduced by Hibler (1980a) into the ice thickness distribution equation, the changes to the mixed layer temperature may be described by the following equations

$$\frac{\partial T_{mix}}{\partial t} = \frac{Q_I}{C_w d_{mix}} \left\{ \int_0^{\infty} F_L(g, h, T_{mix}) h dh + (1 - G_1) f^b - G_1 \min\{0, f_b(0)\} + F_o \right\} \quad (41)$$

$$F_L(h, g, T_{mix}) = \begin{cases} -C(T_{mix})g(h) & h > 0 \\ C(T_{mix})(1 - G_1)\delta(h) & h = 0 \end{cases} \quad (42)$$

where

$$C(T_{mix}) = \min \left\{ \frac{(T_{mix} - 271.2)}{Q_I h} C_w d_{mix}, 1 \right\} \quad (43)$$

and  $\bar{h}$  is the mean ice thickness

$$\bar{h} = \int_0^{\infty} g(h)h dh \quad (44)$$

Here,  $d_{\text{mix}}$  is the mixed layer depth (taken to be 30m),  $Q_I$  is the volumetric heat of fusion of ice ( $302 \text{ MJm}^{-3}$ ) and  $C_w$  is the volumetric heat capacity of water ( $4.19 \text{ MJm}^{-3}$ ), and the freezing temperature of sea water has been taken as  $271.2 \text{ K}$ . The term  $F_o$  is the upward oceanic heat flux into the mixed layer. The factor  $C_w d_{\text{mix}}/Q_I$  when multiplied by a temperature difference gives an ice volume difference. Equation (41) is a modification of Hibler's (1980a) equation (6). The last two terms of (41) are dealt with simply by evaluating the volumes of ice before and after melting by amount  $f^b \Delta t$  and comparing the result with the volume that should be melted according to the heat budget (as described above) rather than attempting a direct numerical integration.

The changes to the thickness distribution due to the melting of all the thickness categories by  $f^b \Delta t$  cannot be done by using the methods described in the previous section. This is because the melting rate here may be very much larger than the heat budget growth and melt rates, especially when the ice concentration is low so that large amounts of heat can enter the ocean. Thus the amount of melting required during a single time step may be considerably larger than the width of the thickness levels involved. Indeed it may be the case that an entire thickness distribution is melted. If a distribution, initially described by  $g(h)$ , is melted by an amount  $f^b \Delta t$  from all levels, then the subsequent distribution is

$$g'(h) = \delta(h) \int_0^{f^b \Delta t} g(h) dh + g(h + f^b \Delta t) \quad (45)$$

This represents a shifting to the left of the function  $g(h)$  and is achieved in the code by interpolating the values  $G_L$  from the old thickness grid onto a new grid with values specified at the nodes

$$f^b \Delta t + h_L \quad (46)$$

The new amount of open water is obtained by adding the value

$$\int_0^{f^b \Delta t} g(h) dh \quad (47)$$

to the old value, and in the code is evaluated in the obvious manner, by summing up the values of  $g_L$  for which  $h_L < f^b \Delta t$  together with the appropriate fractional part of the thickness distribution level within which  $h = f^b \Delta t$  lies.

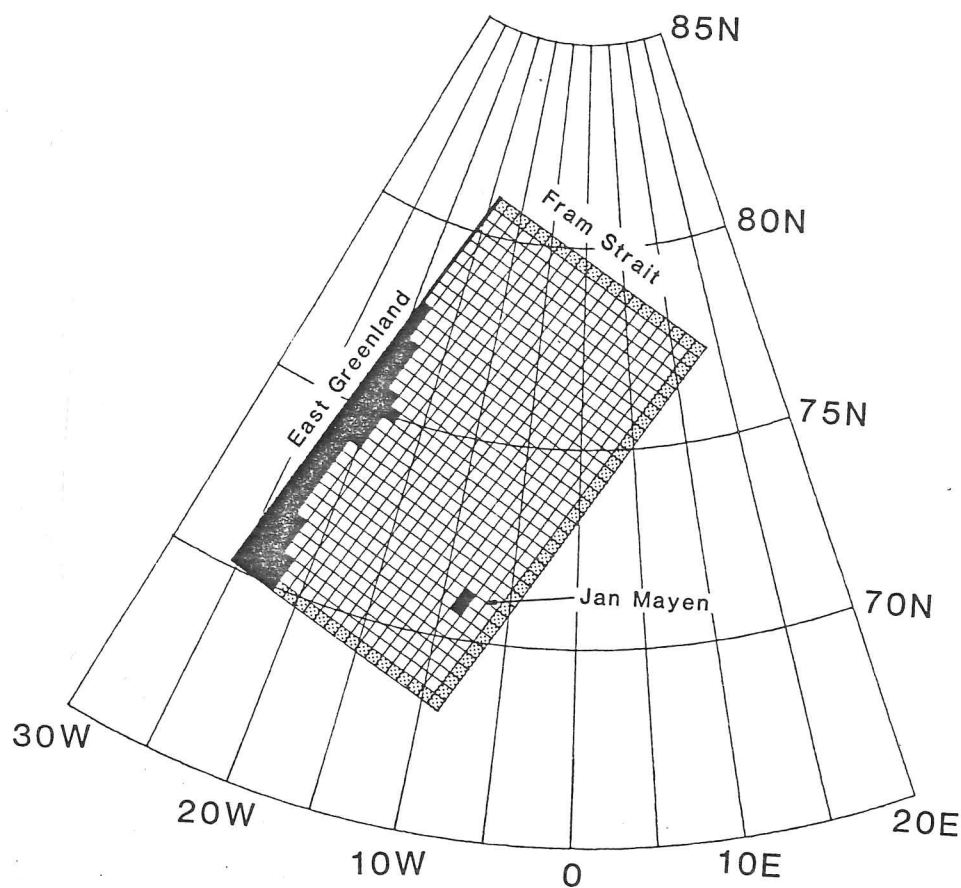
## 6. THE MODEL SIMULATIONS

### 6.1 Model inputs

#### **6.1.1 The model grid**

The model described thus far is applicable to any geographic region. In this section we describe the input fields, boundaries and other special features associated with modelling the sea ice off East Greenland. Figure (6.1) shows the grid employed for this purpose. The grid is rectangular if plotted on a map with a Lambert equal area projection. There are  $21 \times 36$  velocity points or  $22 \times 37$  cells in which the physical properties are defined. The grid length is 35 km. The northern boundary represents the Greenland-Spitsbergen passage (Fram Strait). The western boundary includes part of the east coast of Greenland extending from Nordostrundingen in the north to roughly Scoresby Sund at the south. The east and south sides of the grid lie in the open sea. This grid was chosen so that the sea ice off Greenland would cover as much of the grid as possible, such that both the coast of Greenland and, for as much of the year as possible, the ice edge are included. The orientation of the grid is chosen so that the initial ice edge position lies roughly vertically from the top to bottom of the grid.

The northern, eastern and southern boundaries consist of outflow cells in which the ice viscosities are set to zero and natural outflow or inflow is allowed. At the northern boundary, the ice thickness distribution is specified as a function of the time of the year. This is because the ice thicknesses there cannot be predicted by a local model since they depend upon the processes occurring in the Central Arctic. The ice flux through Fram Strait is not specified as it depends upon the ice velocities there, and these are calculated in the model.



Figure(6.1)

The grid representing the part of the Greenland Sea modelled in the standard simulations.

### 6.1.2 Initial thickness distribution

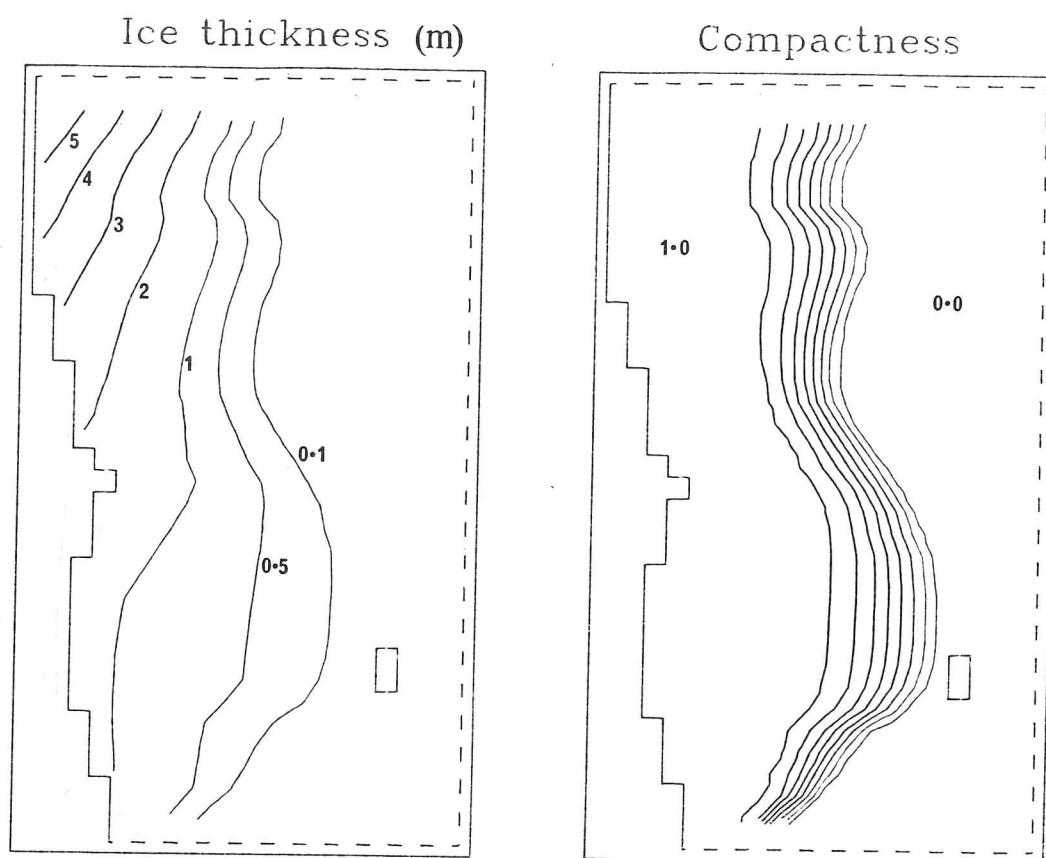
For a short term simulation, the initial variables used for input are of greater importance than in a long term climate study where an equilibrium solution is obtained from arbitrary initial data.

In this study, the initial conditions were those of November 30, 1978. The initial ice thickness distribution was obtained from charts produced by Vinje (1979). These charts however, gave only the the position of the 3/8 ice concentration line. Thus, the ice concentration was assumed to be total from the coast out to a certain distance at which point it drops as a cosine function until zero half as far away again from the coast. The average ice thickness was taken to drop linearly from a maximum at the coast to zero where the ice concentration is zero. The linear change in thickness across Fram Strait is consistent with the observations of Wadhams (1983b). This data, which was obtained from a submarine, suggests a maximum mean thickness in Fram Strait of 6m near the western coast.

The average ice thickness of the pack ice at its western limit was taken to vary as the function  $a + by^3$  ( $a$  and  $b$  constants) where  $y$  is the distance along the vertical axis of the grid (with increasing  $y$  towards north). This is so that the initial ice thickness increases from south to north, with enhanced thickness in the Fram Strait region. The initial ice thickness distribution at each point was then determined by assuming that the probability density decreases linearly from  $h = 0$  to  $h = h_{\max}$ , the maximum thickness. For such a linear distribution,  $h_{\max}$  is three times the mean ice thickness. In addition, where the compactness was set to unity, the thin ice in level 2 was redistributed to level 3, and very close to the coast it was further redistributed to level 4. Figure (6.2) shows contours of the mean ice thickness, and the compactness used to initialize the model run.

The thickness distribution at the northern boundary is specified not only initially, but throughout the integration. The procedure for determining this is the same as that used in obtaining the initial distribution except that now the position of the 3/8 compactness line is specified as a function of time. Monthly values of the position of this

Figure(6.2)



Contours of the initial ice thickness and compactness used in the standard model simulation. The contour interval for the compactness diagram is 0.125.

line were obtained from Vinje (1979, 1980), and interpolated to weekly values.

Initially, the floe sizes are set to the largest value allowed in the model, the winds acting immediately to break up floes that are too large. In addition, the floes entering the grid through Fram Strait are specified to be equal to the maximum allowable floe size.

### 6.1.3 Oceanic heat flux and initial mixed layer temperature

The mixed layer temperature in the model is defined where an ice cover exists, to be  $271.2^{\circ}\text{K}$ , the freezing point of sea water. Where the initial ice distribution consisted entirely of open water, the initial mixed layer temperature was increased linearly away from the ice edge, the heat contained in the mixed layer at a given distance away from the ice edge being just enough to melt all the ice at an equivalent distance into the pack. This is the result of extrapolating the linear ice thickness profile away from the ice edge and converting the resulting negative ice thicknesses into a mixed layer temperature increase. A rise of one degree Kelvin for a 30m mixed layer would be enough to melt a layer of ice of about 42cm in thickness, before the mixed layer temperature returned to freezing point.

Little is known of the magnitude and distribution of the oceanic heat flux, the heat entering the surface mixed layer from the deep sea levels. Thermodynamic sea ice models have been found to produce excessive ice growth if the oceanic heat flux is set to zero. Maykut and Untersteiner (1971) used a constant value of  $2\text{Wm}^{-2}$  (equivalent to  $0.057\text{ cm/day}$  of melting) in their standard simulation although the model can be made to give reasonable ice thicknesses in the Central Arctic without oceanic heat flux if the other forcing parameters are suitably tuned (personal communication, K. Shine, University of Liverpool). Tucker (1982), in modelling the East Greenland area uses an oceanic heat flux equivalent to a melt of  $10\text{cm/day}$  in the regions east of a band roughly corresponding to the expected position of the ice edge. By adjusting the oceanic heat flux in this way, one can control the ice edge position, and for the model here, Tucker's (1982) value of the heat flux is high enough to do this. It was

felt undesirable to force the results of the model in this way so the simulations here were run with lower heat flux values. The heat flux distribution used in the model was such as to have a  $3.5 \text{ cm day}^{-1}$  melt at the grid point (20,30) with a  $\frac{1}{2}(1-\cos\theta)$  decrease away from this maximum, reaching zero on the southern edge of the grid and at the East Greenland coast. This oceanic heat flux distribution was found to stabilize the ice distribution changes for early December and is also similar to the oceanic heat flux derived from the Hibler and Bryan (1983) ocean-ice model.

To give an idea of how much the oceanic heat flux can influence the position of the ice edge when melting and advection are taking place, a simplified version of the ice thickness distribution equation may be considered.

$$\frac{\partial h}{\partial t} + \frac{\partial(uh)}{\partial x} = f(x) \quad (1)$$

where  $h$  is the average ice thickness (the volume of ice per unit area). If  $u$  is constant, then to maintain an ice edge at a constant position, take

$$\frac{\partial h}{\partial x} = \frac{\partial h}{\partial t} = 0 \quad (2)$$

so that

$$f = u \frac{\partial h}{\partial x} \quad (3)$$

For the initial conditions near the northern part of the grid,

$$\frac{\partial h}{\partial x} \approx -8 \times 10^{-6} \quad (4)$$

for which a velocity of about  $5 \text{ cms}^{-1}$  away from the ice edge would be

Table 1

Values of humidity and cloudiness (percentage)  
used as input to the thermodynamic calculations.

Humidity

Month	Jan Mayen	Myggbukta	Average
January	82	76	79
February	81	74	78
March	81	76	78
April	83	81	82
May	86	78	82
June	90	82	86
July	87	83	85
August	84	75	80
September	81	70	76
November	82	74	78
December	82	78	80

Cloudiness

Month	N.E. Greenland	Svalbard	Jan Mayen	Myggbukta	Average
January	53	66	83	58	65
February	45	73	82	48	62
March	48	64	78	49	60
April	50	59	81	44	58
May	51	79	83	83	61
June	58	83	83	64	72
July	58	86	88	61	73
August	71	87	86	66	78
September	72	78	80	57	72
October	67	78	82	57	61
November	60	79	82	62	71
December	51	69	81	51	63

sufficient to balance a melt of 3.5 cm/day.

#### 6.1.4 Input winds and temperatures

Both the temperature and the wind speed are important in determining the thermodynamic growth rates, the wind field also being important in the dynamics. Spatially varying temperature fields are needed in this study because of the large variation that can exist across the Greenland Sea. This is particularly the case in the winter months when the mean monthly temperatures can vary from  $-28^{\circ}\text{C}$  in the north-western corner of the grid to about  $0^{\circ}\text{C}$  in the south-east (Crutcher and Merserve 1970). Both the spatial and temporal variations in the wind field are important.

Wind and temperature data was available from the ECMWF FGGE IIIB dataset, which had a spatial resolution of  $1.875^{\circ}$  (ECMWF: The Global Weather Experiment daily global analysis). The data was given for 12 hour intervals, zero and 12 hours GMT. Surface temperature and 1000mbar winds were used. Hibler's (1980b) model code was written for geostrophic wind input and so the input winds used here were converted to geostrophic winds using a turning angle and modifying the magnitude (McPhee 1980). The input fields were interpolated to the model grid using simple bilinear interpolation.

#### 6.1.5 Other thermodynamic inputs

To complete the list of inputs, we consider those for which average values over the grid are sufficient, and a representative value is more important to the results than are the variations from that value. Monthly averaged cloud cover values are used and obtained from Huschke (1969) and Hovmöller (1945). The values obtained are those of stations in North Greenland (Huschke 1969) and Jan Mayen and Myggbukta (Hovmöller 1945) which correspond roughly to the four corners of the grid used. The mean of the four sets of data are used and the monthly values are given in table 1.

The humidities are those given by Hovmöller averaged from the two stations at Myggbukta and Jan Mayen.

The atmospheric pressure values were obtained from the FGGE dataset and averaged over the East Greenland grid.

All the quantities described here were either interpolated from monthly values or averaged from half-day intervals to weekly values.

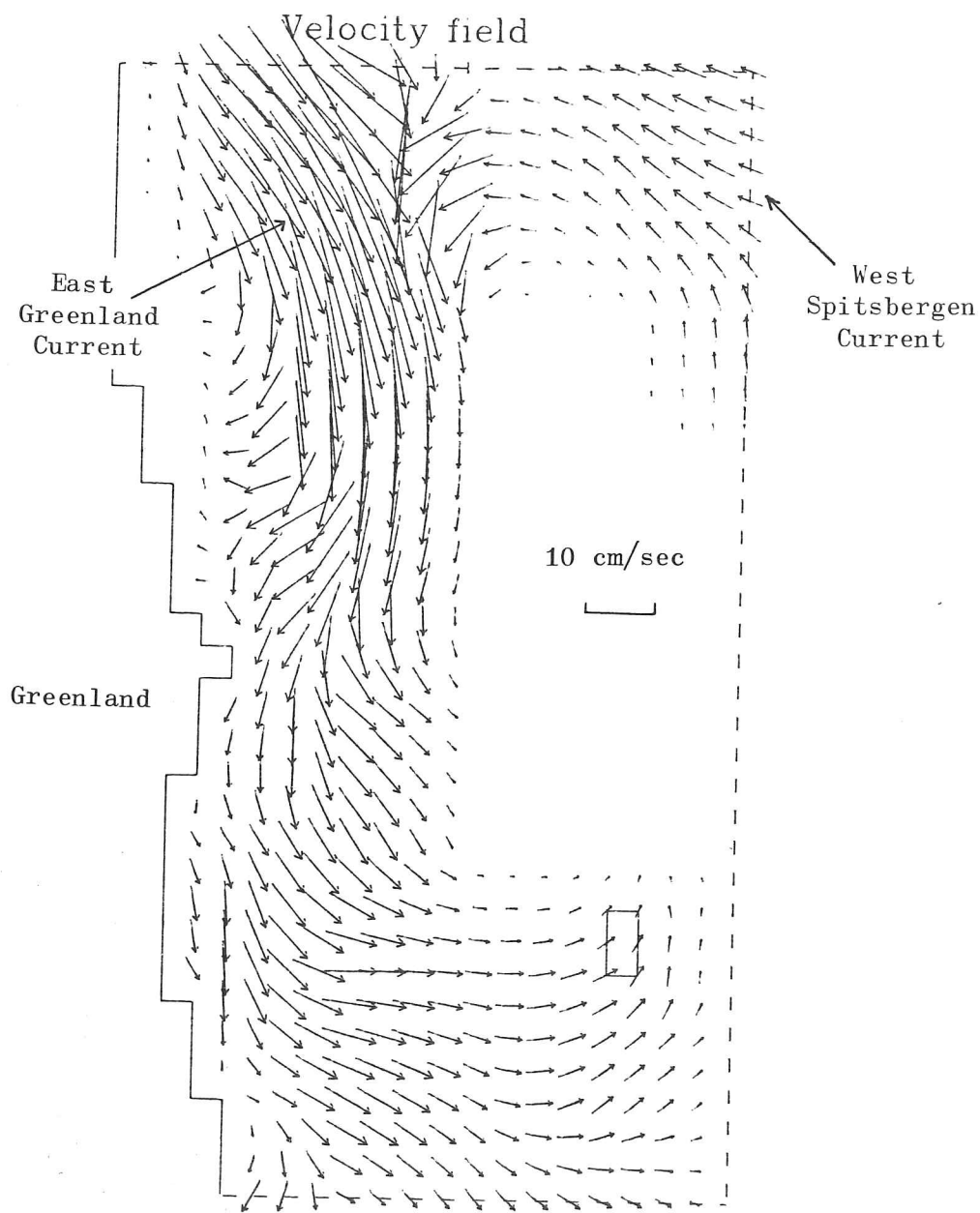
#### 6.1.6 Ocean currents

The geostrophic current with its associated sea surface tilt are of sufficient magnitude to affect the ice distribution in the Arctic (Hibler 1979). In one of Tucker's (1982) sensitivity studies however, he found that for the East Greenland region the inclusion of geostrophic currents had negligible effect upon the ice distribution simulation. The geostrophic current field as used in Tucker's (1982) simulations was not of a sufficiently high resolution to include the high speed ( $\sim 30 \text{ cm s}^{-1}$ ) parts of the East Greenland Current. The highest speeds occur just to the south of Fram Strait in the region near the shelf break (Wadhams 1981). In another sensitivity study Tucker used long term wind driven ice velocities obtained from a previous run, as an ocean current input for a test run. Although there is no physical justification for such a procedure, in this particular case the current velocities used more closely resembled the observed long term currents than did the geostrophic currents that he used. This test indicated that by not including the high speed East Greenland Current, the results could be adversely affected.

In view of these points, it was decided to use modified observed long term currents as the current input. The observed currents used are those of Kiillerich (1945), adjusted to include some measurements given by Coachman and Aagaard (1974). For the model run, the values were reduced by a constant factor to parameterize the effect of meandering or snaking of the path of the current and to attempt to counter the effect by which parameterizing any time varying forcing by using constant time averaged values overestimates the true response. The resulting field is shown in figure (6.3). Time-varying wind-induced currents were also parameterized as described in section 6.3.3.

The sensitivity of the motion of sea ice to ocean currents, together with the fact that that long term currents are specified, mean that errors in the oceanic forcing will build up. As an example, errors in the

## Ocean current input



Figure(6.3) The long term ocean current input for the model interpolated from a map produced by Kiilerich (1945) supplemented with data from Coachman and Aagaard (1974).

specified currents can upset the delicate balance between advection and melting at the ice edge. Also, near coasts, specifying too large a current could result in excessive build up of ice there. In the standard run we have opted to have currents on the low side. In this way, errors are not compounded, and also it allows the time varying wind fields to be the dominant forcing, the effects of a long term current field being more intuitively obvious. The lack of accurate time varying data for the oceanic forcing terms (including the heat flux) is perhaps the major source of error in the model. Coupled ocean-sea ice models which are now being developed should be the answer to these difficulties.

## 6.2 Application of the model to a standard simulation

### 6.2.1 Introduction

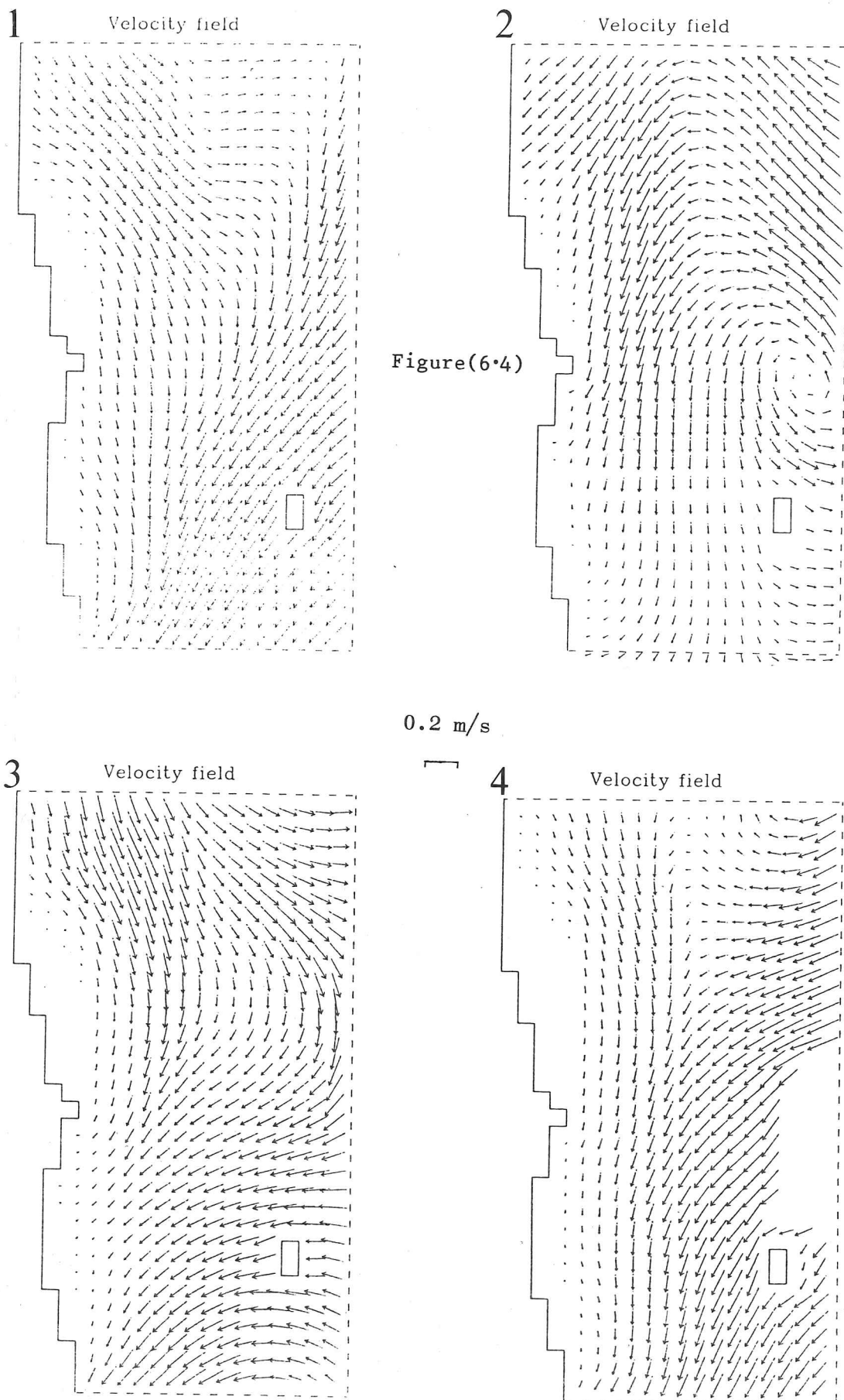
The model was run through a standard simulation with initial conditions for 30 November 1978. The time step used was six hours and with a grid length of 35 km this meant that for expected ice velocities, the Courant-Friedrichs-Lewy stability requirement for the advection equations would be satisfied. This states that the following inequality involving the ice velocity should hold,

$$\Delta x > \Delta t \sqrt{2(u^2 + v^2)} \quad (5)$$

where  $\Delta x$  is the grid length and  $\Delta t$  is the time step.

### 6.2.2 Variability of the model results

There is considerable day to day variability in some of the output fields. Figure (6.4) shows ice velocity fields 84 hours apart. The applied wind field changes from day to day and it is this that is responsible for the rapid changes in the resulting ice velocity field. The average floe size varies in some places fairly rapidly. This would be expected to occur where the compactness was high and converging conditions occurred abruptly giving rise to large numbers of floes coming together. The ice



Instantaneous ice velocity vector plots from the model for periods 84 hours apart showing the rapid changes possible. The period covered by the figures is from 13 to 23 April 1979.

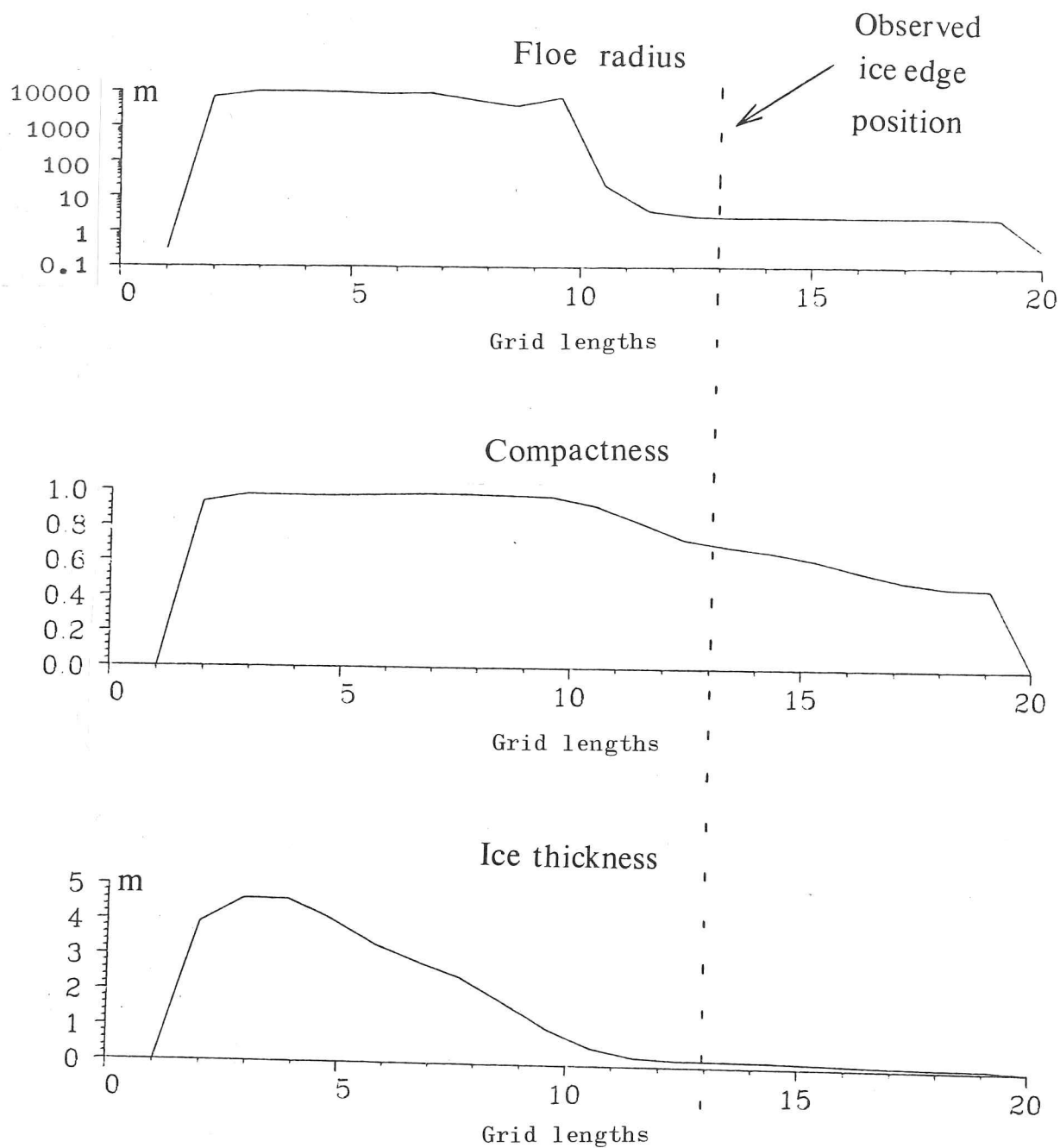
thickness distribution does not change so rapidly, although where the ice is thin, the higher velocities mean that features can advect tens of kilometres in a few days.

The floe size fields show a greater spatial variation than the ice thickness fields, as might be expected (see figures 6.11, 6.12 and 6.13 for some examples). First of all, there is a large range of possible values that floe size can take, and secondly it is quite possible for neighbouring grid squares to have floe size values that span this entire range (the wind field may break large floes in one grid square but not in the neighbouring square). Despite this, some coherent structures appear to be visible, particularly in regions of large floes. For the regions in which very large floes are indicated, the interpretation should be that the region consists essentially of a continuous ice cover. At the other end of the floe size spectrum, predicted floe sizes of less than 1 or 2 m should be regarded as meaning simply that the ice cover is highly broken up. This occurs for thin ice very near the ice edge where the effects of ocean waves have been parameterized by artificially weakening the ice there.

### 6.2.3 General features of the output fields

We must be careful when interpreting features of the output that occur near the start of the simulation because they may be due to the form of the initial distribution specified. We thus regard the first two or three months of the simulation as the (settling down) period during which the thickness distributions develop their own characteristic profiles.

During the first week or so of the simulation, which would be expected to be a period of ice growth (in thickness and extent), the position of the  $3/8$  ice concentration line advanced at an expected rate. However the fairly high initial sea surface temperatures in some regions dropped despite the imposed oceanic heat flux term, down to freezing when a thin ice layer of high compactness (greater than 90%) formed over most of the formerly open water region. The layer remained thin for a considerable amount of time and a sharp increase in the ice thickness within the pack persisted. Figure (6.5) shows the ice characteristics along a transect



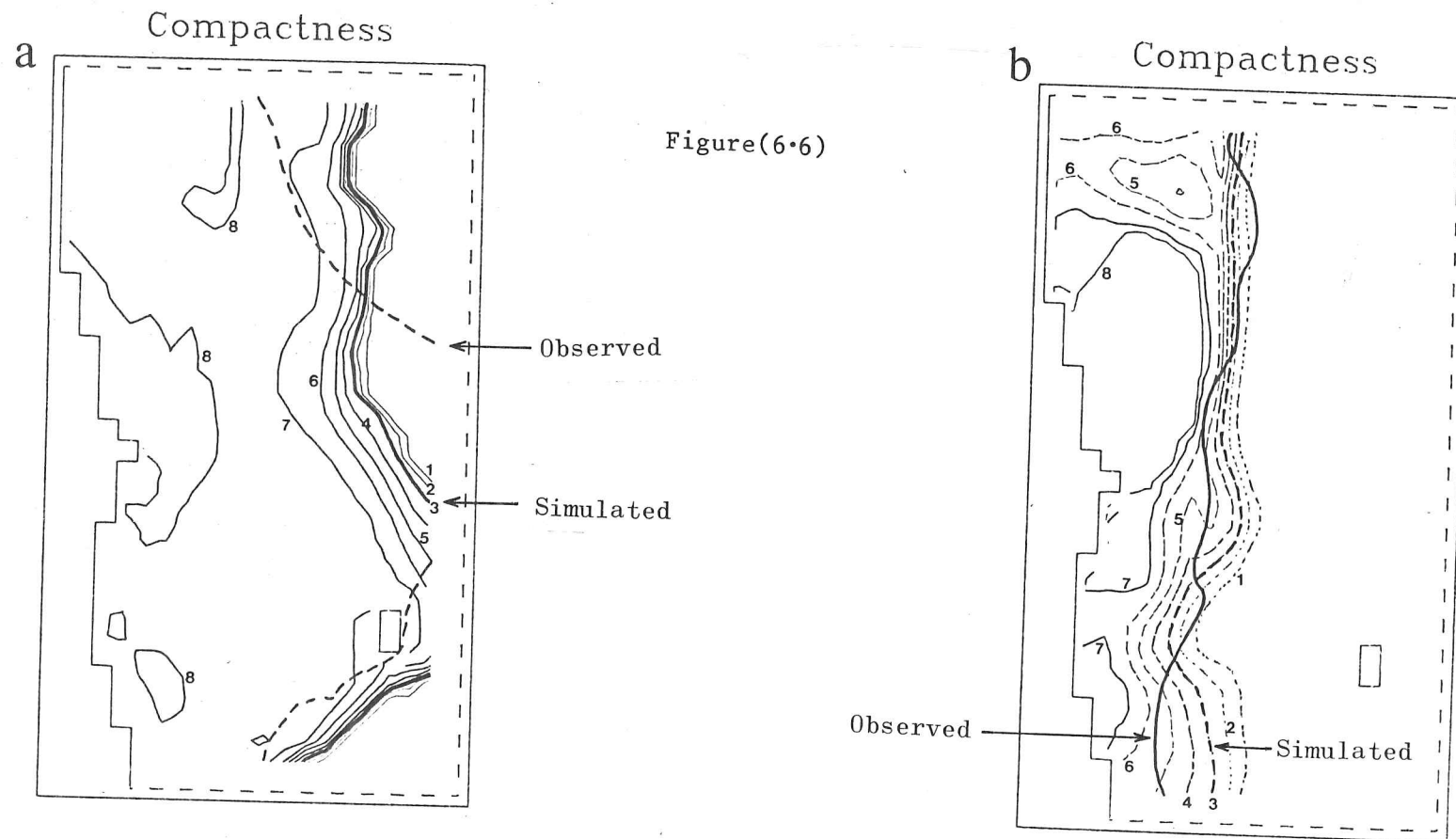
Figure(6.5)

Ice characteristics along a transect during a period when the model output included a large area of thin ice (in this example the date is April 12 1979). The observed ice edge at that time is also indicated.

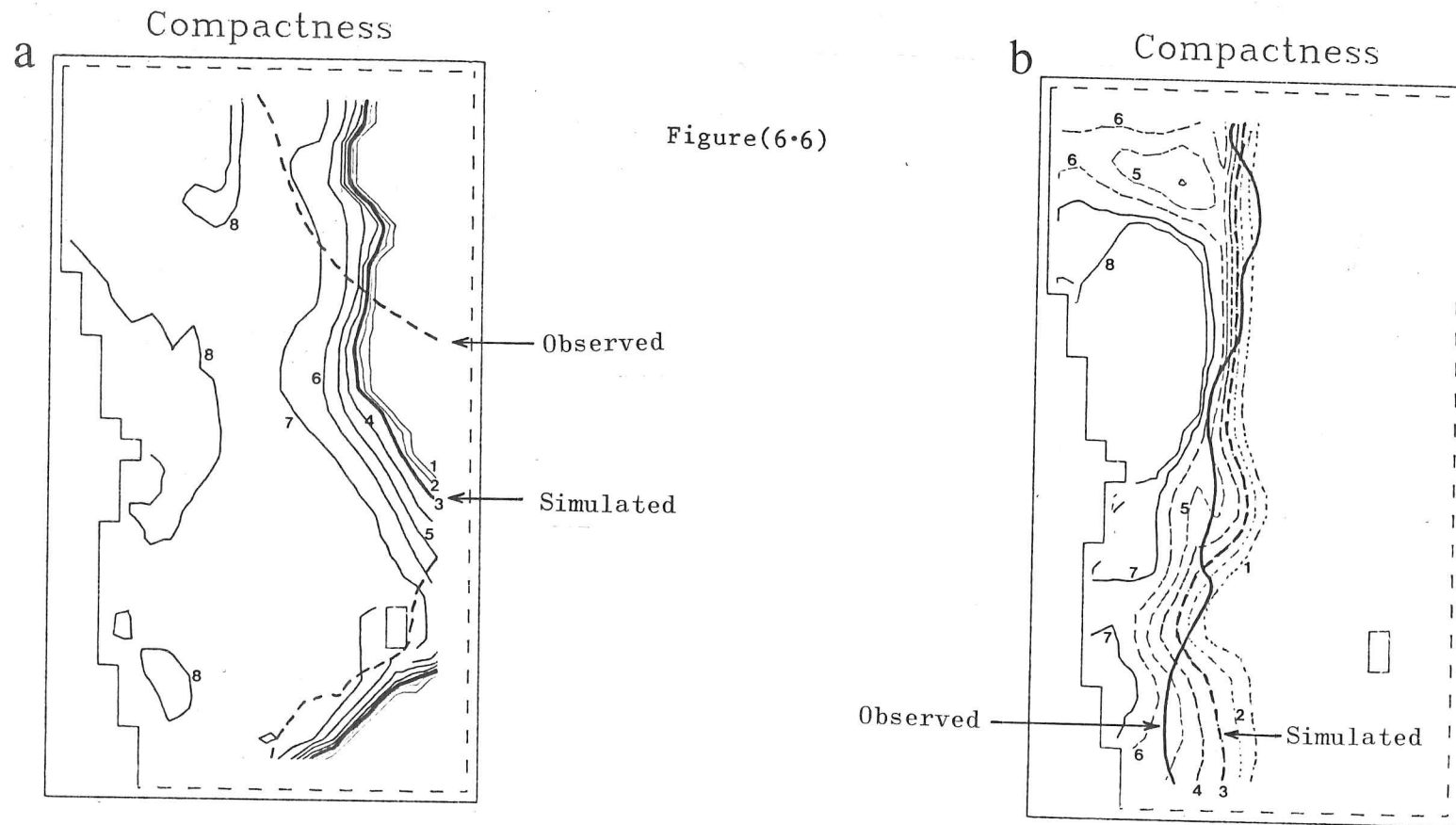
across the Greenland Sea toward the end of this period. It is this thin layer of ice that can be removed by specifying an oceanic heat flux as high as that specified by Tucker (1982) in his Greenland Sea simulation. An oceanic heat flux that effectively defines the position of the ice edge might also undesirably affect the type of ice edge profiles developed. Since the ice edge profile is of interest in this study, the lower values of heat flux used here allowed more natural ice edges to appear during the spring melting. The compactness field for the end of December (after one month's simulation) is shown in figure (6.6a) which also includes the observed  $3/8$  concentration line (Vinje 1979). It shows that by then, the observed and simulated ice edge positions had already started to diverge. The initial oceanic heat flux and sea surface temperature distributions could of course be adjusted (by trial and error) to give the correct ice edge position after a month's simulation, but this might be regarded as excessive 'tuning'. The inability of the model to predict the correct lateral extent of the thin ice during winter meant that observed features of the ice edge for the year 1979 were not modelled. These include a large tongue of sea ice extending northward from the ice edge north of Jan Mayen (Vinje 1980). The same feature occurs in other years (it previously appeared in 1971) in the same location and has acquired the name "Odden" (Vinje 1980). In 1979, Odden appeared in February and became detached by April, melting completely by May.

The compactness values which in winter were found difficult to simulate show much better agreement at the start of June. This can be seen clearly if we compare the model results with Vinje's (1980) data (figure 6.6b).

An energy source, not yet considered, that is available in the winter for ice melting is that due to wave action, the energy ultimately deriving from the wind. This would have the desirable effect, as far as this model is concerned, of melting ice near areas of open water, but leaving unaffected the thick ice away from the ice edge. Wadhams *et al* (1979) calculate that for typical conditions near the ice edge in the Greenland Sea, wave-induced melting can destroy a 3 metre floe in a matter of days (if the wave has a 5m amplitude, the floes will melt in about 1-2 days; for a 1m amplitude wave, the melting would take about one week). The melting is caused by a turbulent heat exchange between the lower surface of the ice



Comparison of observed and simulated  $3/8$  concentration line. Diagram (a) refers to the end of December after one months simulation. Diagram (b) is for the end of May after the spring melting of the thin ice. The compactness contours are measured in eighths.

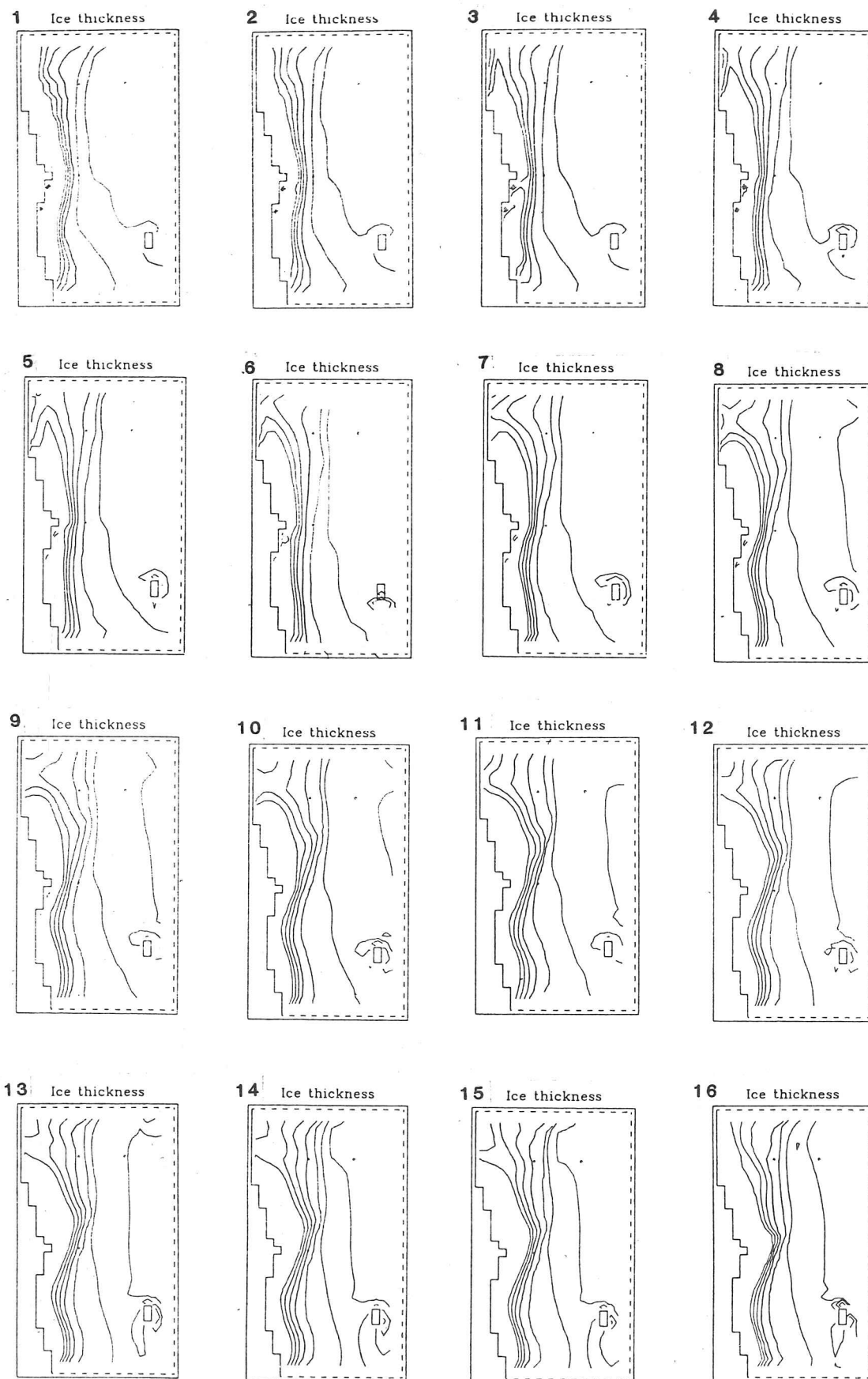


Comparison of observed and simulated  $3/8$  concentration line. Diagram (a) refers to the end of December after one months simulation. Diagram (b) is for the end of May after the spring melting of the thin ice. The compactness contours are measured in eighths.

and the ocean. This requires the water near the ice surface to be above the melting point of ice. For the model simulations, no such temperature difference is possible so that more elaborate oceanic boundary layer formulations would be required to model wave and shear current-induced melting.

Some features of the ice thickness distribution near the East Greenland coast are interesting. When the ice velocity is towards the coast, the ice thickness there increases. However, when wind changes result in an ice velocity away from the coast, the rheology in the model is such that the formation of open water occurs comparatively easily. This, as was shown in chapter 4, considerably reduces the resistance of the ice to deformation, which results in a large shear and further opening. The effect, which can be seen in figure (6.7) is to peel off a layer of thick ice which becomes caught in the East Greenland drift stream and is advected south. This situation stops, usually in a matter of days, when the wind again turns. The open water formed near the coast soon becomes frozen in winter (figure (6.7) starts in March). The ice still has a low compressive strength so that the thick ice can return to the coast.

Figures (6.8a-f) show the changes to the mean ice thickness distribution, the compactness and the mean floe size distribution at times throughout the model integration. For comparison, observed ice limits from charts produced by the United States Naval Polar Oceanography Centre are shown which include more detail than Vinje's data. We see from figure (6.8a) that one month after the start of the simulation, a large amount of new ice has formed near the centre-right of the grid. In the model simulations, a large area of new ice forms, but in a region too far south. By early February (figure (6.8b)), the initial errors have compounded and there are few features, other than very general ones, in the simulated output that can be equated with the observed sea ice distribution. Four weeks later (figure 6.8c) things have started to improve. The region of open sea in the map of the observed conditions seems to correspond to the areas of reduced compactness and very small floes suggested from the model output. Figure (6.8c) shows a much reduced area of large floes compared to that in figure (6.8b). In addition, the area of the observed ice of high concentration (7/8 to total) also undergoes a considerable reduction. In



Figure(6.7)

The contours are (from left to right) 5m, 4m, 3m, 2m, 1m and 0.5m.

Continued on the next page.

Figure (6.7)

Continued from the previous page.

The development of features near the coast of East Greenland. Notice the changes occurring in the top left area of each picture. An area of thick ice becomes detached (Picture 3), gets advected south until it hits a larger area of thick ice (Picture 6). Eventually (Picture 16) the ice thickness pattern again resembles the original (Picture 1).

Other smaller areas of thin ice near the coasts can be seen further south. (Pictures 1-9).

Picture 1 refers to 12 March 1979 and picture 16 refers to 4 May 1979, each picture being 84 hours apart.

Figure(6.8)

The next 6 figures show the development of ice characteristics throughout the model run. For comparison, we show the observed ice conditions as presented by the United States Naval Polar Oceanography Centre. Suitland, Md.

Figure (6.8a)

26 December 1978

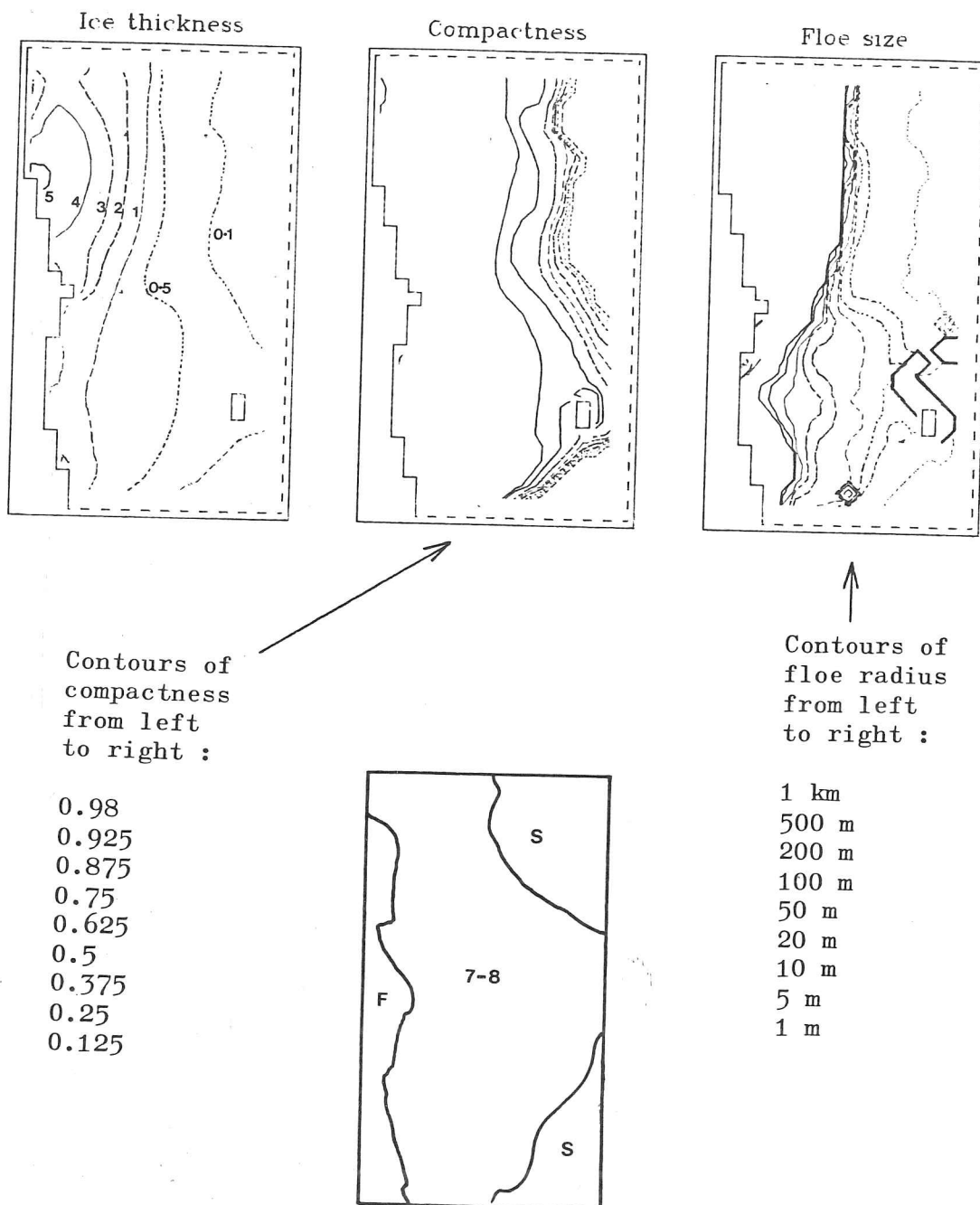


Figure (6.8b)

7 February 1979

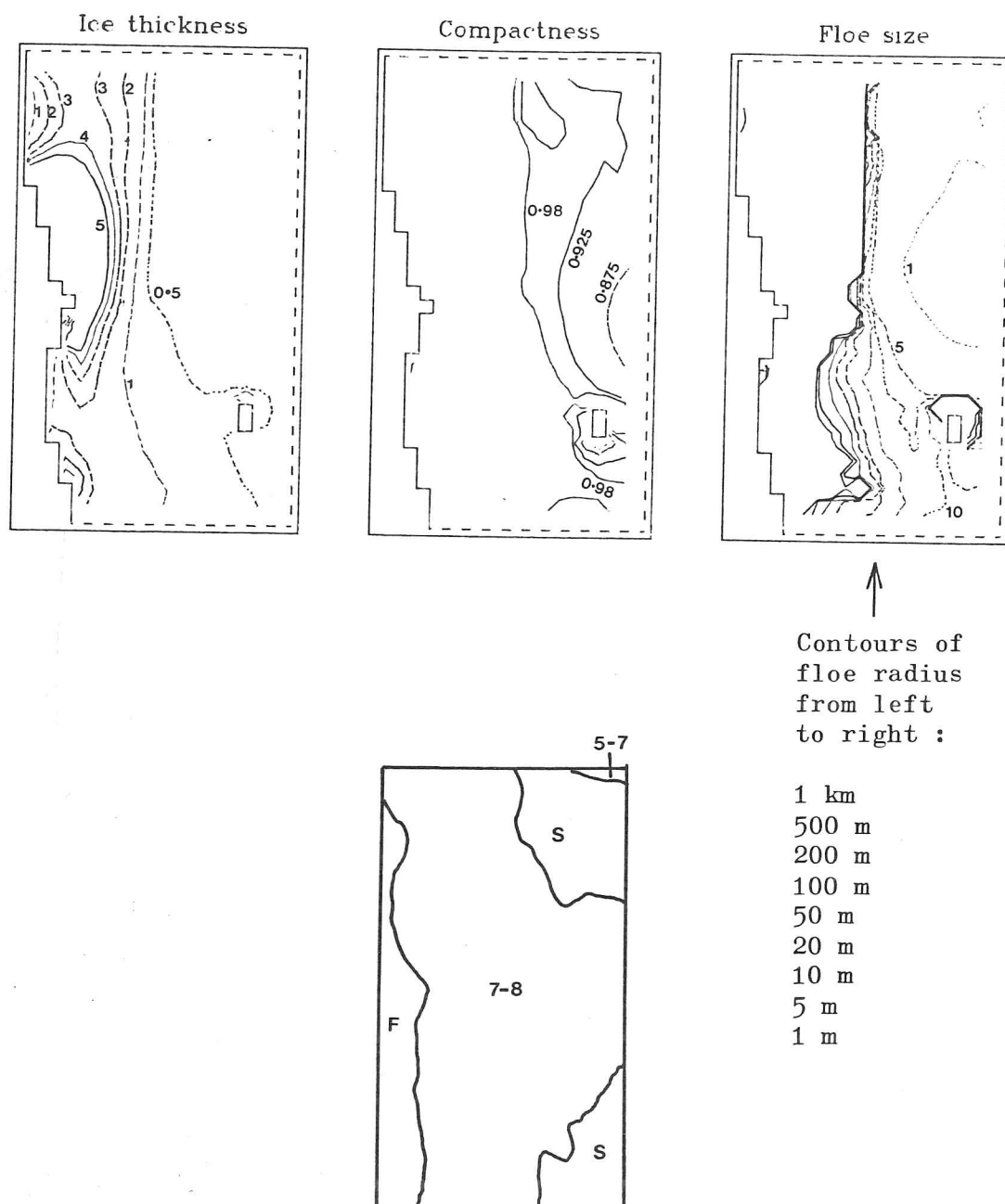
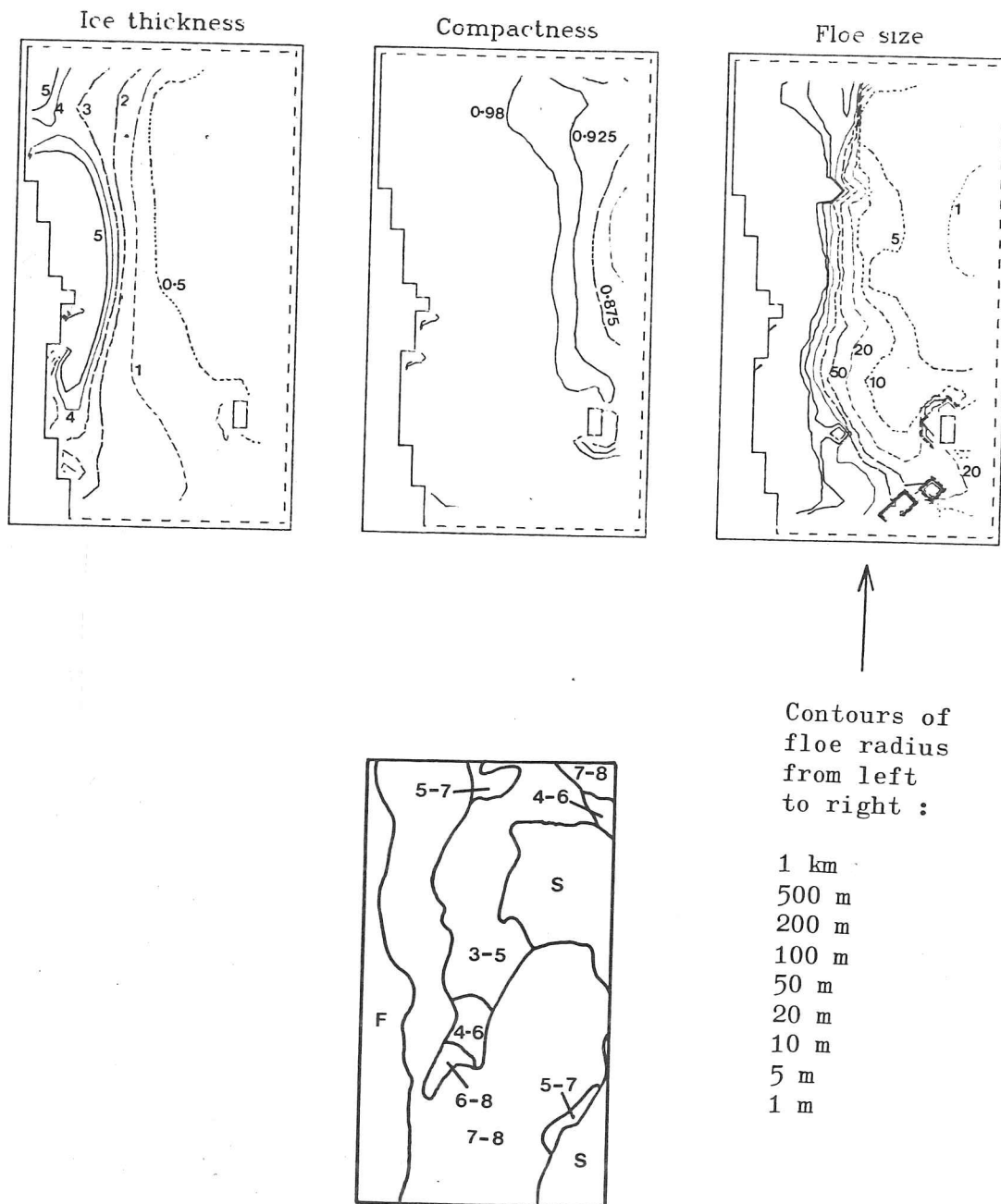


Figure (6.8c)

6 March 1979



Contours of  
floe radius  
from left  
to right :

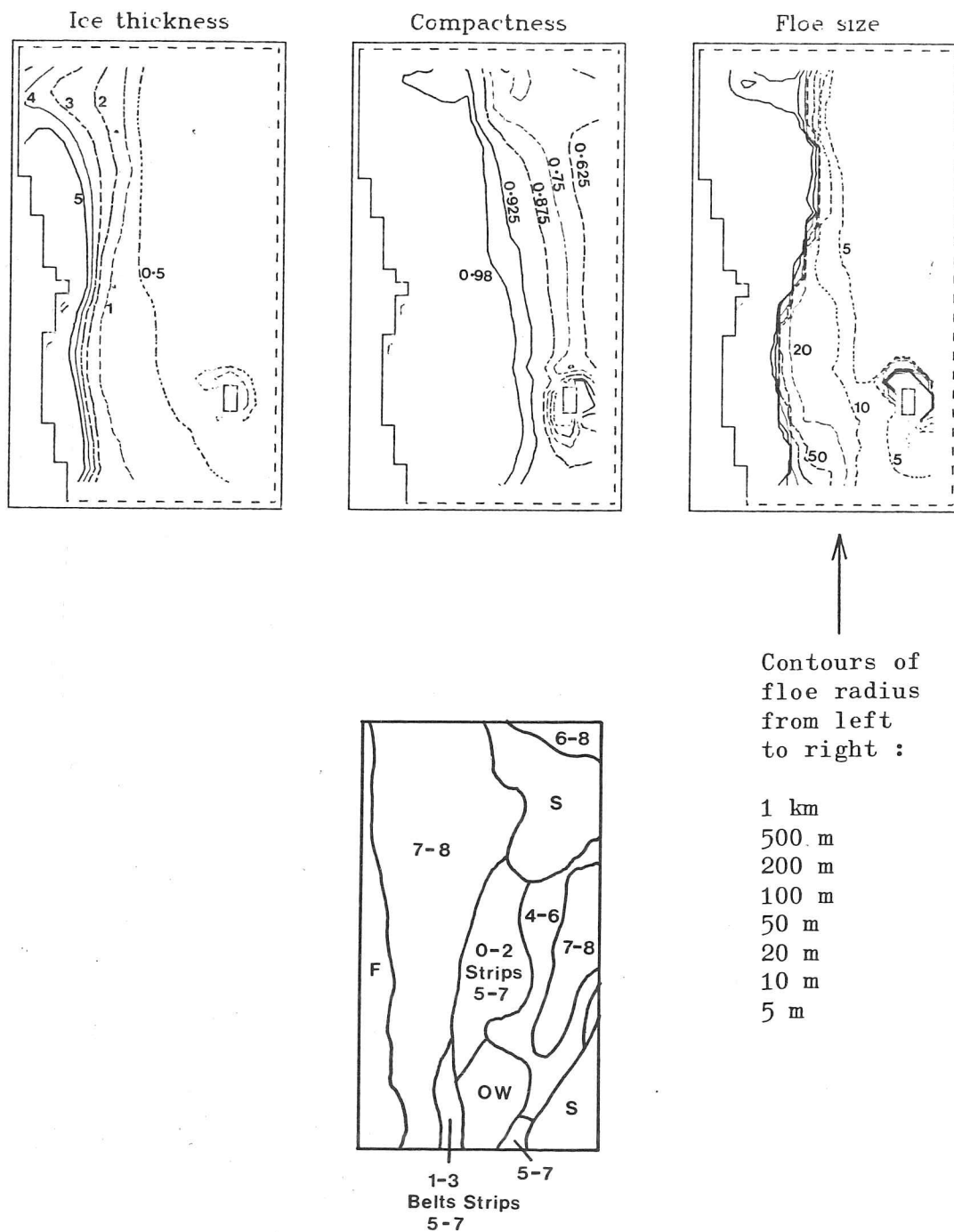
1 km  
500 m  
200 m  
100 m  
50 m  
20 m  
10 m  
5 m  
1 m

## Key to symbols

- S Sea  
F Land and fast ice  
OW Open water (Within ice limit)  
7-8 Fractional ice area (Eighths)

Figure (6.8d)

3 April 1979

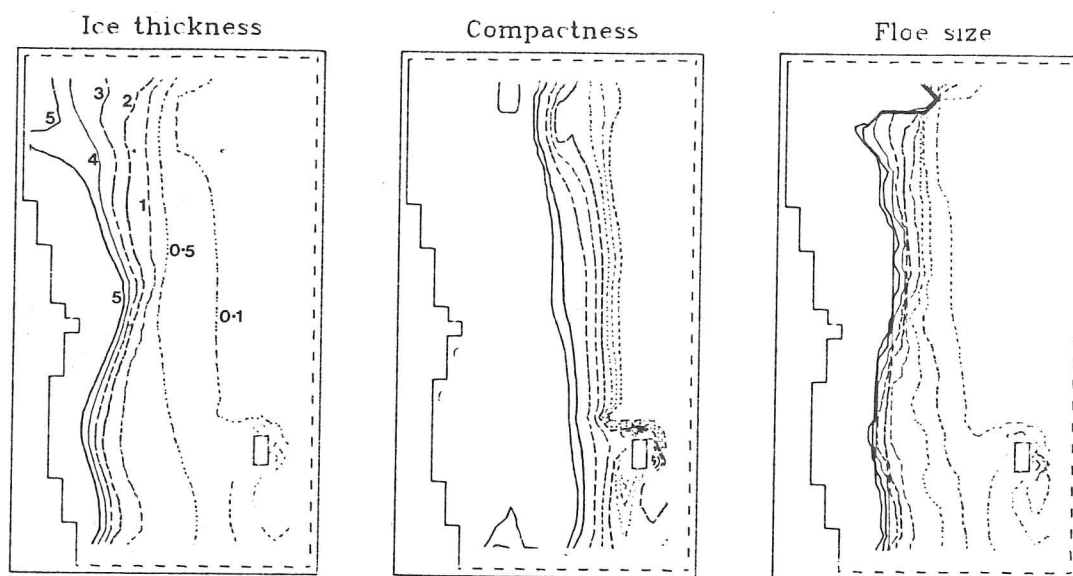


## Key to symbols

- S      Sea
- F      Land and fast ice
- OW      Open water (Within ice limit)
- 7-8      Fractional ice area (Eighths)

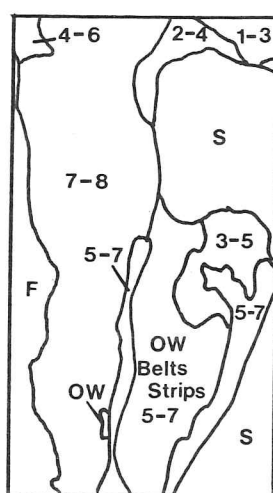
Figure (6.8e)

1 May 1979



Contours of  
compactness  
from left  
to right :

0.98  
0.925  
0.875  
0.75  
0.625  
0.5  
0.375  
0.25  
0.125



Contours of  
floe radius  
from left  
to right :

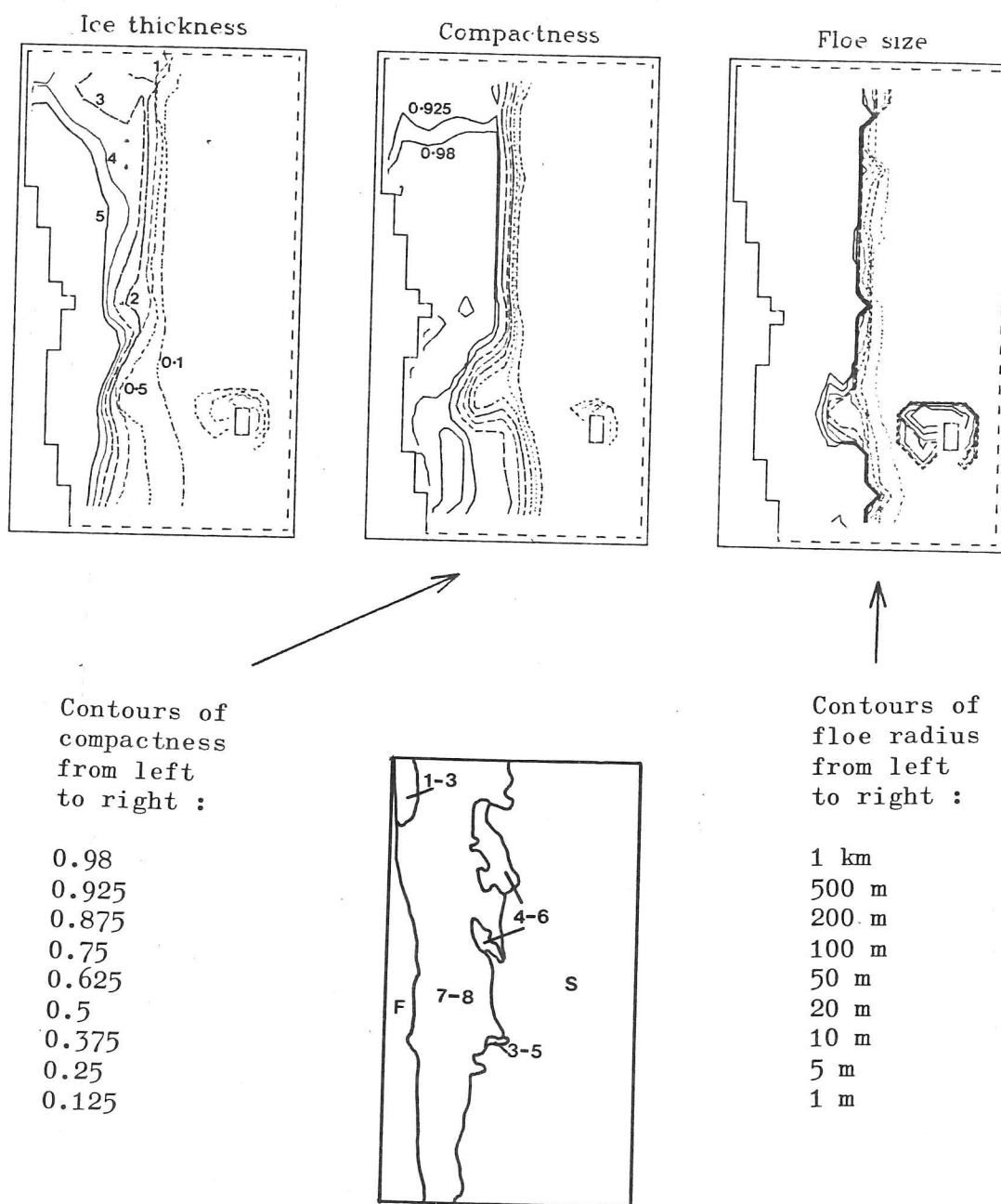
1 km  
500 m  
200 m  
100 m  
50 m  
20 m  
10 m  
5 m  
1 m

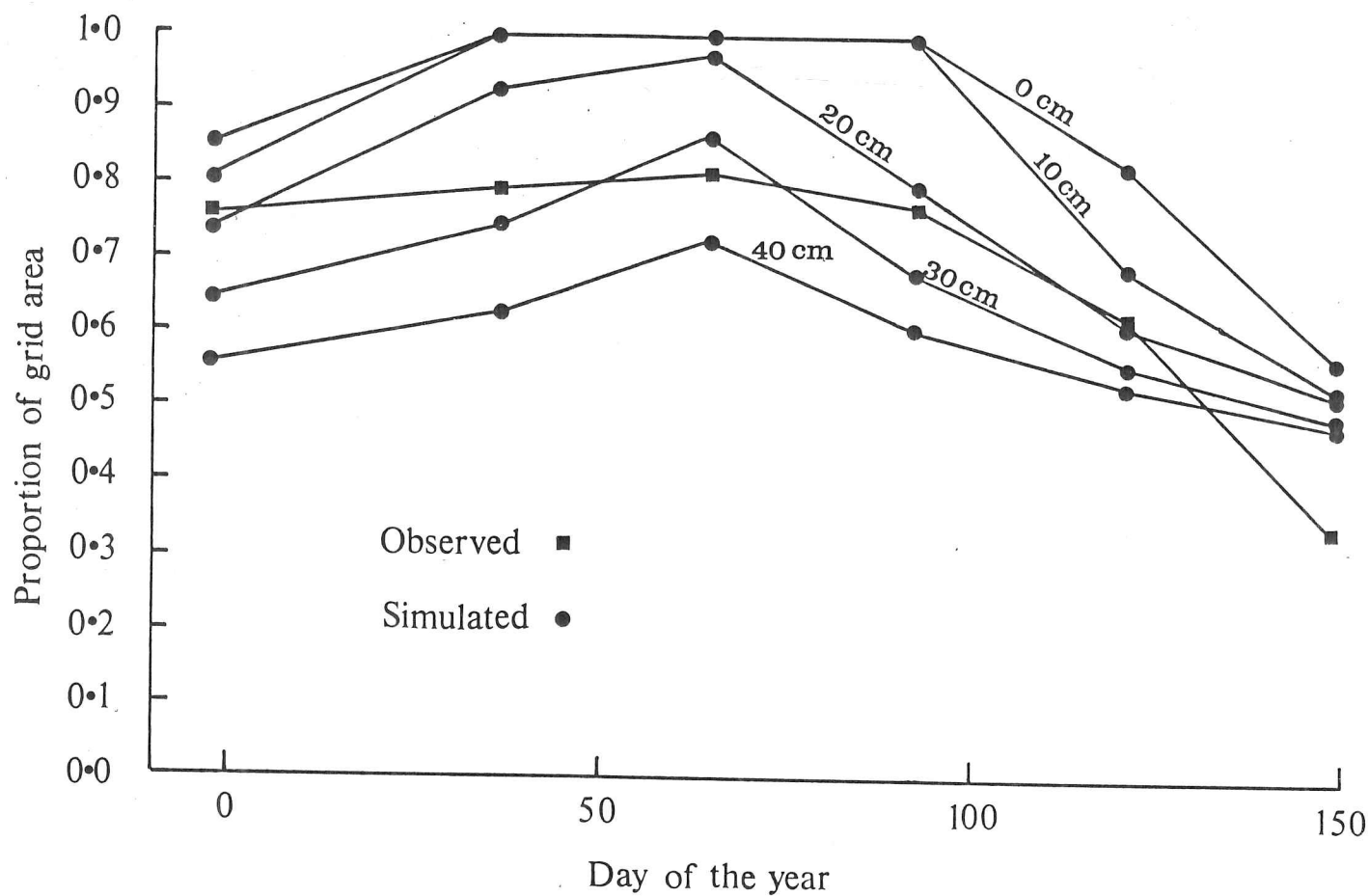
## Key to symbols

- S Sea  
F Land and fast ice  
OW Open water (Within ice limit)  
7-8 Fractional ice area (Eighths)

Figure (6.8f)

29 May 1979





Figure(6.9)

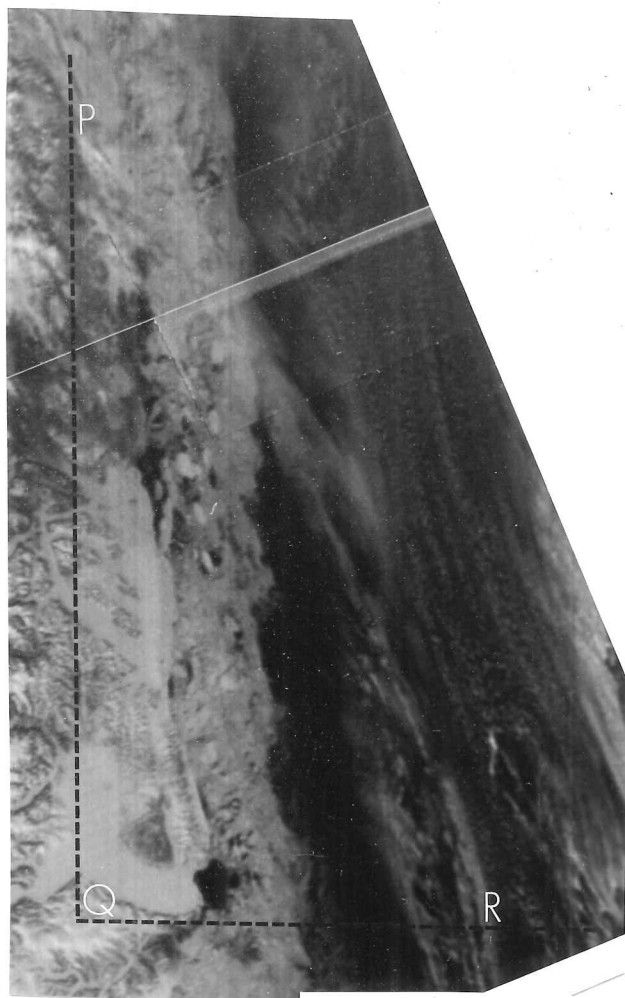
The observed extent of ice in the region covered by the model grid (given as a proportion of the area of sea in the grid) is compared with the extent predicted by the model. Also shown are the extents of ice of thicknesses greater than certain values (10 cm, 20 cm, 30 cm and 40 cm).

The proportions can be multiplied by  $0.69 \times 10^6$  to give actual areas ( $\text{km}^2$ ).

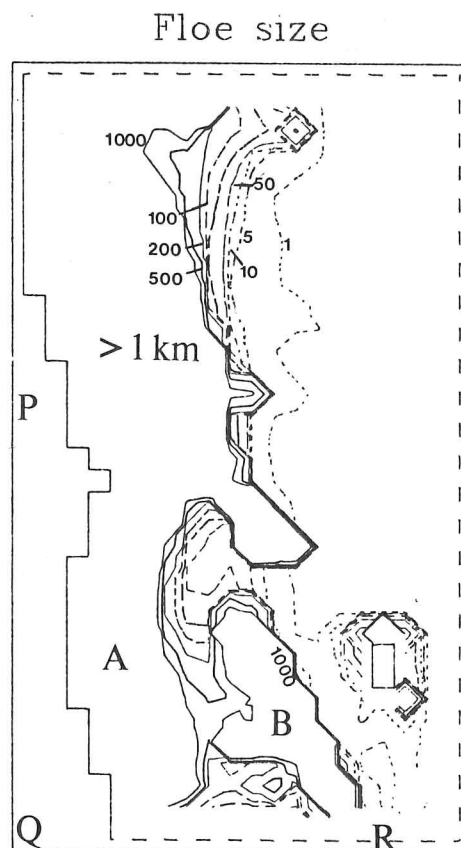
figure (6.8c), the area of large floes at the top left of the grid area seems to correspond quite closely with the observed area of high concentration. However, the large area of ice of high concentration observed near the south-west part of the grid is not simulated. After a further 4 weeks (figure (6.8d)), the area covered by compact ice increases slightly. Also, the simulated area of large floes shows a similar increase in extent, the resulting area corresponding very closely to the observed high compactness region. This correspondence remained close for the rest of the simulation. The area of compact ice at the eastern side of the grid started to melt at this time (early April 1979) so that by the start of May (figure (6.8e)) a general agreement between the observed and simulated compactness fields occurs, although the details of the observed picture are not simulated. The best agreement between the observed and simulated compactness fields occurs in the second half of May by which time most of the thin ice areas have melted (both in reality and in the model) (figure (6.8f)). By May the ice edge is essentially determined by the limit of the extent of thick ice. The representation of the thick ice which is naturally less responsive to forcing is also less susceptible to errors in the forcing and this could explain the improvement in the results compared to those of winter. A sharp change in ice concentration and floe size at the ice edge is then predicted, in contrast with the situation for most of the winter months.

We have seen that in the winter months, the model produces too large an extent of ice and that most of the excess area consists of very thin ice. Figure (6.9) shows the variation throughout the model run of the proportion of the sea area within the grid that is ice covered. The observed areas are those obtained from figures (6.8a-f). Figure (6.9) also shows values for total area obtained by not including ice less than a certain thickness. We see that if ice less than about 30cm is neglected in the area evaluation, then the model would predict more or less correct values for total ice extent during most of the run.

Figure (6.10) is a satellite photograph of part of the area covered by the model grid. The model floe size distribution for the same date (9 May 1979) is shown in figure (6.11). The large area of ice classified by the model as consisting of very large floes, and is marked A in the diagram

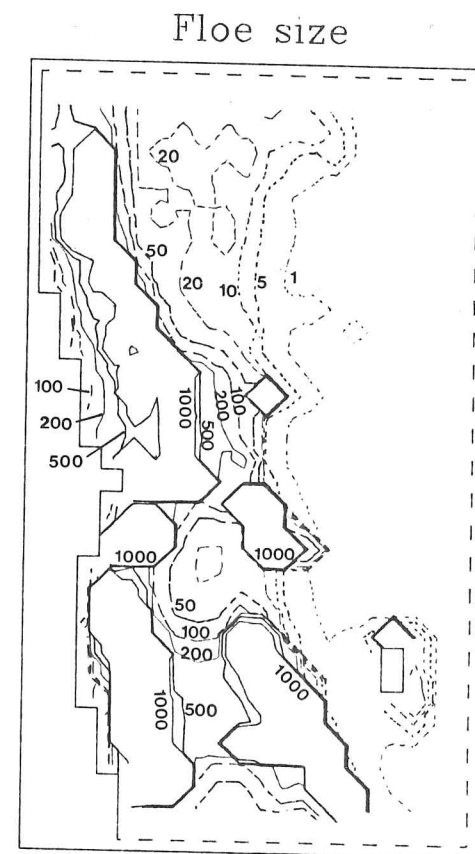


Note that the white areas to the right in the photograph are clouds rather than sea ice.  
Figure(6.10)



Figure(6.11)

Comparison of features visible in a satellite picture and a floe size contour diagram for 9 May 1979.



Figure(6.12)

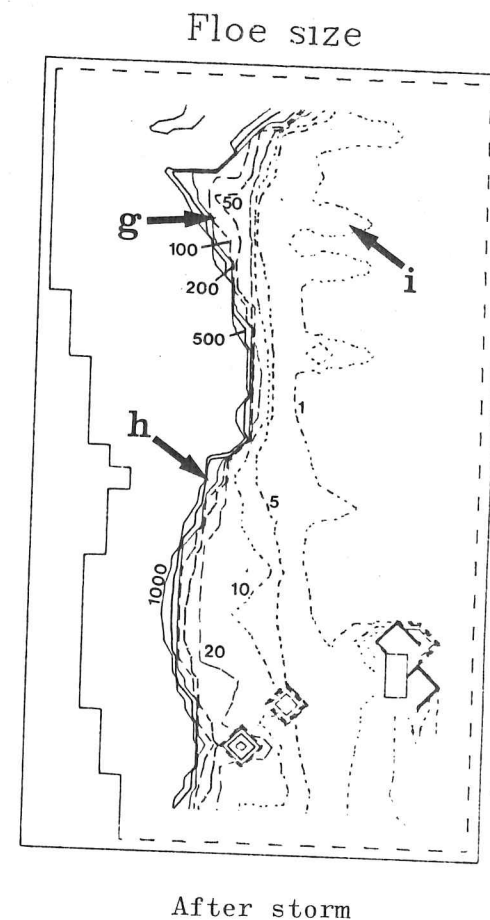
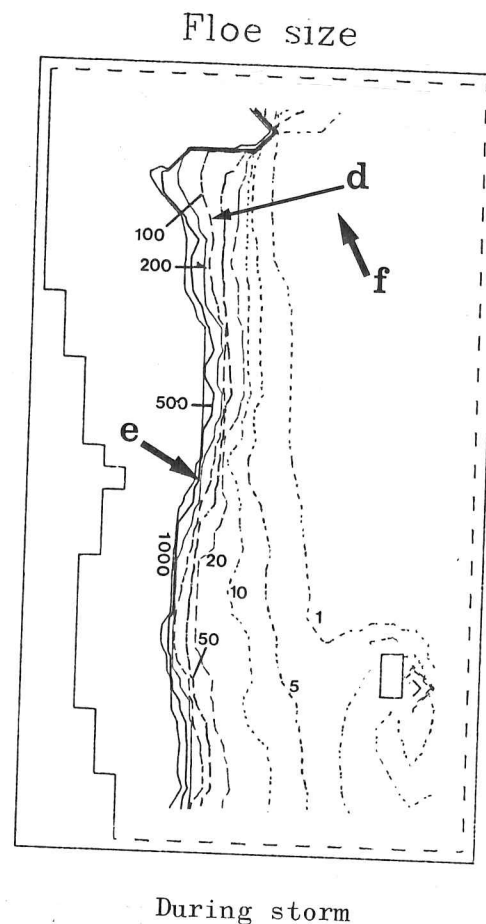
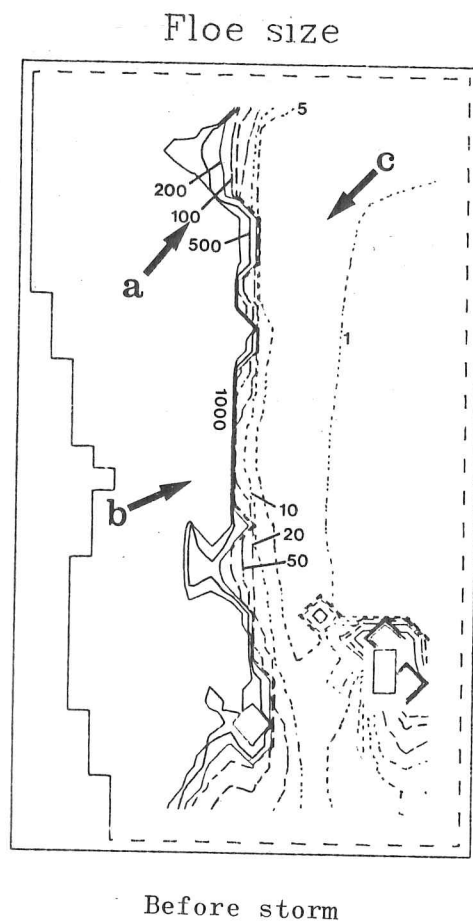
The average floe size of selected thickness categories (levels 4 and 5 of the model grid) for 9 May 1979.

corresponds well with what appears to be the main pack in the satellite image. A narrow area slightly lighter than the sea touching the main pack in the photograph suggests an area of loose pack. A larger area of loose pack (small floes) is indicated from the model results. This may be because there was ice there that cannot be detected in the image or that there was no ice there in reality. The area marked B in figure (6.11) also indicates the presence of very large floes, but again there is no sign in the image of any features there. The ice in B is however very much thinner (0.3m) than that in A (about 4m) and would thus be expected to appear (if at all) differently than thick ice in the image.

Another point to note from the satellite photograph is the detailed structure of the sea ice distribution that is visible, and in particular, the ice edge. We would not expect to simulate these details with the grid resolution used in the model. The wind fields used for forcing the model were not sufficiently detailed to include, for instance, the small scale wind anomalies that occur near the ice edge due to variations in the atmospheric drag coefficients and boundary layer stability (Overland et al 1983).

Although figure (6.11) shows a large area of continuous ice, this does not mean that there are no small floes there but that large floes dominate the field. This is illustrated in figure (6.12) which shows the average floe size for thickness levels 4 and 5 revealing that there are floes even near the coast. The diagram must be interpreted with care because it gives the floe size without any indication of the proportion of area covered by those floes. In this example, the actual number of floes near the coast would be very small.

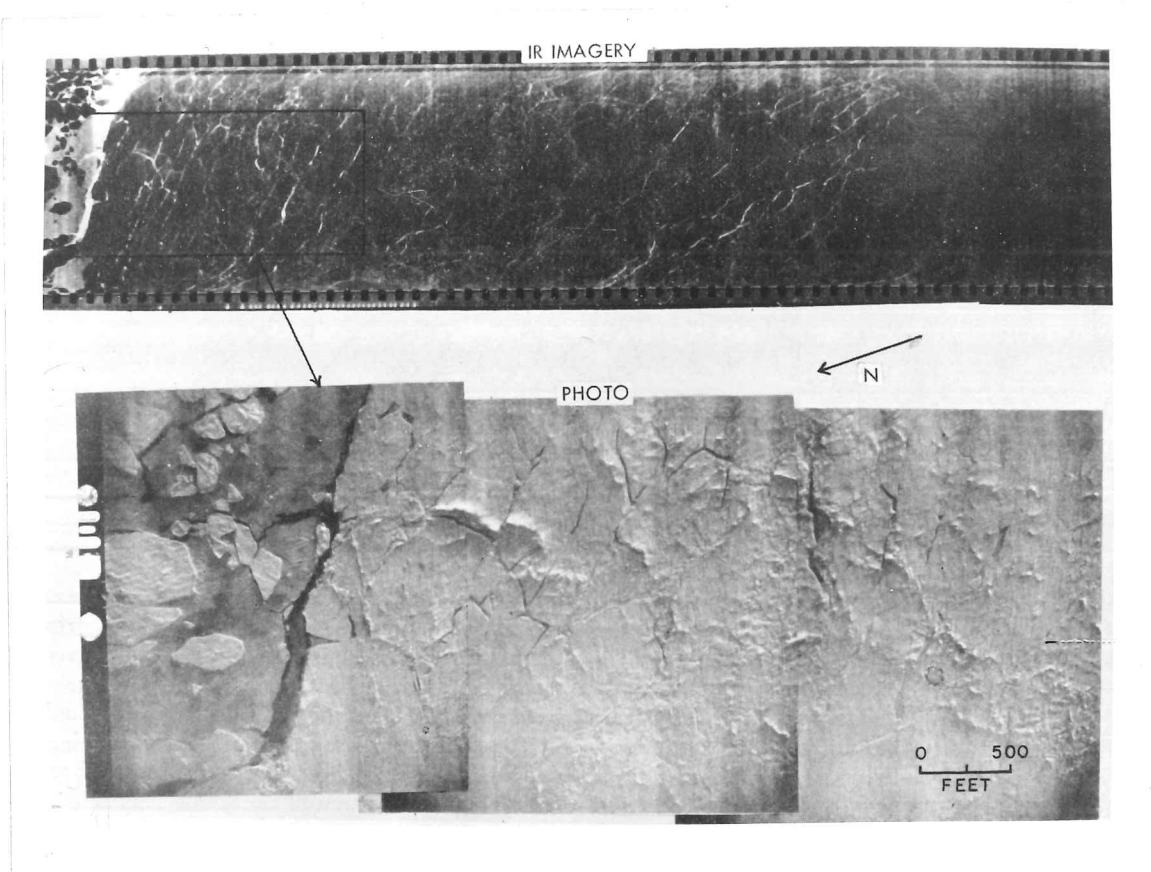
During the period April 29 to May 2, a storm passed through the region covered by the model and at this time the ice edge had returned to the model grid. The model response to the storm is shown in figure (6.13) which gives the floe size distributions during a period of a week. The floe size maps show the effects of the storm more graphically than the thickness distribution or compactness maps. The dramatic effect of the storm can be seen by the considerable reduction in the area of large floes. The surviving large floes are confined to a narrow band near the coast. Floe



Figure(6.13)

The letters a-i show where the floe size distributions are given in figure 6.18

The effect of a storm on the floe size distribution in the Greenland Sea. The three diagrams correspond roughly to the situation before, during and after the storm.



Figure(6.14)

A large floe, well within the ice pack in the Greenland Sea, starting to break up during a storm. Photograph from Ketchum and Wittmann 1972.

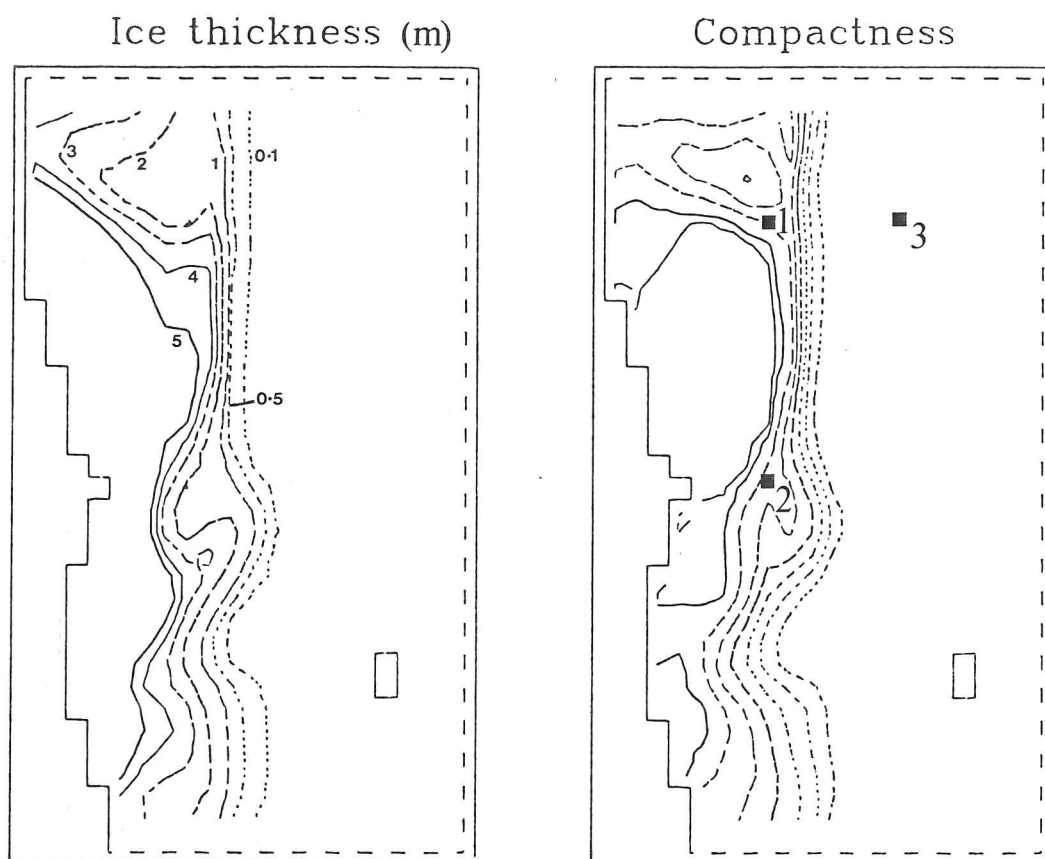
breaking like this, well away from the ice edge, has been observed from aircraft by Ketchum and Wittmann (1972) who show photographs of fragments of a large floe that appears to have broken up in a way consistent with the long floe break up mechanism suggested in chapter 3 (see figure (6.14)). Ketchum and Wittmann were fortunate enough to have made their observations around the time of a severe storm similar to that occurring during the time of the simulation.

An area of reduced ice concentration and ice thickness appears at the beginning of May and persists until the ice edge approaches when it develops an eddy-like structure (figure (6.15)). This does not seem to correspond to any real feature in that location, although polynyas and eddies are observed in the East Greenland pack ice (Wadhams 1981, Wadhams and Squire 1983). The feature in the model seems to derive from a divergence of the applied ocean current field. The map from which the current field was digitized has the diverging region, but whether or not this is a permanent feature is not known.

#### 6.2.4 Distributions within single grid squares

The full information regarding floe sizes produced by the model can be seen only by looking at the floe size distribution at each grid point. Figures (6.16a-c and 6.17) show floe size distributions obtained from digitized photographs along a 37km transect of a region near the ice edge (data provided by A. Cowan, Scott Polar Research Institute). The area from which the data was collected ( $72^{\circ}\text{N}$ ) falls near the southern edge of the model grid. The areas of a total of 4256 floes were sampled. Figures (6.16a-c) are the floe size distributions of three 12km sections of the transect. Figure (6.17) shows the floe size distribution for the transect as a whole. We see from these diagrams that variations in the floe size distribution would be expected even within one model grid square. We also see that although there is quite a variation in the range of floe sizes, there does seem to be a dominating floe size in this region. The data for figures (6.16a-c and 6.17) were obtained from photographs taken from aircraft. Much larger floes, further north, have been measured from satellite imagery (Vinje 1977).

Figure(6.15)

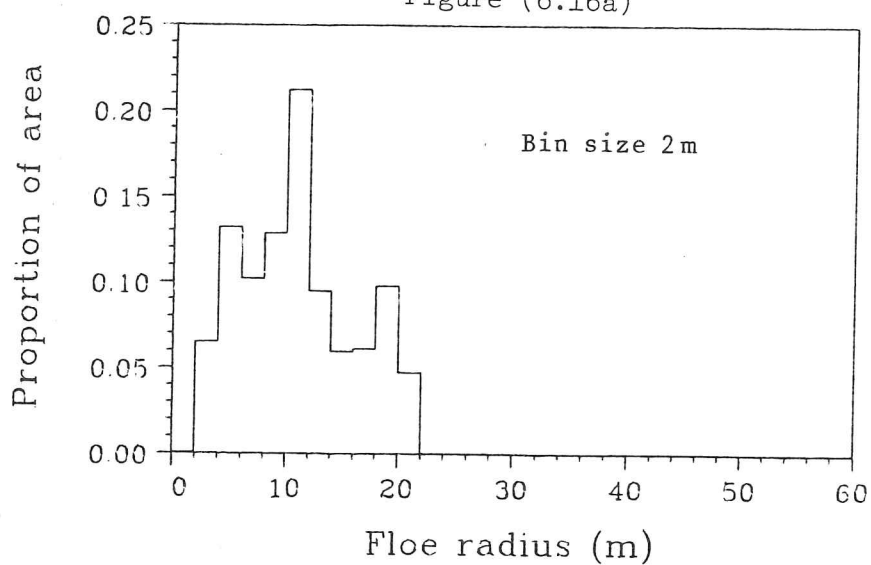


Anomalies in the long term oceanic current input as used by the model produce features at the ice edge.

Contours of  
compactness  
from left  
to right :

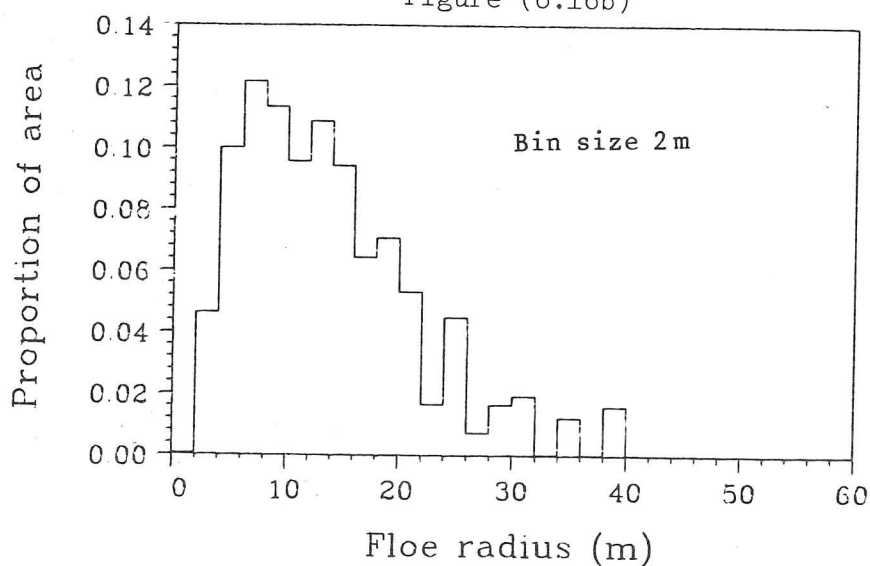
0.98  
0.925  
0.875  
0.75  
0.625  
0.5  
0.375  
0.25  
0.125

Figure (6.16a)



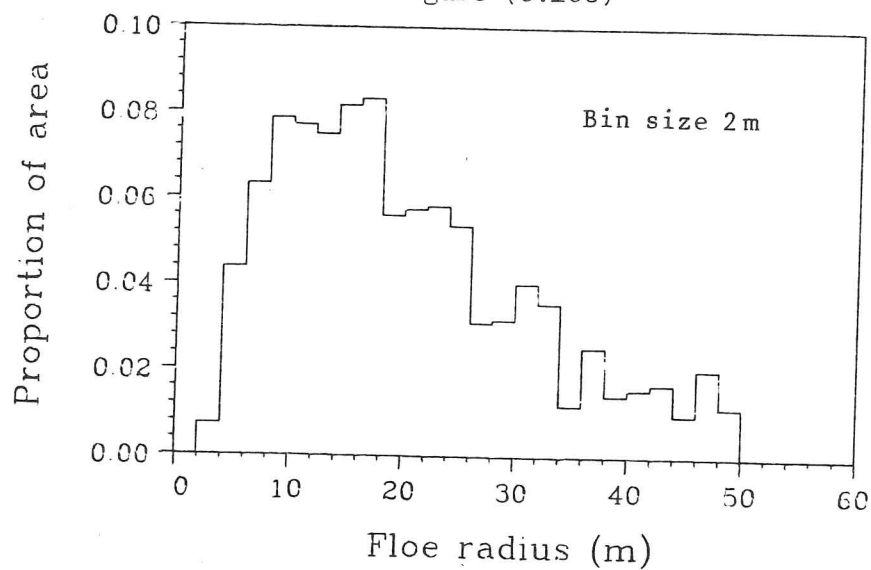
Observed floe size distribution in a region 0-12 km from the ice edge in the Greenland Sea.

Figure (6.16b)



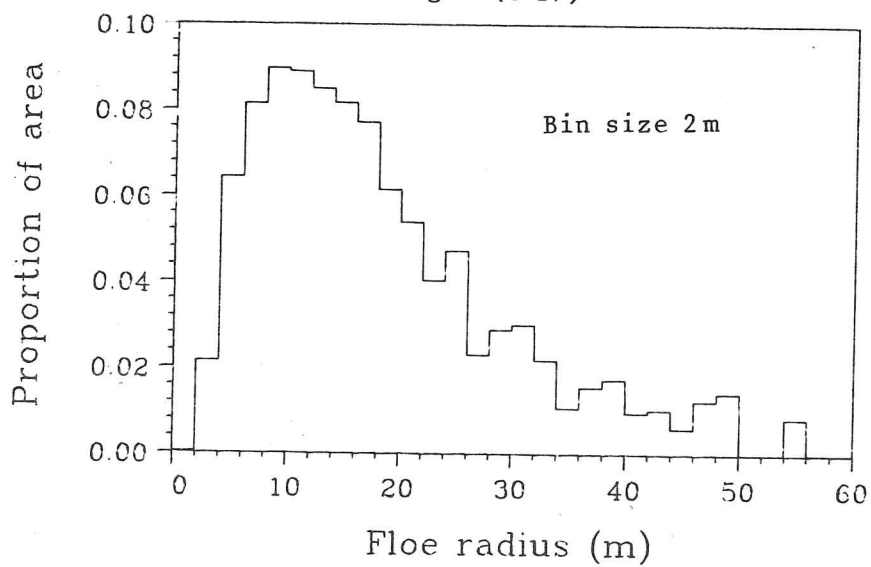
Observed floe size distribution in a region 12-24 km from the ice edge in the Greenland Sea.

Figure (6.16c)

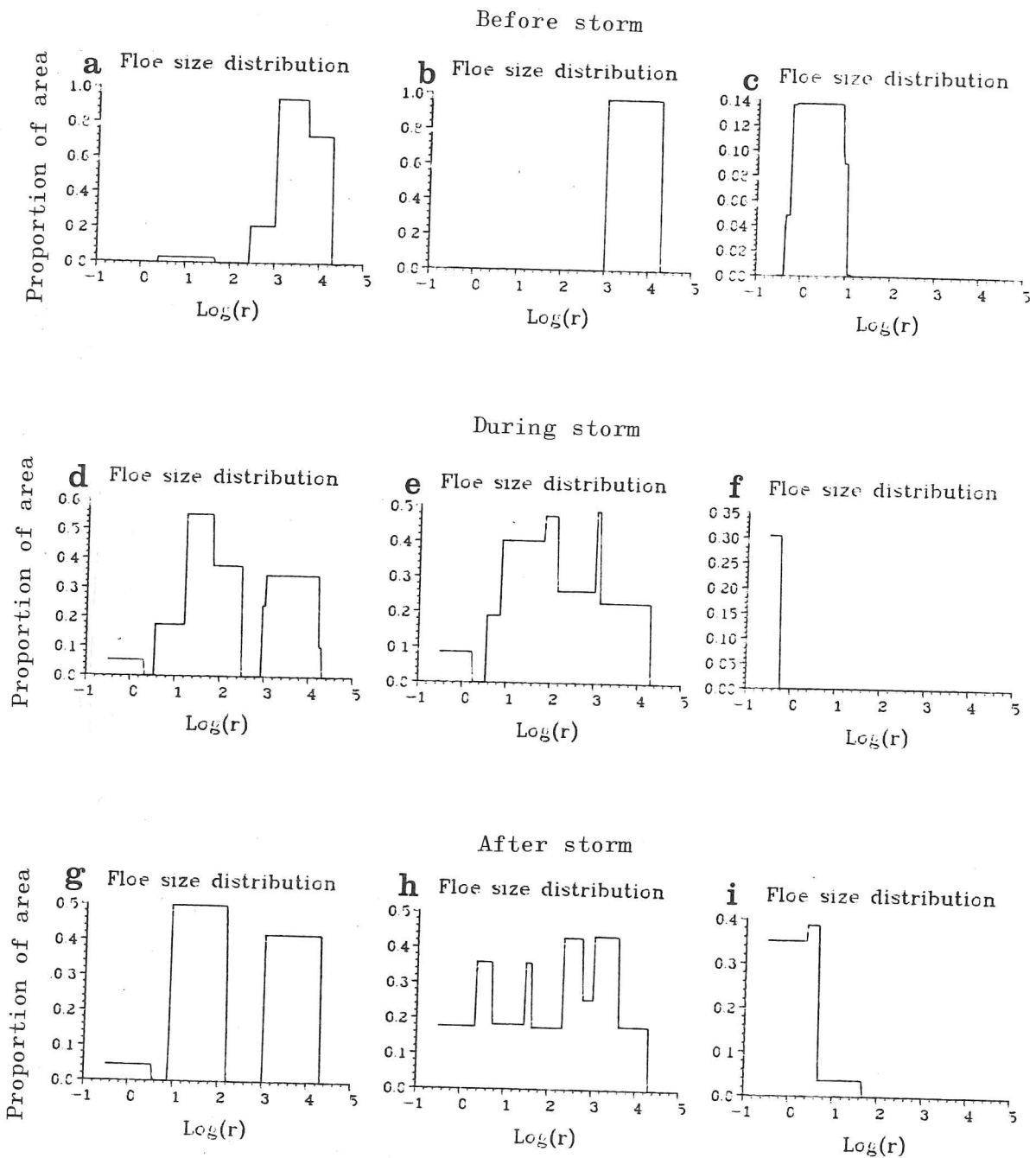


Observed floe size distribution in a region  
24-36 km from the ice edge in the Greenland Sea.

Figure(6.17)



Observed floe size distribution in a region 0-  
37 km from the ice edge in the Greenland Sea.



Figure(6.18)

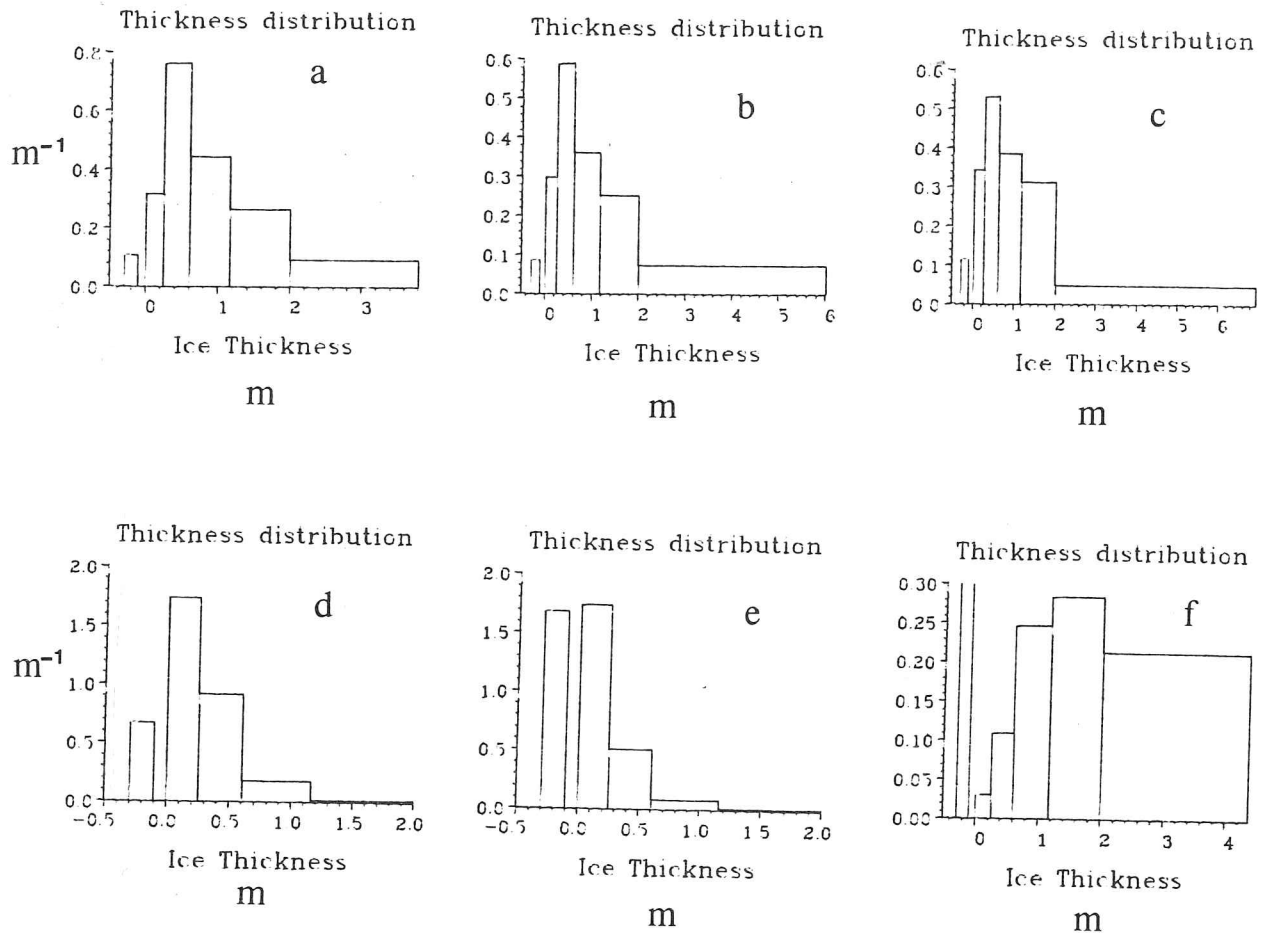
These diagrams show the shift of the floe size distribution toward the lower end of the spectrum due to a storm, and a slight readjustment back to larger floes after the storm.

The letters a-i refer to positions in the grid as indicated in figure 6.13

To illustrate the relative areal proportions of floes of various radii, the floe distribution within each thickness category is needed (the model gives only the mean floe size within each thickness level). Here, we have assumed a rectangular distribution for each of the thickness levels, although this is not the only possibility. The total distribution is obtained by summing the separate distributions for each of the thickness levels.

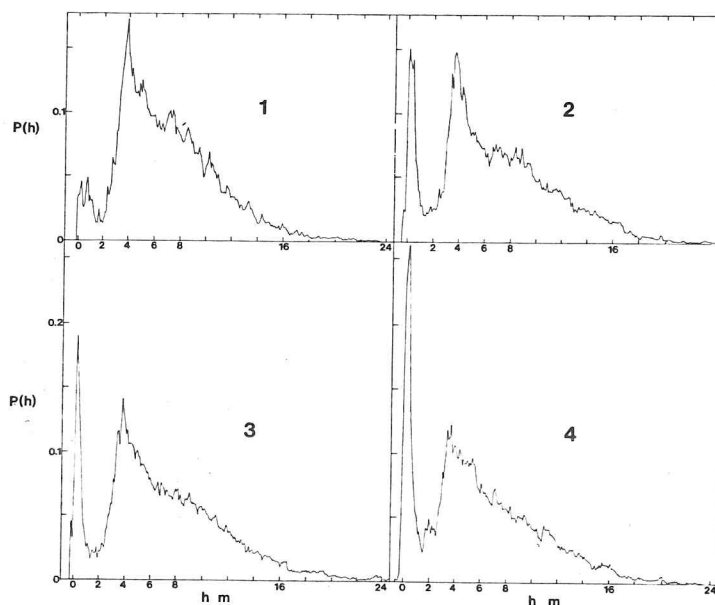
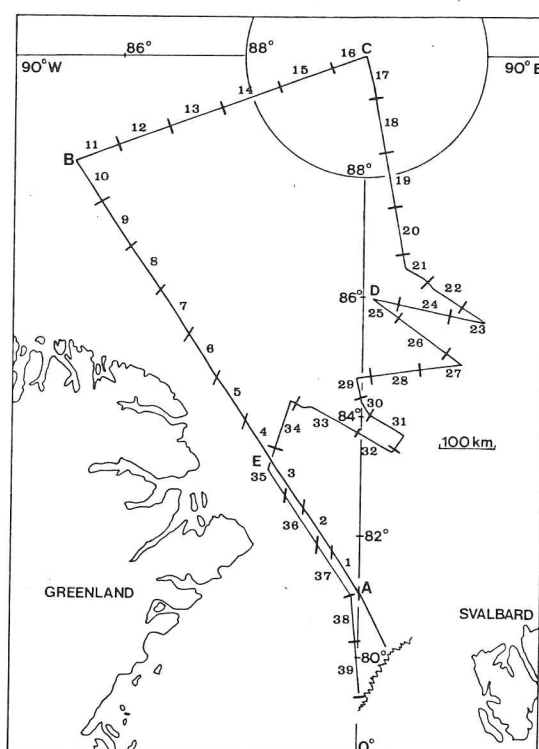
Figures (6.18) showing the simulated floe size distributions indicate the same kind of variation as in the observed data. There are large variations in the floe size in a single region with perhaps some particular floe sizes dominating. There can, however, be no real comparison between this sort of data and the model results unless far more than 6 ice thickness levels are used. A one grid cell study with perhaps 100 ice thickness levels would be more useful in trying to generate results to compare with figure (6.17), however a three-dimensional model with this resolution is not yet feasible.

The model ice thickness distributions show the characteristic shape seen in observed profiles of a tailing off towards larger ice thicknesses. The values of the thickness distribution for thin ice will depend on its recent history. Divergence with freezing will cause large amounts of thin ice. Convergence will cause ridging of the thin ice reducing the thin ice amounts and increasing the thick ice. Figure (6.19) shows some typical profiles obtained by the model and for comparison we show some profiles obtained from upward-looking sonar data from submarine (figure (6.20)). These profiles were observed in the shear zone north of Fram Strait (shown in segments 1-4 in figure(6.20)) and so generally have more thick ice than in most of the Greenland Sea. During summer the melting of the thin ice in regions where the average ice thickness was high gives rise to flatter distributions. This could be an artifact of the model due to the lack of thickness distribution structure defined within the top level which could be overcome by increasing the thickness of the maximum fixed thickness level and increasing the number of levels. However, this would involve using much larger amounts of computer store.



Figure(6.19)

Figures (a), (b) and (c) show the thickness distribution at point 2 of the grid for the following dates: 17 March, 12 April and 28 April 1979. Figures (d) and (e) are for point 3 which is nearer the ice edge and for 17 March and 12 April 1979. Figure (f) is the thickness distribution further south (point 1) and later (26 May) when melting has started. The positions of the points 1, 2 and 3 within the grid are shown in figure (6.15).



Figure(6·20)

Observed ice thickness distributions along four 100 km sections of the track of H.M.S. Sovereign. The cruise was made during October 1976 (Wadhams 1980a). The labels 1-4 refer to the numbered 100 km sections marked in the map starting at point A.

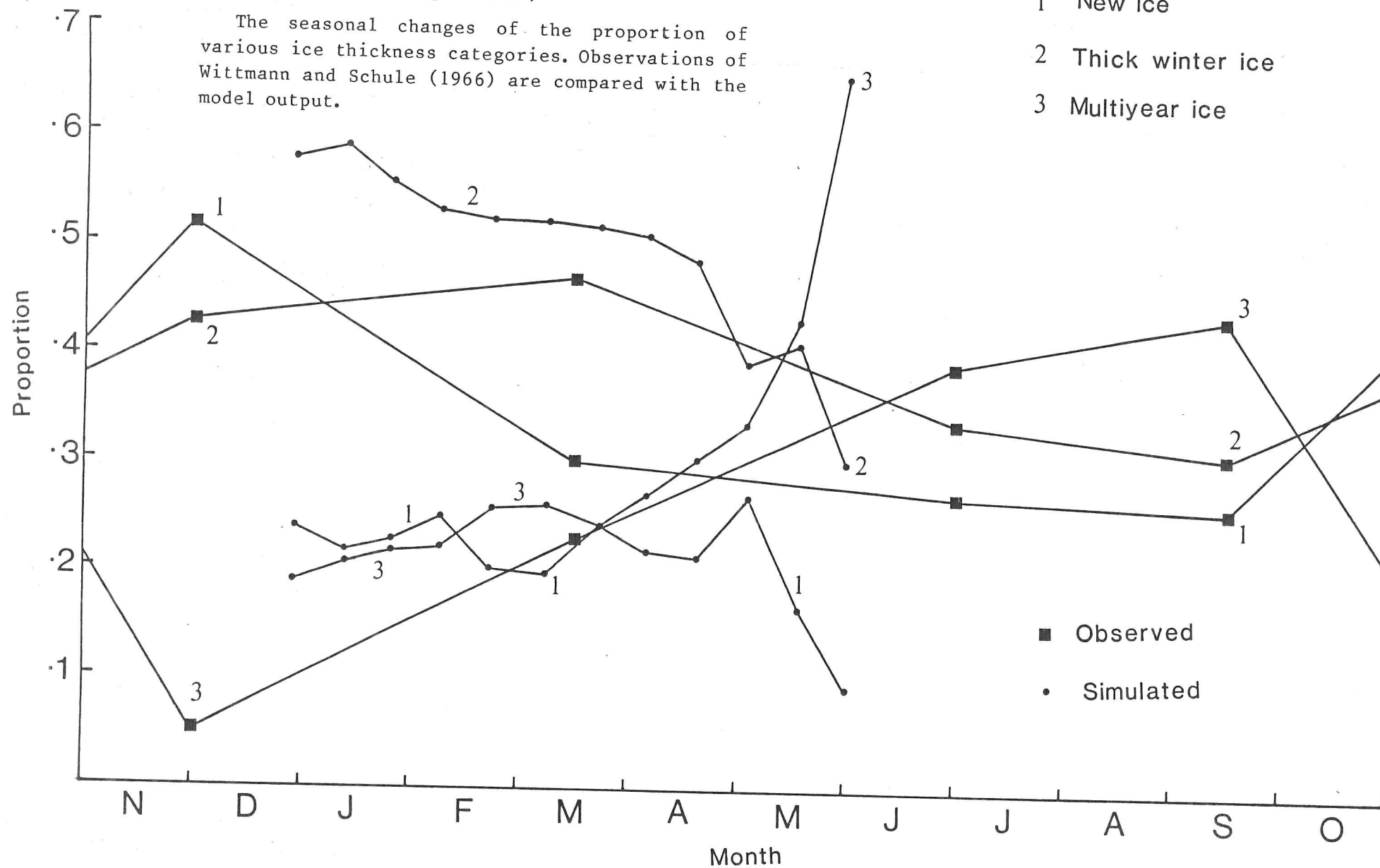
Wittmann and Schule (1966), in their early study on the proportions of ice types in the Arctic gave seasonal values of the percentages of three categories of ice in the East Greenland region. The categories were new ice, thick winter ice and a third category consisting of second-year and multiyear ice. Their values were made from a number of visual observations from aircraft so at best their data should be regarded only as estimates. If we assume that the three categories correspond to level 2, levels 3 to 5 and level 6 of the model thickness distribution, then a comparison can be made between the observations and the model results. The amounts were summed over the ice covered portions of the grid and the results plotted for every two weeks. The result is shown in figure (6.21). Definite seasonal responses of the model are shown, particularly the rapid decrease in the thin ice proportion at the onset of summer melting. The amount of thin ice drops to well below the Wittmann and Schule results during spring; Wittmann and Schule's data for East Greenland included more of the area north of Fram Strait than in the model grid and this is where the extra amounts of thin ice would be expected in spring.

#### 6.2.5 Transects

The change of some ice properties along a transect in Denmark Strait was investigated by Kozo and Tucker (1974). The observations were carried out from a submarine and amongst the properties they measured was floe size. Figure (6.22) shows a representation of their data, in which the boxes denote the sizes and distances from the ice edge of various regimes of ice types observed. They collected data to a distance of 229 km from the ice edge which would be between 6 and 7 of the grid lengths used in the model. Although the grid employed for this study did not include Denmark Strait, a comparison between the Tucker and Kozo data and model results for transects further north would still be useful. The data suggests an order of magnitude increase in floe size for each 150 km or so into the pack. At the same rate, the floes would become large at a distance of about 12 grid squares from the edge. Figure (6.23) shows some profiles from the model for times when the ice edge appeared on the grid. In fact, these are transects for the period during the storm discussed above. There are differences due to latitude changes but the general trend shows some agreement. A steeper profile is suggested for the spring simulations

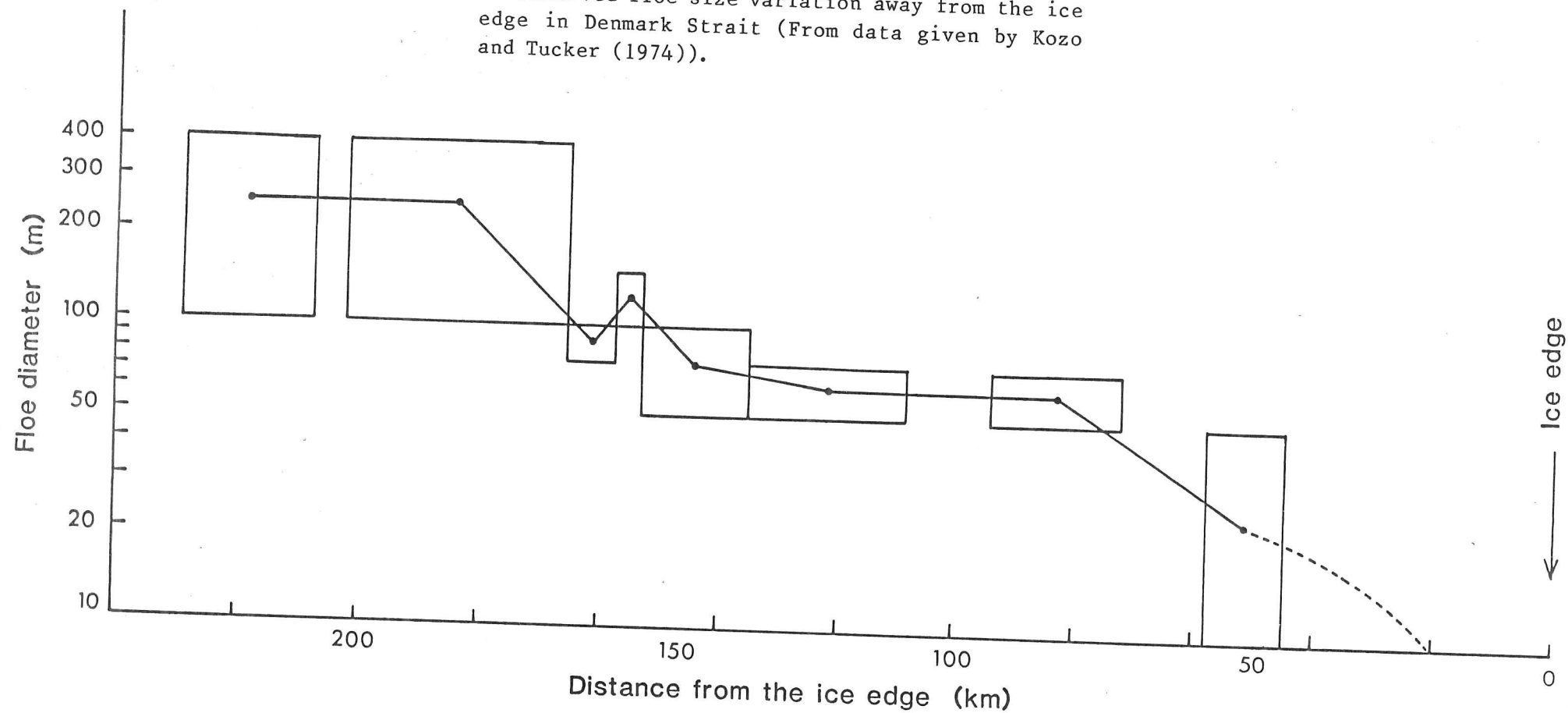
Figure(6.21)

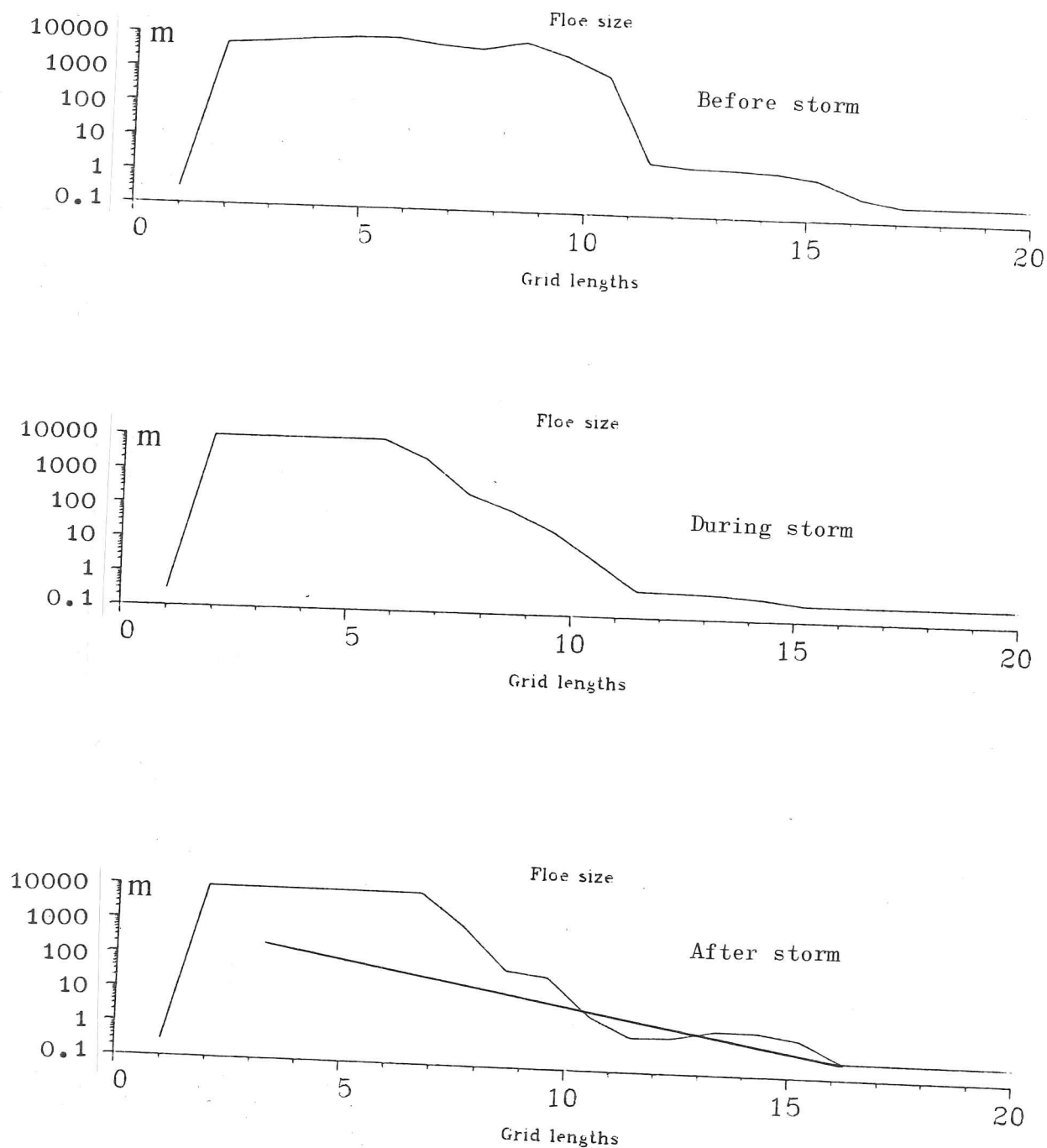
The seasonal changes of the proportion of various ice thickness categories. Observations of Wittmann and Schule (1966) are compared with the model output.



Figure(6.22)

Observed floe size variation away from the ice edge in Denmark Strait (From data given by Kozo and Tucker (1974)).





Figure(6.23)

Changes in floe size distribution as a result of a storm. The straight line in the third transect shows the gradient of the floe size line if there is an order of magnitude increase in floe size for each 150km into the pack (as is the case for the Kozo and Tucker (1974) data).

however.

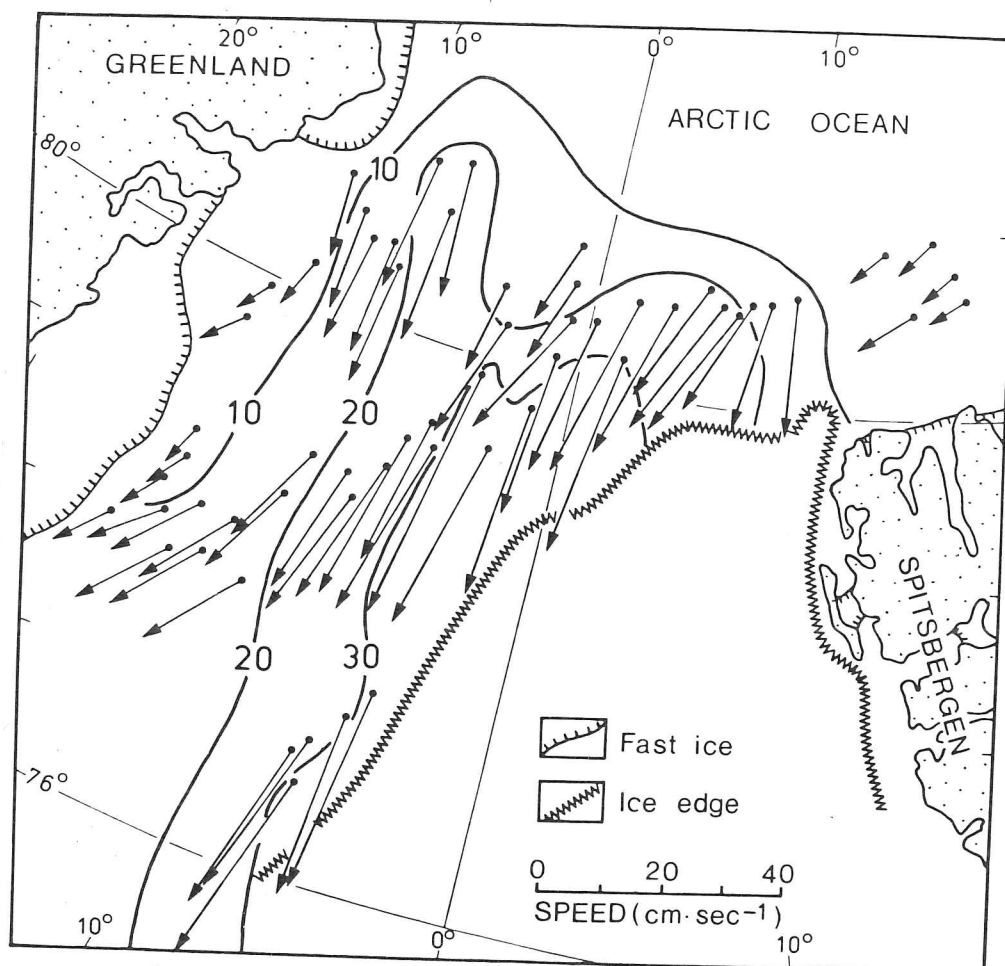
Figure (6.24) shows observed ice velocity vectors south of Fram Strait during a period of fairly strong northerly winds of up to  $15 \text{ ms}^{-1}$ . As we have seen, the model ice velocities can vary over over a few days but figure (6.25) shows simulated ice speed contours at a time when the general wind pattern was similar to that occurring when the observed drift rates were obtained. The distribution of ice drift speeds in the observed and simulated cases is similar although in the model results, a greater area of the region is contoured because the model included a larger area of ice than observed at that time.

Wadhams (1983b) estimated the ice volume flux across Fram Strait using ice thickness data derived from measurements that were made from the submarine *Sovereign* during the period April-May 1979. The ice velocity profile across Fram Strait was obtained from Vinje (1982) which together with the ice thickness gives the ice volume flux. Figures (6.26, 6.27 and 6.28) show the results obtained by Wadhams (1983b) (dashed lines) together with the results obtained from the model (solid lines). The agreement is quite good both qualitatively and quantitatively, although the model does not produce a zone of fast ice in the grid cell closest to the coast of Greenland. Also the position at which the ice flux curve reaches a maximum is slightly displaced. The total ice volume flux across Fram Strait according to the model is 0.25 Sverdrup (1 Sverdrup is equivalent to  $10^6 \text{ m}^3 \text{ s}^{-1}$ ). This is a little lower than Wadhams' (1983b) value of 0.29 Sv.

### 6.3 Variations to the model

#### 6.3.1 Introduction

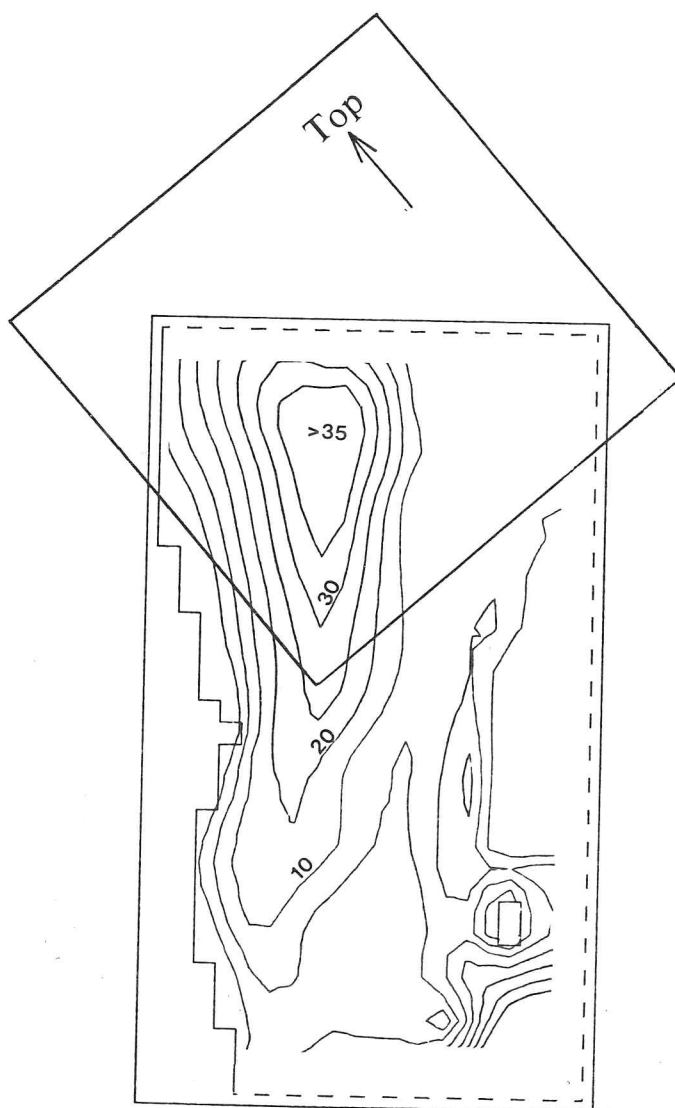
Here we present some more model results obtained by varying some of the input parameters. Ideally the model should be run over a number of seasonal cycles for an equilibrium solution to be reached. In addition, the entire Arctic should also be included in the model simulation to provide an ice volume transport through Fram Strait. The effect of modifying a model parameter should be tested by running the modified model through an



Figure(6.24)

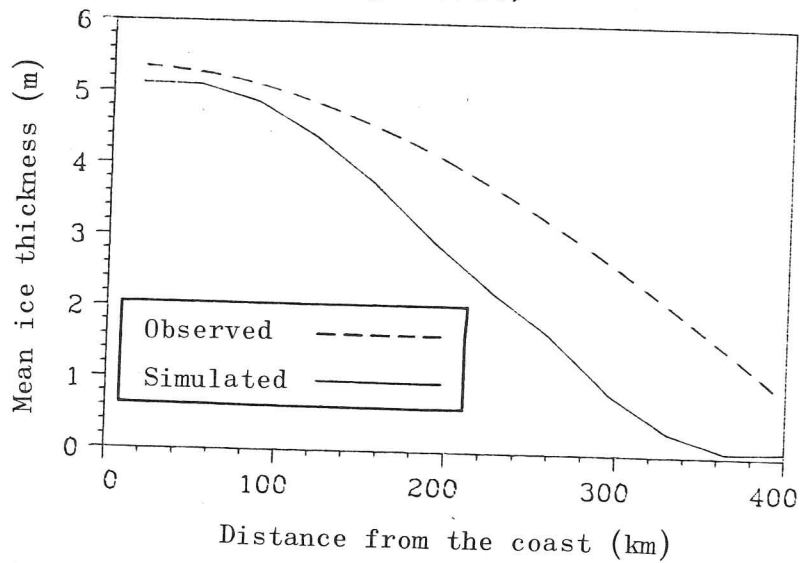
Drift observations from Landsat imagery, April 21 to May 7, 1976 [after SCOR, 1979 and Wadhams 1981].

Figure(6.25)



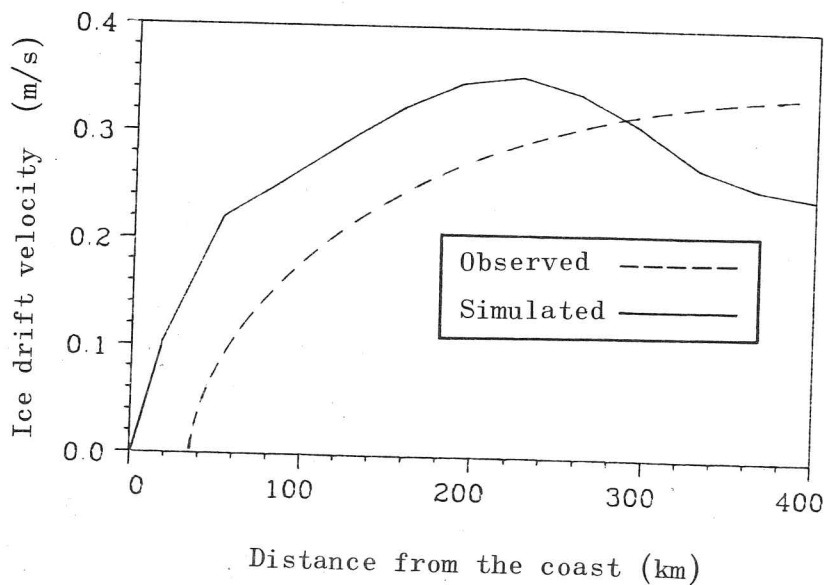
Contours of ice drift speed ( $\text{cm s}^{-1}$ ) for 30 April 1979 (produced by the model). The square shows the area covered by the map in the previous figure.

Figure(6.26)

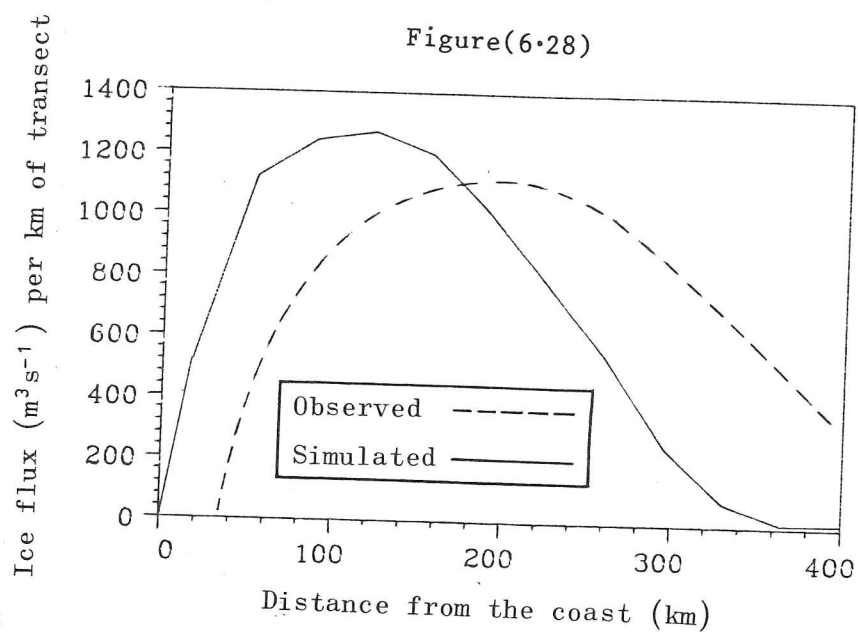


Comparison of the observed (Wadhams 1983b) mean ice thickness across Fram Strait with the model results. The ice thickness along the northern edge of the grid is specified in the model run, however the thicknesses given here correspond to the position of the submarine track which was a little further south.

Figure(6.27)



Comparison of the observed (Wadhams 1983b) ice velocity profile across Fram Strait with the model results.



Comparison of the ice flux profile across Fram Strait derived from observations (Wadhams 1983b) and the model results.

entire equilibrium run, but at present this is prohibitively expensive in terms of computer resources.

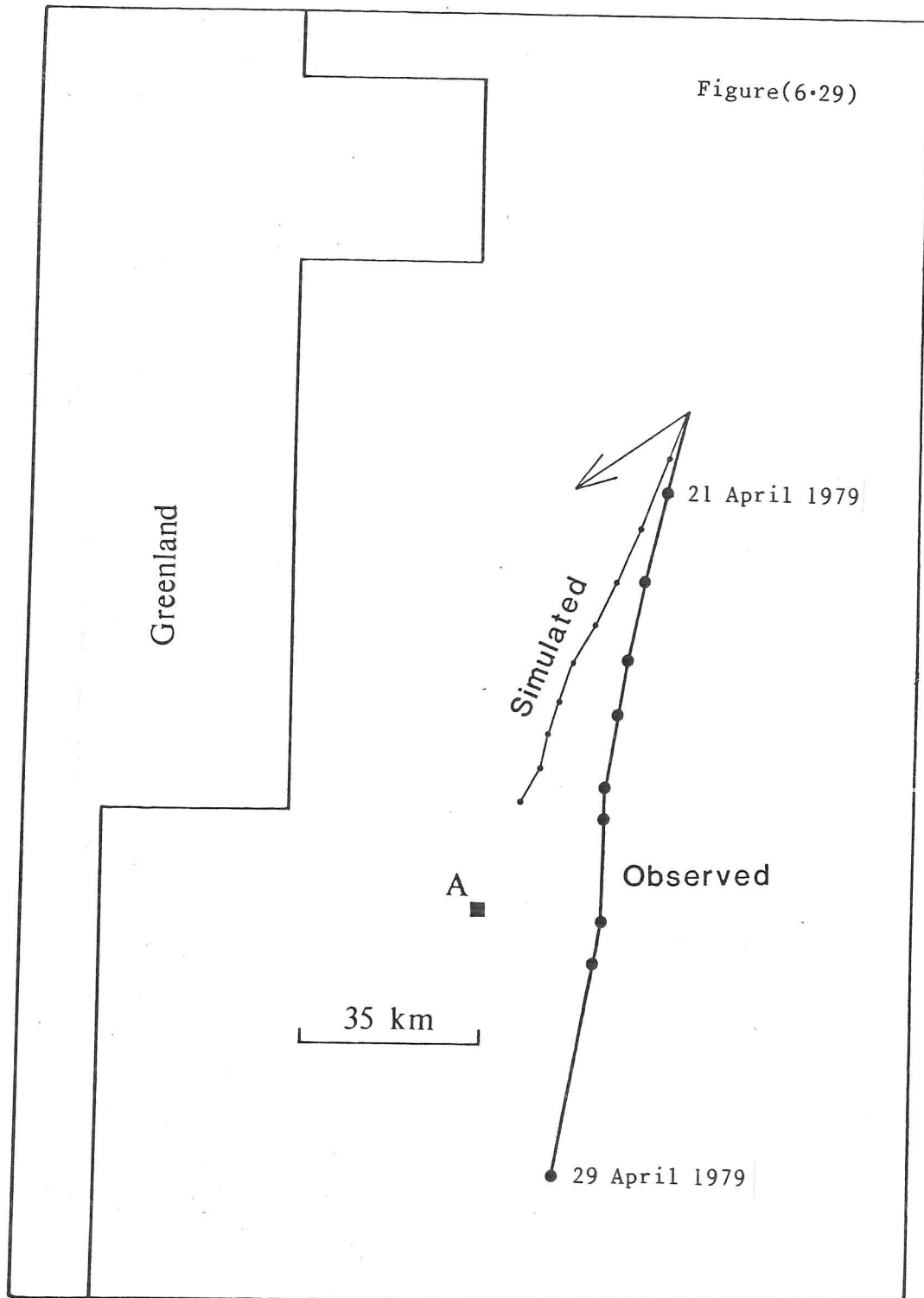
In this section we restrict our attention to particular parts of the model run and compare the standard results with those from a modified program. This is found to produce results of a quality sufficient to suggest improvements to the model.

### 6.3.2 Drift trajectories

During the time of the model simulation, a satellite-tracked buoy (number 1924 of the Arctic Ocean Buoy Program, Thorndike and Colony 1980) drifted southwards near the East Greenland coast. It passed through the region of fairly thick ice where the ice interaction term is important. In the standard simulation the observed ocean currents were reduced so that the resulting ice velocities along the East Greenland Current reach  $0.3 \text{ ms}^{-1}$ . However the mean velocities that resulted from this were too low to give the correct mean drift rates. Thus, for the drift tests no such adjustments to the ocean currents were made.

There is some difficulty in interpreting the results of drift track calculations in regions where the thickness distribution has not been verified. Studies of this sort are more useful where a concurrent set of drift track measurements and wind and current velocities are made. Such studies made during the AIDJEX programme resulted in the determination of the air and water turning angles used in the model described here. There, calculated and observed drift tracks were made to coincide by adjusting these turning angles (McPhee 1980).

Figure (6.29) shows the simulated drift trajectories and the observed trajectory of the buoy for a 9 day period. The simulated drift rates are too small, something that may be due to a number of causes. The most probable cause is from errors in the imposed ocean current field. This could also explain the slight difference in the direction of the real and simulated drift. Also, because the simulated buoy moves too quickly towards the coast where the ice is thicker it slows down too much, compounding the error.



Drift trajectories: The track of a buoy is compared to that predicted by the model. The dots along the paths show the positions at times one day apart.

Point A shows the position reached by the buoy for a run in which the shear viscosity is reduced by a factor of four.

The arrow shows the simulated initial direction of the buoy if the ice strength is set to zero.

Changing the viscosities used can affect the drift. Point A in figure (6.29) shows the position reached by the buoy in a model run in which the shear viscosity is reduced by a factor of four. This gives a result significantly closer to the observed buoy position. Neglecting the shear viscosity altogether would in this case improve the result further. The bulk viscosity term cannot be neglected however and this is shown by the arrow at the start of the drift tracks which shows the direction of a buoy obtained by setting the ice strength to zero (which gives rise to small viscosity terms). The effect of the bulk viscosity term is seen to prevent excessive drift towards the coast.

It should be noted that the buoy in question was within only one or two grid lengths of the coast suggesting the possibility of problems associated with the resolution of the grid.

### 6.3.3 Wind-induced currents

The momentum equation in Hibler's (1979) model includes forcing due to long term geostrophic currents. No attempt had been made to account for the effect of the long term ice circulation upon the current, and neither had the effect of short term wind conditions upon the surface current been included. The surface current is in fact a combination of the long term geostrophic, wind-induced (directly or indirectly via the ice) and tidal currents. The Greenland Sea is fairly open and not shallow enough for the tidal current to be significant there, although in other areas, the tides can affect the sea ice velocities (for example, in the Laptev Sea (Zubov (1943))). The influence of the ice motion on the ocean currents would repay study as part of a fully interacting ocean ice model. As far as the short term wind-induced current is concerned, an attempt could be made to simulate this by adding an Ekman surface current with a magnitude modified by the amount of ice present. This was done for the standard simulations, and here we compare results obtained by running the model without a wind-induced current parameterization.

Ekman's solution for the water velocity due to a steady wind stress acting on an infinitely deep ocean with no boundaries and an eddy viscosity constant with depth, gave a surface current acting at  $45^\circ$  to the

right of the surface wind (in the northern Hemisphere) (see for example Pond and Pickard 1978). Ekman found experimentally that the magnitude of the surface current is related to the surface wind speed  $|U|$  by the relation

$$\frac{|U_e|}{|U|} = \frac{0.0127}{\sqrt{\sin|\phi|}} \quad (6)$$

where  $\phi$  is the latitude. Thus in complex notation

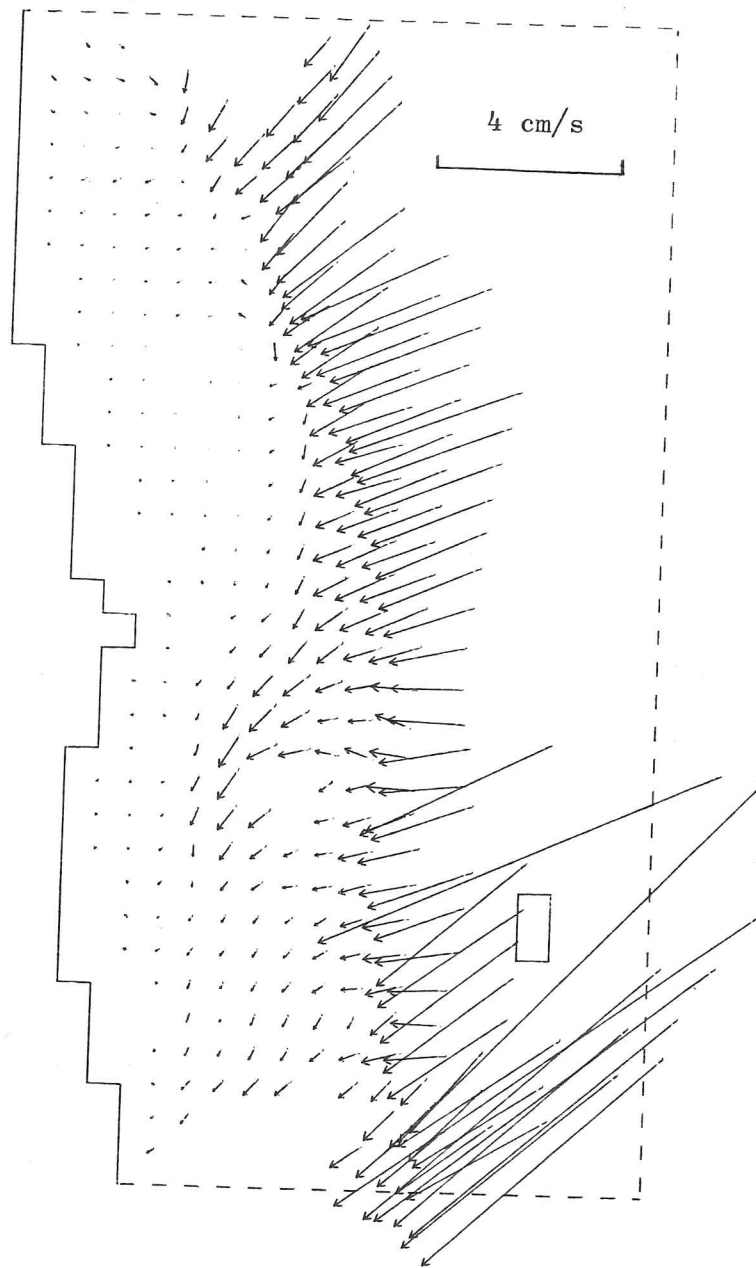
$$U_e = \frac{0.0127}{\sqrt{\sin|\phi|}} U_g e^{-i\pi/4} \quad (7)$$

The simplest way to include the modified Ekman current into the the current stress formulation of the model is to turn the Ekman current by the geostrophic current turning angle (but with the opposite sense) and add it to the geostrophic current. The quadratic water stress formula for the geostrophic current will then turn the geostrophic current, as it should do, and also turn the Ekman component back again to its surface direction before evaluating the ice-water stress.

In figure (6.30), the effect on the ice velocity field due to the introduction of a wind-induced current parameterization is shown. The figure shows the difference between the velocity solutions after running the model through 18 time steps both with and without a modified current. As can be seen, the effect is to enhance the velocity toward the ice pack near the ice edge. The change is large enough near to the ice edge to significantly affect the solution there. The velocity within the pack is almost unchanged.

The effect of wind-induced currents is thus of importance when modelling the ice pack very near the ice edge.

# Difference velocity field (5 May 1979)



Figure(6.30)

The diagram shows the difference between the resulting ice velocity vector fields after running the model for 28 timesteps with and without including a parameterization of the effects of wind-induced currents.

## 7. CONCLUSIONS AND FURTHER WORK

### 7.1 A summary of the new features in this model

We have shown that it is possible to construct a sea ice model that predicts floe size, as well as ice thickness and velocity, giving a comprehensive description of the ice conditions in a region. The floe size is a particularly useful parameter to include as it is easily measurable from aerial photographs and this model is the first to incorporate specific representation of floes. The Greenland Sea region was chosen for the simulations, for which reasonable agreement with observations has been obtained. The floe size distribution maps seem to give a very good indication of the sea ice conditions with respect to what is seen in satellite imagery. Where the results are not so good, the path towards more complete coupled models is indicated.

The introduction of floes into an already fairly complex sea ice model allows for the possibility of many feedback mechanisms. Included in the model here is a lateral melting feedback in which the amount of lateral melting occurring in the model depends upon the average floe size.

The model developed here represented the ice with a multi-level formulation, this type of model not having previously been applied to the East Greenland region. This enabled estimates to be made of the various ice types present in the Greenland Sea, and their variation with time, giving a general agreement with observations.

The model represents an advance over those large scale sea ice models that do not include a full rheology as part of the momentum equation. This means that better ice thicknesses are predicted (particularly where any interaction with land is likely) than models such as that of Parkinson and Washington (1979) which uses ad hoc methods when dealing with the ice interaction. Parkinson and Washington solve the momentum equation without

the ice interaction terms, and subsequently adjust the velocity solution so that the resulting ice concentrations do not exceed a given maximum value. Compared to those models that do have sophisticated rheologies (Hibler 1979, Tucker 1982), our model is of more direct use in that easily verifiable sea ice properties are dealt with. Also, because many of the processes included are based on physics at a fundamental level, there is less tuning needed to run the model. For instance, the ice strength is determined completely from the ice thickness distribution, whereas Hibler's model has an adjustable parameter in the strength determination.

Many theoretical results concerning the behaviour of randomly distributed circular floes have been obtained. Previous studies of the mathematics of finite sized floes have been very limited and are not easily extended. In particular, they were restricted to one dimension and thus avoided the difficulties involved in the more realistic two-dimensional problem. The treatment here is two-dimensional and is such that many aspects of pack ice behaviour not derivable from a consideration of ice as a continuum can be made. In particular, the idea of pack ice as consisting of floes was used to derive relationships for the ice strength for various conditions.

A number of results concerning the physics of ice floes were obtained that are of interest not just from the modelling point of view, but also in their own right. In particular, very little work on the wind-induced break up of floes has been done before.

A full treatment of the ice dynamics applicable to ice modelling was made, resulting in the theoretical derivation of a plastic yield curve for the determination of the ice interaction terms. The results from the drifting buoy calculations suggest that factors neglected in the yield curve calculation may yet be important; however the fact that a yield curve has been derived at all is significant here. Previous studies have assumed the shape of a yield curve as the starting point. The derivation here can serve as a basis for designing new yield curves.

## 7.2 Future development of sea ice modelling

There are essentially two directions in which the future course of sea ice modelling can go. One direction is towards complexity and the inclusion of more and more factors to try to represent the many physical processes occurring in nature. To model fully the entire range of ice types found in the (East) Greenland Sea, from the fast ice at the coast to the active region very near the ice edge with its complicated physics, more comprehensive models will be needed than exist at present. Instead of making models more complicated, we could aim for simplicity, to model sea ice using only the most important factors. The advantages would be economy and speed of operation. Such models, if they can be made to provide good results, would be most useful for coupling with ocean and atmosphere models. The most difficult aspect of the simplification would be to retain ice interaction terms which, as we have seen, are vital. The most important part of the rheology appears from the results here to be the bulk viscosity. A simplified rheology involving only the bulk viscosity and neglecting the shear viscosity may be more economical and produce reasonable results in the East Greenland region, although it may not be valid in the Central Arctic.

There is no reason why the model cannot be applied to regions other than the Greenland area. The model could be used in the Arctic Basin although the parts of the model concerned with floes would be wasted since large floes would be predicted everywhere. A more useful exercise would be to model the marginal ice zone in the Bering Sea where floes are observed and have been measured. The ice there is generally thinner near the ice edge than in the Greenland Sea, and so different floe size profiles would be expected. The Antarctic with its large seasonal sea ice zone and unique climate could also be usefully modelled. The model is sufficiently general to cope with a wide range of conditions.

The representation of floes in the model can be used to provide a feedback mechanism for the dynamics, in that different rheologies may be used in regions of small floes and where the ice is continuous. The research has not yet been done for determining the various rheologies to use in various regions, but the model here provides a framework in which

the results of such studies may be incorporated.

Without going as far as coupling ice models with ocean and atmosphere models, the most promising improvement to the model for studying the East Greenland region would be to have a more dynamic upper ocean layer forced by the factors already used for the ice forcing. This has been partly investigated here with the introduction of a parameterization of the wind-induced currents. Further improvements could involve the lateral transport of the oceanic mixed layer together with its heat content. This could, for instance, advect warmer water with the West Spitsbergen Current to increase the ice-free area within Fram Strait. Without an ocean model however, no forcing of the mixed layer from below can be achieved.

Although the problems of modelling sea ice are great, particularly in marginal ice zones, there are many avenues open for further research. Improvement to the models and interesting results will surely come.

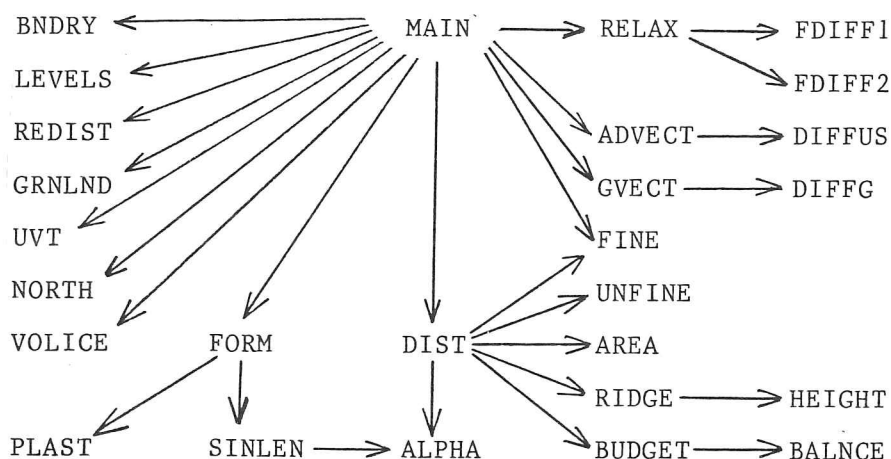
## APPENDIX

# APPENDIX

## Listing of the code

In this appendix, we give an outline of the contents of the model code with some details of the numerical methods used, not mentioned in the text. A description of the main subroutines are given, although the code contains sufficient comment lines for the logic to be followed.

The figure here shows the subroutine structure of the program and is up to four levels deep.



Subroutines ADVECT, BNDRY, DIFFUS, FORM, PLAST and VOLICE are essentially the same as used in Hibler's (1980b) code. However PLAST is retained only for comparison with SINLEN which has replaced it. Subroutine RELAX and its associated subroutines FDIFF1 and FDIFF2 have had only minor modifications, as outlined below. GVECT and DIFFG are simply multi-level versions of ADVECT and DIFFUS and are trivially obtained. The rest of the subroutines are new and the other subroutines in Hibler's code are no longer needed. The basic numerical methods for performing the time integration to second order accuracy are retained as are the second order accurate spatial finite differences. The reader is referred to Hibler (1979, 1980b) for a full description of the numerical methods, but here we will mention some of the salient features.

The advection (ADVECT) is performed by a conservative 2-2 (second order accuracy in space and time) explicit scheme (modified Euler step) together with small harmonic and biharmonic diffusion (DIFFUS) terms that prevent numerical instabilities. The advection equations are staggered in time with respect to the momentum equations which gives an efficient scheme for coupled equations of this sort. The momentum equations are also 2-step so that two relaxation solutions are needed at each time step (RELAX), the first giving an approximate velocity solution at half the time step to use in the non-linear velocity terms during the second relaxation solution to give the solution after the full time step.

For each grid cell, the velocities are specified at the corners, and physical properties such as the thickness distribution and floe number density are specified at the centres of the grid cells. Near coasts, the velocity points are forced to be zero in the solution to the momentum equation. The cells are of four types. 1) ordinary ice or open water, 2) land cells in which no ice is allowed to advect or diffuse, 3) open boundary cells which allow free inflow and outflow of ice by setting the viscosities and strengths to zero, and resetting the ice properties within the cell to be a weighted average of the properties in the non-open boundary cells neighbouring it, and finally 4) cells in which the ice amounts are specified as input boundary conditions. Subroutines BNDRY and NORTH deal with type 4) cells.

Of the other subroutines, the most important is DIST which deals with the redistribution of the ice thickness levels due to both dynamic and thermodynamic causes. The corresponding changes to the number of floes within each thickness level are also handled here. In addition, any temperature changes to the mixed layer are made at this stage. Subroutine DIST calls subroutine RIDGE which redistributes ice between the thickness levels during ridging to produce a normalized thickness distribution.

Subroutines SINLEN and ALPHA take the ice velocity field as input and give the viscosities for use in solving the momentum equation for which subroutines FORM and RELAX are used. Subroutines BUDGET and BALANCE evaluate the ice growth rates as functions of the ice thickness, the time of the year, and thermodynamic input parameters such as the wind speed, the

cloud amount, the relative humidity, and the air temperature.

Subroutine NORTH provides the boundary conditions for the northern part of the grid corresponding to Fram Strait. A subroutine of this type would not be needed in a study of the central Arctic where all the ice would be generated within the system.

Subroutine GRNLND reads in data concerning the ocean currents and heat flux specific to the Greenland grid used in this study.

Finally, subroutine UVT reads in the winds and surface air temperatures when they are needed.

### 1. Solution of the momentum equation in RELAX

The solution of the momentum equation by over-relaxation involves considerable computation, especially when the grid is large. Thus any time saving techniques for this part of the model would be useful.

At those points in the model grid at which there is no ice, one method is to set the ice mass and strength to zero and solve for the ice velocity in the usual way. The solutions obtained at the no-ice points are then disregarded or set to zero. If however, solutions at such points can be specified a priori then the computations need be performed only at the points where there is ice. To do this though, one must be careful not to specify an unreasonable ice velocity that would occur if a small amount of ice were allowed to drift there. This is because an obviously incorrect velocity would influence the solution in the region where there is ice. For example, specifying the velocity to be zero at no-ice points would make the ice edge behave as a coastline. Thus although the value of the velocity solution at these points is not of interest, their influence on other solution points is.

A possible method is to specify the solution at the no-ice points to be the drift velocity suggested by Zubov (1943) where the ice velocity is given as 2% of the wind speed and in the direction of the geostrophic wind. A modern study of the data from buoys in the Arctic ocean (Thorndike and

Colony 1982) suggest that for summer the ice velocity is related to the geostrophic wind according to

$$u = U_g 0.011 e^{-i18^\circ} \quad (1)$$

although the constant of proportionality and the turning angle ( $18^\circ$  to the right in this case) vary seasonally. The situation in Greenland more closely resembles the situation in the Arctic during summer than for other times so (1) will be used here. It should be noted that near the ice edge, the ice interaction term is negligible so that empirical formulae of the form of (1) are more applicable there.

When modelling real geographical regions, the time saving involved by passing the solution calculation at land points and zero-ice points may be significant. Also, because fewer unknowns are calculated the number of iterations needed for convergence may well be less than otherwise.

Another way in which slightly faster evaluation of the velocity solution can be obtained is to use values of the relaxation parameter  $\omega$  that varies over the grid. Hibler's model uses  $\omega = 1.5$  for all the points. The relaxation parameter is used as follows. Suppose  $f(u) = u$  requires a numerical solution for  $u$ . If  $u^n$  is the solution after  $n$  iterations, then  $u^{n+1}$  the solution at the next iteration is given by

$$u^{n+1} = u^n + \omega \{f(u^n) - u^n\} \quad (2)$$

If  $\omega = 1$ ,  $u^{n+1} = u^n$  and there is no relaxation. For  $\omega > 1$  and  $\omega < 1$ , we have over-relaxation and under-relaxation respectively.

The optimal relaxation parameter to use depends on the particular equation involved. The best results obtained in practice with this model were obtained by initializing the relaxation parameter for each equation of the system to  $\omega_{ijk} = 1.48$ . The suffices  $i$  and  $j$  refer to the grid point and the suffix  $k=1$  or  $2$ , for the  $u$  or the  $v$  equation. At each iteration a simple test is done to compare the changes to the velocity solution. If the differences appear to be increasing,  $\omega$  is decreased by  $0.02$ . If the

differences are decreasing, indicating stability,  $\omega$  is allowed to increase by 0.01. However,  $\omega$  is kept within the limits (1.0, 1.5). Formally,

$$\begin{aligned}\omega^1 &= 1.48 \\ \omega^{n+1} &= \begin{cases} \omega^n + 0.01 & \text{if } f(u^n) - u^n < f(u^{n-1}) - u^{n-1} \\ \omega^n - 0.02 & \text{otherwise} \end{cases} \end{aligned} \quad (3)$$

Over a number of time steps, this scheme showed a 4% decrease in the number of iterations needed for convergence, compared with taking  $\omega = 1.5$  everywhere.

# The listing

```

1 C Main driving program for viscous plastic sea ice model
2 C incorporating floe size number densities
3   IMPLICIT REAL*8 (A-H,O-Z)
4   DIMENSION U(21,36,3),V(21,36,3),ETA(22,37),PRESS(22,37),ZETA(22,37
5   1),DRAGS(21,36),DRAGA(21,36),GAIRX(21,36),GAIRY(21,36),GWATX(21,36)
6   2,GWATY(21,36),G(6,22,37,3),GAMMA(18,18),AMASS(21,36),FORCEX(21,36)
7   3,FORCEY(21,36),TMIX(22,37),G1(6),G2(18),G3(18),UC(21,36),VC(21,36)
8   4,FND(5,22,37,3),GAMMAF(18),EKMANX(21,36),EKMANZ(21,36),PHI(21,36),
9   5,TAIR(21,36),C(52),P(52),RHUM(52),EDGE(52),HTSEA(22,37),AVV(22,37,3
10  6),UAV(21,36),VAV(21,36)
11   COMMON/EE/ECCEN
12   COMMON/GRIDI/NX,NY,NX1,NY1,NXM1,NYM1,NL,NLM1,NFINE,NS,NSM1
13   COMMON/GRIDR/HI(22,37,3),HMS(18),HWS(18),HS(17),HM(6),HW(6),H(6),T
14   IOP
15   COMMON/STEP/DT,DX,DY
16   COMMON/ARRAY/GMASK(22,37),UVM(21,36)
17   COMMON/OUTFLO/OUT(22,37)
18   COMMON/SIGMA/ALPHR(22,37),ALPHO(22,37),EI,EII2,COTT
19   COMMON/PHYS/CB,CF,STREN,RHOICE,RHOWAT,GRAV,COT,UA,UB,AH,BH,RHOAIR,
20   1QI,CW,DMIX,SIDER,TI,SIGMAX,PI,ARMAX,CPLF,CON1,CON2,STFN,CON,ERROR2
21   2,D1,D3,TINC,CH,SIN20,COS20,SIN25,COS25
22 C Various modes of printout
23 C   Set IP1=1 for output of information at start of run
24   IP1=1
25 C   Set IP2=1 for basic information every NFULL'th time step
26   IP2=1
27 C   Set IP3=1 for more information every NFULL'th time step
28   IP3=1
29 C   Set INIT=1 if reading in input from previous run
30   INIT=0
31 C   Set IWIND=1 if using new wind file
32   IWIND=1
33 C   Set IOUT=1 if final variables are to be output
34   IOUT=1
35 C   Set ITMIX=1 if using artificial TMIX field as input
36   ITMIX=1
37 C Decide on basic parameters
38   NUMIT=6
39   NFULL=5
40   NX=21
41   NY=36
42   NL=6
43   NX1=NX+1
44   NY1=NY+1
45   NXM1=NX-1
46   NYM1=NY-1
47   NLM1=NL-1
48   NFINE=4
49   NS=((NL-2)*NFINE)+2
50   NSM1=NS-1
51   NG=5
52   TOP=1.0D-06
53   STREN=9.0D+03
54   DELTT=2.16D+04
55   DT=2.16D+04
56   DX=3.5D+04
57   DY=3.5D+04
58   ERROR=1.0D-02
59   ERROR2=0.01D0
60   TINC=ERROR2*1.0D-02
61   DIFF1=4.0D-03*DX
62   ECCEN=2.0D0
63   RHOAIR=1.3D0
64   RHOICE=0.922D+03
65   RHOWAT=0.1025D+04
66   GRAV=9.82868D0
67   COT=1.428D0
68   SIN20=0.342D0
69   COS20=0.9397D0
70   SIN25=0.4226D0
71   COS25=0.9063D0
72   UA=0.5D0
73   UB=0.5D0
74   CB=((RHOWAT-RHOICE)/RHOWAT)*RHOICE*GRAV*0.5D0
75   CF=CB*COT*(UA+UB)*RHOICE/RHOWAT
76   AH=RHOWAT*0.5D0/(COT*(UA+UB)*RHOICE)
77   BH=2.0D0*STREN/CB
78   CH=BH/(4.0D0-AH)
79   QI=3.02D+08
80   CW=4.19D+06
81   DMIX=3.0D+01
82   TI=QI/(CW*DMIX)
83   SIGMAX=1.0D+05
84   PI=3.141592653589793D0
85   STFN=5.67D-08
86   CON=2.1656D0
87   D1=2.28D0
88   D3=5.5D-08
89   CON1=4.5D0*SIGMAX/(RHOWAT*GRAV*3.43D-06)
90   CPLF=(1.0D+10/(3.0D0*RHOWAT*GRAV))*0.25D0
91   CON2=3.0D0*RHOWAT*GRAV*3.43D-06/(DSQRT(2.0D0)*DEXP(PI/4.0D0))
92   SIDER=(PI/4.0D0)+(4.0D0/PI)
93   RRMAT=1.0D+04
94   ARMAX=PI*RRMAX*RRMAX
95   LAD=2
96   IUVT=1
97 C Initialise counter
98   DAY=334.75D0
99   ICOUNT=0
100  TOUT=0.0D0

```

```

101 C Define boundaries
102 CALL BNDRY
103 C Set up vertical thickness levels
104 CALL LEVELS
105 C Calculate coefficients used in redistribution
106 CALL REDIST(GAMMA,GAMMAF)
107 C Input test data
108 DO 2 J=1,NY1
109 DO 2 I=1,NX1
110 TMIX(I,J)=2.712D+02
111 DO 2 K=1,3
112 DO 1 L=2,NL
113 G(L,I,J,K)=0.0D0
114 1 CONTINUE
115 G(2,I,J,K)=0.25D0*OUT(I,J)
116 G(3,I,J,K)=0.25D0*OUT(I,J)
117 G(4,I,J,K)=0.25D0*OUT(I,J)
118 G(5,I,J,K)=0.25D0*OUT(I,J)
119 G(1,I,J,K)=0.0D0*OUT(I,J)
120 2 CONTINUE
121 DO 3 J=1,NY
122 DO 3 I=1,NX
123 PHI(I,J)=75.0D0*PI/180.0D0
124 TAIR(I,J)=274.0D0
125 3 CONTINUE
126 DO 4 NWEK=1,52
127 C(NWEK)=0.75D0
128 RHUM(NWEK)=0.7D0
129 P(NWEK)=101400.0D0
130 4 CONTINUE
131 DO 5 J=1,NY
132 DO 5 I=1,NX
133 GAIRX(I,J)=5.0D0
134 GAIRY(I,J)=0.0D0
135 GWATX(I,J)=0.0D0
136 GWATY(I,J)=0.0D0
137 5 CONTINUE
138 C Call data specific to Greenland
139 CALL GRNLND(GWATX,GWATY,PHI,C,RHUM,P,EDGE,HTSEA)
140 C Read initial thickness distribution and mixed layer temperature
141 IF(INIT.EQ.0)READ(13)G,HI,TMIX
142 C If observed surface temperature field is available, read it in
143 IF(ITMIX.EQ.0)READ(12)TMIX
144 DO 6 K=1,3
145 DO 6 J=1,NY1
146 DO 6 I=1,NX1
147 IF(OUT(I,J).EQ.0.0D0)HI(I,J,K)=H(NLM1)+TOP
148 DO 6 L=1,NL
149 G(L,I,J,K)=G(L,I,J,K)*OUT(I,J)
150 6 CONTINUE

```

```

151 DO 7 K=1,3
152 DO 7 J=1,NY1
153 DO 7 I=1,NX1
154 DO 7 L=1,NLM1
155 FND(L,I,J,K)=G(L+1,I,J,K)/ARMAX
156 7 CONTINUE
157 C Zero out velocity
158 DO 8 J=1,NY
159 DO 8 I=1,NX
160 GWATX(I,J)=GWATX(I,J)+1.0D-08
161 U(I,J,3)=0.0D0
162 U(I,J,2)=0.0D0
163 U(I,J,1)=0.0D0
164 V(I,J,3)=0.0D0
165 V(I,J,2)=0.0D0
166 V(I,J,1)=0.0D0
167 UC(I,J)=0.0D0
168 VC(I,J)=0.0D0
169 UAV(I,J)=0.0D0
170 VAV(I,J)=0.0D0
171 8 CONTINUE
172 C Zero out viscosities
173 DO 9 J=1,NY1
174 DO 9 I=1,NX1
175 ETA(I,J)=0.0D0
176 ZETA(I,J)=0.0D0
177 9 CONTINUE
178 C Get first value of U and V
179 THETA=1.0D0
180 C Evaluate strength
181 DO 11 J=1,NY1
182 DO 11 I=1,NX1
183 DO 10 L=1,NL
184 G1(L)=G(L,I,J,1)*(1.0D0+1.0D-04)
185 10 CONTINUE
186 C Refine the grid
187 CALL FINE(G1,G2)
188 C Call RIDGE to determine the initial ice strength
189 CALL RIDGE(I,J,G2,G3,GAMMA,GAMMAF,PRESS(I,J))
190 11 CONTINUE
191 C Read in winds and air temperature
192 CALL UVT(GAIRX,GAIRY,TAIR,ICOUNT,INIT,IUVT)
193 CALL FORM(U,V,ETA,ZETA,DRAGS,DRAGA,GAIRX,GAIRY,GWATX,GWATY,FORCEX,
194 1FORCEY,G,AMASS,PRESS,PHI,EKMANX,EKMANX)
195 DO 13 J=1,NY1
196 DO 13 I=1,NX1
197 HM(NL)=(HI(I,J,1)+H(NLM1))*0.5D0
198 C Define initial viscosity
199 ZETA(I,J)=0.0D0
200 DO 12 L=2,NL

```

```

201      ZETA(I,J)=ZETA(I,J)+(G(L,I,J,1)*1.0D+11*HM(L))
202 12    CONTINUE
203      ETA(I,J)=ZETA(I,J)/(ECCEN*ECCEN)
204 13    CONTINUE
205 C Write out thickness levels
206      IF(IPL.EQ.1) WRITE (6,14) H,HI(2,2,1)
207 14    FORMAT(////,1X,'Thickness levels ',9X,6(2X,F7.4))
208      IF(IPL.EQ.1) WRITE(6,15)HM
209 15    FORMAT(1X,'Midpoints of levels',7X,6(2X,F7.4))
210      IF(IPL.EQ.1) WRITE(6,16)HW
211 16    FORMAT(1X,'level widths',14X,6(2X,F7.4),/)
212 C      IF(IPL.EQ.1) WRITE(6,11)
213 C11    FORMAT(///,31X,'Redistribution coefficients, GAMMA(L1,L2) '/')
214 C      IF(IPL.EQ.1) WRITE(6,12)((GAMMA(L1,L2),L1=1,NS),L2=1,NS)
215 C12    FORMAT(1X,18(1X,F6.4))
216 C Calculate ice velocities if this is the first run
217      IFIRST=1
218      IF(INIT.EQ.0) CALL RELAX(U,V,ETA,ZETA,DRAGS,DRAGA,AMASS,FORCEX,FOR
219 ICEY,ERROR,THETA,UC,VC,IFIRST,GAIRX,GAIRY,EKMANX,EKMANY)
220      IFIRST=0
221      ERROR=1.0D-05
222      DO 17 J=1,NY
223      DO 17 I=1,NX
224      U(I,J,2)=U(I,J,1)
225      U(I,J,3)=U(I,J,2)
226      V(I,J,2)=V(I,J,1)
227      V(I,J,3)=V(I,J,2)
228 17    CONTINUE
229 C Read in output from previous run if available.
230      IF(INIT.EQ.1) READ(10)G,HI,FND,U,V,TMIX,TOUT,DAY,ICOUNT,POSX,POSY
231      POSX=5.15D0
232      POSY=16.2D0
233      IF(IWIND.EQ.1)ICOUNT=0
234      CALL VOLICE(G,VOL)
235      DO 18 J=1,NY
236      DO 18 I=1,NX
237      UC(I,J)=U(I,J,1)
238      VC(I,J)=V(I,J,1)
239 18    CONTINUE
240 C Predictor corrector procedure starts here
241 19    CONTINUE
242 C Update timestep and calculate day and week of the year
243      ICOUNT=ICOUNT+1
244      NUMIT=NUMIT-1
245      DAY=DAY+DELTT/8.64D+04
246      DAY=DMOD(DAY,365.0D0)
247      NW=IDINT(DAY*52.0D0/365.0D0)+1
248      WRITE(6,58)ICOUNT,DAY
249 C Read in winds and temperature
250      CALL UVT(GAIRX,GAIRY,TAIR,ICOUNT,INIT,IUVT)

```

```

251      IUVT=0
252 C Set reasonable thickness and floe number distribution at outflow cells
253      DO 22 L=1,NL
254      DO 20 J=2,NY
255      DO 20 I=2,NX
256      UC(I,J)=(G(L,I-1,J-1,1)*OUT(I-1,J-1)+G(L,I+1,J-1,1)*OUT(I+1,J-1)+G
257 1(L,I-1,J+1,1)*OUT(I-1,J+1)+G(L,I+1,J+1,1)*OUT(I+1,J+1)+4.0D0*(G(L,
258 2I,J-1,1)*OUT(I,J-1)+G(L,I-1,J,1)*OUT(I-1,J)+G(L,I+1,J,1)*OUT(I+1,J
259 3)+G(L,I,J+1,1)*OUT(I,J+1))/(OUT(I-1,J-1)+OUT(I+1,J-1)+OUT(I-1,J+1
260 4)+OUT(I+1,J+1)+4.0D0*(OUT(I,J-1)+OUT(I-1,J)+OUT(I+1,J)+OUT(I,J+1))
261 5+1.0D-15)
262 20    CONTINUE
263      DO 21 J=2,NY
264      DO 21 I=2,NX
265      G(L,I,J,1)=G(L,I,J,1)+(GMASK(I,J)-OUT(I,J))*UC(I,J)
266 21    CONTINUE
267 22    CONTINUE
268      DO 25 L=1,NLM1
269      DO 23 J=2,NY
270      DO 23 I=2,NX
271      UC(I,J)=(FND(L,I-1,J-1,1)*OUT(I-1,J-1)+FND(L,I+1,J-1,1)*OUT(I+1,J-
272 11)+FND(L,I-1,J+1,1)*OUT(I-1,J+1)+FND(L,I+1,J+1,1)*OUT(I+1,J+1)+4.0
273 2D0*(FND(L,I,J-1,1)*OUT(I,J-1)+FND(L,I-1,J,1)*OUT(I-1,J)+FND(L,I+1,
274 3J,1)*OUT(I+1,J)+FND(L,I,J+1,1)*OUT(I,J+1))/(OUT(I-1,J-1)+OUT(I+1,
275 4J-1)+OUT(I-1,J+1)+OUT(I+1,J+1)+4.0D0*(OUT(I,J-1)+OUT(I-1,J)+OUT(I+
276 51,J)+OUT(I,J+1))+1.0D-15)
277 23    CONTINUE
278      DO 24 J=2,NY
279      DO 24 I=2,NX
280      FND(L,I,J,1)=FND(L,I,J,1)+(GMASK(I,J)-OUT(I,J))*UC(I,J)
281 24    CONTINUE
282 25    CONTINUE
283      DO 26 J=2,NY
284      DO 26 I=2,NX
285      UC(I,J)=(HI(I-1,J-1,1)*OUT(I-1,J-1)+HI(I+1,J-1,1)*OUT(I+1,J-1)+HI(
286 1I-1,J+1,1)*OUT(I-1,J+1)+HI(I+1,J+1,1)*OUT(I+1,J+1)+4.0D0*(HI(I,J-1
287 2,1)*OUT(I,J-1)+HI(I-1,J,1)*OUT(I-1,J)+HI(I+1,J,1)*OUT(I+1,J)+HI(I,
288 3J+1,1)*OUT(I,J+1))/(OUT(I-1,J-1)+OUT(I+1,J-1)+OUT(I-1,J+1)+OUT(I+
289 41,J+1)+4.0D0*(OUT(I,J-1)+OUT(I-1,J)+OUT(I+1,J)+OUT(I,J+1))+1.0D-15
290 5)
291 26    CONTINUE
292      DO 27 J=2,NY
293      DO 27 I=2,NX
294      HI(I,J,1)=HI(I,J,1)+(GMASK(I,J)-OUT(I,J))*UC(I,J)
295 27    CONTINUE
296 C Read in imposed northern boundary conditians (Greenland)
297      CALL NORTH(G,EDGE(NW),FND,TMIX)
298      CALL VOLICE(G,VOL1)
299      VOL1=VOL1-VOL
300 C First do predictor

```

```

301      DO 28 J=1,NY
302      DO 28 I=1,NX
303      U(I,J,3)=U(I,J,1)
304      V(I,J,3)=V(I,J,1)
305      UC(I,J)=U(I,J,1)
306      VC(I,J)=V(I,J,1)
307 28    CONTINUE
308      THETA=1.0D0
309      DT=DELTT/2.0D0
310      DO 30 J=1,NY1
311      DO 30 I=1,NX1
312      DO 29 L=1,NL
313      G1(L)=G(L,I,J,1)*(1.0D0+1.0D-04)
314 29    CONTINUE
315      CALL FINE(G1,G2)
316 C Determine ice strength
317      CALL RIDGE(I,J,G2,G3,GAMMA,GAMMAF,PRESS(I,J))
318 30    CONTINUE
319 Calculate forcing
320      CALL FORM(U,V,ETA,ZETA,DRAGS,DRAGA,GAIRX,GAIRY,GWATX,GWATY,FORCEX,
321      IFORCEY,G,AMASS,PRESS,PHI,EKMANX,EKMANY)
322      CALL RELAX(U,V,ETA,ZETA,DRAGS,DRAGA,AMASS,FORCEX,FORCEY,ERROR,THET
323      1A,UC,VC,IFIRST,GAIRX,GAIRY,EKMANX,EKMANY)
324 C Do regular time step
325 C Do backwards time step
326      THETA=1.0D0
327      DT=DELTT
328      CALL FORM(U,V,ETA,ZETA,DRAGS,DRAGA,GAIRX,GAIRY,GWATX,GWATY,FORCEX,
329      IFORCEY,G,AMASS,PRESS,PHI,EKMANX,EKMANY)
330 C Set U(1)=U(2) and same for V
331      DO 31 J=1,NY
332      DO 31 I=1,NX
333      U(I,J,3)=U(I,J,1)
334      V(I,J,3)=V(I,J,1)
335      UC(I,J)=U(I,J,1)
336      VC(I,J)=V(I,J,1)
337      U(I,J,1)=U(I,J,2)
338      V(I,J,1)=V(I,J,2)
339 31    CONTINUE
340      CALL RELAX(U,V,ETA,ZETA,DRAGS,DRAGA,AMASS,FORCEX,FORCEY,ERROR,THET
341      1A,UC,VC,IFIRST,GAIRX,GAIRY,EKMANX,EKMANY)
342 C Advect each thickness level
343      NUM=NL
344      CALL GVECT(U,V,G,DIFF1,LAD,NUM)
345 C Calculate new maximum thickness by advecting total volume,
346 C and using conservation.
347      DO 35 J=1,NY1
348      DO 35 I=1,NX1
349      DO 32 K=1,3
350      AVV(I,J,K)=0.0D0

```

```

351 32    CONTINUE
352      DO 34 K=1,3
353      DO 33 L=2,NLM1
354      AVV(I,J,K)=AVV(I,J,K)+G(L,I,J,K)*HM(L)
355 33    CONTINUE
356      AVV(I,J,K)=AVV(I,J,K)+G(NL,I,J,K)*0.5D0*(H(NLM1)+HI(I,J,K))
357 34    CONTINUE
358 35    CONTINUE
359      CALL ADVECT(U,V,AVV,DIFF1,LAD)
360      DO 36 J=1,NY1
361      DO 36 I=1,NX1
362      HI(I,J,2)=HI(I,J,1)
363 36    CONTINUE
364      DO 40 J=1,NY1
365      DO 40 I=1,NX1
366      IF(G(NL,I,J,1).LE.0.0D0) GOTO 38
367      SUM=0.0D0
368      DO 37 L=2,NLM1
369      SUM=SUM+G(L,I,J,1)*HM(L)
370 37    CONTINUE
371      HI(I,J,1)=(2.0D0*(AVV(I,J,1)-SUM)/G(NL,I,J,1))-H(NLM1)
372      GOTO 39
373 38    HI(I,J,1)=H(NLM1)+TOP
374 39    CONTINUE
375 40    CONTINUE
376 C Advect floe number densities
377      NUM=NLM1
378      CALL GVECT(U,V,FND,DIFF1,LAD,NUM)
379      DO 41 J=1,NY1
380      DO 41 I=1,NX1
381      IF(GMASK(I,J).EQ.0.0D0) HI(I,J,1)=H(NLM1)+TOP
382      HI(I,J,1)=DMAX1(HI(I,J,1),H(NLM1)+TOP)
383      HI(I,J,1)=DMIN1(HI(I,J,1),25.0D0)
384 41    CONTINUE
385 C Carry out thickness and floe size redistributions
386      CALL DIST(U,V,G,GAMMA,GAMMAF,PRESS,TMIX,FND,GAIRX,GAIRY,DAY,NW,PHI
387      1,TAIR,C,P,RHUM,HTSEA)
388 C Correct outflow points and get outflow ice
389      CALL VOLICE(G,VOL)
390      DO 44 J=1,NY1
391      DO 44 I=1,NX1
392      HI(I,J,1)=DMAX1(HI(I,J,1),H(NLM1)+TOP)
393      DO 42 LF=1,NLM1
394      FND(LF,I,J,1)=FND(LF,I,J,1)*OUT(I,J)
395 42    CONTINUE
396      DO 43 LG=1,NL
397      G(LG,I,J,1)=G(LG,I,J,1)*OUT(I,J)
398 43    CONTINUE
399      IF(G(NL,I,J,1).EQ.0.0D0) HI(I,J,1)=H(NLM1)+TOP
400 44    CONTINUE

```

```

401 CALL VOLICE(G,VOL2)
402 TOUT1=VOL-VOL2-VOL1
403 VOL=VOL2
404 TOUT=TOUT+TOUT1
405 II=POSX
406 JJ=POSY
407 SY=POSY-DFLOAT(JJ)
408 SX=POSX-DFLOAT(II)
409 U1=SY*U(II+1,JJ+2,1)+(1.0D0-SY)*U(II+1,JJ+1,1)
410 U2=SY*U(II+2,JJ+2,1)+(1.0D0-SY)*U(II+2,JJ+1,1)
411 U3=SX*U2+(1.0D0-SX)*U1
412 V1=SY*V(II+1,JJ+2,1)+(1.0D0-SY)*V(II+1,JJ+1,1)
413 V2=SY*V(II+2,JJ+2,1)+(1.0D0-SY)*V(II+2,JJ+1,1)
414 V3=SX*V2+(1.0D0-SX)*V1
415 POSX=POSX+DT*U3/DX
416 POSY=POSY+DT*V3/DY
417 WRITE(6,45)DAY,POSX,POSY
418 45 FORMAT(1X,'POSITION',3G20.6)
419 DO 46 J=1,NY
420 DO 46 I=1,NX
421 UAV(I,J)=UAV(I,J)+U(I,J,1)
422 VAV(I,J)=VAV(I,J)+V(I,J,1)
423 46 CONTINUE
424 WRITE(6,66)VOL
425 WRITE(6,67)TOUT1
426 WRITE(6,68)TOUT
427 C Print out every K'th point
428 KTH=MOD(ICOUNT,NFULL)
429 IF(KTH.EQ.0) GO TO 47
430 GO TO 54
431 47 CONTINUE
432 C Output information at each time step
433 IF(IP2.EQ.1) WRITE(6,59)
434 IF(IP2.EQ.1) WRITE(6,60)
435 IF(IP2.EQ.1) WRITE(6,56)((U(I,J,1),I=1,NX,NG),J=1,NY,NG)
436 IF(IP2.EQ.1) WRITE(6,61)
437 IF(IP2.EQ.1) WRITE(6,56)((V(I,J,1),I=1,NX,NG),J=1,NY,NG)
438 IF(IP2.EQ.1) WRITE(6,48)
439 48 FORMAT(/,1X,'FLOE NUMBER DENSITY',/)
440 IF(IP2.EQ.1) WRITE(6,49)((FND(1,I,J,1),I=1,NX1,NG),J=1,NY1,NG)
441 IF(IP2.EQ.1) WRITE(6,57)
442 IF(IP2.EQ.1) WRITE(6,49)((FND(2,I,J,1),I=1,NX1,NG),J=1,NY1,NG)
443 IF(IP2.EQ.1) WRITE(6,57)
444 IF(IP2.EQ.1) WRITE(6,49)((FND(3,I,J,1),I=1,NX1,NG),J=1,NY1,NG)
445 49 FORMAT(1X,5G17.10)
446 IF(IP2.EQ.1) WRITE(6,62)
447 IF(IP2.EQ.1) WRITE(6,50)(G(L,10,10,1),G(L,20,10,1),L=1,NL)
448 IF(IP2.EQ.1) WRITE(6,50)(G(L,10,20,1),G(L,20,20,1),L=1,NL)
449 50 FORMAT(/,(1X,G20.12,5X,G20.12))
450 IF(IP3.EQ.1) WRITE(6,63)

```

```

451 IF(IP3.EQ.1) WRITE(6,49)((ZETA(I,J),I=1,NX1,NG),J=1,NY1,NG)
452 IF(IP3.EQ.1) WRITE(6,51)
453 51 FORMAT(/,1X,'SHEAR VISCOSITY, ETA',/)
454 IF(IP3.EQ.1) WRITE(6,49)((ETA(I,J),I=1,NX1,NG),J=1,NY1,NG)
455 IF(IP3.EQ.1) WRITE(6,52)
456 52 FORMAT(/,1X,'RIDGING AMOUNT, ALPHR',/)
457 IF(IP3.EQ.1) WRITE(6,49)((ALPHR(I,J),I=1,NX1,NG),J=1,NY1,NG)
458 IF(IP3.EQ.1) WRITE(6,53)
459 53 FORMAT(/,1X,'OPEN WATER OPENING, ALPHO',/)
460 IF(IP3.EQ.1) WRITE(6,49)((ALPHO(I,J),I=1,NX1,NG),J=1,NY1,NG)
461 IF(IP3.EQ.1) WRITE(6,64)
462 IF(IP3.EQ.1) WRITE(6,49)((PRESS(I,J),I=1,NX1,NG),J=1,NY1,NG)
463 IF(IP3.EQ.1) WRITE(6,65)
464 IF(IP3.EQ.1) WRITE(6,49)((TMIX(I,J),I=1,NX1,NG),J=1,NY1,NG)
465 C Check counter and decide if new winds needed
466 C Decide if done
467 54 CONTINUE
468 IF(NUMIT.EQ.0) GO TO 55
469 GO TO 19
470 55 CONTINUE
471 C Output information for next run
472 IF(IOUT.EQ.1) WRITE(14)UAV,VAV
473 IF(IOUT.EQ.1) WRITE(11)G,HI,FND,U,V,TMIX,TOUT,DAY,ICOUNT,POSX,POSY
474 STOP
475 56 FORMAT(1X,5G17.10)
476 57 FORMAT(/)
477 58 FORMAT(1X,'**** TIME STEP ',I6,' DAY ',F7.2)
478 59 FORMAT(6X,'FULL DATA PRINTED FOR THIS TIME STEP')
479 60 FORMAT(/,1X,'X-COMPONENT OF ICE VELOCITY')
480 61 FORMAT(/,1X,'Y-COMPONENT OF ICE VELOCITY')
481 62 FORMAT(/,1X,'ICE THICKNESS DISTRIBUTION AT SELECTED POINTS')
482 63 FORMAT(/,1X,'BULK VISCOSITY, ZETA')
483 64 FORMAT(/,1X,'STRENGTH')
484 65 FORMAT(/,1X,'MIXED LAYER TEMPERATURE')
485 66 FORMAT(6X,'TOTAL VOLUME ',G20.12)
486 67 FORMAT(6X,'OUTFLOW ',G14.7)
487 68 FORMAT(6X,'NET:',4X,G14.7)
488 END
489 C
490 C
491 C
492 C
493 SUBROUTINE ADVECT(U,V,AD,DIFF1,LAD)
494 C
495 C Advection
496 IMPLICIT REAL*8 (A-H,O-Z)
497 DIMENSION AD(22,37,3),U(21,36,3),V(21,36,3)
498 COMMON/GRID1/NX,NY,NX1,NY1,NXMI,NL,NLMI,NFINE,NS,NSMI
499 COMMON/GRIDR/HI(22,37,3),HMS(18),HWS(18),HS(17),HM(6),HW(6),H(6),T
500 10P

```

```

501 COMMON/STEP/DT,DX,DY
502 COMMON/ARRAY/GMASK(22,37),UVM(21,36)
503 C Decide if backward euler or leapfrog
504 LL=LAD
505 IF(LL.EQ.1) GO TO 1
506 C Backward euler
507 DELTT=DT
508 K3=2
509 GO TO 2
510 C Leapfrog
511 1 DELTT=DT*2.0D0
512 K3=3
513 2 CONTINUE
514 C Rearrange
515 DO 3 J=1,NY1
516 DO 3 I=1,NX1
517 AD(I,J,3)=AD(I,J,2)
518 AD(I,J,2)=AD(I,J,1)
519 3 CONTINUE
520 C Go through conservative advection
521 DELTX=DELTT/(4.0D0*DX)
522 DELTY=DELTT/(4.0D0*DY)
523 4 CONTINUE
524 DO 5 J=2,NY
525 DO 5 I=2,NX
526 AD(I,J,1)=AD(I,J,K3)-DELTXX*((AD(I,J,2)+AD(I+1,J,2))*U(I,J,1)+U(I,
527 1J-1,1))-AD(I,J,2)+AD(I-1,J,2))*U(I-1,J,1)+U(I-1,J-1,1))-DELTYY*(
528 2(AD(I,J,2)+AD(I,J+1,2))*V(I-1,J,1)+V(I,J,1))-AD(I,J,2)+AD(I,J-1,
529 32))*V(I-1,J-1,1)+V(I,J-1,1)))
530 5 CONTINUE
531 C Decide if done
532 GO TO (10,8,6),LL
533 6 CONTINUE
534 DO 7 J=1,NY1
535 DO 7 I=1,NX1
536 AD(I,J,2)=AD(I,J,3)
537 7 CONTINUE
538 GO TO 10
539 8 CONTINUE
540 C Do backward euler correction
541 DO 9 J=1,NY1
542 DO 9 I=1,NX1
543 AD(I,J,3)=AD(I,J,2)
544 AD(I,J,2)=0.5D0*(AD(I,J,1)+AD(I,J,2))
545 9 CONTINUE
546 LL=3
547 K3=3
548 GO TO 4
549 10 CONTINUE
550 DO 14 KD=1,2

```

```

551 IF(KD.EQ.2) GO TO 11
552 CALL DIFFUS(AD,DIFF1,DELTT)
553 GOTO 12
554 11 DIFF2=-(DX*DX)/DELTT
555 CALL DIFFUS(AD,DIFF2,DELTT)
556 12 CONTINUE
557 DO 13 J=1,NY1
558 DO 13 I=1,NX1
559 AD(I,J,1)=(AD(I,J,1)+AD(I,J,3))*GMASK(I,J)
560 13 CONTINUE
561 14 CONTINUE
562 RETURN
563 END
564 C
565 C
566 SUBROUTINE DIFFUS(AD,DIFF1,DELTT)
567 C
568 IMPLICIT REAL*8 (A-H,O-Z)
569 DIMENSION AD(22,37,3),AD1(22,37)
570 COMMON/GRID1/NX,NY,NX1,NY1,NXM1,NYM1,NL,NLM1,NFINE,NS,NSM1
571 COMMON/GRIDR/HI(22,37,3),HMS(18),HWS(18),HS(17),HM(6),HW(6),H(6),T
572 1OP
573 COMMON/STEP/DT,DX,DY
574 COMMON/ARRAY/GMASK(22,37),UVM(21,36)
575 C Subroutine diffuses AD,multiplies by DELT,and puts result in AD
576 C Zero out AD1
577 DO 1 J=1,NY1
578 DO 1 I=1,NX1
579 AD1(I,J)=0.0D0
580 1 CONTINUE
581 C Do diffusion
582 DELTXX=DELTT*DIFF1/(DX*DX)
583 DELTYY=DELTT*DIFF1/(DY*DY)
584 DO 2 J=2,NY
585 DO 2 I=2,NX
586 AD1(I,J)=DELTXX*((AD(I+1,J,3)-AD(I,J,3))*GMASK(I+1,J)-(AD(I,J,3)-A
587 1D(I-1,J,3))*GMASK(I-1,J))+DELTYY*((AD(I,J+1,3)-AD(I,J,3))*GMASK(I,
588 2J+1)-(AD(I,J,3)-AD(I,J-1,3))*GMASK(I,J-1))
589 2 CONTINUE
590 DO 3 J=1,NY1
591 DO 3 I=1,NX1
592 AD(I,J,3)=AD1(I,J)
593 3 CONTINUE
594 RETURN
595 END
596 C
597 SUBROUTINE GVECT(U,V,G,DIFF1,LAD,NUM)
598 C
599 IMPLICIT REAL*8 (A-H,O-Z)
600 DIMENSION G(NUM,22,37,3),U(21,36,3),V(21,36,3)

```

```

601      COMMON/GRIDI/NX,NY,NX1,NY1,NXM1,NYM1,NL,NLM1,NFINE,NS,NSM1
602      COMMON/GRIDR/HI(22,37,3),HMS(18),HWS(18),HS(17),HM(6),HW(6),H(6),T
603      IOP
604      COMMON/STEP/DT,DX,DY
605      COMMON/ARRAY/GMASK(22,37),UVM(21,36)
606  C Decide if backward euler or leapfrog
607      LL=LAD
608      IF(LL.EQ.1) GO TO 1
609  C Backward euler
610      DELTT=DT
611      K3=2
612      GO TO 2
613  C Leapfrog
614  1      DELTT=DT*2.0D0
615      K3=3
616  2      CONTINUE
617  C Rearrange
618      DO 3 J=1,NY1
619      DO 3 I=1,NX1
620      DO 3 L=1,NUM
621      G(L,I,J,3)=G(L,I,J,2)
622      G(L,I,J,2)=G(L,I,J,1)
623  3      CONTINUE
624  C Go through conservative advection
625      DELTX=DELTT/(4.0D0*DX)
626      DELTY=DELTT/(4.0D0*DY)
627  4      CONTINUE
628      DO 5 J=2,NY
629      DO 5 I=2,NX
630      DO 5 L=1,NUM
631      G(L,I,J,1)=G(L,I,J,K3)-DELTXX*((G(L,I,J,2)+G(L,I+1,J,2))*(U(I,J,1)+
632      1U(I,J-1,1))-G(L,I,J,2)+G(L,I-1,J,2))*(U(I-1,J,1)+U(I-1,J-1,1))-D
633      2ELTY*((G(L,I,J,2)+G(L,I,J+1,2))*(V(I-1,J,1)+V(I,J,1))-G(L,I,J,2)+
634      3G(L,I,J-1,2))*(V(I-1,J-1,1)+V(I,J-1,1)))
635  5      CONTINUE
636  C Decide if done
637      GO TO (10,8,6),LL
638  6      CONTINUE
639      DO 7 J=1,NY1
640      DO 7 I=1,NX1
641      DO 7 L=1,NUM
642      G(L,I,J,2)=G(L,I,J,3)
643  7      CONTINUE
644      GO TO 10
645  8      CONTINUE
646  C Do backward euler correction
647      DO 9 J=1,NY1
648      DO 9 I=1,NX1
649      DO 9 L=1,NUM
650      G(L,I,J,3)=G(L,I,J,2)

```

```

651      G(L,I,J,2)=0.5D0*(G(L,I,J,1)+G(L,I,J,2))
652  9      CONTINUE
653      LL=3
654      K3=3
655      GO TO 4
656  10     CONTINUE
657      DO 15 L=1,NUM
658      DO 14 KD=1,2
659      IF(KD.EQ.2) GO TO 11
660      CALL DIFFG(G,DIFF1,DELTT,L,NUM)
661      GOTO 12
662  11     DIFF2=-(DX*DX)/DELTT
663      CALL DIFFG(G,DIFF2,DELTT,L,NUM)
664  12     CONTINUE
665      DO 13 J=1,NY1
666      DO 13 I=1,NX1
667      G(L,I,J,1)=(G(L,I,J,1)+G(L,I,J,3))*GMASK(I,J)
668  13     CONTINUE
669  14     CONTINUE
670  15     CONTINUE
671      RETURN
672      END
673  C
674  C
675      SUBROUTINE DIFFG(G,DIFF1,DELTT,L,NUM)
676  C
677      IMPLICIT REAL*8 (A-H,O-Z)
678      DIMENSION G(NUM,22,37,3),G1(22,37)
679      COMMON/GRIDI/NX,NY,NX1,NY1,NXM1,NYM1,NL,NLM1,NFINE,NS,NSM1
680      COMMON/GRIDR/HI(22,37,3),HMS(18),HWS(18),HS(17),HM(6),HW(6),H(6),T
681      IOP
682      COMMON/STEP/DT,DX,DY
683      COMMON/ARRAY/GMASK(22,37),UVM(21,36)
684  C Subroutine diffuses ad,multiplies by deltt,and puts result in ad
685  C Zero out adl
686      DO 1 J=1,NY1
687      DO 1 I=1,NX1
688      G1(I,J)=0.0D0
689  1      CONTINUE
690  C Do diffusion
691      DELTXX=DELTT*DIFF1/(DX*DX)
692      DELTYY=DELTT*DIFF1/(DY*DY)
693      DO 2 J=2,NY
694      DO 2 I=2,NX
695      G1(I,J)=DELTXX*((G(L,I+1,J,3)-G(L,I,J,3))*GMASK(I+1,J)-(G(L,I,J,3)
696      1-G(L,I-1,J,3))*GMASK(I-1,J))+DELTYY*((G(L,I,J+1,3)-G(L,I,J,3))*GMA
697      2SK(I,J+1)-(G(L,I,J,3)-G(L,I,J-1,3))*GMASK(I,J-1))
698  2      CONTINUE
699      DO 3 J=1,NY1
700      DO 3 I=1,NX1

```

```

701      G(L,I,J,3)=G1(I,J)
702 3     CONTINUE
703      RETURN
704      END
705 C
706      SUBROUTINE BNDRY
707 C
708 C Subroutine sets up boundary mask
709      IMPLICIT REAL*8 (A-H,O-Z)
710      COMMON/GRID1/NX,NY,NX1,NY1,NXM1,NYM1,NL,NLM1,NFINE,NS,NSM1
711      COMMON/GRIDR/HI(22,37,3),HMS(18),HWS(18),HS(17),HM(6),HW(6),H(6),T
712      IOP
713      COMMON/ARRAY/GMASK(22,37),UVM(21,36)
714      COMMON/OUTFLO/OUT(22,37)
715      READ(5,1)((UVM(I,J),I=1,NX),J=1,NY)
716 1      FORMAT(21G1.0)
717      READ(5,2)((GMASK(I,J),I=1,NX1),J=1,NY1)
718      READ(5,2)((OUT(I,J),I=1,NX1),J=1,NY1)
719 2      FORMAT(22G1.0)
720      RETURN
721      END
722 C
723 C
724      SUBROUTINE LEVELS
725 C
726      IMPLICIT REAL*8 (A-H,O-Z)
727      COMMON/GRID1/NX,NY,NX1,NY1,NXM1,NYM1,NL,NLM1,NFINE,NS,NSM1
728      COMMON/GRIDR/HI(22,37,3),HMS(18),HWS(18),HS(17),HM(6),HW(6),H(6),T
729      IOP
730 C Determine fixed vertical thickness spacings
731      ERR=1.0D0
732 C C1 is width of thinnest ice layer
733      C1=0.25D0
734 C C2 is a constant to be determined iteratively
735      C2=0.0D0
736 C C3 is a scaling constant
737      C3=6.6D+01
738 C HNLM1 is max of the fixed thickness levels
739      HNLM1=2.0D0
740      HM(2)=C1*0.5D0
741 C Convenient definitions of hm(1) etc
742      HM(1)=0.0D0
743      HW(1)=1.0D0
744      H(1)=0.0D0
745      H(2)=C1
746 1      DO 2 L=3,NLM1
747          HM(L)=HM(L-1)+C1+C2*(1.0D0-DEXP(-(DFLOAT(L)-2.0D0)*(DFLOAT(L)-2.0D
748          10)/C3))
749          H(L)=(2.0D0*HM(L))-H(L-1)
750 2      CONTINUE

```

```

751      IF(DABS(H(NLM1)-HNLM1).LT.1.0D-15) GO TO 4
752      IF(H(NLM1).LT.HNLM1) GO TO 3
753      C2=C2-ERR
754      ERR=ERR/2.5D0
755      GO TO 1
756 3      C2=C2+ERR
757      GO TO 1
758 4      DO 5 L=2,NLM1
759          HW(L)=H(L)-H(L-1)
760 5      CONTINUE
761 C Set max thickness just above hnlm1
762      DO 6 K=1,3
763          DO 6 J=1,NY1
764              DO 6 I=1,NX1
765                  HI(I,J,K)=HNLM1+TOP
766 6      CONTINUE
767 C Set up fine grid
768      NN=1
769      HS(1)=H(1)
770      DO 7 L=2,NLM1
771          DO 7 N=1,NFINE
772              NN=NN+1
773              HS(NN)=H(L-1)+(DFLOAT(N)*HW(L)/DFLOAT(NFINE))
774 7      CONTINUE
775      DO 8 L=2,NSM1
776          HMS(L)=0.5D0*(HS(L-1)+HS(L))
777          HWS(L)=HS(L)-HS(L-1)
778 8      CONTINUE
779      HMS(1)=HM(1)
780      HWS(1)=HW(1)
781      RETURN
782      END
783 C
784 C
785      SUBROUTINE FINE(GL,GS)
786 C
787 C Refines the grid from 6 to 18 layers
788      IMPLICIT REAL*8 (A-H,O-Z)
789      DIMENSION GL(6),GS(18)
790      COMMON/GRID1/NX,NY,NX1,NY1,NXM1,NYM1,NL,NLM1,NFINE,NS,NSM1
791      COMMON/GRIDR/HI(22,37,3),HMS(18),HWS(18),HS(17),HM(6),HW(6),H(6),T
792      IOP
793      GS(1)=GL(1)
794      NN=1
795      DO 1 L=2,NLM1
796          DO 1 N=1,NFINE
797              NN=NN+1
798              GS(NN)=GL(L)/DFLOAT(NFINE)
799 1      CONTINUE
800      GS(NS)=GL(NL)

```

```

801     RETURN
802     END
803 C
804 C
805     SUBROUTINE UNFINE(GS, GL)
806 C
807 C Interpolates the thickness distribution from fine to normal grid
808     IMPLICIT REAL*8 (A-H,O-Z)
809     DIMENSION GL(6), GS(18)
810     COMMON/GRID1/NX, NY, NX1, NY1, NXM1, NYM1, NL, NLM1, NFINE, NS, NSM1
811     COMMON/GRIDR/HI(22,37,3), HMS(18), HWS(18), HS(17), HM(6), HW(6), H(6), T
812     IOP
813     GL(1)=GS(1)
814     NN=1
815     DO 1 L=2, NLM1
816         GL(L)=0.0D0
817     DO 1 N=1, NFINE
818         NN=NN+1
819         GL(L)=GL(L)+GS(NN)
820 1     CONTINUE
821     GL(NL)=GS(NS)
822     RETURN
823     END
824 C
825     SUBROUTINE REDIST(GAMMA, GAMMAF)
826 C
827 C Calculates the coefficients used in redistributing
828 C ice between the layers when ridging. Also the coefficients
829 C used in evaluating the ice strength are determined
830     IMPLICIT REAL*8 (A-H,O-Z)
831     DIMENSION GAMMA(18,18), GAMMAF(18), OVRLP(18)
832     COMMON/GRID1/NX, NY, NX1, NY1, NXM1, NYM1, NL, NLM1, NFINE, NS, NSM1
833     COMMON/GRIDR/HI(22,37,3), HMS(18), HWS(18), HS(17), HM(6), HW(6), H(6), T
834     IOP
835     COMMON/PHYS/CB, CF, STREN, RHOICE, RHOWAT, GRAV, COT, UA, UB, AH, BH, RHOAIR,
836     IQI, CW, DMIX, SIDER, TI, SIGMAX, PI, ARMAX, CPLF, CON1, CON2, STFN, CON, ERROR2
837     2, D1, D3, TINC, CH, SIN20, COS20, SIN25, COS25
838     DO 1 L1=1, NS
839         GAMMAF(L1)=0.0D0
840     DO 1 L2=1, NS
841         GAMMA(L1, L2)=0.0D0
842 1     CONTINUE
843     NDH=25
844     DO 5 L1=2, NSM1
845         DO 4 M=1, NDH
846             H1=HS(L1-1)+(((DFLOAT(M)-0.5D0)/DFLOAT(NDH))*HWS(L1))
847             CALL HEIGHT(H1, H2)
848             GAMMAF(L1)=GAMMAF(L1)+(CF*(H2-H1)*(H2-H1)/DFLOAT(NDH))
849             GAMMAF(L1)=GAMMAF(L1)+(CB*H1*(2.0D0*H2+H1)*(H2-H1)/(3.0D0*(H2+H1)*
850             1DFLOAT(NDH)))

```

```

851     DO 2 L2=L1, NSM1
852     OVRLP(L2)=DMIN1(H2, HS(L2))-DMIN1(H2, HS(L2-1))
853 2     CONTINUE
854     OVRLP(NS)=DMAX1(H2, HS(NSM1))-HS(NSM1)
855     OVRLP(L1)=HS(L1)-H1
856     DO 3 L2=L1, NS
857     GAMMA(L1, L2)=GAMMA(L1, L2)+(2.0D0*H1*OVRLP(L2)/(DFLOAT(NDH))*((H2*H2
858     1)-(H1*H1))))
859 3     CONTINUE
860 4     CONTINUE
861 5     CONTINUE
862     RETURN
863     END
864 C
865 C
866     SUBROUTINE HEIGHT(H1, H2)
867 C
868 C Ridge height H2 in terms of the parent ice thickness H1
869     IMPLICIT REAL*8 (A-H,O-Z)
870     COMMON/PHYS/CB, CF, STREN, RHOICE, RHOWAT, GRAV, COT, UA, UB, AH, BH, RHOAIR,
871     IQI, CW, DMIX, SIDER, TI, SIGMAX, PI, ARMAX, CPLF, CON1, CON2, STFN, CON, ERROR2
872     2, D1, D3, TINC, CH, SIN20, COS20, SIN25, COS25
873     IF(H1.GE.CH) GOTO 1
874     H2=H1*(1.0D0-AH)+DSQRT(((AH-4.0D0)*H1+BH)*AH*H1)
875     H2=DMAX1(H1, H2)
876     RETURN
877 1     H2=H1
878     RETURN
879     END
880 C
881 C
882     SUBROUTINE RIDGE(I, J, G1, G2, GAMMA, GAMMAF, PR)
883 C
884 C Initial distribution G1(L) is renormalized to G2(L)
885     IMPLICIT REAL*8 (A-H,O-Z)
886     DIMENSION GAMMA(18,18), GAMMAF(18), G1(18), G2(18), GD(18), TOTAL(18)
887     COMMON/GRID1/NX, NY, NX1, NY1, NXM1, NYM1, NL, NLM1, NFINE, NS, NSM1
888     COMMON/GRIDR/HI(22,37,3), HMS(18), HWS(18), HS(17), HM(6), HW(6), H(6), T
889     IOP
890     COMMON/PHYS/CB, CF, STREN, RHOICE, RHOWAT, GRAV, COT, UA, UB, AH, BH, RHOAIR,
891     IQI, CW, DMIX, SIDER, TI, SIGMAX, PI, ARMAX, CPLF, CON1, CON2, STFN, CON, ERROR2
892     2, D1, D3, TINC, CH, SIN20, COS20, SIN25, COS25
893     INEG=0
894 C Up to a fraction ARIDGE of the ice area is involved in ridging.
895     ARIDGE=0.15D0
896     HI(I, J, 3)=HI(I, J, 1)
897     PR=0.0D0
898 1     HMAX=0.0D0
899     GTOT=G1(1)
900     HMS(NS)=(HI(I, J, 1)+HS(NSM1))*0.5D0

```

```

901     HWS(NS)=HI(I,J,1)-HS(NSM1)
902     DO 2 L=1,NS
903     GD(L)=0.0D0
904     G2(L)=G1(L)
905 2    CONTINUE
906     TOT=0.0D0
907     DO 3 L=1,NS
908     TOT=TOT+G1(L)
909     TOTAL(L)=TOT
910 3    CONTINUE
911 C Find cumulative thickness totals
912     IF(TOT.EQ.1.0D0.OR.TOT.LT.0.1D0)RETURN
913     IF((TOT.GT.1.0D0.AND.G1(1).LT.ARIDGE).OR.TOT.GT.(1.0D0+ARIDGE))GOT
914     IO 4
915 C Add open water if initial distribution is undernormalized.
916     G2(1)=1.0D0-TOT+G2(1)
917     RETURN
918 4    DO 5 L=2,NS
919     G2(L)=0.0D0
920 5    CONTINUE
921 C Determine relative amounts of each thickness category to be ridged
922     DO 8 L=2,NS
923     IF(GTOT.GE.ARIDGE.OR.(GTOT+G1(L)).LT.ARIDGE) GOTO 7
924     HST=HS(L-1)+((ARIDGE-GTOT)*HWS(L)/G1(L))
925 C Find maximum height of new ridges formed
926     CALL HEIGHT(HST,HMAX)
927     GD(L)=((1.0D0-(GTOT/ARIDGE))*2)
928     IF(L.EQ.2) GOTO 7
929     DO 6 L1=3,L
930     GD(L1-1)=(2.0D0-((TOTAL(L1-2)+TOTAL(L1-1))/ARIDGE))*G1(L1-1)/ARIDG
931     IE
932 6    CONTINUE
933 7    GTOT=GTOT+G1(L)
934 8    CONTINUE
935 C Tentative open water loss
936     G2(1)=-(2.0D0-(G1(1)/ARIDGE))*(G1(1)/ARIDGE)
937 C Evaluate GAMMA(NS,NS)
938     HMD=H(NLM1)+((DMAX1(HST,H(NLM1))-H(NLM1))/3.0D0)
939     CALL HEIGHT(HMD,H2)
940 C Redistribution coefficient for the top layer
941     GAMMA(NS,NS)=2.0D0*HMD/(HMD+H2)
942 C Calculate net changes to each layer, G2(L)
943     DO 10 L2=2,NS
944     DO 9 L1=2,L2
945     G2(L2)=G2(L2)+GD(L1)*GAMMA(L1,L2)
946 9    CONTINUE
947     G2(L2)=G2(L2)-GD(L2)
948 10   CONTINUE
949     DEN=0.0D0
950     GNUM=GTOT-1.0D0

```

```

951     DO 11 L=1,NS
952     DEN=DEN+G2(L)
953 11   CONTINUE
954 C Update maximum ice thickness if HMAX exceeds current value
955     HI(I,J,3)=DMAX1(HMAX,HI(I,J,1))
956     DO 12 L=1,NS
957 C Modify the changes G2(L) so resulting distribution is normalized
958     G2(L)=(-(GNUM/DEN)*G2(L))+G1(L)
959 12   CONTINUE
960     DO 13 L=1,NS
961     IF(G2(L).LT.0.0D0) GOTO 14
962 13   CONTINUE
963     GOTO 19
964 C If more that ARIDGE needs to be ridged allow this and start again
965 14   ARIDGE=ARIDGE+0.05D0
966     IF(ARIDGE.LE.3.0D0)GOTO 1
967 C Debugging aid
968     WRITE(6,15)
969 15   FORMAT(1X,'NO RIDGING POSSIBLE, INVESTIGATE',/,1X,'LAST ICE THICKN
970     LESS DISTRIBUTION WAS...')
971     WRITE(6,16)G1,HI(I,J,1)
972 16   FORMAT(1X,G17.10)
973     WRITE(6,17)I,J
974 17   FORMAT(1X,'GRID POINT',2I4)
975     ARIDGE=0.15D0
976     INEG=INEG+1
977     G1(1)=0.0D0
978     G1(NS)=1.0D0
979     DO 18 L=2,NSM1
980     G1(L)=0.0D0
981 18   CONTINUE
982     IF(INEG.EQ.4)STOP
983     GOTO 1
984 C Calculate strength
985 19   GAMMAF(NS)=(CF*(H2-HMD)*(H2-HMD))
986     GAMMAF(NS)=GAMMAF(NS)+(CB*HMD*(2.0D0*H2+HMD)*(H2-HMD)/(3.0D0*(H
987     12+HMD)))
988     DO 20 L=2,NS
989     PR=PR-(GAMMAF(L)*GD(L)*GNUM/(DEN*1.0D-04))
990 20   CONTINUE
991     RETURN
992     END
993 C
994 C
995     SUBROUTINE DIST(U,V,G,GAMMA,GAMMAF,PRESS,TMIX,FND,GAIRX,GAIRY,DAY,
996     INW,PHI,TAIR,C,P,RHUM,HTSEA)
997 C
998 C Thermodynamic and Dynamic redistribution
999 C Floe size and number density are updated
1000     IMPLICIT REAL*8 (A-H,O-Z)

```

```

1001 DIMENSION G(6,22,37,3),GAMMA(18,18),GAMMAF(18),PRESS(22,37),FGROW(
1002 121),F(6),TMIX(22,37),FND(5,22,37,3),GAIRX(21,36),GAIRY(21,36),U(21
1003 2,36,3),V(21,36,3),G1(6),G2(18),G3(18),RR(22,37),PHI(21,36),TAIR(21
1004 3,36),C(52),P(52),RHUM(52),HTSEA(22,37)
1005 COMMON/GRID1/NX,NY,NX1,NY1,NXM1,NYM1,NL,NLM1,NFINE,NS,NSM1
1006 COMMON/GRIDR/HI(22,37,3),HMS(18),HWS(18),HS(17),HM(6),HW(6),H(6),T
1007 IOP
1008 COMMON/STEP/DT,DX,DY
1009 COMMON/ARRAY/GMASK(22,37),UVM(21,36)
1010 COMMON/SIGMA/ALPHR(22,37),ALPHO(22,37),EI,EII2,COTT
1011 COMMON/PHYS/CB,CF,STREN,RHOICE,RHOWAT,GRAV,COT,UA,UB,AH,BH,RHOAIR,
1012 IQI,CW,DMIX,SIDER,TI,SIGMAX,PI,ARMAX,CPLF,CON1,CON2,STFN,CON,ERROR2
1013 2,D1,D3,TINC,CH,SIN20,COS20,SIN25,COS25
1014 DO 36 J=2,NY
1015 DO 36 I=2,NX
1016 C Calculate actual area of open water produced
1017 C when ice area is lost through ridging
1018 CALL ALPHA(I,J,U,V)
1019 IF(G(NL,I,J,1).EQ.0.0D0.OR.GMASK(I,J).EQ.0.0D0)HI(I,J,1)=H(NLM1)+T
1020 IOP
1021 HM(NL)=(HI(I,J,2)+H(NLM1))*0.5D0
1022 H(NL)=HI(I,J,2)
1023 C Evaluate wind speed
1024 UG=(DSQRT(GAIRX(I-1,J-1)*GAIRX(I-1,J-1)+GAIRY(I-1,J-1)*GAIRY(I-1,J
1025 1-1))+DSQRT(GAIRX(I,J-1)*GAIRX(I,J-1)+GAIRY(I,J-1)*GAIRY(I,J-1)))+DS
1026 2QRT(GAIRX(I-1,J)*GAIRX(I-1,J)+GAIRY(I-1,J)*GAIRY(I-1,J))+DSQRT(GAI
1027 3RX(I,J)*GAIRX(I,J)+GAIRY(I,J)*GAIRY(I,J)))*0.25D0
1028 C Find average air temperature in grid cell
1029 TA=0.25D0*(TAIR(I-1,J-1)+TAIR(I,J-1)+TAIR(I-1,J)+TAIR(I,J))
1030 DO 1 L=1,NL
1031 THKNSS=H(L)
1032 C Evaluate growth rates F(L)
1033 CALL BUDGET(PHI(I,J),TA,UG,DAY,C(NW),P(NW),TMIX(I,J),THKNSS,F(L),
1034 1RHUM(NW))
1035 1 CONTINUE
1036 DO 2 L=2,NL
1037 G(L,I,J,3)=0.0D0
1038 2 CONTINUE
1039 C Open water formed when ridging
1040 G(1,I,J,3)=DT*ALPHO(I,J)
1041 HW(NL)=HI(I,J,2)-H(NLM1)
1042 C Melt and growth of middle levels
1043 LI=0
1044 IF(F(1).GE.0.0D0)L1=1
1045 DO 3 L=1,NLM1
1046 MELT=0
1047 IF(F(L).LT.0.0D0)MELT=1
1048 IF(L.EQ.NLM1.AND.MELT.EQ.1) GOTO 4
1049 DG=DT*G(L,MELT,I,J,2)*F(L)/HW(L+MELT+L1)
1050 G(L+1,I,J,3)=G(L+1,I,J,3)+DG

```

```

1051 G(L,I,J,3)=G(L,I,J,3)-DG
1052 LI=0
1053 3 CONTINUE
1054 GOTO 5
1055 C Melt of possibly thin top level
1056 4 DG=DMIN1(G(NL,I,J,2),-DT*G(NL,I,J,2)*F(NL)/HW(NL))
1057 G(NL,I,J,3)=G(NL,I,J,3)-DG
1058 G(NLM1,I,J,3)=G(NLM1,I,J,3)+DG
1059 C Adjust HI due to possible growth from NLM1 level
1060 5 IF(G(NLM1,I,J,2).GT.0.0D0.AND.G(NL,I,J,2).LE.0.0D0.AND.F(NLM1).GT.
1061 10.0D0)HI(I,J,1)=H(NLM1)+DMAX1(TOP,DT*F(NLM1))
1062 IF(F(NL).LT.0.0D0)GOTO 6
1063 C Growth of top layer
1064 IF(G(NL,I,J,2).GT.0.0D0)HI(I,J,1)=HI(I,J,1)+(DT*F(NL))
1065 GOTO 7
1066 C Melt of top layer
1067 6 HI(I,J,1)=DMAX1(HI(I,J,1)+(DT*F(NL)),H(NLM1)+TOP)
1068 7 CONTINUE
1069 C Thermodynamic changes to the floe number density
1070 DO 8 L=1,NLM1
1071 FND(L,I,J,3)=0.0D0
1072 8 CONTINUE
1073 DO 9 L=2,NLM1
1074 MELT=-1
1075 IF(F(L).LT.0.0D0)MELT=0
1076 IF(L.EQ.NLM1.AND.MELT.EQ.0)GOTO 10
1077 DFND=DT*FND(L,MELT,I,J,2)*F(L)/HW(L+MELT+1)
1078 FND(L,I,J,3)=FND(L,I,J,3)+DFND
1079 FND(L-1,I,J,3)=FND(L-1,I,J,3)-DFND
1080 9 CONTINUE
1081 GOTO 11
1082 10 DFND=DMIN1(FND(NLM1,I,J,2),-DT*FND(NLM1,I,J,2)*F(NL)/HW(NL))
1083 FND(NLM1,I,J,3)=FND(NLM1,I,J,3)-DFND
1084 FND(NLM1-1,I,J,3)=FND(NLM1-1,I,J,3)+DFND
1085 11 CONTINUE
1086 C Number density increases in level 2 only if level 3 floes melt
1087 FND(1,I,J,3)=FND(1,I,J,3)+DT*DMIN1(F(1),0.0D0)*FND(1,I,J,2)/HW(2)
1088 DO 12 L=1,NLM1
1089 FND(L,I,J,1)=FND(L,I,J,1)+FND(L,I,J,3)
1090 12 CONTINUE
1091 DO 13 L=1,NL
1092 G(L,I,J,1)=G(L,I,J,1)+G(L,I,J,3)
1093 13 CONTINUE
1094 C calculate mixed layer warming
1095 C Eliminate negative ice areas (Resulting from Numerical
1096 C errors associated with advection). Store amount as a
1097 C heat input.
1098 GNEG=0.0D0
1099 DO 14 L=1,NL
1100 IF(G(L,I,J,1).LE.1.0D-18.AND.G(L,I,J,1).GT.0.0D0)G(L,I,J,1)=0.0D0

```

```

1101 GNORM=DMAX1(G(L,I,J,1),0.0D0)
1102 GNEG=GNEG+((GNORM-G(L,I,J,1))*HM(L))
1103 G(L,I,J,1)=GNORM
1104 G1(L)=G(L,I,J,1)
1105 14 CONTINUE
1106 C Perform ridging
1107 CALL FINE(G1,G2)
1108 CALL RIDGE(I,J,G2,G3,GAMMA,GAMMAF,PR)
1109 CALL UNFINE(G3,G1)
1110 C Update G due to ridging
1111 DO 15 L=1,NL
1112 G(L,I,J,1)=G1(L)*GMASK(I,J)
1113 15 CONTINUE
1114 C Impose maximum possible floe size
1115 DO 16 L=2,NL
1116 FND(L-1,I,J,1)=DMAX1(G(L,I,J,1)/ARMAX,FND(L-1,I,J,1))*GMASK(I,J)
1117 IF(G(L,I,J,1).LE.0.0D0)FND(L-1,I,J,1)=0.0D0
1118 16 CONTINUE
1119 C Must use total floe number density here
1120 C Floes increase in size due to coalescing
1121 TOTFND=0.0D0
1122 DO 17 L=2,NL
1123 TOTFND=TOTFND+FND(L-1,I,J,1)
1124 17 CONTINUE
1125 C If compactness is high, treat cover as continuous
1126 IF(G(1,I,J,1).LT.1.0D-12)GOTO 18
1127 A=1.0D0-G(1,I,J,1)
1128 CL=-((2.0D0*A*ALPHR(I,J)*DT)/((1.0D0-(1.0D0-DSQRT(2.0D0/3.0D0))*A*
1129 1A)*(1.0D0-(1.0D0-DSQRT(2.0D0/3.0D0))*A*A)-(2.0D0*A/3.0D0)+1.0D-12)
1130 2)
1131 C If -CL is large, cover becomes continuous
1132 IF(CL.LT.-5.0D+01)GOTO 18
1133 C Integration of floe number density
1134 FND1=TOTFND*DEXP(CL)
1135 GOTO 19
1136 C Treat ice cover as continuous
1137 18 FND1=(1.0D0-G(1,I,J,1))/ARMAX
1138 19 FND1=DMAX1(FND1,(1.0D0-G(1,I,J,1))/ARMAX)
1139 DO 20 L=2,NL
1140 FND(L-1,I,J,1)=(FND(L-1,I,J,1)/(TOTFND+1.0D-18))*FND1
1141 20 CONTINUE
1142 HI(I,J,1)=HI(I,J,3)
1143 AVG=0.0D0
1144 HM(NL)=(HI(I,J,1)+H(NLM1))*0.5D0
1145 H(NL)=HI(I,J,1)
1146 C Adjust thickness distribution due to lateral melting
1147 HW(NL)=HI(I,J,1)-H(NLM1)
1148 VOLUM=0.0D0
1149 DO 21 L=2,NL
1150 VOLUM=VOLUM+G(L,I,J,1)*HM(L)

```

```

1151 21 CONTINUE
1152 SIDES=0.0D0
1153 DO 22 L=2,NL
1154 C Calculate total floe perimeter
1155 SIDES=SIDES+2.0D0*HM(L)*SIDER*DSQRT(PI*FND(L-1,I,J,1)*G(L,I,J,1))*
1156 1RHOICE/RHOWAT
1157 22 CONTINUE
1158 C VMELT is volume to be melted
1159 VMELT=GNEG-DMIN1(F(1),0.0D0)*G(1,I,J,1)*DT-HTSEA(I,J)*DT
1160 IF(VMELT.LE.0.0D0)GOTO 30
1161 FBDTO=VMELT/(1.0D0-G(1,I,J,1)+1.0D-18)
1162 NUM=NL
1163 CALL AREA(I,J,G,0.0D0,FBDTO,G1(1),NUM)
1164 DO 23 L=1,NLM1
1165 X1=FBDTO+H(L)
1166 X2=FBDTO+H(L+1)
1167 CALL AREA(I,J,G,X1,X2,G1(L+1),NUM)
1168 23 CONTINUE
1169 C VDIFF0 is vertical volume melt if SIDES=0
1170 H1=DMAX1(HI(I,J,1)-FBDTO,H(NLM1)+TOP)
1171 VDIFF0=0.0D0
1172 DO 24 L=2,NLM1
1173 VDIFF0=VDIFF0+(G(L,I,J,1)-G1(L))*HM(L)
1174 24 CONTINUE
1175 VDIFF0=VDIFF0+G(NL,I,J,1)*0.5D0*(H(NL)+H(NLM1))-G1(NL)*0.5D0*(H(NL
1176 1M1)+H1)
1177 C FBDT is vertical melt
1178 FBDT=VMELT/(SIDES+1.0D0-G(1,I,J,1)+1.0D-18)
1179 C Melt all ice by amount FBDT
1180 NUM=NL
1181 CALL AREA(I,J,G,0.0D0,FBDT,G(1,I,J,3),NUM)
1182 DO 25 L=1,NLM1
1183 X1=FBDT+H(L)
1184 X2=FBDT+H(L+1)
1185 CALL AREA(I,J,G,X1,X2,G(L+1,I,J,3),NUM)
1186 25 CONTINUE
1187 C VDIFF is vertical melt with SIDES
1188 VDIFF=0.0D0
1189 DO 26 L=2,NLM1
1190 VDIFF=VDIFF+(G(L,I,J,1)-G(L,I,J,3))*HM(L)
1191 26 CONTINUE
1192 VDIFF=VDIFF+G(NL,I,J,1)*0.5D0*(H(NL)+H(NLM1))-G(NL,I,J,3)*0.5D0*(H
1193 1(NLM1)+HI(I,J,1))
1194 NUM=NLM1
1195 DO 27 L=2,NL
1196 X1=FBDT+H(L-1)
1197 X2=FBDT+H(L)
1198 FND(L-1,I,J,3)=0.0D0
1199 IF(G(L,I,J,3).GT.0.0D0)CALL AREA(I,J,FND,X1,X2,FND(L-1,I,J,3),NUM)
1200 27 CONTINUE

```

```

1201      HI(I,J,1)=DMAX1(HI(I,J,1)-FBDT,H(NLM1)+TOP)
1202 C VMELT is volume to be melted by heat absorbed by leads
1203 C VDIFF is Actual volume melted vertically
1204 C Update G(1)
1205      DO 28 L=1,NL
1206      G(L,I,J,1)=G(L,I,J,3)
1207 28      CONTINUE
1208      DO 29 L=1,NLM1
1209      FND(L,I,J,1)=FND(L,I,J,3)
1210 29      CONTINUE
1211 C Raise temperature by amount not used to melt ice
1212      H(NL)=HI(I,J,1)
1213      HM(NL)=0.5D0*(H(NLM1)+H(NL))
1214      HW(NL)=H(NL)-H(NLM1)
1215 30      CONTINUE
1216      DO 31 L=2,NL
1217      AVG=AVG+HM(L)*G(L,I,J,1)
1218 31      CONTINUE
1219 C TUP is residual temperature increase to mixed layer after
1220 C performing vertical melt. If all the ice is lost, a net
1221 C temperature increase to the mixed layer results.
1222      IF(AVG.GT.0.0D0)TUP=TI*(VDIFF0-VDIFF)
1223      IF(AVG.LE.0.0D0)TUP=TI*(VMELT-VOLUM)
1224      TMIX(I,J)=TMIX(I,J)+TUP
1225      CMIX=DMIN1((TMIX(I,J)-2.712D+02)/((AVG*TI)+1.0D-18),1.0D0)
1226 C Calculate new amount of open water from lateral melt
1227      G(1,I,J,1)=G(1,I,J,1)+(CMIX*(1.0D0-G(1,I,J,1)))
1228 C Do lateral melt
1229      DO 32 L=2,NL
1230      G(L,I,J,3)=G(L,I,J,1)*(1.0D0-CMIX)
1231 C Adjust mixed layer temperature from lateral melting
1232      TMIX(I,J)=TMIX(I,J)+((G(L,I,J,3)-G(L,I,J,1))*HM(L)*TI)
1233 C Update G(1)
1234      G(L,I,J,1)=G(L,I,J,3)
1235 32      CONTINUE
1236 C Include next line since rounding errors may
1237 C put TMIX below freezing
1238      TMIX(I,J)=DMAX1(2.712D+02,TMIX(I,J))
1239 C Cracking of floes in a wind U10
1240      U10=UG/1.5D0
1241      HM(NL)=0.5D0*(H(NLM1)+HI(I,J,1))
1242      DO 35 L=2,NL
1243      RH=DSQRT(G(L,I,J,1)/(PI*FND(L-1,I,J,1)+1.0D-18))
1244 C Characteristic plate length CPL
1245      CPL=CPLF*(HM(L)**0.75D0)
1246 C Is floe long or short
1247      IF(RH.LE.CPL) GOTO 33
1248 C Find the maximum bending moment in long floe
1249      A=1.0D0-G(1,I,J,1)
1250      SIG=CON2*CPL*CPL*CPL*U10*U10/((HM(L)**3.5D0)*A+1.0D-18)

```

```

1251 C Will the floe break
1252      IF(SIG.LT.SIGMAX) GOTO 34
1253 C If so then pieces have radius RH
1254      RH=CPL*PI/8.0D0
1255 C Short floe formulae
1256 33      RMAX=CON1*(HM(L)**3.5D0)*A/((CPL*CPL*U10*U10+1.0D-18)
1257      RH=DMIN1(RH,RMAX)
1258 34      FND(L-1,I,J,1)=G(L,I,J,1)/(PI*RH*RH+1.0D-18)
1259 35      CONTINUE
1260 36      CONTINUE
1261 C Output information about floe sizes
1262 C      WRITE(6,997)
1263 C997      FORMAT(1X,'FLOE RADII')
1264 C      DO 74 L=2,NL
1265 C      WRITE(6,998)L
1266 C998      FORMAT(1X,'LEVEL NUMBER ',I4)
1267 C      DO 73 J=2,NY
1268 C      DO 73 I=2,NX
1269 C      RR(I,J)=DSQRT(G(L,I,J,1)/(PI*FND(L-1,I,J,1)+1.0D-18))
1270 C73      CONTINUE
1271 C      WRITE(6,996)((RR(I,J),I=1,NX,5),J=1,NY,5)
1272 C996      FORMAT(1X,5G17.10)
1273 C74      CONTINUE
1274      RETURN
1275      END
1276 C
1277 C
1278      SUBROUTINE RELAX(U,V,ETA,ZETA,DRAGS,DRAGA,AMASS,FORCEX,FORCEY,ERRO
1279      1R,THETA,UC,VC,IFIRST,GAIRX,GAIRY,EKMANX,EKMANY)
1280 C
1281      IMPLICIT REAL*8 (A-H,O-Z)
1282      DIMENSION U(21,36,3),V(21,36,3),ETA(22,37),ZETA(22,37),DRAGS(21,36
1283      1),DRAGA(21,36),GAIRX(21,36),GAIRY(21,36),FORCEX(21,36),FORCEY(21,3
1284      26),FXETA(4),FXZETA(4),FYETA(4),FYZETA(4),UERR(21,36),VERR(21,36),C
1285      3OEF(21,36),EKMANX(21,36),EKMANY(21,36),AMASS(21,36),FXM(21,36),FYM
1286      4(21,36),UC(21,36),VC(21,36),FXE(4,21,36),FYE(4,21,36),FXZ(4,21,36)
1287      5,FYZ(4,21,36),WFA(21,36,2)
1288      COMMON/GRID1/NX,NY,NX1,NY1,NXM1,NYM1,NL,NLM1,NFINE,NS,NSM1
1289      COMMON/DINV/DELIN2
1290      COMMON/STEP/DT,DX,DY
1291      COMMON/ARRAY/GMASK(22,37),UVM(21,36)
1292      ICOUNT=0
1293 C Initialize relaxation parameter
1294      DO 1 KXY=1,2
1295      DO 1 J=1,NY
1296      DO 1 I=1,NX
1297      WFA(I,J,KXY)=1.48D0
1298      IF(AMASS(I,J).LT.1.0D-08)WFA(I,J,KXY)=0.0D0
1299 1      CONTINUE
1300      DELIN=1.0D0/DX

```

```

1301      DELIN2=0.5D0/(DX*DX)
1302 C First set U(2)=U(1)
1303      DO 2 J=1,NY
1304      DO 2 I=1,NX
1305 C Make sure bdry pts are equal to zero
1306      U(I,J,2)=U(I,J,1)
1307      V(I,J,2)=V(I,J,1)
1308      U(I,J,1)=U(I,J,3)*UVM(I,J)
1309      V(I,J,1)=V(I,J,3)*UVM(I,J)
1310 C Use Zubov's law for velocity solution where there is no ice
1311      IF(AMASS(I,J).LT.1.0D-08)U(I,J,1)=0.011D0*(GAIRX(I,J)*0.95106D0+GA
1312      IIRY(I,J)*0.30902D0)*UVM(I,J)
1313      IF(AMASS(I,J).LT.1.0D-08)V(I,J,1)=0.011D0*(GAIRY(I,J)*0.95106D0-GA
1314      IIRX(I,J)*0.30902D0)*UVM(I,J)
1315      UERR(I,J)=1.0D+12
1316      VERR(I,J)=1.0D+12
1317      IF(IFIRST.EQ.1)AMASS(I,J)=0.0D0
1318 C Set up coeffs of diagonal components
1319      COEF(I,J)=AMASS(I,J)/DT+2.0D0*THETA*(0.5D0*DRAGS(I,J)+2.0D0*((ETA(
1320      I,I,J)+ETA(I+1,J)+ETA(I,J+1)+ETA(I+1,J+1))+.5D0*(ZETA(I,J)+ZETA(I+1,
1321      2J)+ZETA(I,J+1)+ZETA(I+1,J+1)))/(4.0D0*(DX*DX)))+1.0D-08
1322 2      CONTINUE
1323 C Calculate all functions of previous U and V values
1324      TTHETA=2.0D0*(1.0D0-THETA)
1325      DO 3 J=2,NYMI
1326      DO 3 I=2,NXMI
1327      IF(WFA(I,J,1).EQ.0.0D0)GOTO 3
1328      CALL FDIFF1(U,V,ETA,FXETA,I,J)
1329      CALL FDIFF1(U,V,ZETA,FXZETA,I,J)
1330      CALL FDIFF1(V,U,ETA,FYETA,I,J)
1331      CALL FDIFF1(V,U,ZETA,FYZETA,I,J)
1332      FXO=0.5D0*TTHETA*(FXETA(1)+FXZETA(1)+FXETA(2)+FXETA(3)+FXZETA(4)-F
1333      IXETA(4))
1334      FX1=(AMASS(I,J)/DT-TTHETA*0.5D0*DRAGS(I,J))*U(I,J,2)
1335      FX2=TTHETA*0.5D0*DRAGA(I,J)*V(I,J,2)
1336      FYO=0.5D0*TTHETA*(FYETA(1)+FYETA(2)+FYZETA(2)+FYZETA(3)-FYETA(3)+F
1337      IYETA(4))
1338      FY1=(AMASS(I,J)/DT-TTHETA*0.5D0*DRAGS(I,J))*V(I,J,2)
1339      FY2=-TTHETA*0.5D0*DRAGA(I,J)*U(I,J,2)
1340      FXC=AMASS(I,J)*0.5D0*TTHETA*(UC(I,J)*(U(I+1,J,2)-U(I-1,J,2))+VC(I,
1341      1J)*(U(I,J+1,2)-U(I,J-1,2)))/(2.0D0*DX)
1342      FXM(I,J)=FXO+FX1+FX2+FORCEX(I,J)+FXC
1343      FYC=AMASS(I,J)*0.5D0*TTHETA*(UC(I,J)*(V(I+1,J,2)-V(I-1,J,2))+VC(I,
1344      1J)*(V(I,J+1,2)-V(I,J-1,2)))/(2.0D0*DX)
1345      FYM(I,J)=FYO+FY1+FY2+FORCEY(I,J)+FYC
1346 3      CONTINUE
1347 C Set u(3)=u(1)
1348 4      CONTINUE
1349      DO 5 J=1,NY
1350      DO 5 I=1,NX

```

```

1351      U(I,J,3)=U(I,J,1)
1352      V(I,J,3)=V(I,J,1)
1353 5      CONTINUE
1354 C Begin sweep
1355      CALL FDIFF2(U,V,ETA,FXE,WFA)
1356      CALL FDIFF2(U,V,ZETA,FXZ,WFA)
1357      CALL FDIFF2(V,U,ETA,FYE,WFA)
1358      CALL FDIFF2(V,U,ZETA,FYZ,WFA)
1359      DO 6 J=2,NYMI
1360      DO 6 I=2,NXMI
1361      IF(WFA(I,J,1).EQ.0.0D0)GOTO 6
1362      FXETA(1)=FXE(1,I,J)+DELIN2*(U(I-1,J,1)*(ETA(I,J+1)+ETA(I,J)))
1363      FXETA(2)=FXE(2,I,J)+DELIN2*(U(I,J-1,1)*(ETA(I,J)+ETA(I+1,J)))
1364      FXETA(3)=FXE(3,I,J)+0.5D0*DELIN2*(V(I-1,J-1,1)*ETA(I,J)+V(I,J-1,1)
1365      1*(-ETA(I,J)+ETA(I+1,J))-V(I+1,J-1,1)*ETA(I+1,J)+V(I-1,J,1)*(-ETA(I
1366      2,J+1)+ETA(I,J))-V(I-1,J+1,1)*ETA(I,J+1))
1367      FXETA(4)=FXE(4,I,J)+DELIN2*0.5D0*(V(I-1,J-1,1)*ETA(I,J)+V(I,J-1,1)
1368      1*(-ETA(I+1,J)+ETA(I,J))-V(I+1,J-1,1)*ETA(I+1,J)+V(I-1,J,1)*ETA(I,
1369      2J+1)-ETA(I,J))-V(I-1,J+1,1)*ETA(I,J+1))
1370      FYETA(1)=FYE(1,I,J)+DELIN2*(V(I-1,J,1)*(ETA(I,J+1)+ETA(I,J)))
1371      FYETA(2)=FYE(2,I,J)+DELIN2*(V(I,J-1,1)*(ETA(I,J)+ETA(I+1,J)))
1372      FYETA(3)=FYE(3,I,J)+0.5D0*DELIN2*(U(I-1,J-1,1)*ETA(I,J)+U(I,J-1,1)
1373      1*(-ETA(I,J)+ETA(I+1,J))-U(I+1,J-1,1)*ETA(I+1,J)+U(I-1,J,1)*(-ETA(I
1374      2,J+1)+ETA(I,J))-U(I-1,J+1,1)*ETA(I,J+1))
1375      FYETA(4)=FYE(4,I,J)+DELIN2*0.5D0*(U(I-1,J-1,1)*ETA(I,J)+U(I,J-1,1)
1376      1*(-ETA(I+1,J)+ETA(I,J))-U(I+1,J-1,1)*ETA(I+1,J)+U(I-1,J,1)*ETA(I,
1377      2J+1)-ETA(I,J))-U(I-1,J+1,1)*ETA(I,J+1))
1378      FXZETA(1)=FXZ(1,I,J)+DELIN2*(U(I-1,J,1)*(ZETA(I,J+1)+ZETA(I,J)))
1379      FXZETA(4)=FXZ(4,I,J)+DELIN2*0.5D0*(V(I-1,J-1,1)*ZETA(I,J)+V(I,J-1,
1380      11)*(-ZETA(I+1,J)+ZETA(I,J))-V(I+1,J-1,1)*ZETA(I+1,J)+V(I-1,J,1)*(Z
1381      2ETA(I,J+1)-ZETA(I,J))-V(I-1,J+1,1)*ZETA(I,J+1))
1382      FYZETA(2)=FYZ(2,I,J)+DELIN2*(V(I,J-1,1)*(ZETA(I,J)+ZETA(I+1,J)))
1383      FYZETA(3)=FYZ(3,I,J)+0.5D0*DELIN2*(U(I-1,J-1,1)*ZETA(I,J)+U(I,J-1,
1384      11)*(-ZETA(I,J)+ZETA(I+1,J))-U(I+1,J-1,1)*ZETA(I+1,J)+U(I-1,J,1)*(-
1385      2ZETA(I,J+1)+ZETA(I,J))-U(I-1,J+1,1)*ZETA(I,J+1))
1386      FX3=THETA*(FXETA(1)+FXZETA(1)+FXETA(2)+FXETA(3)+FXZETA(4)-FXETA(4)
1387      1)
1388      FXCP=AMASS(I,J)*THETA*(UC(I,J)*(U(I+1,J,1)-U(I-1,J,1))+VC(I,J)*(U(
1389      1I,J+1,1)-U(I,J-1,1)))*0.5D0*DELIN
1390      FX3=FX3-FXCP
1391      FY3=THETA*(FYETA(1)+FYETA(2)+FYZETA(2)+FYZETA(3)-FYETA(3)+FYETA(4)
1392      1)
1393      FYCP=AMASS(I,J)*THETA*(UC(I,J)*(V(I+1,J,1)-V(I-1,J,1))+VC(I,J)*(V(
1394      1I,J+1,1)-V(I,J-1,1)))*0.5D0*DELIN
1395      FY3=FY3-FYCP
1396      FL11=THETA*DRAGA(I,J)/COEF(I,J)
1397      FL1=(FXM(I,J)+FX3)/COEF(I,J)
1398      F22=(FYM(I,J)+FY3)/COEF(I,J)
1399      FL1IS=1.0D0+(FL11*FL11)
1400      FL1ISI=1.0D0/FL1IS

```

```

1401 VICOR=((F11+FL11*F22)*FL11SI)*UVM(I,J)
1402 VICOR=((F22-FL11*F11)*FL11SI)*UVM(I,J)
1403 U(I,J,1)=U(I,J,1)+WFA(I,J,1)*(VICOR-U(I,J,1))
1404 V(I,J,1)=V(I,J,1)+WFA(I,J,2)*(VICOR-V(I,J,1))
1405 6 CONTINUE
1406 ICOUNT=ICOUNT+1
1407 IF(ICOUNT.GT.200) GO TO 9
1408 SI=0.0D0
1409 DO 7 J=1,NY
1410 DO 7 I=1,NX
1411 IF(WFA(I,J,1).EQ.0.0D0)GOTO 7
1412 UR=U(I,J,1)-U(I,J,3)
1413 VR=V(I,J,1)-V(I,J,3)
1414 DW=0.01D0
1415 IF(DABS(UR).GT.DABS(UERR(I,J)))DW=-0.02D0
1416 WFA(I,J,1)=DMIN1(1.5D0,DMAX1(WFA(I,J,1)+DW,1.0D0))
1417 DW=0.01D0
1418 IF(DABS(VR).GT.DABS(VERR(I,J)))DW=-0.02D0
1419 WFA(I,J,2)=DMIN1(1.5D0,DMAX1(WFA(I,J,2)+DW,1.0D0))
1420 SI=DMAX1(SI,DABS(UR))
1421 SI=DMAX1(SI,DABS(VR))
1422 UERR(I,J)=UR
1423 VERR(I,J)=VR
1424 7 CONTINUE
1425 IF(SI.LT.ERROR)GOTO 11
1426 IF(ICOUNT.LT.70)GOTO 4
1427 DO 8 KXY=1,2
1428 DO 8 J=1,NY
1429 DO 8 I=1,NX
1430 WFA(I,J,KXY)=DMIN1(1.0D0,WFA(I,J,KXY))
1431 8 CONTINUE
1432 GO TO 4
1433 9 CONTINUE
1434 WRITE(6,10)
1435 10 FORMAT(IX,'NO CONVERGENCE AFTER 200 ITERATIONS')
1436 C Now end
1437 11 CONTINUE
1438 WRITE(6,12)ICOUNT,SI
1439 12 FORMAT(6X,'RELAX CALLED: NO. OF ITERATIONS ',I4,5X,'MAX ERROR',G12
1440 1.5)
1441 RETURN
1442 END
1443 C
1444 C
1445 SUBROUTINE FDIFF2(U,V,ETA,FXE,WFA)
1446 C
1447 C Subroutine for use by RELAX
1448 IMPLICIT REAL*8 (A-H,O-Z)
1449 DIMENSION U(21,36,3),V(21,36,3),ETA(22,37),FXE(4,21,36),WFA(21,36,
1450 12)

```

```

1451 COMMON/GRID1/NX,NY,NX1,NY1,NXM1,NYM1,NL,NLM1,NFINE,NS,NSM1
1452 COMMON/GRIDR/HI(22,37,3),HMS(18),HWS(18),HS(17),HM(6),HW(6),H(6),T
1453 IOP
1454 COMMON/DINV/DELIN2
1455 DO 1 J=2,NYM1
1456 DO 1 I=2,NXM1
1457 IF(WFA(I,J,1).EQ.0.0D0)GOTO 1
1458 FXE(1,I,J)=DELIN2*(U(I+1,J,1)*(ETA(I+1,J+1)+ETA(I+1,J)))
1459 FXE(2,I,J)=DELIN2*(U(I,J+1,1)*(ETA(I+1,J+1)+ETA(I,J+1)))
1460 FXE(3,I,J)=DELIN2*(V(I,J,1)*(-ETA(I,J)-ETA(I+1,J+1)+ETA(I+1,J)+ETA
1461 1(I,J+1))+V(I+1,J,1)*(-ETA(I+1,J)+ETA(I+1,J+1))+V(I,J+1,1)*(-ETA(I+
1462 21,J+1)+ETA(I,J+1))+V(I+1,J+1,1)*ETA(I+1,J+1))*0.5D0
1463 FXE(4,I,J)=DELIN2*(V(I,J,1)*(ETA(I,J+1)+ETA(I+1,J)-ETA(I,J)-ETA(I+
1464 11,J+1))+V(I+1,J,1)*(ETA(I+1,J)-ETA(I+1,J+1))+V(I,J+1,1)*(ETA(I+1,J
1465 2+1)-ETA(I,J+1))+V(I+1,J+1,1)*ETA(I+1,J+1))*0.5D0
1466 1 CONTINUE
1467 RETURN
1468 END
1469 C
1470 C
1471 SUBROUTINE FDIFF1(U,V,ETA,FXETA,I,J)
1472 C
1473 C Subroutine for use by RELAX
1474 IMPLICIT REAL*8 (A-H,O-Z)
1475 DIMENSION U(21,36,3),V(21,36,3),ETA(22,37),FXETA(4)
1476 COMMON/GRID1/NX,NY,NX1,NY1,NXM1,NYM1,NL,NLM1,NFINE,NS,NSM1
1477 COMMON/GRIDR/HI(22,37,3),HMS(18),HWS(18),HS(17),HM(6),HW(6),H(6),T
1478 IOP
1479 COMMON/DINV/DELIN2
1480 FXETA(1)=DELIN2*(U(I+1,J,2)*(ETA(I+1,J+1)+ETA(I+1,J))-U(I,J,2)*(ET
1481 1A(I+1,J+1)+ETA(I,J)+ETA(I+1,J)+ETA(I,J+1))+U(I-1,J,2)*(ETA(I,J+1)+
1482 2ETA(I,J)))
1483 FXETA(2)=DELIN2*(U(I,J+1,2)*(ETA(I+1,J+1)+ETA(I,J+1))-U(I,J,2)*(ET
1484 1A(I+1,J+1)+ETA(I,J)+ETA(I+1,J)+ETA(I,J+1))+U(I,J-1,2)*(ETA(I,J)+ET
1485 2A(I+1,J)))
1486 FXETA(3)=DELIN2*(V(I-1,J-1,2)*ETA(I,J)+V(I,J-1,2)*(-ETA(I,J)+ETA(I
1487 1+1,J))-V(I+1,J-1,2)*ETA(I+1,J)+V(I-1,J,2)*(-ETA(I,J+1)+ETA(I,J))+V
1488 2(I,J,2)*(-ETA(I,J)-ETA(I+1,J+1)+ETA(I+1,J)+ETA(I,J+1)))
1489 FXETA(3)=FXETA(3)+DELIN2*(V(I+1,J,2)*(-ETA(I+1,J)+ETA(I+1,J+1))-V(
1490 1I-1,J+1,2)*ETA(I,J+1)+V(I,J+1,2)*(-ETA(I+1,J+1)+ETA(I,J+1))+V(I+1,
1491 2J+1,2)*ETA(I+1,J+1))
1492 FXETA(4)=DELIN2*(V(I-1,J-1,2)*ETA(I,J)+V(I,J-1,2)*(-ETA(I+1,J)+ETA
1493 1(I,J))-V(I+1,J-1,2)*ETA(I+1,J)+V(I-1,J,2)*(ETA(I,J+1)-ETA(I,J))+V(
1494 2I,J,2)*(ETA(I,J+1)+ETA(I+1,J)-ETA(I,J)-ETA(I+1,J+1)))
1495 FXETA(4)=FXETA(4)+DELIN2*(V(I+1,J,2)*(ETA(I+1,J)-ETA(I+1,J+1))-V(I
1496 1-1,J+1,2)*ETA(I,J+1)+V(I,J+1,2)*(ETA(I+1,J+1)-ETA(I,J+1))+V(I+1,J+
1497 21,2)*ETA(I+1,J+1))
1498 FXETA(3)=FXETA(3)*0.5D0
1499 FXETA(4)=FXETA(4)*0.5D0
1500 RETURN

```

```

1501      END
1502 C
1503 C
1504      SUBROUTINE VOLICE(G,VOL)
1505 C
1506 C calculates total volume of ice
1507      IMPLICIT REAL*8 (A-H,O-Z)
1508      DIMENSION G(6,22,37,3)
1509      COMMON/GRIDI/NX,NY,NX1,NY1,NXM1,NYM1,NL,NLM1,NFINE,NS,NSM1
1510      COMMON/GRIDR/HI(22,37,3),HMS(18),HWS(18),HS(17),HM(6),HW(6),H(6),T
1511      IOP
1512      VOL=0.0D0
1513      DO 2 J=1,NY1
1514      DO 2 I=1,NX1
1515      DO 1 L=2,NLM1
1516      VOL=VOL+(G(L,I,J,1)*HM(L))
1517 1      CONTINUE
1518      VOL=VOL+(G(NL,I,J,1)*(H(NLM1)+HI(I,J,1))*0.5D0)
1519 2      CONTINUE
1520      RETURN
1521      END
1522 C
1523 C
1524      SUBROUTINE AREA(I,J,G,X1,X2,Y,NUM)
1525 C
1526 C Finds ice area between any two thickness values
1527      IMPLICIT REAL*8 (A-H,O-Z)
1528      DIMENSION G(NUM,22,37,3)
1529      COMMON/GRIDI/NX,NY,NX1,NY1,NXM1,NYM1,NL,NLM1,NFINE,NS,NSM1
1530      COMMON/GRIDR/HI(22,37,3),HMS(18),HWS(18),HS(17),HM(6),HW(6),H(6),T
1531      IOP
1532      IFND=NUM-NLM1
1533      Y=0.0D0
1534      IF(X1.GE.X2)RETURN
1535      L1=0
1536      L2=0
1537      DO 1 L=1,NL
1538      IF(X1.GT.H(L))L1=L
1539      IF(X2.GT.H(L))L2=L
1540 1      CONTINUE
1541      IF(L1.EQ.NL.OR.L2.EQ.0)RETURN
1542      IF(L1.EQ.L2)GOTO 3
1543      Y=(H(L1+1)-X1)*G(L1+IFND,I,J,1)/HW(L1+1)
1544      IF(L1.EQ.0.AND.IFND.EQ.1)Y=G(1,I,J,1)
1545      IF(L2.NE.NL)Y=Y+((X2-H(L2))*G(L2+IFND,I,J,1)/HW(L2+1))
1546      IF((L2-L1).LE.1)RETURN
1547      L1P2=L1+2
1548      DO 2 LL=L1P2,L2
1549      Y=Y+G(LL-1+IFND,I,J,1)
1550 2      CONTINUE

```

```

1551      RETURN
1552 3      Y=(X2-X1)*G(L1+IFND,I,J,1)/HW(L1+1)
1553      RETURN
1554      END
1555 C
1556 C
1557      SUBROUTINE FORM(U,V,ETA,ZETA,DRAGS,DRAGA,GAIRX,GAIRY,GWATX,GWATY,F
1558      IORCEX,FORCEY,G,AMASS,PRESS,PHI,EKMANX,EKMANY)
1559 C
1560 C Program forms basic input parameters for relaxation
1561      IMPLICIT REAL*8 (A-H,O-Z)
1562      DIMENSION U(21,36,3),V(21,36,3),ETA(22,37),ZETA(22,37),DRAGS(21,36
1563      1),DRAGA(21,36),GAIRX(21,36),GAIRY(21,36),GWATX(21,36),GWATY(21,36)
1564      2,G(6,22,37,3),FORCEX(21,36),FORCEY(21,36),AMASS(21,36),PRESS(22,37
1565      3),PHI(21,36),EKMANX(21,36),EKMANY(21,36)
1566      COMMON/EE/ECCEN
1567      COMMON/GRIDI/NX,NY,NX1,NY1,NXM1,NYM1,NL,NLM1,NFINE,NS,NSM1
1568      COMMON/GRIDR/HI(22,37,3),HMS(18),HWS(18),HS(17),HM(6),HW(6),H(6),T
1569      IOP
1570      COMMON/STEP/DT,DX,DY
1571      COMMON/ARRAY/GMASK(22,37),UVM(21,36)
1572      COMMON/OUTFLO/OUT(22,37)
1573      COMMON/PHYS/CB,CF,STREN,RHOICE,RHOWAT,GRAV,COT,UA,UB,AH,BH,RHOAIR,
1574      IQI,CW,DMIX,SIDER,TI,SIGMAX,PI,ARMAX,CPLF,CON1,CON2,STFN,CON,ERROR2
1575      2,D1,D3,TINC,CH,SIN20,COS20,SIN25,COS25
1576 C First set up basic constants
1577 C Set LENS=1 if SINLEN to be used
1578 C Set LENS=0 if PLAST to be used (Elliptical yield curve)
1579      LENS=1
1580      SINWIN=0.4226D0
1581      COSWIN=0.9063D0
1582      SINWAT=0.4226D0
1583      COSWAT=0.9063D0
1584 C Estimate amass
1585      DO 1 J=1,NY
1586      DO 1 I=1,NX
1587      AMASS(I,J)=RHOICE*0.125D0*(((H(NLM1)+HI(I,J,1))*G(NL,I,J,1))+((H(N
1588      1LM1)+HI(I+1,J,1))*G(NL,I,J+1,1))+((H(NLM1)+HI(I,J+1,1))*G(NL,I,J+1
1589      2,1))+((H(NLM1)+HI(I+1,J+1,1))*G(NL,I+1,J+1,1)))
1590      DO 1 L=2,NLM1
1591      AMASS(I,J)=AMASS(I,J)+(RHOICE*0.25D0*HM(L)*(G(L,I,J,1)+G(L,I+1,J,1
1592      1)+G(L,I,J+1,1)+G(L,I+1,J+1,1)))
1593 1      CONTINUE
1594 C Set up non-linear wind and water drag
1595      DO 2 J=1,NY
1596      DO 2 I=1,NX
1597      COR=AMASS(I,J)*1.4544D-04*DSIN(PHI(I,J))
1598      DAIRN=RHOAIR*.12D-02*DSQRT((GAIRX(I,J)*GAIRX(I,J))+GAIRY(I,J)*GAI
1599      1RY(I,J)))
1600      EKMANX(I,J)=1.27D-02*(GAIRX(I,J)*COS20+GAIRY(I,J)*SIN20)/DSQRT(DSI

```

```

1601 IN(PHI(I,J))/1.5D0
1602 EKMANX(I,J)=1.27D-02*(GAIRY(I,J)*COS20-GAIRX(I,J)*SIN20)/DSQRT(DSI
1603 IN(PHI(I,J))/1.5D0
1604 OPEN=0.25D0*(G(1,I,J,1)+G(1,I+1,J,1)+G(1,I,J+1,1)+G(1,I+1,J+1,1))
1605 CURRX=GWATX(I,J)+OPEN*(EKMANX(I,J)*COS25-EKMANX(I,J)*SIN25)
1606 CURRY=GWATY(I,J)+OPEN*(EKMANX(I,J)*COS25-EKMANX(I,J)*SIN25)
1607 DWATN=5.5D0*DSQRT((U(I,J,1)-CURRX)**2+(V(I,J,1)-CURRY)**2)
1608 C Set up symmetric drag
1609 DRAGS(I,J)=DWATN*COSWAT
1610 C Set up anti-symmetric drag plus coriolis
1611 DRAGA(I,J)=DWATN*SINWAT+COR
1612 C Set up forcing field
1613 C First do wind
1614 FX=DAIRN*(COSWIN*GAIRX(I,J)-SINWIN*GAIRY(I,J))
1615 FY=DAIRN*(SINWIN*GAIRX(I,J)+COSWIN*GAIRY(I,J))
1616 C Add in current force
1617 FX=FX+DWATN*(COSWAT*CURRX-SINWAT*CURRY)
1618 FY=FY+DWATN*(SINWAT*CURRX+COSWAT*CURRY)
1619 C Add in tilt
1620 FORCEX(I,J)=FX-COR*GWATY(I,J)
1621 FORCEY(I,J)=FY+COR*GWATX(I,J)
1622 2 CONTINUE
1623 IF(LENS.EQ.1) CALL SINLEN(U,V,PRESS,ETA,ZETA)
1624 IF(LENS.EQ.0) CALL PLAST(U,V,PRESS,ETA,ZETA)
1625 C Set viscosities and pressure equal to zero at outflow points
1626 DO 3 J=1,NY1
1627 DO 3 I=1,NX1
1628 PRESS(I,J)=PRESS(I,J)*OUT(I,J)
1629 ETA(I,J)=ETA(I,J)*OUT(I,J)
1630 ZETA(I,J)=ZETA(I,J)*OUT(I,J)
1631 IF(GMASK(I,J).LT.0.5D0)ETA(I,J)=1.0D+14
1632 IF(GMASK(I,J).LT.0.5D0)ZETA(I,J)=1.0D+14
1633 3 CONTINUE
1634 C Calculate pressure force and add to external force
1635 DO 4 J=1,NY
1636 DO 4 I=1,NX
1637 FORCEX(I,J)=FORCEX(I,J)-(0.25D0/DX)*(PRESS(I+1,J)+PRESS(I+1,J+1)-P
1638 PRESS(I,J)-PRESS(I,J+1))
1639 FORCEY(I,J)=FORCEY(I,J)-(0.25D0/DY)*(PRESS(I,J+1)+PRESS(I+1,J+1)-P
1640 PRESS(I,J)-PRESS(I+1,J))
1641 4 CONTINUE
1642 RETURN
1643 END
1644 C
1645 C
1646 SUBROUTINE SINLEN(U,V,PRESS,ETA,ZETA)
1647 C
1648 C Subroutine calculates strain rates and viscous parameters
1649 C A sine wave lens yield curve is implied
1650 IMPLICIT REAL*8 (A-H,O-Z)

```

```

1651 DIMENSION U(21,36,3),V(21,36,3),PRESS(22,37),ETA(22,37),ZETA(22,37
1652 I)
1653 COMMON/GRID1/NX,NY,NX1,NY1,NXM1,NYM1,NL,NLM1,NFINE,NS,NSM1
1654 COMMON/GRIDR/HI(22,37,3),HMS(18),HWS(18),HS(17),HM(6),HW(6),H(6),T
1655 IOP
1656 COMMON/STEP/DT,DX,DY
1657 COMMON/SIGMA/ALPHR(22,37),ALPHO(22,37),EI,EII2,COTT
1658 COMMON/ARRAY/GMASK(22,37),UVM(21,36)
1659 COMMON/PHYS/CB,CF,STREN,RHOICE,RHOWAT,GRAV,COT,UA,UB,AH,BH,RHOAIR,
1660 IQI,CW,DMIX,SIDER,TI,SIGMAX,PI,ARMAX,CPLF,CON1,CON2,STFN,CON,ERROR2
1661 2,D1,D3,TINC,CH,SIN20,COS20,SIN25,COS25
1662 C Evaluate strain rates
1663 DO 1 J=2,NY
1664 DO 1 I=2,NX
1665 CALL ALPHA(I,J,U,V)
1666 ETA(I,J)=PRESS(I,J)*DSQRT(DMAX1(EII2-EI*EI,0.0D0))/(PI*EII2+1.0D-2
1667 I0)
1668 ZETA(I,J)=(0.5D0-(DARCOS(COTT)/PI))*PRESS(I,J)/(EI+1.0D-20)
1669 C Formula for ZETA is inaccurate when EI is close to 0
1670 IF(DABS(COTT).LT.1.0D-08)ZETA(I,J)=ETA(I,J)
1671 EII=DSQRT(EII2)
1672 1 CONTINUE
1673 C Put min and max viscosities in
1674 DO 2 J=1,NY1
1675 DO 2 I=1,NX1
1676 C Confine ZETA within limits
1677 ZCON=DMIN1(2.5D+08*PRESS(I,J),ZETA(I,J))
1678 ZCON=DMAX1(4.0D+08,ZCON)
1679 C If ZETA changes, then change ETA by the same proportion
1680 ETA(I,J)=(ETA(I,J)/(ZETA(I,J)+1.0D-18))*ZCON
1681 ZETA(I,J)=ZCON
1682 ETA(I,J)=ETA(I,J)/4.0D0
1683 2 CONTINUE
1684 RETURN
1685 END
1686 C
1687 C
1688 SUBROUTINE ALPHA(I,J,U,V)
1689 C
1690 C Calculates kinematic parameters of the velocity field
1691 IMPLICIT REAL*8 (A-H,O-Z)
1692 DIMENSION U(21,36,3),V(21,36,3)
1693 COMMON/STEP/DT,DX,DY
1694 COMMON/SIGMA/ALPHR(22,37),ALPHO(22,37),EI,EII2,COTT
1695 COMMON/ARRAY/GMASK(22,37),UVM(21,36)
1696 COMMON/PHYS/CB,CF,STREN,RHOICE,RHOWAT,GRAV,COT,UA,UB,AH,BH,RHOAIR,
1697 IQI,CW,DMIX,SIDER,TI,SIGMAX,PI,ARMAX,CPLF,CON1,CON2,STFN,CON,ERROR2
1698 2,D1,D3,TINC,CH,SIN20,COS20,SIN25,COS25
1699 E11=(0.5D0/DX)*(U(I,J,1)+U(I,J-1,1)-U(I-1,J,1)-U(I-1,J-1,1))
1700 E22=(0.5D0/DY)*(V(I,J,1)+V(I-1,J,1)-V(I,J-1,1)-V(I-1,J-1,1))

```

```

1701     E12=(0.25D0/DY)*(U(I,J,1)+U(I-1,J,1)-U(I,J-1,1)-U(I-1,J-1,1))+(0.2
1702 15D0/DX)*(V(I,J,1)+V(I,J-1,1)-V(I-1,J,1)-V(I-1,J-1,1))
1703     EI=E11+E22
1704     EII2=(E11-E22)*(E11-E22)+4.0D0*E12*E12
1705     EII=DSQRT(EII2)
1706     COTT=EI/(EII+1.0D-20)
1707     COTT=DMAX1(COTT,-1.0D0)
1708     COTT=DMIN1(COTT,1.0D0)
1709     IF(EII.GT.DABS(EI)) GOTO 1
1710     ALPHR(I,J)=0.0D0
1711     IF(EI.LT.0.0D0)ALPHR(I,J)=-EI
1712     GOTO 2
1713 1 ALPHR(I,J)=(DSQRT(EII2-EI*EI)-DARCOS(EI/EII)*EI)/PI
1714 2 ALPHR(I,J)=ALPHR(I,J)*GMASK(I,J)
1715     ALPHO(I,J)=(ALPHR(I,J)+EI)*GMASK(I,J)
1716     RETURN
1717     END
1718 C
1719 C
1720     SUBROUTINE PLAST(U,V,PRESS,ETA,ZETA)
1721 C
1722 C Subroutine calculates strain rates and viscous parameters
1723 C using an elliptical yield curve
1724     IMPLICIT REAL*8 (A-H,O-Z)
1725     DIMENSION U(21,36,3),V(21,36,3),PRESS(22,37),ETA(22,37),ZETA(22,37
1726 1)
1727     COMMON/EE/ECCEN
1728     COMMON/GRIDI/NX,NY,NX1,NY1,NXMI,NYMI,NL,NLMI,NFINE,NS,NSMI
1729     COMMON/GRIDR/HI(22,37,3),HMS(18),HWS(18),HS(17),HM(6),HW(6),H(6),T
1730 1OP
1731     COMMON/STEP/DT,DX,DY
1732     COMMON/SIGMA/ALPHR(22,37),ALPHO(22,37),EI,EII2,COTT
1733     COMMON/ARRAY/GMASK(22,37),UVM(21,36)
1734     ECM2=1.0D0/(ECCEN*ECCEN)
1735     GMIN=1.0D-20
1736 C Evaluate strain rates
1737     DO 1 J=2,NY
1738     DO 1 I=2,NX
1739     E11=(0.5D0/DX)*(U(I,J,1)+U(I,J-1,1)-U(I-1,J,1)-U(I-1,J-1,1))
1740     E22=(0.5D0/DY)*(V(I,J,1)+V(I-1,J,1)-V(I,J-1,1)-V(I-1,J-1,1))
1741     E12=(0.25D0/DY)*(U(I,J,1)+U(I-1,J,1)-U(I,J-1,1)-U(I-1,J-1,1))+(0.2
1742 15D0/DX)*(V(I,J,1)+V(I,J-1,1)-V(I-1,J,1)-V(I-1,J-1,1))
1743     EI=E11+E22
1744     EII2=(E11-E22)*(E11-E22)+4.0D0*E12*E12
1745     EII=DSQRT(EII2)
1746     DELT=DMAX1(GMIN,DSQRT(EI*EI+ECM2*EII2))
1747     ZETA(I,J)=0.5D0*PRESS(I,J)/DELT
1748     ALPHR(I,J)=(0.5D0*(DELT-EI))*GMASK(I,J)
1749     ALPHO(I,J)=(ALPHR(I,J)+EI)*GMASK(I,J)
1750 1 CONTINUE

```

```

1751 C Put min and max viscosities in
1752     DO 2 J=1,NY1
1753     DO 2 I=1,NX1
1754     ZETA(I,J)=DMIN1(.25D+09*PRESS(I,J),ZETA(I,J))
1755     ZETA(I,J)=DMAX1(4.0D+08,ZETA(I,J))
1756     ETA(I,J)=ECM2*ZETA(I,J)
1757 2 CONTINUE
1758     RETURN
1759     END
1760 C
1761 C
1762     SUBROUTINE BUDGET(PHI,TAIR,UG,DAY,C,P,TMIX,H,FB,RHUM)
1763 C
1764 C Evaluate heat budget
1765     IMPLICIT REAL*8 (A-H,O-Z)
1766     COMMON/PHYS/CB,CF,STREN,RHOICE,RHOWAT,GRAV,COT,UA,UB,AH,BH,RHOAIR,
1767 1QI,CW,DMIX,SIDER,TI,SIGMAX,PI,ARMAX,CPLF,CON1,CON2,STFN,CON,ERROR2
1768 2,D1,D3,TINC,CH,SIN20,COS20,SIN25,COS25
1769 C Set up constants
1770     D2=6450.0D0
1771     A=9.5D0
1772     B=7.66D0
1773     IF(H.GT.0.0D0)GO TO 1
1774     H=0.05D0
1775     D2=5690.0D0
1776     A=7.5D0
1777     B=35.86D0
1778 1 FS=0.0D0
1779 C Declination of sun
1780     DEC=(23.44D0*PI/180.0D0)*DCOS((172.0D0-DAY)*PI/180.0D0)
1781     ES=611.0D0*(10.0D0*(A*(TAIR-273.16D0)/(TAIR-B)))
1782     QS=EP*ES/(P-0.378D0*ES)
1783     E=RHUM*QS*P/(EP+(0.378D0*RHUM*QS))
1784 C Integrate Zillman's formula for short-wave radiation
1785     DO 2 ITIME=1,12
1786     HA=(12.5D0-DFLOAT(ITIME))*PI/12.0D0
1787     COSZ=DSIN(PHI)*DSIN(DEC)+DCOS(PHI)*DCOS(DEC)*DCOS(HA)
1788     Q=1353.0D0*COSZ*COSZ/((COSZ+2.7D0)*E*1.0D-05+1.085D0*COSZ+0.1D0)
1789     IF(COSZ.LE.0.0D0)Q=0.0D0
1790     FS=FS+(Q/12.0D0)
1791 2 CONTINUE
1792 C Short-wave radiation
1793     FS=FS*(1.0D0-0.6D0*C*C)
1794 C Long-wave radiation
1795     FL=STFN*(TAIR**4)*(1.0D0-0.261D0*DEXP(-7.77D-04*(273.0D0-TAIR))*(27
1796 13.0D0-TAIR)))*(1.0D0+C*0.275D0)
1797     QA=0.622D0*E/(P-0.378D0*E)
1798     IF(H.GT.0.055D0) GOTO 3
1799     T=TMIX
1800     GOTO 6

```

```

1801 C Calulate T (surface ice temperature) required for heat flux balance
1802 3 T1=200.0D0
1803 T2=300.0D0
1804 CALL BALNCE(P,T1,A,B,E,FS,FL,TAIR,QA,UG,H,TMIX,D2,BAL1,BALA)
1805 CALL BALNCE(P,T2,A,B,E,FS,FL,TAIR,QA,UG,H,TMIX,D2,BAL2,BALA)
1806 DO 5 NN=1,12
1807 T=0.5D0*(T1+T2)
1808 CALL BALNCE(P,T,A,B,E,FS,FL,TAIR,QA,UG,H,TMIX,D2,BAL,BALA)
1809 IF(BAL*BAL1.LT.0.0D0)GOTO 4
1810 T1=T
1811 BAL1=BAL
1812 GOTO 5
1813 4 T2=T
1814 BAL2=BAL
1815 5 CONTINUE
1816 T=DMIN1(T,273.16D0)
1817 6 CALL BALNCE(P,T,A,B,E,FS,FL,TAIR,QA,UG,H,TMIX,D2,BAL,BALA)
1818 C Obtain growth rate implied by linear temperature profile
1819 FB=-BALA/QI
1820 RETURN
1821 END
1822 C
1823 C
1824 SUBROUTINE BALNCE(P,T,A,B,E,FS,FL,TAIR,QA,UG,H,TMIX,D2,BAL,BALA)
1825 C
1826 C Calculates heat flux balance
1827 IMPLICIT REAL*8 (A-H,O-Z)
1828 COMMON/PHYS/CB,CF,STREN,RHOICE,RHOWAT,GRAV,COT,UA,UB,AH,BH,RHOAIR,
1829 IQI,CW,DMIX,SIDER,TI,SIGMAX,PI,ARMAX,CPLF,CON1,CON2,STFN,CON,ERROR2
1830 2,D1,D3,TINC,CH,SIN20,COS20,SIN25,COS25
1831 ES=611.0D0*(10.0D0*(A*(T-273.16D0)/(T-B)))
1832 QS=0.622D0*ES/(P-0.378D0*ES)
1833 C Thickness dependent albedo
1834 ALB=0.44D0*(H**0.28D0)+0.08D0
1835 C Reduce albedo due to melt ponds
1836 IF(T.EQ.273.16D0) ALB=ALB*0.8213D0
1837 IF(H.EQ.0.05D0)ALB=0.08D0
1838 C Consider stability of atmospheric boundary layer.
1839 STB=1.0D0
1840 IF(T.LE.TAIR)STB=0.571428D0
1841 BALA=(1.0D0-ALB)*FS+FL+UG*STB*(D1*(TAIR-T)+D2*(QA-QS))-D3*(T**4)
1842 BAL=BALA+(CON/H)*(TMIX-T)
1843 RETURN
1844 END
1845 C
1846 C
1847 SUBROUTINE NORTH(G,X38,FND,TMIX)
1848 C
1849 C Calculate input parameters for Fram Strait
1850 IMPLICIT REAL*8 (A-H,O-Z)

```

```

1851 DIMENSION G(6,22,37,3),FND(5,22,37,3),TMIX(22,37)
1852 COMMON/PHYS/CB,CF,STREN,RHOICE,RHOWAT,GRAV,COT,UA,UB,AH,BH,RHOAIR,
1853 IQI,CW,DMIX,SIDER,TI,SIGMAX,PI,ARMAX,CPLF,CON1,CON2,STFN,CON,ERROR2
1854 2,D1,D3,TINC,CH,SIN20,COS20,SIN25,COS25
1855 COMMON/GRID1/NX,NY,NX1,NY1,NXM1,NYM1,NL,NLM1,NFINE,NS,NSM1
1856 COMMON/GRIDR/HI(22,37,3),HMS(18),HWS(18),HS(17),HM(6),HW(6),H(6),T
1857 IOP
1858 J=36
1859 ALP=0.5D0
1860 BETA=0.7552854129D0
1861 X1=(1.0D0+ALP-ALP*BETA)*X38
1862 X2=(1.0D0-ALP*BETA)*X38
1863 Y=36.0D0-0.5D0
1864 DO 7 I=2,NX
1865 HI(I,J,1)=H(NLM1)+TOP
1866 H(NL)=HI(I,J,1)
1867 HW(NL)=H(NL)-H(NLM1)
1868 HM(NL)=0.5D0*(H(NL)+H(NLM1))
1869 X=DFLOAT(I)-0.5D0
1870 A=DCOS((X-X2)*1.570796327D0/(X1-X2))
1871 IF(X.LE.X2)A=1.0D0
1872 IF(X.GE.X1)A=0.0D0
1873 G(1,I,J,1)=1.0D0-A
1874 HX0=1.0D-04*Y*Y*Y+0.9D0
1875 HMAX=0.0D0
1876 IF(X.LT.X1)HMAX=((X1-X)/X1)*HX0*3.0D0
1877 IF(A.EQ.0.0D0)GOTO 4
1878 NLMAX=NLM1
1879 DO 1 L=1,NLM1
1880 G(L+1,I,J,1)=0.0D0
1881 IF(H(L).LE.HMAX.AND.HMAX.LT.H(L+1))NLMAX=L
1882 1 CONTINUE
1883 IF(NLMAX.EQ.1)GOTO 3
1884 DO 2 L=2,NLMAX
1885 G(L,I,J,1)=2.0D0*A*HW(L)*((1.0D0-(HM(L)/HMAX))/HMAX
1886 2 CONTINUE
1887 3 G(NLMAX+1,I,J,1)=2.0D0*A*(HMAX-H(NLMAX))*((1.0D0-((HMAX+H(NLMAX)))/(
1888 12.0D0*HMAX)))/HMAX
1889 TMIX(I,J)=271.2D0
1890 4 HI(I,J,1)=DMAX1(HI(I,J,1),HMAX)
1891 IF(G(1,I,J,1).NE.0.0D0) GOTO 5
1892 G(3,I,J,1)=G(3,I,J,1)+G(2,I,J,1)
1893 G(2,I,J,1)=0.0D0
1894 IF(I.GT.5) GOTO 5
1895 G(4,I,J,1)=G(4,I,J,1)+G(3,I,J,1)
1896 G(3,I,J,1)=0.0D0
1897 5 CONTINUE
1898 DO 6 L=2,NL
1899 FND(L-1,I,J,1)=G(L,I,J,1)/ARMAX
1900 IF(G(L,I,J,1).LE.0.0D0)FND(L-1,I,J,1)=0.0D0

```

```

1801 C Calulate T (surface ice temperature) required for heat flux balance
1802 3 T1=200.0D0
1803 T2=300.0D0
1804 CALL BALNCE(P,T1,A,B,E,FS,FL,TAIR,QA,UG,H,TMIX,D2,BAL1,BALA)
1805 CALL BALNCE(P,T2,A,B,E,FS,FL,TAIR,QA,UG,H,TMIX,D2,BAL2,BALA)
1806 DO 5 NN=1,12
1807 T=0.5D0*(T1+T2)
1808 CALL BALNCE(P,T,A,B,E,FS,FL,TAIR,QA,UG,H,TMIX,D2,BAL,BALA)
1809 IF(BAL*BAL1.LT.0.0D0)GOTO 4
1810 T1=T
1811 BAL1=BAL
1812 GOTO 5
1813 4 T2=T
1814 BAL2=BAL
1815 5 CONTINUE
1816 T=DMIN1(T,273.16D0)
1817 6 CALL BALNCE(P,T,A,B,E,FS,FL,TAIR,QA,UG,H,TMIX,D2,BAL,BALA)
1818 C Obtain growth rate implied by linear temperature profile
1819 FB=-BALA/QI
1820 RETURN
1821 END
1822 C
1823 C
1824 SUBROUTINE BALNCE(P,T,A,B,E,FS,FL,TAIR,QA,UG,H,TMIX,D2,BAL,BALA)
1825 C
1826 C Calculates heat flux balance
1827 IMPLICIT REAL*8 (A-H,O-Z)
1828 COMMON/PHYS/CB,CF,STREN,RHOICE,RHOWAT,GRAV,COT,UA,UB,AH,BH,RHOAIR,
1829 IQI,CW,DMIX,SIDER,TI,SIGMAX,PI,ARMAX,CPLF,CON1,CON2,STFN,CON,ERROR2
1830 2,D1,D3,TINC,CH,SIN20,COS20,SIN25,COS25
1831 ES=611.0D0*(10.0D0**((A*(T-273.16D0)/(T-B)))
1832 QS=0.622D0*ES/(P-0.378D0*ES)
1833 C Thickness dependent albedo
1834 ALB=0.44D0*(H**0.28D0)+0.08D0
1835 C Reduce albedo due to melt ponds
1836 IF(T.EQ.273.16D0) ALB=ALB*0.8213D0
1837 IF(H.EQ.0.05D0)ALB=0.08D0
1838 C Consider stability of atmospheric boundary layer.
1839 STB=1.0D0
1840 IF(T.LE.TAIR)STB=0.571428D0
1841 BALA=(1.0D0-ALB)*FS+FL+UG*STB*(D1*(TAIR-T)+D2*(QA-QS))-D3*(T**4)
1842 BAL=BALA+(CON/H)*(TMIX-T)
1843 RETURN
1844 END
1845 C
1846 C
1847 SUBROUTINE NORTH(G,X38,FND,TMIX)
1848 C
1849 C Calculate input parameters for Fram Strait
1850 IMPLICIT REAL*8 (A-H,O-Z)

```

```

1851 DIMENSION G(6,22,37,3),FND(5,22,37,3),TMIX(22,37)
1852 COMMON/PHYS/CB,CF,STREN,RHOICE,RHOWAT,GRAV,COT,UA,UB,AH,BH,RHOAIR,
1853 IQI,CW,DMIX,SIDER,TI,SIGMAX,PI,ARMAX,CPLF,CON1,CON2,STFN,CON,ERROR2
1854 2,D1,D3,TINC,CH,SIN20,COS20,SIN25,COS25
1855 COMMON/GRID1/NX,NY,NX1,NY1,NXM1,NYM1,NL,NLM1,NFINE,NS,NSM1
1856 COMMON/GRIDR/HI(22,37,3),HMS(18),HWS(18),HS(17),HM(6),HW(6),H(6),T
1857 IOP
1858 J=36
1859 ALP=0.5D0
1860 BETA=0.7552854129D0
1861 X1=(1.0D0+ALP-ALP*BETA)*X38
1862 X2=(1.0D0-ALP*BETA)*X38
1863 Y=36.0D0-0.5D0
1864 DO 7 I=2,NX
1865 HI(I,J,1)=H(NLM1)+TOP
1866 H(NL)=HI(I,J,1)
1867 HW(NL)=H(NL)-H(NLM1)
1868 HM(NL)=0.5D0*(H(NL)+H(NLM1))
1869 X=DFLOAT(I)-0.5D0
1870 A=DCOS((X-X2)*1.570796327D0/(X1-X2))
1871 IF(X.LE.X2)A=1.0D0
1872 IF(X.GE.X1)A=0.0D0
1873 G(1,I,J,1)=1.0D0-A
1874 HX0=1.0D-04*Y*Y*Y+0.9D0
1875 HMAX=0.0D0
1876 IF(X.LT.X1)HMAX=((X1-X)/X1)*HX0*3.0D0
1877 IF(A.EQ.0.0D0)GOTO 4
1878 NLMAX=NLM1
1879 DO 1 L=1,NLM1
1880 G(L+1,I,J,1)=0.0D0
1881 IF(H(L).LE.HMAX.AND.HMAX.LT.H(L+1))NLMAX=L
1882 1 CONTINUE
1883 IF(NLMAX.EQ.1)GOTO 3
1884 DO 2 L=2,NLMAX
1885 G(L,I,J,1)=2.0D0*A*HW(L)*(1.0D0-(HM(L)/HMAX))/HMAX
1886 2 CONTINUE
1887 3 G(NLMAX+1,I,J,1)=2.0D0*A*(HMAX-H(NLMAX))*(1.0D0-((HMAX+H(NLMAX)))/(
1888 12.0D0*HMAX)))/HMAX
1889 TMIX(I,J)=271.2D0
1890 4 HI(I,J,1)=DMAX1(HI(I,J,1),HMAX)
1891 IF(G(1,I,J,1).NE.0.0D0)GOTO 5
1892 G(3,I,J,1)=G(3,I,J,1)+G(2,I,J,1)
1893 G(2,I,J,1)=0.0D0
1894 IF(I.GT.5)GOTO 5
1895 G(4,I,J,1)=G(4,I,J,1)+G(3,I,J,1)
1896 G(3,I,J,1)=0.0D0
1897 5 CONTINUE
1898 DO 6 L=2,NL
1899 FND(L-1,I,J,1)=G(L,I,J,1)/ARMAX
1900 IF(G(L,I,J,1).LE.0.0D0)FND(L-1,I,J,1)=0.0D0

```

```

1901 6 CONTINUE
1902 7 CONTINUE
1903 RETURN
1904 END
1905 C
1906 C
1907 SUBROUTINE GRNLND(GWATX,GWATY,PHI,C,RHUM,P,EDGE,HTSEA)
1908 C
1909 IMPLICIT REAL*8 (A-H,O-Z)
1910 COMMON/GRIDI/NX,NY,NX1,NY1,NXM1,NYM1,NL,NLM1,NFINE,NS,NSM1
1911 COMMON/PHYS/CB,CF,STREN,RHOICE,RHOWAT,GRAV,COT,UA,UB,AH,BH,RHOAIR,
1912 IQI,CW,DMIX,SIDER,TI,SIGMAX,PI,ARMAX,CPLF,CON1,CON2,STFN,CON,ERROR2
1913 2,D1,D3,TINC,CH,SIN20,COS20,SIN25,COS25
1914 DIMENSION GWATX(21,36),GWATY(21,36),PHI(21,36),C(52),RHUM(52),P(52
1915 1),EDGE(52),HTSEA(22,37)
1916 READ(1,1)(C(I),RHUM(I),P(I),I=1,52)
1917 1 FORMAT(3G8.0)
1918 READ(1,2)(EDGE(I),I=1,52)
1919 2 FORMAT(G6.0)
1920 C Read in long term ocean currents
1921 READ(3)GWATX,GWATY
1922 DO 3 J=1,NY
1923 DO 3 I=1,NX
1924 GWATX(I,J)=GWATX(I,J)
1925 GWATY(I,J)=GWATY(I,J)
1926 GX=GWATX(I,J)*COS25+GWATY(I,J)*SIN25
1927 GY=GWATY(I,J)*COS25-GWATX(I,J)*SIN25
1928 GWATX(I,J)=GX
1929 GWATY(I,J)=GY
1930 3 CONTINUE
1931 C Read in latitude values at grid points
1932 READ(4)PHI
1933 C Set up oceanic heat flux field
1934 X1=1.0D0
1935 X2=20.0D0
1936 SEA=-3.5D0/8.64D+06
1937 DO 4 J=1,NY1
1938 SA=SEA*0.5D0*(1.0D0-DCOS(PI*DFLOAT(J)/30.0D0))
1939 DO 4 I=1,NX1
1940 HTSEA(I,J)=0.5D0*SA*(1.0D0-DCOS(PI*(DFLOAT(I)-X1)/(X2-X1)))
1941 IF(I.GE.20)HTSEA(I,J)=SA
1942 IF(I.LE.1)HTSEA(I,J)=0.0D0
1943 4 CONTINUE
1944 RETURN
1945 END
1946 C
1947 C
1948 SUBROUTINE UVT(GAIRX,GAIRY,TAIR,ICOUNT,INIT,IUVT)
1949 C
1950 REAL*4 SGAIRX(21,36),SGAIRY(21,36),STAIR(21,36)

```

```

1951 REAL*8 GAIRX(21,36),GAIRY(21,36),TAIR(21,36)
1952 COMMON/GRIDI/NX,NY,NX1,NY1,NXM1,NYM1,NL,NLM1,NFINE,NS,NSM1
1953 IF(ICOUNT.EQ.1.AND.INIT.EQ.0)RETURN
1954 C Read in winds and temperature
1955 NUMFLD=0
1956 IF((INIT.EQ.0.AND.ICOUNT.EQ.0).OR.MOD(ICOUNT,2).EQ.1)NUMFLD=1
1957 IF(INIT.EQ.1.AND.IUVT.EQ.1)NUMFLD=(ICOUNT/2)+1
1958 IF((INIT.EQ.1.AND.ICOUNT.EQ.0).OR.NUMFLD.EQ.0)RETURN
1959 DO 2 N=1,NUMFLD
1960 READ(2)SGAIRX,SGAIRY,STAIR
1961 WRITE(6,1)
1962 1 FORMAT(1X,'WIND AND TEMPERATURE FILE READ ONCE')
1963 2 CONTINUE
1964 DO 3 J=1,NY
1965 DO 3 I=1,NX
1966 GAIRX(I,J)=1.5*(SGAIRX(I,J)*0.9063+SGAIRY(I,J)*0.4226)
1967 GAIRY(I,J)=1.5*(SGAIRY(I,J)*0.9063-SGAIRX(I,J)*0.4226)
1968 TAIR(I,J)=STAIR(I,J)
1969 3 CONTINUE
1970 RETURN
1971 END

```

## The output

WIND AND TEMPERATURE FILE READ ONCE

Thickness levels	0.0	0.2500	0.6055	1.1626	2.0000	-0.0000
2.0000						
Midpoints of levels	0.0	0.1250	0.4278	0.8841	1.5813	2.0000
level widths	1.0000	0.2500	0.3555	0.5571	0.8374	-0.0000

```

RELAX CALLED: NO. OF ITERATIONS 32    MAX ERROR .97085D-02
**** TIME STEP 1 DAY 335.00
RELAX CALLED: NO. OF ITERATIONS 31    MAX ERROR .81424D-05
RELAX CALLED: NO. OF ITERATIONS 31    MAX ERROR .98272D-05
POSITION 335.000 5.27889 16.1800
TOTAL VOLUME 431.356046103
OUTFLOW -6.181303
NET: -6.181303
**** TIME STEP 2 DAY 335.25
RELAX CALLED: NO. OF ITERATIONS 25    MAX ERROR .91648D-05
RELAX CALLED: NO. OF ITERATIONS 24    MAX ERROR .62637D-05
POSITION 335.250 5.43457 16.1576
TOTAL VOLUME 431.000494675
OUTFLOW -6.914162
NET: -13.09546
**** TIME STEP 3 DAY 335.50
WIND AND TEMPERATURE FILE READ ONCE
RELAX CALLED: NO. OF ITERATIONS 33    MAX ERROR .84667D-05
RELAX CALLED: NO. OF ITERATIONS 35    MAX ERROR .73470D-05
POSITION 335.500 5.46213 16.0752
TOTAL VOLUME 435.370187203
OUTFLOW -8.766854
NET: -21.86232
**** TIME STEP 4 DAY 335.75
RELAX CALLED: NO. OF ITERATIONS 20    MAX ERROR .79765D-05
RELAX CALLED: NO. OF ITERATIONS 29    MAX ERROR .86755D-05
POSITION 335.750 5.46323 16.0044
TOTAL VOLUME 440.555927308
OUTFLOW -9.040284
NET: -30.90260
**** TIME STEP 5 DAY 336.00
WIND AND TEMPERATURE FILE READ ONCE
RELAX CALLED: NO. OF ITERATIONS 24    MAX ERROR .57374D-05
RELAX CALLED: NO. OF ITERATIONS 32    MAX ERROR .86341D-05
POSITION 336.000 5.49240 16.0044
TOTAL VOLUME 438.748579794
OUTFLOW -.9579669
NET: -31.86057
FULL DATA PRINTED FOR THIS TIME STEP

```

## X-COMPONENT OF ICE VELOCITY

.0	.0	.0	.0	.0
.0	-.3105038395D-01	-.7090668542D-02	-.5200650416D-02	.0
.0	.9293394750D-01	.1109645415	.6619184922D-01	.0
.0	.4871843570D-01	.1944705420	.2506536305	.0
.0	.5005692442D-01	.3338169365	.1296760889	.0
.0	.1132368337	.4068779663	.1319461303	.0
.0	.1288521988	.2881886907	.1274435170	.0
.0	.0	.0	.0	.0

## Y-COMPONENT OF ICE VELOCITY

.0	.0	.0	.0	.0
.0	.1023818950D-01	.1107732253	.1139191078	.0
.0	.1366843052D-01	.8795392231D-01	.1726953539	.0
.0	.7595177703D-03	.7931579803D-01	.3206200784	.0

.0	.5634955024D-01	.2638644639	.6829193563D-01	.0
.0	.7451490554D-01	.3484362157	.4387192074D-01	.0
.0	-.2674565943D-01	.2022760537	-.1701246158D-01	.0
.0	.0	.0	.0	.0

## FLOE NUMBER DENSITY

.0	.0	.0	.0	.0
.0	.2750180735D-03	.1096185814D-01	.0	.0
.0	.9981429823D-04	.2332027623D-03	.6611309131D-01	.0
.0	.1014151682D-03	.4871191795D-03	.1996824763	.0
.0	.1803283251D-03	.6810533466D-01	.0	.0
.0	.1781163404D-03	.1272327791	.0	.0
.0	.4848284624D-03	.1575645400D-01	.0	.0
.0	.0	.0	.0	.0

.0	.0	.0	.0	.0
.0	.2022082297D-02	.1905831061D-02	.0	.0
.0	.3168191094D-02	.1521679427D-02	.2051673547D-02	.0
.0	.1557761745D-02	.1946563369D-02	.5030122683D-02	.0
.0	.1799266279D-02	.4876829533D-02	.0	.0
.0	.1209163148D-02	.1211953314D-01	.0	.0
.0	.5329698482D-04	.2196141150D-02	.0	.0
.0	.0	.0	.0	.0

.0	.0	.0	.0	.0
.0	.1310137030D-04	.5731718733D-05	.0	.0
.0	.1518286356D-02	.2548198015D-03	.3347898891D-04	.0
.0	.6851716353D-03	.3936485051D-03	.9643199641D-04	.0
.0	.1730699351D-04	.6378890565D-03	.0	.0
.0	.9283334952D-11	.8675465480D-03	.0	.0
.0	.2423516246D-05	.5486861522D-03	.0	.0
.0	.0	.0	.0	.0

## ICE THICKNESS DISTRIBUTION AT SELECTED POINTS

.713857542288D-01	1.000000000000
.124933091651D-01	.0
.503079942980	.0
.298952916710	.0
.113920381882	.0
.167695033636D-03	.0

.169063889104	1.000000000000
.115517607501	.0
.265092112425	.0
.242459828699	.0
.207866562271	.0
.0	.0

## BULK VISCOSITY, ZETA

.1000000000D+15	.1000000000D+15	.1000000000D+15	.1000000000D+15	.1000000000D+15
.1000000000D+15	400000000.0	400000000.0	400000000.0	.0
.1000000000D+15	400000000.0	1261337622.	400000000.0	.0
.1000000000D+15	400000000.0	400000000.0	400000000.0	.0
.1000000000D+15	400000000.0	400000000.0	400000000.0	.0
.1000000000D+15	446184565.9	400000000.0	400000000.0	.0
.1000000000D+15	475716525.0	400000000.0	400000000.0	.0
.1000000000D+15	.0	.0	.0	.0

## SHEAR VISCOSITY, ETA

.1000000000D+15	.1000000000D+15	.1000000000D+15	.1000000000D+15	.1000000000D+15
.1000000000D+15	95998407.77	87251015.07	.0	.0
.1000000000D+15	63655008.29	289423850.9	.0	.0
.1000000000D+15	.0	86897564.25	.0	.0
.1000000000D+15	92416697.77	.0	.0	.0
.1000000000D+15	80444759.70	.0	.0	.0
.1000000000D+15	104407294.1	.0	.0	.0
.1000000000D+15	.0	.0	.0	.0

## RIDGING AMOUNT, ALPHR

-.2154116179D-26	-.2154116179D-26	-.2154116179D-26	-.2154116179D-26	-.2154116179D-26
-.2154116179D-26	.2327202660D-06	.5165083634D-06	.1970238047D-06	.7855160803D-06
-.2154116179D-26	.3999514791D-07	.3939711896D-06	.5996104804D-07	.1077869592D-05
-.2154116179D-26	.3352887927D-06	.2420644460D-06	.1377650517D-05	.1765303628D-05
-.2154116179D-26	.4497742760D-06	.3599316456D-07	.2827201339D-06	.2376215088D-05
-.2154116179D-26	.6717434115D-06	.8318341972D-06	.3668635776D-06	.3286920362D-05
-.2154116179D-26	.5941041654D-06	.1226072867D-05	.4548905122D-06	.3674979915D-05
-.2154116179D-26	.3499299728D-06	.6827316801D-06	.4681611318D-05	.1147183998D-05

## OPEN WATER OPENING, ALPHO

-.2154116179D-26	-.2154116179D-26	-.2154116179D-26	-.2154116179D-26	-.2154116179D-26
-.2154116179D-26	.2973621442D-06	.3543722124D-06	.3883281488D-07	.1234058187D-05
-.2154116179D-26	.6054287125D-06	.3126197932D-06	.1180541237D-05	.4745627325D-06
-.2154116179D-26	.2061657913D-06	.1153104473D-05	.0	.6351697152D-07
-.2154116179D-26	.3963688412D-06	.5052280725D-05	.8963723064D-09	.0
-.2154116179D-26	.4324915321D-07	.3363626913D-05	.1206300990D-07	.0
-.2154116179D-26	.3768485842D-06	.2076650835D-05	.1117424776D-06	.2270364608D-07
-.2154116179D-26	.2744526737D-05	.4558018235D-05	.1782523318D-05	.1098585468D-05

## STRENGTH

.0	.0	.0	.0	.0
.0	710.9509204	33.76574347	.0	.0
.0	300.6551840	1574.998346	.0	.0
.0	658.3601275	839.5225336	.0	.0
.0	3288.410915	.0	.0	.0
.0	3676.058916	.0	.0	.0
.0	2355.159303	.0	.0	.0
.0	.0	.0	.0	.0

## MIXED LAYER TEMPERATURE

271.2000000	271.2000000	272.4780163	275.9183538	279.3586912
271.2000000	271.2000000	271.2000000	271.8526248	273.1358492
271.2000000	271.2000000	271.2000000	271.2000000	271.8650621
271.2000000	271.2000000	271.2000000	271.2000000	272.3528315
271.2000000	271.2000000	271.2000000	272.3314632	274.5447666
271.2000000	271.2000000	271.2000000	272.7513367	275.6227700
271.2000000	271.2000000	271.2000000	273.5532844	277.4405386
271.2000000	271.2000000	271.2000000	273.4011479	278.3582854

## \*\*\*\* TIME STEP

6 DAY 336.25

RELAX CALLED: NO. OF ITERATIONS 23 MAX ERROR .79660D-05

RELAX CALLED: NO. OF ITERATIONS 31 MAX ERROR .85239D-05

POSITION 336.250

5.53519

16.0145

TOTAL VOLUME 437.306506862

OUTFLOW -.6669196

NET: -32.52749

## BIBLIOGRAPHY

## BIBLIOGRAPHY

- Ackley, S. F. and Hibler, W. D. III., 1974: Measurement of Arctic Ocean ice deformation and fracture patterns from satellite imagery. AIDJEX Bull. 26, 33-47.
- Ackley, S. F., Hibler, W. D. III, and Kugzrug, F. K., 1976: Misgivings on isostatic imbalance as a mechanism for sea ice cracking. AIDJEX Bull. 33, 85-94.
- Alekseev, G. V. and Buzuev A. Yu., 1973: Bokovoe tayanie l'da v razvod'yakh (Lateral melting of ice in leads). Trudy AANII, 307, 169-178.
- Andreas, E. L., and Ackley, S. F., 1982: On the differences in ablation seasons of the Arctic and Antarctic sea ice. Journal of the Atmospheric Sciences, 39(2), 440-47.
- Bauer, J., and Martin, S., 1983: A model of grease ice growth in small leads. Journal of Geophysical Research, 88, 2917-2925.
- Brown, R. A., 1973: On the atmospheric boundary layer: Theory and methods, AIDJEX Bull., 20, 1-142.
- Browne, I. M., and Crary, A. P., 1958: The movement of ice in the Arctic Ocean. (In Thurston, W. R., ed. Arctic Sea Ice. Conference held at Easton, Maryland, February 24-27, 1958. Washington, D. C., National Academy of Sciences-National Research Council. 191-209. (Publication 598))
- Campbell, W. J., 1964: On the steady-state flow of sea ice. Seattle. Univ. of Washington, Dept. of Meteorology. Sci. Report to ONR under contract NR 307-352. 167p.
- Coachman, L. K., and Aagaard, K., 1974: Physical oceanography of Arctic and Subarctic seas, edited by Y. Herman, pp. 1-72, Springer, New York.
- Colony, R., 1976: The simulation of arctic sea ice dynamics. POAC 76. The third international conference on port and ocean engineering under arctic conditions, 469-86.
- Coon, M. D., and Evans, R. J., 1977: On wind-induced cracking of sea-ice sheets. Journal of Glaciology., 18, 152-154.

- Cox, G. F. N., and Weeks, W. F., 1982: Equations for determining the gas and brine volumes in sea ice samples. CRREL Report 82-30. 11pp.
- Crutcher, H. L., and J. M. Meserve, 1970: Selected level heights, temperatures and dew points for the Northern Hemisphere. NAVAIR 50-iC-52, Naval Weather Service Command, Washington, DC.
- Doronin, Yu. P., 1970: On a method of calculating the compactness and drift of ice floes. Tr. Arkt. Antarkt. Inst. T291, 5-17 (in Russian). English transl. AIDJEX Bull. 3, 22-39.
- Drogaishev, D. A., 1956. Zones of compression and rarefaction of ice in the atmospheric pressure field. Izv. Akad. Nauk, Geophysical Series, 11, 1332-1337, Translation by E. R. Hope in Ice-drift and its calculation (Recent Russian papers), October 1957. Canadian Defence Research Board.
- Drucker, D. C., 1950: Some implications of work hardening and ideal plasticity, Quart. Appl. Math., 7, 411-418.
- Evans, R. J., 1971: Cracks in perennial sea ice due to thermally induced stress. Journal of Geophysical Research. 76(33), 8153-55.
- Evans, R. J., and Untersteiner, N., 1971: Thermal cracks in floating ice sheets. Journal of Geophysical Research. 76(3), 694-703.
- Felzenbaum, A. I., 1958: The theory of the steady drift of ice and the calculation of the long period mean drift in the central part of the Arctic basin. Problems of the North, 2, 5-15, 13-44.
- Fleagle, R. G., and Businger, J. A., 1963: An introduction to Atmospheric Physics, 346pp., Academic Press, New York.
- Gaskill, H. S., Lopez, R. J., and Swaters, G. E., 1980: Free drift of sea ice: A comparison of models. C-CORE Technical report 80-16. 132pp.
- Gebhart, B., Sammakia, B., and Audunson, T., 1983: Melting characteristics of horizontal ice surfaces in cold saline water. Journal of Geophysical Research, 88, 2935-2942.
- Goodman, D. J., Wadhams, P., and Squire, V. A., 1980: The flexural response of a tabular ice island to ocean swell. Annals of Glaciology, 23-27.
- Gordienko, P., 1958: Arctic ice drift. (In Thurston, W. R., ed. Arctic Sea Ice.

Conference held at Easton, Maryland, February 24-27, 1958. Washington D. C., National Academy of Sciences - National Research Council. 210-222. (Publication 598))

Hetenyi, M., 1946: Beams on elastic foundation, University of Michigan Press, Ann Arbor, Mich.

Hibler, W. D. III, and Ackley, S. F., 1982: On modeling the Weddell Sea pack ice. *Annals of Glaciology*, **3**, 125-130.

Hibler, W. D. III, and Bryan, K., 1983: A large scale ice ocean model for the marginal ice zone. MIZEX modeling workshop, October 18-20, 1983. Fairlee, Vermont.

Hibler, W. D. III, Ackley, S. F., Crowder, W. K., McKim, H. W., and Anderson, D. M., 1974: Analysis of shear zone ice deformation in the Beaufort Sea using satellite imagery. The Coast and Shelf of the Beaufort Sea, J. C. Reed, and J. E. Sater, Eds., Arctic Institute of North America, 285-296.

Hibler, W. D. III, 1979: A dynamic thermodynamic sea ice model. *Journal of Physical Oceanography*, **9**, 815-846.

Hibler, W. D. III, 1980a: Modeling a variable thickness sea ice cover. *Monthly Weather Review*, **108**, 1943-1973.

Hibler, W. D. III, 1980b: Documentation for a two-level dynamic thermodynamic sea ice model. Spec. Rep. 80-8, USACRREL, Hanover, NH, 35pp.

Hovmöller, E., 1945: Climate and weather over the coast-land of Northeast Greenland and the adjacent Sea, *Medd. Groenl.*, **144**(1).

Huschke, R. E. 1969: Arctic cloud statistics from 'air-calibrated' surface weather observations. Memo. RM-6173-PR, The Rand Corporation, 79pp.

Idso, S. B. and R. D. Jackson, 1969: Thermal radiation from the atmosphere. *Journal of Geophysical Research*, **74**, 5397-5403.

Joffre, S. M., 1982: Momentum and heat transfers in the surface layer over a frozen sea. *Boundary-layer Meteorology* **24**, 211-229.

Ketchum, R. D. Jr., and Wittmann, W. I., 1972: Recent Remote Sensing Studies of the East Greenland Pack Ice. Sea ice conference proceedings, Reykjavik, 213-226.

- Kiilerich, A., 1945: On the hydrography of the Greenland Sea, *Medd. Groenl.*, 144(2).
- Koch, L., 1945: The east Greenland ice, *Medd. Groenl.*, 130(3).
- Kozo, T. L., and Tucker, W. B., 1974: Sea ice features in the Denmark Strait, *Journal of Geophysical Research*, 79(30), 4505-4511.
- Kovacs, A., 1972: On pressured sea ice. Sea ice conference proceedings, Reykjavik, 276-295.
- Laevastu, T., 1960: Factors affecting the temperature of the surface layers of the sea, *Commentationes Physico-Mathematicae*, 25:1, 8-134.
- Leppäranta, M., 1981: An ice drift model for the Baltic Sea. *Tellus*, 33, 583-596.
- McPhee, M. G., 1975: Ice-ocean momentum transfer for the AIDJEX ice model. *AIDJEX Bull.*, 29, 93-111.
- McPhee, M. G., 1980: An analysis of pack ice drift in Summer, in *Sea Ice Processes and Models*, edited by R. S. Pritchard. pp62-75, University of Washington Press, Seattle.
- McPhee, M. G. 1982: Sea ice drag laws and simple boundary layer concepts, including application to rapid melting. *CRREL Report 82-4*, 17pp.
- Manabe, S., and Wetherald, R. T., 1980: On the distribution of climate change resulting from an increase in CO<sub>2</sub> content of the atmosphere. *J. of Atmos. Sci.* 37, No. 1, 99-118.
- Maykut, G. A., and Untersteiner, N., 1971: Some results from a time dependent, thermodynamic model of sea ice. *Journal of Geophysical Research*, 76, 1550-1575.
- Maykut, G. A., 1983: Surface heat and mass balance of ice, in *NATO Advanced Study Institute on Air-Sea-Ice Interaction*, Plenum, New York.
- Muench, R. D., and Charnell, R. L., 1977: Observations of medium-scale features along the seasonal ice edge in the Bering Sea. *Journal of Physical Oceanography*, 7, No. 4, 602-606.
- Muench, R. D., Stegen, G. R., and Hachmeister, L., 1983: Prediction of ice

- distribution and movement in the outer marginal ice zone, POAC 83; The seventh international conference on port and ocean engineering under arctic conditions. 1, 190-199.
- Murry, F. W., 1967: On the computation of saturation vapour pressure, *J. Appl. Meteorol.*, **6**, 203-204.
- Neralla, V. R., and Liu, W. S., 1979: A simple model to calculate the compactness of ice floes. *Journal of Glaciology* **24**, No. 90, 407-414.
- Neralla, V. R., Liu, W. D., Venkatesh, S., and Danard, M. B., 1980: Techniques for predicting sea ice motion, in *Sea Ice Processes and Models*, edited by R. S. Pritchard. 197-206, University of Washington, Seattle.
- Overgaard, S., Wadhams, P., and Leppäranta, M., 1983: Ice properties in the Greenland and Barents Seas during Summer. *Journal of Glaciology*, **29**, No. 101, 142-164.
- Overland, J. E., Reynolds, R. M., and Pease, C. M., 1983: A model of the atmospheric boundary layer over the marginal ice zone. *Journal of Geophysical Research*, **88**, No. C5, 2836-2840.
- Ovsiyenko, S. N., 1976: O chislennom modelirovanii dreyfa l'da. (Numerical modelling of the drift of ice). *Izvestiya Akademii Nauk SSSR. Fizika Atmosfera i Okeana*, Tom 12, No. 11, 1201-06. English translation in *Izvestiya. Academy of Sciences, U.S.S.R. Atmospheric and Oceanic Physics*, **12**, No. 11, 1977, 240-43.
- Parkinson, C. L., and Washington, W. M., 1979: A large-scale numerical model of sea ice. *Journal of Geophysical Research*, **84**, 311-337.
- Parkinson, C. L., and Herman, G. F., 1980: Sea ice simulations based on fields generated by the GLAS GCM. *Monthly Weather Review*, **108**, No. 12, 2080-2091.
- Parkinson, C. L., and Good, M. R., 1982: Sensitivity of a climatologically driven sea ice model to the ocean heat flux. *NASA Technical Memorandum* 83.
- Parmerter, R. R., 1974: A mechanical model of rafting, *AIDJEX Bull.* **23**, 97-115. (Also published as PB 230 378/AS, Nat. Tech. Inform. Serv., Springfield, Va.)
- Parmerter, R. R. and Coon, M. D., 1972: Model of pressure ridge formation of

- sea ice. *Journal of Geophysical Research*, **77**, 6565-6575.
- Pritchard, R. S., 1977: The effect of strength on simulations of sea ice dynamics. POAC 77. The fourth international conference on port and ocean engineering under Arctic conditions, **1**, 494-505.
- Pritchard, R. S., Coon, M. D. and McPhee, M. G., 1977: Simulation of sea ice dynamics during AIDJEX. *Journal of Pressure Vessel Technology*, **93**(3), 491-97.
- Pritchard, R. S. and Coon, M. D., 1981: Canadian Beafort sea ice characterization, POAC 81. The sixth international conference on port and ocean engineering under arctic conditions. **2**, 609-18.
- Pond, S., and Pickard, G. L., 1978: *Introductory dynamic oceanography*. Pergamon Press. 241 pp.
- Reed, R. J. and Campbell, W. J., 1962: The equilibrium drift of ice station Alpha, *Journal of Geophysical Research*, **67**, 281-297.
- Røed, L. P., and O'Brien, J. J., 1981: Geostrophic adjustment of highly dispersive media: An application to the marginal ice zone, *J. Geophys. Astrophys. Fluid Dyn.*, **18**, 263-278.
- Røed, L. P., and O'Brien, J. J., 1983: A coupled ice-ocean model of upwelling in the marginal ice zone. *Journal of Geophysical Research*, **86**, 2863-2872.
- Rothrock, D. A., 1975: The energetics of the plastic deformation of pack ice by ridging. *Journal of Geophysical Research*, **80**, 4514-4519.
- Rothrock, D. A., 1983: Ice thickness distribution - Measurement and theory, in *NATO Advanced Study Institute on Air-Sea-Ice Interaction*, Plenum, New York.
- Russel-Head, D. S., 1980: The melting of free-drifting icebergs. *Annals of Glaciology*, **1**, 119-122.
- Schwaegler, R. T., 1974: Fracture of sea ice sheets due to isostatic imbalance. *AIDJEX Bull.* **24**, 131-46.
- SCOR, 1979: The Arctic Ocean heat budget, Report From Working Group 58, Scientific Committee on Oceanic Research, Rep. 52, *Geophys. Inst., Univ. of Bergen, Norway*.

- Semtner, A. J., Jr., 1976: A model for the thermodynamic growth of sea ice in numerical investigations of climate. *J. Phys. Oceanogr.*, **6**, 379-389.
- Sodhi, D. S., 1977: Ice arching and the drift of pack ice through restricted channels. CRREL Report 77-18. Cold Regions research and engineering Laboratory, Hanover, New Hampshire. 11pp.
- Solomon, H., 1973: A one-dimensional collision model for the drift of a compact ice pack. *Geophysical Fluid Dynamics*, **5**, 1-22.
- Sverdrup, H. U., 1928: The wind-drift of the ice on the North Siberian Shelf. The Norwegian North Polar Expedition with the 'Maud' 1918-1925, Scientific results, **4**, 1-46.
- Thorndike, A., and Colony, R., 1980: Arctic Ocean Buoy Program, Data Report, 19 January 1979 to 31 December 1979. 131 pp.
- Thorndike, A., and Colony, R., 1982: Sea ice motion in response to geostrophic winds, *Journal of Geophysical Research*, **87**, 5845-5852.
- Thorndike, A. S., Rothrock, D. A., Maykut, G. A., and Colony, R., 1975: The thickness distribution of sea ice. *Journal of Geophysical Research*, **80**, 4501-4513.
- Timokhov, L. A., 1967a: Odnomernyi stokhasticheskii dreif l'dov (One dimensional stochastic ice drift). *Trudy Arkticheskii i Antarkticheskii Nauchno-issledovatel'skii Institut. Leningrad.* **281**, 121-129. Unpublished English translation by Joachim Büchner and Leda V. Sagen in *AIDJEX Bull.* **3**, November 1970: 80-93.
- Timokhov, L. A., 1967b: K voprosu o dinamike i kinematike l dov. (Dynamics and kinematics of ice floes). **281**, 130-136. Unpublished English translation by Joachim Büchner in *AIDJEX Bull.* **3**, 94-105.
- Tucker, W. B., III, 1982: An application of a numerical sea ice model to the East Greenland area. CRREL Report 82-16, U.S. Army Cold Regions Research and Engineering Laboratory, Hanover, NH, 51 pp.

- Tucker, W. B. III, 1983: A comparison of sea ice model results using three different wind forcing fields. CRREL Report 83-17, U. S. Army Cold Regions Research and Engineering Laboratory, Hanover, NH, 11pp.
- Tucker, W. B. III, and Govoni, J. W., 1981: Morphological investigations of first-year sea ice pressure ridge sails. Cold Regions Sci. Tech., 5, No. 1, 12pp.
- Udin, I., and Ullerstig, A., 1976: A numerical model for forecasting the ice motion in the bay and sea of Bothnia, SMHI, Norrköping.
- Vinje, T. E., 1977: Sea ice studies in the Spitzbergen-Greenland area, Landsat Rep. E77-10206, U. S. Dep. of Commer., Natl. Tech. Inf. Ser., Springfield, Va.
- Vinje, T. E., 1979: Sea ice conditions and drift of Nimbus-6 buoys in 1978, Arbok Nor. Polarinst. 1978, 57-66.
- Vinje, T. E., 1980: On the extreme sea ice conditions observed in the Greenland and Barents Seas in 1979, Arbok Nor. Polarinst. 1979, 57-65.
- Vinje, T. E., 1982: The drift pattern of sea ice in the Arctic with particular reference to the Atlantic approach, in The Arctic Ocean. The Hydrographic Environment and the Fate of Pollutants (ed. L. Rey), Macmillan, London, 83-96.
- Wadhams, P., 1978: Wave decay in the marginal ice zone measured from a submarine, Deep Sea Res., 25, 23-40.
- Wadhams, P., 1980a: A comparison of sonar and laser profiles along corresponding tracks in the Arctic Ocean, in Sea Ice Processes and models, edited by R. S. Pritchard, 283-299, University of Washington Press, Seattle.
- Wadhams, P., 1980b: Ice characteristics in the seasonal sea ice zone. Cold Regions Sci. Tech., 2, 37-88.
- Wadhams, P., 1981: The ice cover in the Greenland and Norwegian Seas, Reviews of Geophysics and Space Physics, 19, No. 3, 345-393.
- Wadhams, P., 1983a: A mechanism for the formation of ice edge bands. Journal of Geophysical Research, 88, No. C5, 2813-2818.
- Wadhams, P., 1983b: Sea ice thickness distribution in Fram Strait. Nature, 305, No. 5930, 108-111.

- Wadhams, P., Gill, A. E., and Linden, P. F., 1979: Transects by submarine of the East Greenland Polar front. *Deep-Sea Research*, **26A**, 1311-1327.
- Wadhams, P., and Squire, V. A., 1983: An ice-water vortex at the edge of the East Greenland Current. *Journal of Geophysical Research*. **88**, C5, 2770-2780.
- Walker, E. R., and Wadhams, P., 1979: On thick sea-ice floes, *Arctic*, **32**(2), 140-147.
- Washington, W. M., Semtner, A. J. Jr., Parkinson, C., and Morrison, L., 1976: On the development of a Seasonal Change Sea-Ice model. *Journal of Physical Oceanography*, **6**, No. 5, 679-685.
- Weber, J. R., and Erdelyi, M., 1976: Ice and ocean tilt measurements in the Beaufort Sea. *Journal of Glaciology*, **17**, 61-71.
- Weller, G., 1972: Radiation flux investigations. *AIDJEX Bull.* **14**, 28-30. (Available as PB 220/859, National Technical Information Service, Springfield, Virginia)
- Wittmann, W. I., and Schule, J. J. Jr., 1966: Comments on the mass budget of arctic pack ice. *Proc Symp. on the Arctic Heat Budget and Atmospheric Circulation*, RM-5233-NSF, ed. J. O. Fletcher, Rand Corp., Santa Monica, Calif., 215-246.
- Zillman, J. W. 1972: A study of some aspects of the radiation and heat budgets of the southern hemisphere oceans, *Meteorol. Stud.* **26**, 562pp., Bureau of Meteorology, Dept. of the interior, Canberra, Australia.
- Zubov, N. N., 1943: *Arctic Ice* (in Russian), Izdatel'stvo Glavsermorputi, Moscow. (English translation, U. S. Naval Oceanographic Office, Washington, D. C., 195.)

#### LIST OF ACRONYMS

AIDJEX	Arctic Ice Dynamics Joint Experiment
ECMWF	European Centre for Medium-range Weather Forecasting
FGGE	First GARP [Global Atmospheric Research Program] Global Experiment
MIZEX	Marginal Ice Zone Experiment
SCOR	Scientific Committee on Oceanic Research

## ADDENDUM

Hunkins, K., 1962: Waves on the Arctic Ocean. *Journal of Geophysics*, 67 , 2477.

Mollo-Christensen E., 1983: Interactions between waves and mean drift in an ice pack. *Journal of Geophysical Research*, 88 , 2971-2972.

Robin G. de Q., 1963: Wave propagation through fields of pack ice. *Philosophical Transactions of the Royal Society of London*, A255 , 313-339.

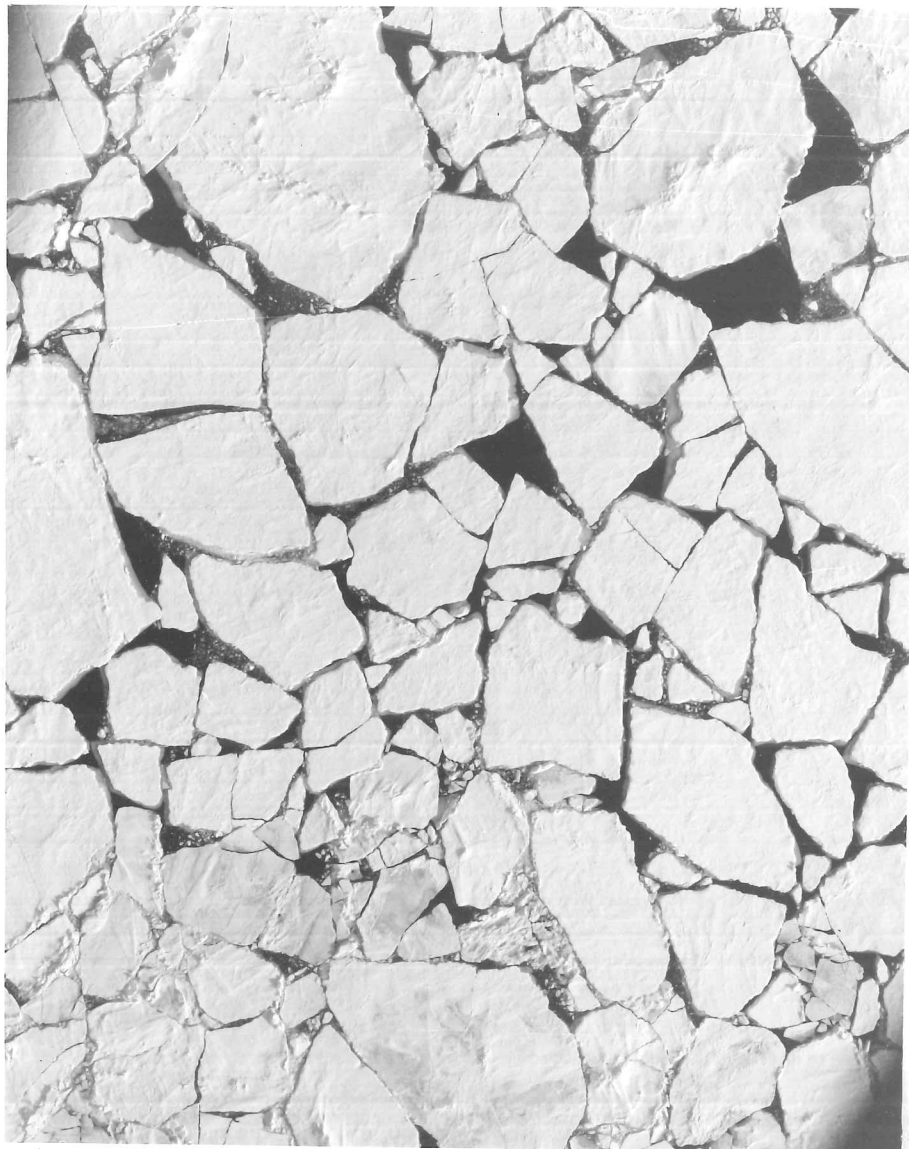
Williams, E., Swithinbank, C.W.M., and Robin G. de Q. 1975: A submarine study of the Arctic pack ice. *Journal of Glaciology*, 15 , 349-362.

## PLATES

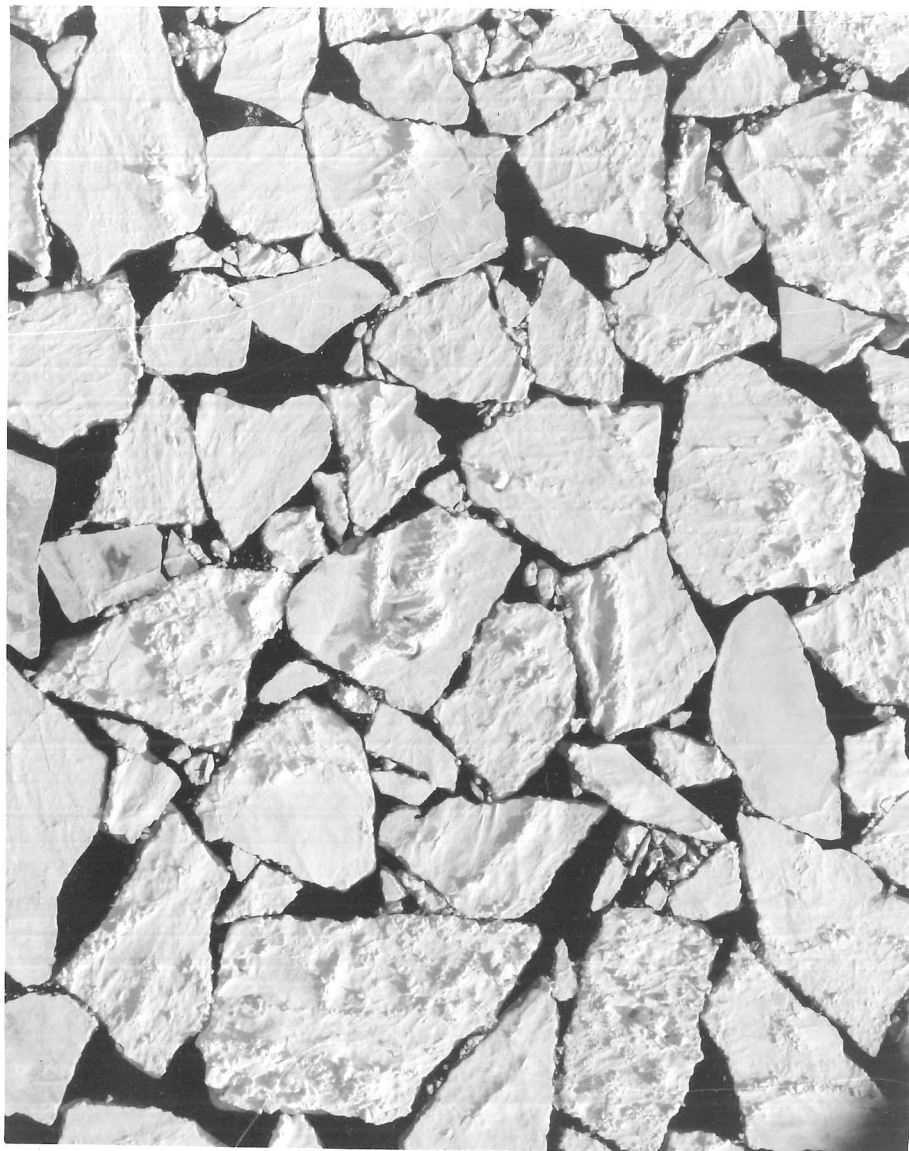
A selection of views of floes from the air in a region near the ice edge in Fram Strait in summer.

Photographs supplied by Vernon Squire.

All the photographs were taken on 27 June 1983.



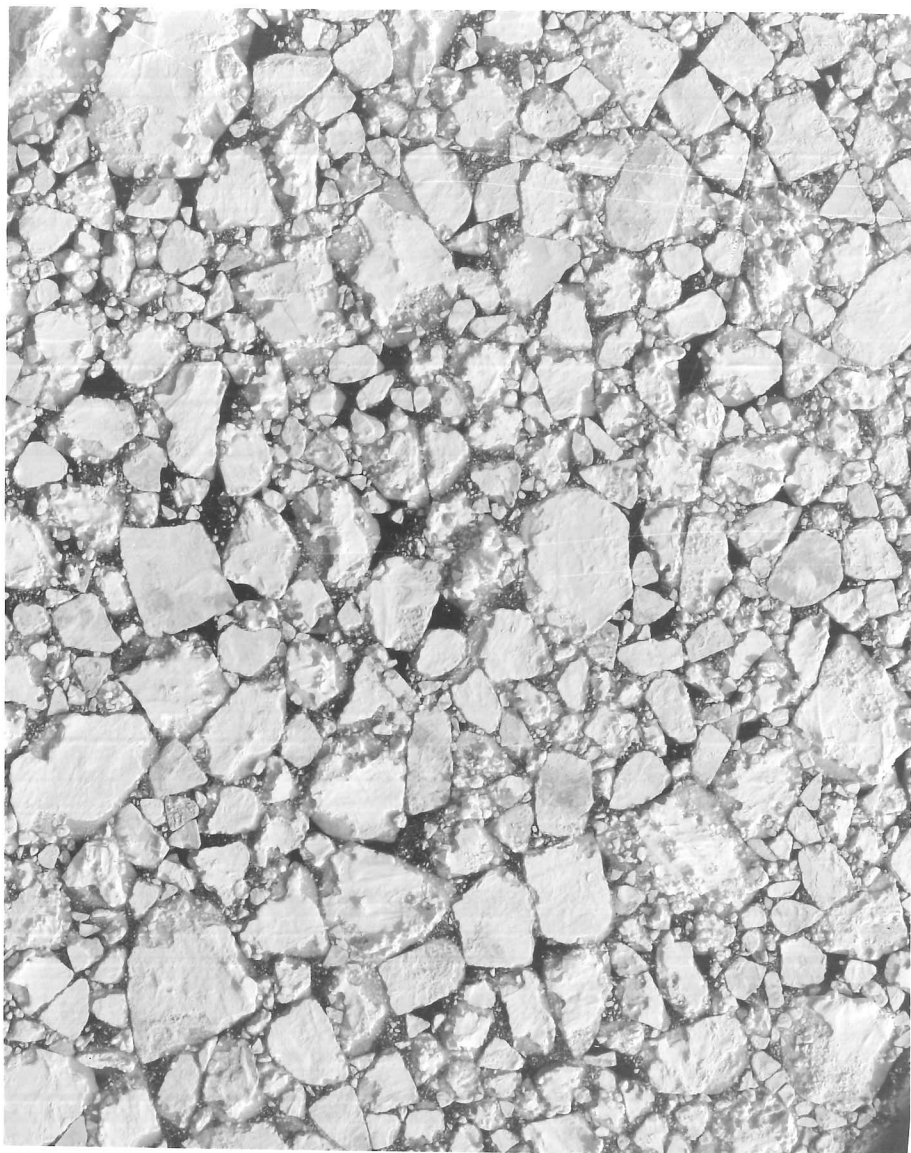
100 m



100 m



100 m



100 m



100 m

UNIVERSITY  
LIBRARY  
CAMBRIDGE